



HAL
open science

Investigation of interpenetrating polymer networks and recent UV curable chemistries

Milena de Brito

► **To cite this version:**

Milena de Brito. Investigation of interpenetrating polymer networks and recent UV curable chemistries. Other. Université de Haute Alsace - Mulhouse, 2011. English. NNT : 2011MULH5772 . tel-01261935

HAL Id: tel-01261935

<https://theses.hal.science/tel-01261935>

Submitted on 26 Jan 2016

HAL is a multi-disciplinary open access archive for the deposit and dissemination of scientific research documents, whether they are published or not. The documents may come from teaching and research institutions in France or abroad, or from public or private research centers.

L'archive ouverte pluridisciplinaire **HAL**, est destinée au dépôt et à la diffusion de documents scientifiques de niveau recherche, publiés ou non, émanant des établissements d'enseignement et de recherche français ou étrangers, des laboratoires publics ou privés.

UNIVERSITE DE HAUTE-ALSACE

Année 2011

n° d'ordre: 2011/01

THESE

pour l'obtention du titre de

Docteur en Chimie des Matériaux

Présentée par

DE BRITO Milèna

Ingénieur de l'Ecole Nationale Supérieure de Chimie de Mulhouse

**INVESTIGATION OF INTERPENETRATING POLYMER
NETWORKS AND
RECENT UV CURABLE CHEMISTRIES**

Soutenue le 25 janvier 2011 devant la commission d'examen

Mme
M
Melle
M
Mme
Mme
M
M

C. CROUTXÉ-BARGHORN
X. ALLONAS
C. DIETLIN
A. MERLIN
N. ARSU
C. CARRE
Z. CHERKAoui
R. FRANTZ

Co-directeur de thèse
Co-directeur de thèse
Examinateur
Examinateur
Rapporteur
Rapporteur
Invité
Invité

A Leninha

ACKNOWLEDGEMENTS

As part of my PhD thesis, I had the opportunity to spend three years within the Department of Photochemistry, in Mulhouse. I worked as a member of both “Photochimie des Matériaux Polymères et Hybrides” (PMPH) and “Photochimie Moléculaire et Photopolymérisation” (PMP) teams.

Today, as I complete my PhD dissertation, I would like to thank all the people I have been working with for their help and their advice.

First and foremost, I would like to express my special thank to my advisors Prof. Céline Croutxé-Barghorn, Prof. Xavier Allonas and Dr. Céline Dietlin for their support, encouragement and guidance throughout my doctoral work.

I would like also to thank Huntsman Advanced Materials for the financial support through this fellowship. Special thanks are owed to Dr. Zoubair Cherkaoui, Dr. Matthias Graeber, Dr. Richard Frantz and Dr. Jean-Jacques Lagref. This collaboration allowed me to gain valuable experiences in rapid prototyping and UV curing fields.

I am also grateful to Prof. Nergis Arsu, Senior Scientist Christiane Carré and Prof. André Merlin for having accepted to serve on my thesis committee and examine my work.

I am also thankful to many others for directly helping with this research.

I would like to thank all the members of the organic laboratory “Chimie Organique et Bioorganique” Prof. Albert Defoin, Prof. Céline Tarnus, Sarah, Lionel, Emel...for their welcome and for providing time, knowledge and equipments necessary to accomplish the organic synthesis. Special thank for Dr Didier le Nouen for all his help with NMR analysis.

I am also grateful to Dr. Koichi Kawamura from the DPG for his support during the organic synthesis.

I would like to thank the Deutsches Kunststoff-Institut and especially Prof. Ingo Alig and Suman for having characterized the rheological properties of the UV cured interpenetrating polymer networks.

I am also grateful to Dr. Loic Vidal for having performed the SEM micrographs.

I am also thankful to the undergraduate students who have helped me a lot during my thesis: Caroline, Marie, Fanny and Corentin.

I would like also to thank all the members of the laboratory, engineers, PhD students (both current and former) for their welcome, their help, and their good mood.

Finally, I would like to express my sincere gratitude to my family for their unconditional love and support.

TABLE OF CONTENTS

LIST OF ABBREVIATIONS.....	i
GENERAL INTRODUCTION.....	1

Chapter I: Rapid prototyping and rapid manufacturing

I	INTRODUCTION	7
I.1	Principle of rapid prototyping.....	9
I.2	Overview of RP technologies	10
I.2.1	Solid-based techniques.....	10
I.2.1.1	Powders.....	10
I.2.1.2	Sheets	13
I.2.1.3	Molten powder particles	14
I.2.2	Liquid-based techniques	16
II	HUNTSMAN COLLABORATION.....	23
III	REFERENCES	26

Chapter II: UV cured Interpenetrating Polymer Networks (IPNs)

I	INTRODUCTION	32
II	GENERAL ASPECTS OF PHOTOPOLYMERIZATION PROCESSES	33
II.1	Introduction.....	33
II.2	Radical photopolymerization.....	33
II.2.1	Radical photoinitiators.....	33
II.2.1.1	α -cleavable photoinitiators (type I)	34
II.2.1.2	Type II photoinitiators	35
II.2.1.3	Photosensitization process	36
II.2.2	Kinetics of radical photopolymerization.....	36
II.2.2.1	Initiation.....	36
II.2.2.2	Propagation	37
II.2.2.3	Termination.....	37
II.2.3	Monomers: acrylic and methacrylic resins	39
II.2.4	Special features of the radical photopolymerization.....	40
II.2.4.1	Side reactions.....	40
II.3	Cationic photopolymerization.....	42
II.3.1	Cationic photoinitiators.....	42
II.3.1.1	Diaryliodonium salts and triarylsulfonium salts	42
II.3.2	Kinetics of cationic photopolymerization.....	48
II.3.2.1	Initiation.....	48
II.3.2.2	Propagation	48
II.3.2.3	Termination.....	48
II.3.3	Cationic monomers and oligomers	49
II.3.3.1	Epoxide monomers	49
II.3.3.2	Vinyl ether monomers.....	50
II.3.4	Special features of the cationic photopolymerization.....	50
II.3.4.1	Deactivation processes.....	50
II.3.4.2	Inhibition.....	50
II.3.4.3	Side reactions.....	51
II.3.4.4	Living character	52
II.3.4.5	Temperature	52
II.4	Conclusion	52
III	IPN PHOTOPOLYMERIZATION	53
III.1	Different ways of UV cured IPN synthesis.....	53
III.1.1	Simultaneous UV IPNs	53
III.1.2	Sequential IPNs.....	53
III.2	Photopolymerization process of IPNs.....	55
III.2.1	Kinetics aspects of photoIPNs	55
III.2.2	Characterization of the photocured IPNs	57
III.2.2.1	IPN morphology.....	57
III.2.2.2	IPN thermomechanical properties.....	59
III.2.2.3	Transparency.....	60

IV	EXPERIMENTAL STUDY	61
IV.1	Understanding of the IPN formation between a diglycidyl ether epoxide and an acrylate under Huntsman industrial specifications.....	61
IV.1.1	Context of the study.....	61
IV.1.2	Characterization of the commercial resin Renshape®SL 7870.....	62
IV.1.2.1	Griffin and SLA 7000 trials.....	62
IV.1.2.2	UV spectroscopy measurements.....	65
IV.1.2.3	Kinetics of photopolymerization at 366 nm	66
IV.1.3	Optimization of the IPN kinetics: Enhancement of the cationic photopolymerization by sensitization processes	68
IV.1.3.1	Compounds used as sensitizers	68
IV.1.3.2	Effect of free radicals from radical photoinitiator photolysis.....	70
IV.1.3.3	Evaluation of the chemical balance between the radical polymerization and the electron transfer reaction	76
IV.1.3.4	Effect of the photosensitizers	81
IV.1.3.5	Tests with Griffin	84
IV.1.4	Use of triphenylphosphine for the improvement of the IPN kinetics.....	86
IV.1.4.1	Trials with Griffin	87
IV.1.4.2	RT FTIR spectroscopy	88
IV.1.5	Influence of temperature on the photopolymerization process.....	90
IV.1.5.1	RT FTIR spectroscopy	90
IV.1.5.2	PhotoDSC experiments.....	95
IV.1.6	Characterization of the final properties	99
IV.1.6.1	Thermomechanical properties	99
IV.1.6.2	IPN morphology	101
IV.2	Academic study on the formation of quasi-simultaneous IPNs between a cycloaliphatic epoxide and a methacrylate	103
IV.2.1	Compounds	104
IV.2.2	Kinetics study under broadband irradiation	105
IV.2.2.1	Photopolymerization of the starting monomers	105
IV.2.2.2	Photopolymerization of the hybrid mixture.....	107
IV.2.3	Kinetics study at 366 nm exposure.....	109
IV.2.3.1	Photopolymerization of the starting monomers	109
IV.2.3.2	Photopolymerization of the hybrid mixture.....	110
IV.2.4	Final properties	112
IV.2.4.1	Thermomechanical analysis of the UV cured analysis	112
IV.2.4.2	Morphology of the UV cured IPNs.....	115
IV.2.4.3	Rheological properties of the UV cured analysis.....	116
V	CONCLUSIONS AND PERSPECTIVES.....	119
VI	REFERENCES	121

Chapter III: Alternatives to IPN chemistries

I	INTRODUCTION	127
II	LITERATURE SURVEY	129
II.1	Basics of thiol-ene chemistry	129
II.1.1	History	129
II.1.2	The reactants	129
II.1.2.1	Thiol compounds	129
II.1.2.2	Ene compounds	130
II.1.2.3	Kinetics of photopolymerization	131
II.1.2.4	Properties of thiol-ene chemistry	133
II.2	Silane-ene	135
II.3	Maleimide chemistry	137
II.3.1	Donor/acceptor copolymerization	138
II.3.1.1	Definition	138
II.3.1.2	Polymerization mechanism: Description of the different steps	139
II.3.2	Maleimide/vinyl ether system	142
III	STUDY OF MALEIMIDE /VINYL ETHER MIXTURES IN PRESENCE OF RADICAL PHOTOINITIATOR	146
III.1	Chemicals	146
III.2	Variation of the proportions between N-tertbutylmaleimide and Tris[4-(vinylloxy)butyl] trimellitate	147
III.3	Variation of vinyl ether nature	150
III.4	Variation of MI structure	151
III.5	Influence of the photoinitiator system	153
III.5.1	Addition of a cationic photoinitiator to the formulation BMI-2300® 2575 DIVE	153
III.5.2	Modification of the radical photoinitiator in presence of the cationic photoinitiators TAS and I 250	155
III.6	Influence of the post-curing treatment	158
III.7	Thermomechanical properties	160
III.8	Determination of the volumetric shrinkage and linear Deflection	162
IV	INVESTIGATIONS ON THE POLYMERIZATION OF MALEIMIDE / NORBORNENE MIXTURES IN PRESENCE OF RADICAL PHOTOINITIATOR	164
IV.1	Introduction	164
IV.2	Thermomechanical properties	168
IV.3	Volumetric shrinkage and linear deflection	169
V	CONCLUSIONS AND PERSPECTIVES	170
VI	REFERENCES	172

Chapter IV: Linear shrinkage measurement

I	INTRODUCTION	179
II	DESCRIPTION OF THE SELECTED METHODS TO MEASURE VOLUMETRIC AND LINEAR SHRINKAGES	181
II.1	Measurement of the volumetric shrinkage.....	181
II.2	Measurement of the linear shrinkage	182
II.2.1	Principle	182
II.2.2	Experimental set up.....	184
II.2.2.1	Substrate.....	184
II.2.2.2	Application of the coating.....	184
II.2.2.3	Light sources	184
II.2.2.4	Deflection measurement	184
II.2.3	Assessment of the linear shrinkage technique and its optimization	186
II.2.3.1	Nature of the substrate	187
II.2.3.2	Sample thickness.....	187
II.2.3.3	Light intensity	189
III	RESULTS	191
III.1	Selected formulations.....	191
III.2	Comparison of the performances between the two linear methods	193
III.3	Comparison between the volumetric and linear shrinkages	194
III.4	Kinetic monitoring of the cantilever deflection	196
IV	CONCLUSIONS AND PERSPECTIVES.....	198
V	REFERENCES	200
	GENERAL CONCLUSION	205

Annexes

Experimental part.....	211
Annexe I: Irradiation sources.....	212
Annex I.1: Arc mercury-xenon (Hg-Xe) Hamamatsu lamp.....	212
Annex I.2: UV conveyor belt.....	213
Annex I.3: Arc Hg Oriel lamp.....	214
Annex I.4: Hg flood lamp.....	214
Annexe II: Real time techniques.....	215
Annex II.1: Real Time Fourier Transform Infra Red (RT FTIR) spectroscopy	215
Annex II.2: Photo Differential Scanning Calorimetry	218
Annexe III: Thermoanalytical techniques	221
Annex III.1: Dynamic Mechanical Analysis (DMA).....	221
Annex III.2: Modulated Differential Scanning Calorimetry (MDSC)	223
Annexe IV: Electronic microscopy technique	226
Annex IV.1: Scanning Electronic Microscopy (SEM).....	226
Annexe V: Rheological technique.....	227
Annex V.1: Combination of Real time dynamic ultrasound reflectometry and time resolved near infrared spectroscopy	227
 Synthesis procedures.....	 229
Annexe VI: Synthesis of liquid bismaleimides	230
Annexe VII: Synthesis of norbornenes	232
 REFERENCES	 234

LIST OF ABBREVIATIONS

910	9,10-diethoxyanthracene
3DP	3D-printing
A	Acceptor monomer
ABS	Acrylonitrile butadiene styrene
ACE	Active chain end mechanism
AFM	Atomic force microscopy
AM	Activated monomer mechanism
BA	Butyl acrylate
BDE	Bond dissociation energy
BDVE	1,4-butadienedioldivinyl ether
BMI-2300®	Phenylmethane maleimide
BP	Benzophenone
CAD	Computer-aided design
C _d	Cure depth
CDDVE	1,4-cyclohexanedimethanol divinyl ether
CQ	Camphorquinone
CMM	Coordinate measuring machine
CT complex	Charge transfer complex
D	donor monomer
D 1173	2-hydroxy-2-methyl-1-phenyl-propan-1-one
DAC	Ethoxylated (3) bisphenol A dimethacrylate
DEP	3,4-epoxycyclohexylmethyl-3'-4'-epoxycyclohexylcarboxylate
DH	H donor
DIVE	Bis[4-(vinylloxy)butyl]isophthalate
DLP	Digital light processing
DMA	Dynamic mechanical analysis
DMD	Digital micromirror device
DMPA	2,2-dimethoxy-2-phenylacetophenone
DMTA	Dynamic mechanical thermal analysis
D _p	Penetration depth
DSC	Differential scanning calorimetry
E5000	Epoxidized hydrogenated bisphenol A
EBANEC	Bis-2,2-[4-(2-[norborn-2-ene-5-carboxylate]ethoxy)phenyl]propane
E _c	Critical exposure
EDB	Ethyl-4-dimethylaminobenzoate
E _{max}	Maximum exposure at the resin surface
FDM	Fused deposition modelling
HDDA	1,6-hexanediol diacrylate
HDDNEC	1,6-hexanediol di (endo,exo-norborn-2-ene-5-carboxylate
I 184	1-hydroxycyclohexylphenyl ketone
I 250	Iodonium, (4-methylphenyl)[4-(2-methylpropyl) phenyl]-, hexafluorophosphate(1-)
I 651	2,2-dimethoxy-2-phenylacetophenone
I 819	Bis(2,4,6-trimethylbenzoyl)-phenylphosphineoxide
I OXE01	1,2-octanedione,1-[4-(phenylthio)phenyl]-, 2-(O-benzoyloxime)
I OXE02	1-[9-ethyl-6-(2-methylbenzoyl)-9H-carbazol-3-yl]-,

	1-(O-acetyloxime)-ethanone
IPNs	Interpenetrating polymer networks
IBOA	Isobornyl acrylate
ITX	Isopropylthioxanthone
LOM	Laminated object manufacturing
L_w	Thickness of the cured line upon laser irradiation
M	Monomer
MDSC	Modulated differential scanning calorimetry
MLS	Microlightswitch®
MI	Maleimide
MIT	Massachusetts Institute of Technology
NMR	Nuclear magnetic resonance
Non rev heat flow	Non reversing heat flow
NOR	Norbornene
NTMI	N-tertbutylmaleimide
OP	Optical pyrometry
PA	Polyamide
PC	Polycarbonate
PEGNEC	Polyethylene glycol (200) di-(norborn-2-ene-5-carboxylate)
PhotoDSC	Photodifferential scanning calorimetry
PI	Photoinitiator
PP	Polypropylene film
PPGBMI	Poly(propylene glycol) bismaleimide
PS	Polystyrene (chapter I)
PS	Photosensitizer (chapter II and III)
Rev heat flow	Reversing heat flow
RH	H donor
RM	Rapid manufacturing
RP	Rapid prototyping
RT FTIR	Real time Fourier transform infra red spectroscopy
RTUR	Real-time ultrasound reflectometry
SCE	Saturated calomel electrode
SEM	Scanning electronic microscopy
SLA	StereoLithography Apparatus, stereolithography process
SLS	Selective laser sintering
SR 833S	Tricyclodecane dimethanol diacrylate
STL	STereoLithography, Standard Triangulation Language
TAS	Triarylsulfonium hexafluoroantimonate mixture salts
TBDNS	1,1,3,3-tetramethyl-1,3-bis [2-(5-norborn-2-yl)ethyl]disiloxane
TEM	Transmission electronic microscopy
T_g	Glass transition temperature
TP	Triphenylphosphine
TPO	2,4,6-trimethylbenzoyldiphenylphosphine oxide
TRIVE	Tris[4-(vinylloxy)butyl]trimellitate
VE	Vinyl ether

GENERAL INTRODUCTION

UV curing technology has become very attractive since in a timescale of few seconds, reactive liquids are converted into solids by light. The UV cured polymers exhibit some advantages compared to the polymers generated thermally such as rapid through-cure, low energy requirements, room temperature treatment, non polluting and solvent free formulations. They find applications in many industrial fields such as protective coatings, varnish industries and electronics. They are also applied in laser technologies such as laser direct imaging or stereolithography (SLA). In stereolithography, a computer-controlled laser beam is used to polymerize a liquid photopolymer layer by layer according to data of a three-dimensional object. The stereolithography technique is the first and the most widely used rapid prototyping (RP) method. This technology emerged because nowadays, the competition between the manufacturers has tremendously intensified. To remain competitive, it has become vital for them to present their new products in the market as early as possible. To that end, they have integrated into their manufacturing process rapid prototyping systems. Rapid prototyping (RP) is merely defined as the fast fabrication of prototypes within a couple of hours or days. As a consequence, it is possible to detect deficiencies early in the process and correct them in order to meet the customer expectations. The use of this laser-induced technique exhibits several advantages in terms of fast curing, beam directivity, accuracy and spatial and temporal control of the process. However, since during the stereolithography process, the laser reproduces point by point the shape of the layer digitally defined, a long period of time is required for the conception of a few prototypes with complex shapes. Manufacturers are now interested in extending the fabrication of prototypes to the production of directly functional products in an important scale. They would like to step into rapid manufacturing (RM). To speed up the process, there are two alternatives: either modifying the light source or increasing the number of light sources. It is within this framework that the collaboration between the Department of Photochemistry and Huntsman Advanced Materials has started. Huntsman Advanced Materials, worldwide supplier of UV curable SLA resins, has decided to develop a new rapid manufacturing machine named Araldite®Digitalis. This technology is able to produce quickly and with a high accuracy a large number of pieces. It is based on a new system of irradiation curing selectively a large surface of the photosensitive resin. So far, the Huntsman commercial resins were specifically formulated for stereolithography. Therefore, the topical issue will be to know if these resins will keep their reactivity under Araldite®Digitalis cure.

The aim of this thesis is thus to develop and characterize UV curable resins compatible with Araldite®Digitalis. The study deals with not only the UV curable resins commonly used in stereolithography (acrylates, epoxides, hybrid epoxide/acrylates mixtures) but also with other resins based on unconventional chemistries that could overcome some identified drawbacks in terms of curing rates or final properties.

The thesis dissertation can be divided into 4 chapters.

The first one “Rapid Prototyping & rapid manufacturing” allows us to introduce the rapid prototyping technology. The advantages and the drawbacks of the most used RP techniques are presented in order to highlight both the technical features and the challenges of Araldite®Digitalis.

The second chapter “UV cured Interpenetrating Polymer Networks” is devoted to the UV curable hybrid systems used in SLA. Commonly, the commercial mixture comprises multifunctional acrylate and epoxide monomers that polymerize according to two different mechanisms (i.e. cationic and radical processes) leading to the formation of two interpenetrating polymer networks. It has been shown that commercial resins efficient under SLA exhibit poor reactivity under Araldite®Digitalis. Time has been devoted to identify and understand the differences between these 2 technologies and their influence on the photopolymerization process. Real Time Infra Red spectroscopy (RT FTIR) spectroscopy was the method of choice. The major task has been devoted to speed up the photochemical pathway of the cationic polymerization. Additionally, the final properties such as the thermomechanical properties and morphology will also be studied. Moreover, an academic study will be performed on an epoxide/methacrylate mixture in order to get a better understanding and a control of the IPN formation. The influence of the light intensity and the photoinitiator concentration on the final properties has been examined. Some limitations are underlined due to the lack of efficient cationic photoinitiators in the UVA range, the stability of some existing cationic photoinitiators and the low light intensity of the light source. As a result, we decided to direct our efforts toward other chemistries.

The third chapter “Alternatives to IPN chemistry” is about unconventional chemistries susceptible to replace the IPN chemistry. Based on the literature survey, we have mainly focused on the chemistries combining maleimides with vinyl ethers and norbornenes respectively. To get an overview of the reactivity of these chemistries, the influence of the different parameters such as the nature of the photoinitiator, the proportion between the monomers, has been assessed by RT FTIR spectroscopy. In order to study the influence of the monomer nature, we spent several weeks in order to synthesize monomers owing to the lack of commercial available maleimide and norbornene compounds. The obtained results were interesting in particular the ones got for the totally new maleimide/norbornene system. Consequently, their thermomechanical properties as well as the linear shrinkage have been also investigated.

The last chapter “Linear shrinkage measurement” is dedicated to the measurement of the shrinkage that occurs during photopolymerization. This notion is of paramount importance for stereolithography and Araldite®Digitalis technologies. Indeed, the shrinkage resulting from the conversion of the liquid photosensitive resin into solid during the building-up process yields to residual stresses capable of inducing distortions and problems of part dimensions. The goal of this chapter is to set up a simple method to measure linear shrinkage in order to compare the different systems proposed during the thesis. This method is based on an existing method and was adapted to our study. It lies in the manual and digital measurement of a UV cured brass cantilever deformation. The results obtained will be compared to the results got with a volumetric shrinkage method related to the buoyancy mass determination.

Chapter I: Rapid prototyping & rapid manufacturing

I	INTRODUCTION.....	7
I.1	Principle of rapid prototyping	9
I.2	Overview of RP technologies.....	10
I.2.1	Solid-based techniques	10
I.2.1.1	Powders	10
I.2.1.2	Sheets	13
I.2.1.3	Molten powder particles.....	14
I.2.2	Liquid-based techniques.....	16
II	HUNTSMAN COLLABORATION	23
III	REFERENCES.....	26

I INTRODUCTION

Nowadays, the manufacturers that desire to keep or acquire a market field have to take into account several parameters such as ^{1,2}.

- ⇒ The globalisation of the markets
- ⇒ The tougher competition between the companies
- ⇒ A higher reactivity from the companies
- ⇒ The control of their costs
- ⇒ The improvement of the quality of their products
- ⇒ The reduction of the development time of the product

As a consequence, if the companies want to be competitive, it is essential for them to materialize the product during the development. Indeed, by this way, all the people participating to the development process (engineers, manufacturers, marketing and purchasing managers) can have a look to the design. Thus, they are able to correct the conception mistakes and make the changes before the costs become too expensive ¹. Rapid prototyping (RP) is one technology that allows to shorten the time between the initial concept and the manufactured product. It came out in the eighties with the rapid development of computer-aided design (CAD) ³. Broadly speaking, it can be defined as the process leading to the creation of a three-dimensional (3D) part, a prototype, with arbitrary shapes coming from the execution of a computer program (CAD) or from an existing object. The process is known to be highly automated and flexible ⁴. Lately, some of RP processes are able to directly produce parts whose mechanical properties are similar to those achieved by conventional manufacturing processes. This ability to build functional parts in small series yields to the emergence of rapid manufacturing (RM).

At the beginning, the prototypes were first used as visual aids to control the estheticity of the real part ⁴. But with the development of both new raw materials and processes, the prototypes can play different roles ⁵. For instance, they can be employed for synthesizing the various components of a product in order to test their suitability within the assembly. They can also serve as master patterns for tooling and molding processes. They can be produced as functional parts to check the final properties such as the material quality, the shape accuracy before the mass fabrication process. Finally, they can be built for a given application according to special specifications. Usually, the production of prototypes is limited between 1 and 10 pieces.

RP finds its applications in various industries such as automotive, aerospace, biomedical, consumer product ...⁶. The chart in Figure I. 1 indicates the repartition of RP according to the different industries.

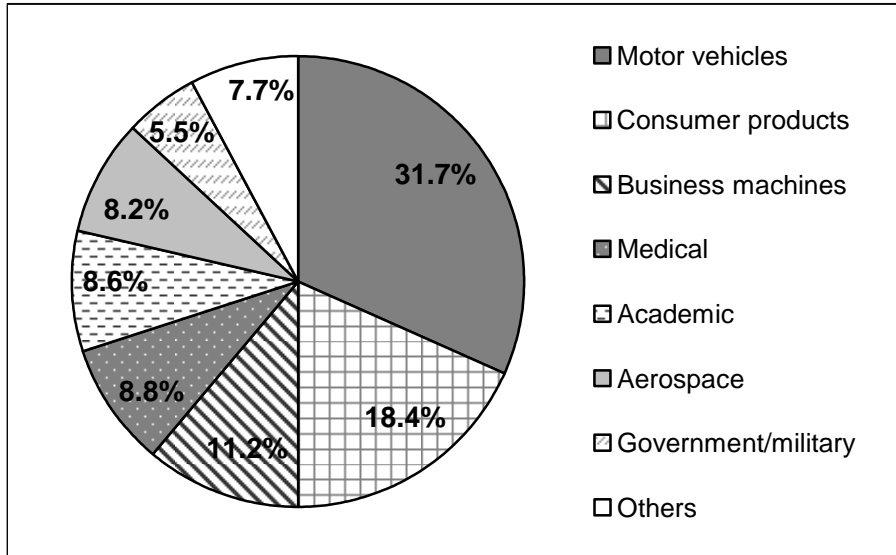


Figure I. 1: Chart representing the different areas of RP

This chapter will present an overview of the rapid prototyping technology. A description of the strengths and the limitations of the commercially available RP technologies will be done. A particular interest will be paid to the processes that use UV curable resins so as to introduce a new technology called Araldite®Digitalis from Huntsman. This process is particularly promising, being capable of producing objects with high accuracy and reproductibility.

1.1 Principle of rapid prototyping

Basically, the fabrication of prototypes can be achieved according to three elementary methods^{2,6}, as it is described in Figure I. 2.

- I. The **subtractive method** consists in removing material from a larger initial solid block.
- II. The **forced forming method** uses the ability of a material to deform under specific binding forces such as molds or dies, so as to produce the object⁶.
- III. The **additive method** lies in the creation of a 3D-part by piling up successive layers of the material.

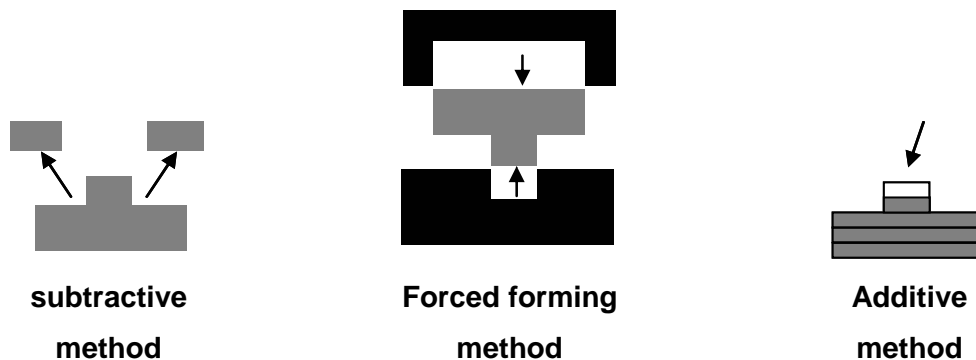


Figure I. 2: The fundamental methods used for the fabrication of a part

The last method emerged in the 80s in order to overcome some limitations of the conventional subtractive and forced forming methods such as the lack of precision and complexity of the geometry shape. It is therefore this methodology that is mostly used in RP⁴.

Additive RP (also called layer manufacturing or solid freeform) can be defined as a manufacturing process for which a three-dimensional (3D) part is fabricated⁴ by using a CAD model. It can be achieved by using either a computer model or by digitalizing a real object. In this case, it is necessary to accurately measure the dimensions size of the object. It is usually performed via a reverse engineering technology such as a laser digitizer or coordinate measuring machine (CMM). All the data acquisition is finally transmitted to the CAD system. Once the CAD model is built, it is not directly sent to the RP machine. It needs first to be converted into a STL file (STereoLithography)⁷⁻⁹. This format of file was created in 1987 by 3D Systems company⁸ for stereolithography application. It is today the most common data interface between CAD software and the rapid prototyping machine. It converts the object into a polyhedral representation.

The role of this format is to approximate the surface of the 3D-part in the shape of triangular facets (Standard Triangulation Language). The quality of the surface is related to the sizes of the facets ⁸⁻¹⁰. The smaller is the facet size, the better is the quality of the surface. Then, the STL file is transmitted to the computer of the RP system that transforms the model into thin, horizontal cross-sections. Finally through laser sintering, guided deposition, photochemical processes ⁴, the model is reproduced layer by layer.

Given that the prototype really looks like the virtual model, this process is named WYSIWYG (What You See Is What You Get). The build-up time of the prototype can vary from hours to days. It is strongly dependent on the size and the complexity of the model.

1.2 Overview of RP technologies

Different RP processes are commercially available. They can be classified into two categories according to the physical state of the base material: solid- and liquid-based techniques.

1.2.1 Solid-based techniques

1.2.1.1 Powders

- **Selective laser sintering (SLS)**

This method was first implemented by CR Deckard at the Texas University in Austin in 1991¹¹. The machines were commercially available starting from 1992. In this process, the base material comes as a heat-fusible powder. Wax powder, metal powder, polystyrene (PS), engineering plastics, acrylonitrile butadiene styrene (ABS), polycarbonate (PC), nylon, coated sand and coated ceramic powder are usually employed ². The overall process takes place in a chamber whose temperature is just below the powder melting point. This heating procedure aims at reducing as much as possible thermal distortion and facilitates the sintering process ¹². The first step lies in the deposition of the powder layer with a roller on the top of the build cylinder. Then, a CO₂ laser beam (the power is ranging from 25 to 50 W) draws the cross-section of the 3D-part on the surface by sintering the powder (cf Figure I. 3).

After the solidification of the fused part, the support platform moves down ¹³. In the meantime, the powder reservoir moves up and a new powder layer is formed by the roller

motion. The repetition of the aforementioned steps continues until the full formation of the 3D-part. The unsintered powder in each layer plays the role of support during the building process.

This excess of powder is at last swept and recycled ¹². According to the end-use applications, post-treatments such as heat treating or infiltration can be performed ^{13,14} in order to improve the final properties of the material. The accuracy is comprised between 50-100 μm ⁷ with a build-up speed ranging from $3\text{-}10 \times 10^{-3} \text{ mm.s}^{-1}$ ^{7,12}. The main advantages of this process are the absence of support, the versatility and the non toxicity of powder materials and the possibility to fabricate large part and use the created pieces as functional parts ^{2,13,14}. The drawbacks should also be listed. The obtained parts are a slightly porous ¹⁴. Moreover, it is difficult to find materials with the suitable processing features ^{2,12}. Furthermore, this process requires both a long warm up time at the beginning of the process ¹⁴ and a long cooling cycle at the end of the process ¹². Additionally, the fire hazard related to the use of a CO_2 laser has also to be taken into consideration not only for this technology but also for all the processes using this kind of laser. The accuracy of this method is low ¹⁴, and the machine price is relatively high ^{7,12}.

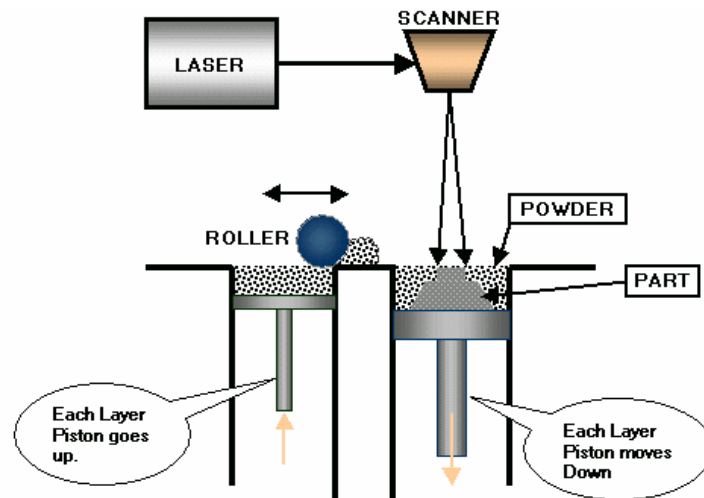


Figure I. 3: Selective laser sintering technique from Arptechⁱ

ⁱ Arptech , How SLS (Selective Laser Sintering) process works, 26/07/2010, <http://www.arptech.com.au/slshelp.htm>

- **3D-printing (3DP)**

3DP technology was developed by Sachs' research group at the Massachusetts Institute of Technology (MIT) in the late 90s^{2,7,15}. Metal and ceramic powders are usually employed as based materials¹². The method consists in selectively spraying a liquid adhesive onto a thin powder layer by means of an ink-jet printing head. The particles of the sprayed powder stick together to form one layer of the 3D piece whereas the unbonded powder is used as support material during the process. The formation of the first layer is followed by the lowering of the building platform and the addition of a fresh powder layer. The procedure is then repeated several times. When the fabrication is finished, the remaining free powder is brushed away and the 3D printed part is treated with a sealant to improve strength and surface finishing. The 3DP procedure is pictured in Figure I. 4.

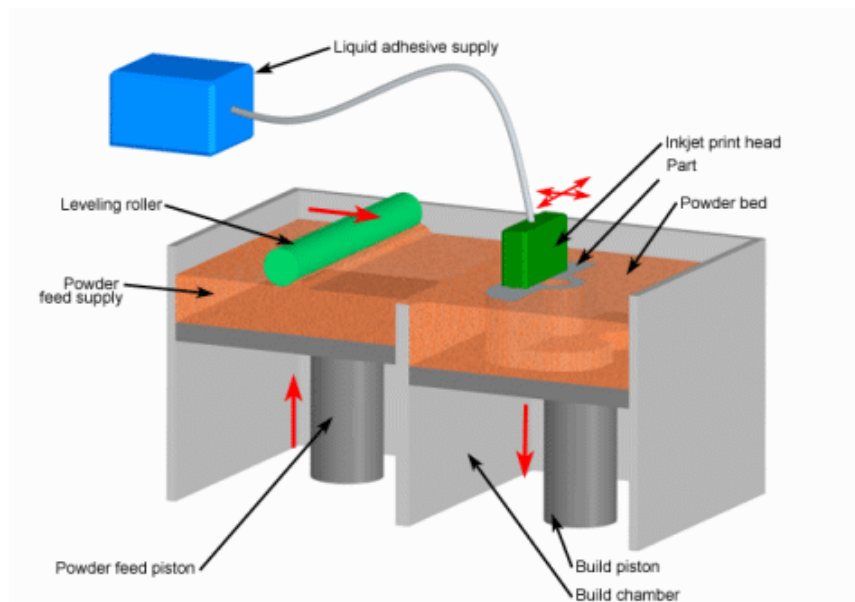


Figure I. 4: 3DP process from customPartNetⁱⁱ

Commonly, the layer thickness achieved by a 3DP machine is around 180 μm . The resolution is roughly 500 μm and the accuracy of $\pm 130 \mu\text{m}$. The build speed is $5\text{-}7 \cdot 10^{-3} \text{ mm}\cdot\text{s}^{-1}$ ¹². 3DP displays several advantages. For instance, the process speed can be increased by using a multi-head system². In addition, the price of the machine is affordable and the maintenance is not complicated. However, this method has some shortcomings. The quality of the final part strongly depends on the precision of the ink-jet heads. Furthermore, only porous items can be built with this machine.

ⁱⁱ Custompartnet , 3D Printing, 26/07/2010, <http://www.custompartnet.com/wu/3d-printing>

I.2.1.2 Sheets

- **Laminated object manufacturing (LOM)**

LOM was coined by Michael Feygin in 1987¹⁶ and was commercially developed by Helisys Corporation in 1991². Paper, ceramics, polymers or metals are commonly employed as base materials. The first step of this process consists in sticking the sheet of paper or other material onto the platform with a special tape. Then, a new layer of sheet is provided by a paper feeding and rolling implement. This new layer glues to the previous layer owing to heat roller that melts the adhesive present on the top of it. The fabrication of the shape of two-dimensional (2D) cross-sections into the top layer of the sheet is performed by means a computer controlled carbon-dioxide laser or a cutter⁷. In fact, the laser not only cuts the outline of the part but also cross hatch parts out of this outline with squares in order to remove them easily after the completion of the prototype. It is noteworthy to indicate that during the building process, these squares act as scaffolds for the building part. As soon as the layer is built, the platform is let down (the depth corresponds to the sheet thickness) so that a new sheet layer is feeding by the rolling implement. Finally, the platform is lifted and the heating roller glues the new layer with the previous one. The overall process is repeated until the prototype is obtained. The principle of this method is shown in Figure I. 5.

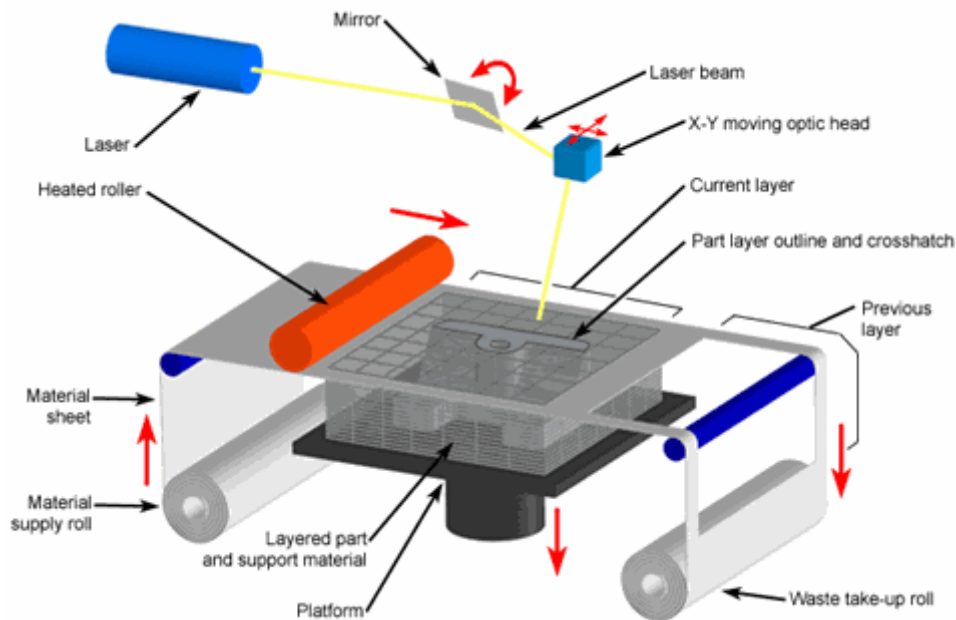


Figure I. 5: LOM principle from customPartNetⁱⁱⁱ

ⁱⁱⁱ Custompartnet , 3D Printing, 26/07/2010, <http://www.custompartnet.com/wu/laminated-object-manufacturing>

Basically, the maximum accuracy of a LOM machine is $\pm 130 \mu\text{m}$, the minimum layer thickness is about $75\text{-}200 \mu\text{m}$ and the cutting speed can reach a maximum speed of $508 \text{ mm}\cdot\text{s}^{-1}$ ¹².

This method is particularly interesting for the creation of very large objects. Moreover, the process is quite fast. The speed is 5-10 times higher than for the other technologies because only the contour has to be drawn¹². However, the removal of the support material can take time since a lot of scraps is produced during the process. The surface finish is rather poor. In addition, it is difficult to produce hollow parts with this technique¹². At last, the prototype needs to be sealed to prevent any water absorption⁷.

1.2.1.3 Molten powder particles

- **Fused deposition modelling (FDM)**

This technology was invented by S. Scott Crump and patented by Stratasys Corporation in 1992¹⁷. It consists in building the part by extruding layer by layer a semi-molten thermoplastic filament (acrylonitrile butadiene styrene (ABS), polycarbonate (PC), polyphenylenesulfone^{7,18}...) or metal wire through a heated nozzle. The nozzle plays an important role in FDM. Indeed, the nozzle motion according to the x and y directions reproduces the shape of the different cross sections created from the CAD system⁹. For the fabrication of complex prototypes with for instance overhangs, the use of a support material is required. In this case, the apparatus displays two nozzles, as it is shown in Figure I. 6. Both the support and the building materials are melted and extruded through the nozzles and deposited onto a platform to produce a layer. Then the platform moves down and the next layer is extruded and bonds with the previous one. The process continues until the entire prototype is built⁹. The overall process is illustrated in Figure I. 6. Finally, the support material is removed. There are two possibilities for removing the substrate part. The first method is to choose a material that can be easily broken away from the building part at the end of the process. The second method is to use a water soluble support material. This material is easily dissolved in warm water. To speed up the dissolution process, the water can be agitated by ultra sounds¹⁴.

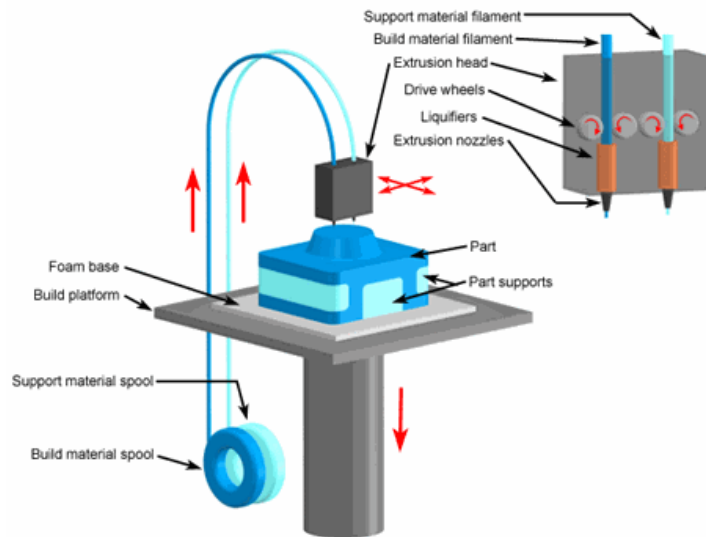


Figure I. 6 : Description of the FDM technology from customPartNet ^{iv}

The deposition speed is approximately 380 mm.s^{-1} . The layer thickness is between $50\text{-}762 \mu\text{m}$ and the accuracy is roughly $127 \mu\text{m}$ ^{9,12}.

The advantages of this technology are numerous. It is a solvent-free method ¹⁸ that leads to strong and heat resistant materials ¹⁴. These materials are suitable for functional testing and can be in some cases directly used as final product ¹⁴. Moreover, many chemicals can be used, even their color can be chosen ¹⁴. Furthermore, FDM does not consume too much heating energy and base material because the material is under the shape of a filament ¹⁸. It is an economical method. Nevertheless, the main drawbacks of FDM are the rough surface of the pieces³, the lack of accuracy of the parts ¹⁴ and the use of a support¹⁴.

^{iv} Custompartnet , 3D Printing, 26/07/2010, <http://www.custompartnet.com/wu/fused-deposition-modeling>

I.2.2 Liquid-based techniques

In this category, all the techniques are working with the same base materials: UV curable resins. The main feature of these liquid resins is their ability to polymerize upon UV irradiation to generate highly crosslinked solid coating according to a photochemical process called UV curing¹⁹⁻²¹. Before introducing the different processes, the basics of UV curing technology will be explained.

- **Principles of UV curing**

UV curing technology is employed in RP processes for several reasons¹⁰. First of all, the polymerization of UV curable resins does not require any solvent (100% of active substances) and is achieved in very short timescales (few seconds). The consumption of energy during the UV process is less important than for thermal process (50 to 100 times less energy). In addition, the process is spatially and temporally controlled. And a broad range of oligomers and monomers can be used in order to achieve the desired final properties. Basically, three compounds are mainly involved in UV curing process: the photoinitiator that generates the reactive species (free radicals, ions), the oligomer that possesses the reactive functions at the chain ends and the monomer that both plays the role of diluent in order to match the right formulation viscosity and participate to the polymerization owing to its reactive functions²². As it can be seen in Scheme I. 1, the UV curing process starts with the absorption of the UV-Visible light by the photoinitiator which leads to the formation of reactive species. These latter are subsequently capable of reacting with the monomer and induce the chain reaction polymerization. All the details about the kinetics of photopolymerization will be given in Chapter II.



Scheme I. 1 : Simplified description of the UV curing process

Photopolymerization process depends not only on the nature of the chemicals but also on the experimental conditions²³. These parameters can influence the kinetics of photopolymerization and thus the final properties. Indeed, the choice of the light source is crucial because the light source must be absorbed by the photoinitiator to create initiating species²⁴. The absorption of the light by the photoinitiator obeys to the Beer-Lambert's law.

In other words, the penetration of light exponentially decreases with the coating thickness^{25,26}. If the photoinitiator concentration is important, the penetration of the light will be limited owing to the inner filter effect. Hence, the cure depth will be low. Moreover, the characteristics of the UV curable oligomers and monomers have also to be borne in mind. Acrylates, which are the most widely used monomers are known to be really sensitive to O₂. Their polymerization can be hindered even inhibited by its presence, yielding to a tacky surface. In practice, during the RP process, this sensitivity towards O₂ means that the acrylate photopolymerization needs a minimum amount of energy to take place because the free radicals have to first react with the O₂ dissolved in the resin. This threshold value is named critical exposure, E_c. It is defined as the minimum laser energy required to reach the resin gel point^{25,26}. However, the effect of O₂ towards acrylates can also have a beneficial impact during the layer by layer building process because it limits the extent of polymerization by scavenging the radicals which could be an asset for stereolithography accuracy. Another drawback of acrylates is their tendency to shrink upon UV irradiation. During the phase change from liquid to solid state, the distance between monomer molecules is reduced which leads to an increase in density and a volume contraction named shrinkage^{23,27-29}. According to the shrinkage magnitude within the processed part, residual stresses can be generated and subsequently be responsible for curl distortion and even cracks^{27,28}. To overcome these limitations, epoxide resins can be employed. These resins do not exhibit any oxygen inhibition but they are affected by humidity. Furthermore, their living character can be a shortcoming for the fabrication of prototypes since the longer is the dark reaction, the lower is the resolution^{25,26}. Many authors have been concerned about the shortcomings of both acrylates and epoxides. They have tried to tackle these issues by playing on the processing conditions and also by using the versatility of the UV curable resins.

- **Stereolithography (SLA)**

SLA is the abbreviation for StereoLithography Apparatus. It was the first RP process that was developed. 3D systems patented this invention in 1986³⁰. It is so far the process that is the most widely used all around the world^{2,3,31}. Typically, an UV curable resin is exposed to a laser beam (Ar⁺ laser 351 and 363 nm, HeCd laser 325 nm and Nd:YVO₄ laser 355 nm) that hardens the top layer^{2,3,12}. Then, the platform carrying the model is lowered to cover the cured layer by a new uncured surface^{12,23,31,32}. The computer controls not only the exact shape of each slice but also the laser beam motion. Indeed, the laser is capable to reproduce point by point the shape of the layer defined

informatically. Given that the building process is achieved in 3D, the term pixel that represents a point in 2D data is replaced by the term voxel (VOLUME piXEL). Finally, the prototype is reconstituted by the successive layer superposition. (cf Figure I. 7).

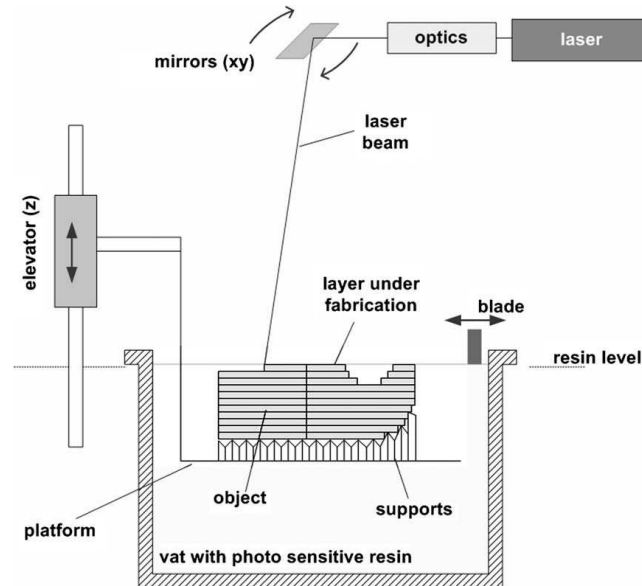


Figure I. 7 : Stereolithography principle from³²

One of the main SLA drawback is the use of supports for the fabrication of objects with overhanging features so as to prevent the building pieces from collapsing¹². In that case, the supports have to be removed at the end of the process. The piece is then submitted to a solvent treatment in order to remove the uncured parts. The obtained part is called “green” because it is not fully cured. Nevertheless, the mechanical properties of the part are good enough so it can be handled. This ability to withstand deformation is defined as green strength³³. It refers to the mechanical properties of the green part. It gathers modulus, strain, strength, hardness notions²⁶. Green strength can be assessed as a function of Young’s modulus, flexural strength and also strain³³.

In Figure I. 8, an attentive observation of the cross-section of a processed part discloses the presence of uncured, partially cured and highly cured areas (due to the overlap of irradiation)^{27,34}. They were formed during the layer by layer process²⁹.

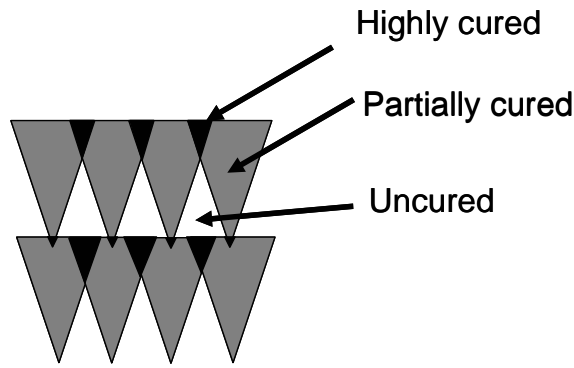


Figure I. 8 : Cross-section of a cured part

This structural inhomogeneity is explained not only by the chemical properties of the UV curable resin but also by the laser beam features^{29,34}. Indeed, the Gaussian energy profile of a laser leads to the formation of a cured line whose outline is in parabolic shape. This line is characterized by the critical exposure (E_c), the minimum energy necessary to cure the photosensitive resin, the cure depth (C_d) and the thickness (L_w), as it is shown in Figure I. 9a and b^{23,32}.

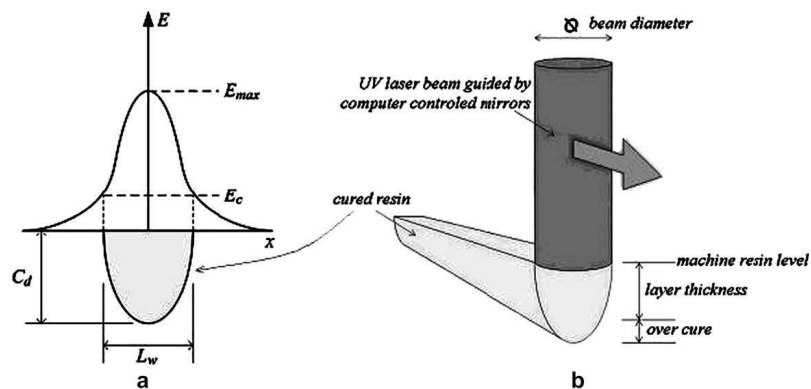


Figure I. 9 : Sketch of the Gaussian energy distribution of the laser (a) and (b) generation of a cured line upon the laser irradiation from³²

The parameters C_d and L_w play an important role in the determination of the resolution and the accuracy of a RP system³⁵.

As illustration, the distance between the new layers can be evaluated with the determination of C_d . C_d can be calculated^{10,32} using the following equation:

$$C_d = D_p \times \ln\left(\frac{E_{\max}}{E_c}\right)$$

with D_p , the resin “penetration depth” at the given wavelength. It indicates how deep the light can go in the resin. And E_{max} is the maximum exposure at the resin surface. Usually, the C_d is plotted versus the logarithm of the UV exposure (mJ/cm^2). A linear dependence is found. This straight line is commonly called “working curve”. Its slope corresponds to D_p and its intercept with the x axis refers to E_c .

Finally, the prototype is subjected to a post-curing with UV lamps in order to achieve a complete polymerization³⁶. Indeed, contrary to a laser whose irradiation penetration depth is accurate but limited, these UV lamps have the capacity to deeply penetrate and lead to the formation of completely insoluble materials. The medium pressure Hg lamps and the UV fluorescent lamps are commonly used because they possess a broad emission spectrum with a continuous background. For a common SLA machine for instance, for ViperTMSLA system, the minimum build layer capability is 20 μm but it is commonly 100 μm . The velocity during the building part is 5 $mm.s^{-1}$. As it can be seen, the real advantage of SLA is its outstanding accuracy^{2,14} leading to a good surface quality^{2,12}. Furthermore, it is possible with SLA to produce large parts (more than 2 meters) by using mammoth SLA machines^v.

Nonetheless, the SLA technology remains one of the most expensive RP technologies. Additionally, the use of support can affect the surface finish during the removal of the part^{2,12}. And at last, the material creep under this process is an issue⁹.

- **Digital light processing (DLP)**

DLP was set up by Texas Instruments in 1987^{vi}. The DLP principle is different from the previous methods. As depicted in Figure I. 10, it is an upside-down process for which the irradiation of a projector (visible light) reproduces the 2D cross-section from the CAD model onto the bottom layer of a photosensitive resin thanks to the digital micromirror device (DMD)³. Upon irradiation, the resin cures very fast. Only few seconds are necessary for its adhesion onto the platform. Subsequently, the platform goes up and a new liquid layer is cured³⁷. The procedure is repeated several times to get the prototype. It is not necessary to carry out a post-processing treatment³⁸.

^v Materialise, About Mammoth Stereolithography, 19/08/2010, <http://www.materialise.com/mammoth-stereolithography>

^{vi} Texas Instruments, How DLP Technology Works, 26/07/2010, <http://www.dlp.com/technology/how-dlp-works/default.aspx>

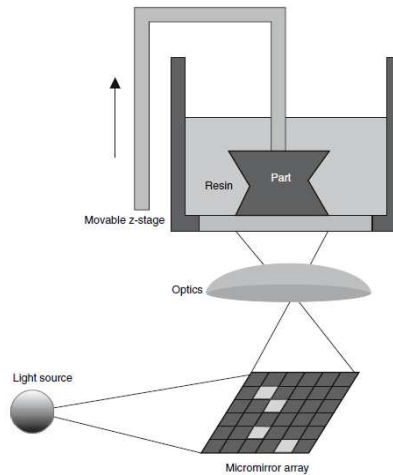


Figure I. 10: DLP principle from ³⁷

Various benefits emerge from this technology. The first one is the reduction of the working hours due to the use of a large irradiation source ³. The second one is the high resolution reached by this method (x and y resolution from 16 μm to 68 μm). In addition, the thickness over z can vary from 15 μm to 150 μm . The upside down process brings another advantage by reducing the need for support structures and by speeding up the replacement of materials. And finally, with the PerfactoryXede® and PerfactoryXtreme® machines, a building speed of $7 \cdot 10^{-3} \text{ mm} \cdot \text{s}^{-1}$ in z direction at a voxel depth of 50 μm can be reached^{vii}. Despite these advantages, DLP exhibits some drawbacks. Some of them are presented here. A high amount of liquid photopolymer is needed in order to fill the material tank. Additionally, the accuracy of this method is directly linked to the high precision of DMD so its cost could be high. Moreover, the photosensitive resins were shown to be really sensitive to the ambient light sources ³. A premature polymerization can occur. As a consequence, the pot life is low.

- **Polyjet system**

Polyjet technology was developed in early 2000 by Objet Geometries^{viii} ³⁹. It is a 3D printing process using UV curable resins. The principle of this technology is different from the traditional rapid prototyping technologies such as stereolithography ⁴⁰. In polyjet system, two different types of photosensitive resins are employed ^{3,38,40}. The first one is the building material. It is a liquid acrylate-based resin. The second one is the support

^{vii} Envisiontec, Perfactory®, Rapid Manufacturing System Rapid Prototyping system Buyers' guide, 27/07/2010, http://www.envisiontec.de/fileadmin/pdf/BuyersGuide_en.pdf

^{viii} Objet, Polyjet™ Technology-3D Printer Video, 27/07/2010, http://www.objet.com/Products/PolyJet_Technology_Movie/.

material. Its chemical properties are different from the build material. Once cured, it becomes a gel³ in order to be easily removed with a water jet after the process⁴⁰. During the process, these photosensitive resins are firstly incorporated into different nozzles so there is no need in using a large vat of liquid UV curable resin. Then, the materials are selectively sprayed in a thin layer onto a building tray according to CAD data. Immediately afterwards, the layer solidifies under a brief UV exposure (UV bulbs)⁴⁰ and a new fresh liquid layer is deposited so that the curing process starts again until the obtention of the 3D part (cf Figure I. 11).

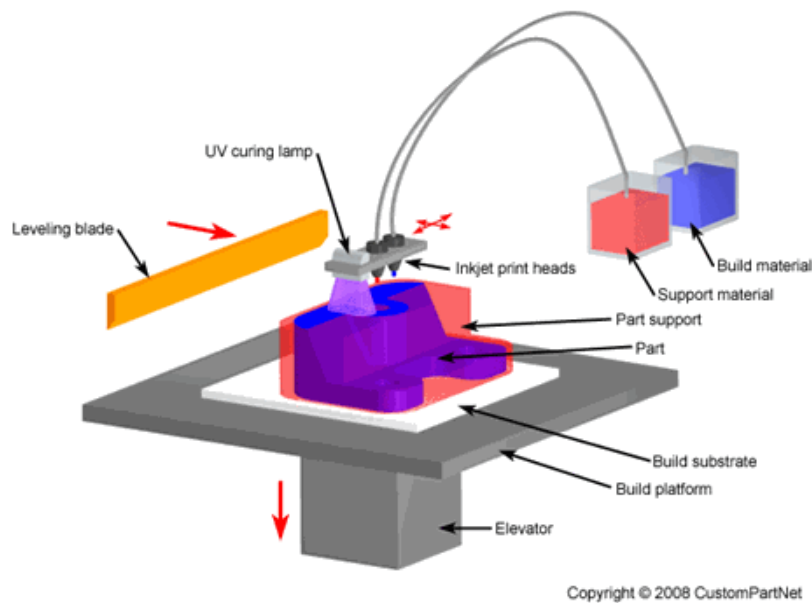


Figure I. 11 : Polyjet system principle from customPartNet^{ix}

No further post curing treatment is required because the material is fully cured at the end of the building process. With this method, the thickness layer is around 16 μm . The build speed is rather fast. The accuracy is high: about 100 μm . It is a particularly attractive technology because the material surfaces are clean and smooth. There is no need in having an important amount of UV curable liquid resin such as for stereolithography. A broad range of materials can be fabricated such as clear materials, coloured materials, hard and tough materials, flexible materials. Despite all these interesting aspects, the feature detail and material properties are lower than for stereolithography^{ix}. Additionally, the precision of finished materials is based on the quality of nozzle. To be competitive, the nozzle precision needs to be high which increases a lot the production cost³. The viscosity of the UV curable resins has also to be considered. It must not be too viscous otherwise the resins are stuck in the nozzles.

^{ix} CustomPartNet, Jetted Photopolymer, 27/07/10, <http://www.custompartnet.com/wu/jetted-photopolymer>

II HUNTSMAN COLLABORATION

Since more than 20 years, Huntsman Advanced Materials is one of the leaders in the development of materials with outstanding properties for design, prototyping and manufacturing. They notably supply a broad range of UV curable resins whose trademark is RenShape®SL for stereolithography applications. These resins were optimized in order to fabricate parts with high accuracy and detail reproduction, good green strength and good mechanical properties. Despite these advances in UV chemistry to accelerate the polymerization process and improve the quality of the part, the time to produce a 3D object increases with the size and the complexity of the object. Recently, Huntsman Advanced Materials has decided to build a manufacturing machine named Araldite® Digitalis^{41,42} using UV curable resins. This device enables to produce at the same time several parts at high speeds and with high accuracy. The key of the process lies in the use of a new exposure system, MicroLightSwitch® (MLS) based on conventional polychromatic UV lamps^x. The UV emission spectrum is shown in Figure I. 12.

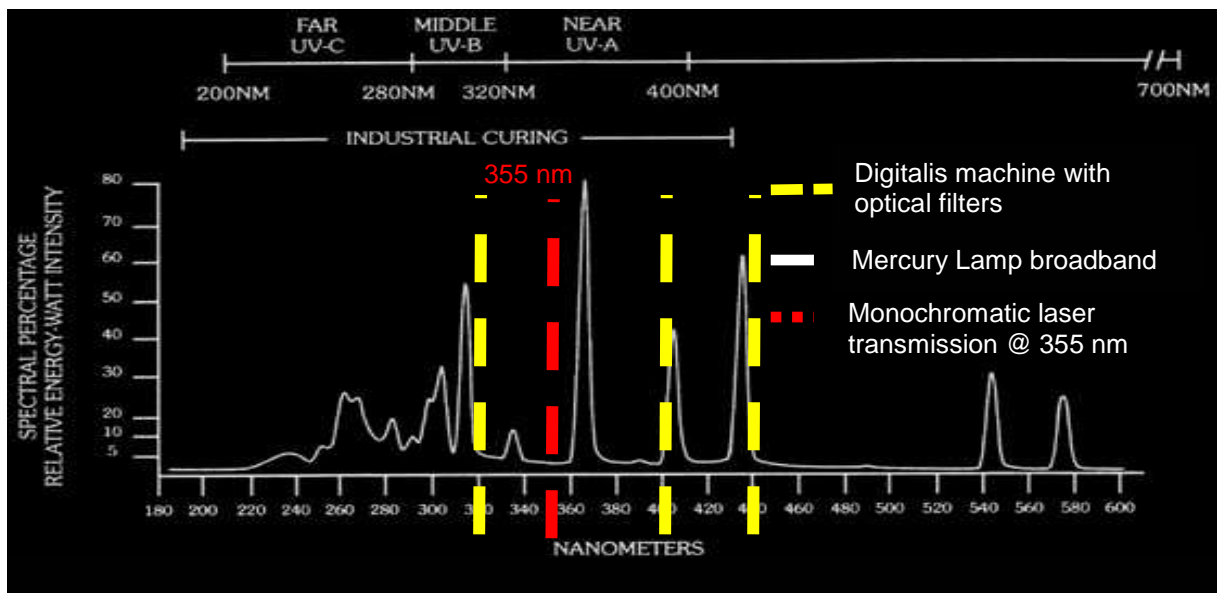


Figure I. 12: UV emission spectra of the MLS exposure system (cf Araldite® Digitalis machine), a mercury broadband lamp and a laser at 355 nm

The light is transmitted via optical fibers to microelectronic shutters present in the MLS system and is refocused onto the resin surface by a set of microlenses. The originality of this technology relies on the shutters that let micro-size spots of radiation to selectively illuminate the liquid photosensitive resin. Contrary to SLA for which the fabrication of 3D object is achieved point by point, the UV exposure for Araldite® Digitalis occurs on a large

^x Araldite® Digitalis literature & FAQ, 27/07/10, http://www.huntsman.com/advanced_materials/index.cfm?PageID=7678

area, 40,000 pixels at a time, thanks to the back-and-forth exposure head scanning in x direction. Once the first layer is cured, the building platform moves down and a fresh layer of liquid resin is subject to the above-mentioned curing process. The process continues until the complete formation of the 3D object. A rough scheme of the Digitalis principle is presented in Figure I. 13.

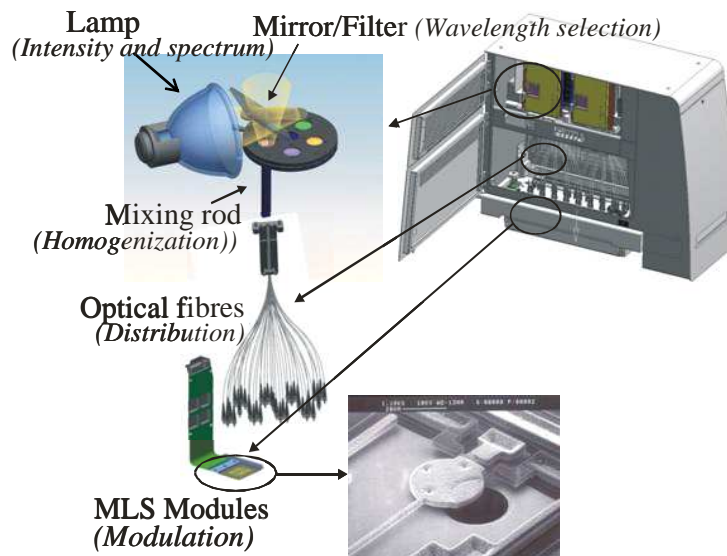


Figure I. 13 : Araldite@Digitalis technology using MicroLightSwitch® (MLS) system

This system has a resolution in $x=10, 50$ or $125 \mu\text{m}$, in $y=10 \mu\text{m}$ and in $z=50, 100, 150 \mu\text{m}$. The exposure speed varies from 3 to $50 \text{ mm}\cdot\text{s}^{-1}$. This new technology is expected to offer significant advantages in comparison with the other technologies using UV curable resins: a) it is a fast process in particular when many parts are built, b) it is also possible to produce large parts by increasing the size of MLS system c) and finally, the use of UV bulb instead of a laser is an important advantage compared to SLA in terms of costs and maintenance. This invention is an important breakthrough in the product manufacturing. Since most of the commercially UV curable resins for RP are formulated and optimized in order to be used in SLA process at an actinic wavelength of 355 nm , the topical issue will be to know if the efficiency of the aforementioned resins will be comparable with Araldite@Digitalis using conventional UV lamps with actinic wavelengths in the UVA area (main emission band at 366 nm cf Figure I. 12). To get a good insight of the full potential of this new technology, it is essential to get a good control of both the processing conditions and the UV curable resin properties. The challenge of this project is to develop and characterize near UV fast responsive resins that can be used with Araldite@Digitalis. Ideally, these resins should fulfil these special specifications: fast curing, high resolution,

Dp~70 μm , flexural green strength~40 MPa, high Tg, high tensile modulus (1400-1500 MPa) and low shrinkage. The investigation presented in the following chapters will not only concern common acrylic, epoxides and IPN UV curable resins used in stereolithography but will also be turned to new routes using unconventional chemistry for RP.

III REFERENCES

1. Dubois, P.; Aoussat, A.; Duchamp, R. *Techniques de l'ingénieur, traité Génie mécanique* **2000**, BM7017, 1-10.
2. Yan, Y.; Li, S.; Zhang, R.; Lin, F.; Wu, R.; Lu, Q.; Xiong, Z.; Wang, X. *Tsinghua Science and Technology* **2009**, *14*, 1-12.
3. Lee, S. Y.; Wang, M. R.; Chen, C. Y.; Chen, C. L.; Hwang, S. J.; Chen, H.; Lai, W. H.; Shyng, L. T.; Wang, C. C. *Journal of Physics: Conferences Series, International Symposium on Instrumentation Science and Technology* **2006**, *48*, 776-779.
4. King, D.; Tansey, T. *Journal of Materials Processing Technology* **2003**, *132*, 42-48.
5. Stampfl, J.; Liska, R. *Macromolecular Chemistry and Physics* **2005**, *206*, 1253-1256.
6. Kochan, D.; Kai, C. C.; Zhaohui, D. *Computers in Industry* **1999**, *39*, 3-10.
7. Wendel, B.; Rietzel, D.; Kuehnlein, F.; Feulner, R.; Huelder, G.; Schmachtenberg, E. *Macromolecular Materials and Engineering* **2008**, *293*, 799-809.
8. Jacob, G. G. K.; Kai, C. C.; Mei, T. *Computers in Industry* **1999**, *39*, 61-70.
9. Chua, C. K.; Chou, S. M.; Wong, T. S. *International Journal of Advanced Manufacturing Technology* **1998**, *14*, 146-152.
10. Jacobs, P. F., CAD processes. In *Rapid Prototyping & Manufacturing, Fundamentals of Stereolithography*, The Society of Manufacturing Engineers: 1992; p 158.
11. Deckard, C. R. U.S. Patent 5017753, 1991.
12. Pham, D. T.; Gault, R. S. *International Journal of Machine Tools and Manufacture* **1998**, *38*, 1257-1287.
13. Freitag, D.; Wohlers, T.; Philippi, T. *Rapid Prototyping: State of the Art Review*; Manufacturing Technology Information Analysis Center: 2003; pp 1-40.
14. Gibson, I., Rapid Prototyping for Medical Applications. In *Advanced Manufacturing Technology for Medical application, Reverse Engineering, Software Conversion and Rapid Prototyping*, Gibson, I., Ed. John Wiley and Sons: 2005.
15. Sachs, E. M.; Haggerty, J. S.; Cima, M. J.; Williams, P. A. US 5204055, 1993.
16. Feygin, M. U.S. Patent 4752352, 1988.
17. Crump, S. S. U.S. Patent 5121329, 1992.
18. Zein, I.; Hutmacher Dietmar, W.; Tan Kim, C.; Teoh Swee, H. *Biomaterials* **2002**, *23*, 1169-1185.
19. Decker, C. *Progress in Polymer Science* **1996**, *21*, 593-650.
20. Decker, C. *Techniques de l'ingénieur* **2000**, Doc AM 3044
21. Fouassier, J.-P. *Hanser Publishers, Munich Vienna N.Y* **1995**.
22. Fuh, J. Y. H.; Choo, Y. S.; Nee, A. Y. C.; Lu, L.; Lee, K. C. *Materials & Design* **1995**, *16*, 23-32.
23. Cheah, C. M.; Nee, A. Y. C.; Fuh, J. Y. H.; Lu, L.; Choo, Y. S.; Miyazawa, T. *Journal of Materials Processing Technology* **1997**, *67*, 41-45.
24. Mehnert, R.; Pincus, A.; Janorsky, I.; Stowe, R.; Berejka, A., UV curing equipment-polychromatic UV lamps. In *volume I UV&EB Curing Technology &*

- Equipment*, John Wiley & Sons Ltd in association with SITA Technology Ltd: London, 1998; p 43.
25. Jacobs, P. F., Basic Polymer Chemistry. In *Rapid Prototyping and Manufacturing, Fundamentals of Stereolithography*, The Society of Manufacturing Engineers: 1992; pp 26-58.
 26. Bernhard, P.; Hofmann, M.; Hunziker, M.; Klingert, B.; Klingert, B.; Schulthess, A.; Steinmann, B., Three-Dimensional Laser Polymerisation. In *Radiation Curing In Polymer Science and Technology Practical Aspects and Applications*, Fouassier, J. P.; Rabek, J. F., Eds. Elsevier Applied Science: London and New York, 1993; Vol. IV.
 27. Fuh, J. Y. H.; Choo, Y. S.; Lu, L.; Nee, A. Y. C.; Wong, Y. S.; Wang, W. L.; Miyazawa, T.; Ho, S. H. *Journal of Materials Processing Technology* **1997**, *63*.
 28. Karalekas, D.; Aggelopoulos, A. *Journal of Materials Processing Technology* **2003**, *136*, 146-150.
 29. Cheah, C. M.; Fuh, J. Y. H.; Nee, A. Y. C.; Lu, L.; Choo, Y. S.; Miyazawa, T. *Journal of Materials Processing Technology* **1997**, *67*, 46-49.
 30. Hull, C. W. US 4575330, 1986.
 31. Yan, X.; Gu, P. *Computer-Aided Design* **1996**, *28*, 307-318.
 32. Salmoria, G. V.; Ahrens, C. H.; Beal, V. E.; Pires, A. T. N.; Soldi, V. *Materials & Design* **2009**, *30*, 758-763.
 33. Jacobs, P. F., Basic Polymer Chemistry. In *Rapid Prototyping and Manufacturing, Fundamentals of Stereolithography*, The Society of Manufacturing Engineers: 1992; p 36.
 34. Fuh, J. Y. H.; Lu, L.; Tan, C. C.; Shen, Z. X.; Chew, S. *Journal of Materials Processing Technology* **1999**, *89-90*, 211-217.
 35. Xu, G.; Zhao, W.; Tang, Y.; Lu, B. *International Journal of Advanced Manufacturing Technology* **2007**, *31*, 941-947.
 36. Fouassier, J.-P.; Rabek, J. F., *Radiation Curing in Polymer Science and Technologie, Practical Aspects and Applications*. Elsevier, Applied Science: 1993; Vol. IV.
 37. Liska, R.; Schuster, M.; Infuehr, R.; Turecek, C.; Fritscher, C.; Seidl, B.; Schmidt, V.; Kuna, L.; Haase, A.; Varga, F.; Lichtenegger, H.; Stampfl, J. *Journal of Coatings Technology and Research* **2007**, *4*, 505-510.
 38. Egodawatta, A. K.; Harrison, D. K.; De Silva, A.; Haritos, G. *Journal of Materials Processing Technology* **2004**, *149*, 604-608.
 39. Kritchman, E.; Gothait, H.; Napadensky, E.; Chechik, D. US2006/0054039 A1, 2006.
 40. Napadenky, E. *RadTech Europe 2005 Conference & Exhibition* **2005**.
 41. Henningsen, H. US2008/0315461 A1, 2008.
 42. Claasen, A. J.; Fienieg, R. US D600,726S, 2009.

Chapter II: UV cured Interpenetrating Polymer Networks (IPNs)

I	INTRODUCTION.....	32
II	GENERAL ASPECTS OF PHOTOPOLYMERIZATION PROCESSES	33
II.1	Introduction	33
II.2	Radical photopolymerization	33
II.2.1	Radical photoinitiators	33
II.2.1.1	α -cleavable photoinitiators (type I).....	34
II.2.1.2	Type II photoinitiators.....	35
II.2.1.3	Photosensitization process.....	36
II.2.2	Kinetics of radical photopolymerization	36
II.2.2.1	Initiation	36
II.2.2.2	Propagation.....	37
II.2.2.3	Termination	37
II.2.3	Monomers: acrylic and methacrylic resins	39
II.2.4	Special features of the radical photopolymerization	40
II.2.4.1	Side reactions	40
II.3	Cationic photopolymerization	42
II.3.1	Cationic photoinitiators	42
II.3.1.1	Diaryliodonium salts and triarylsulfonium salts	42
II.3.2	Kinetics of cationic photopolymerization	48
II.3.2.1	Initiation	48
II.3.2.2	Propagation.....	48
II.3.2.3	Termination	48
II.3.3	Cationic monomers and oligomers.....	49
II.3.3.1	Epoxide monomers.....	49
II.3.3.2	Vinyl ether monomers.....	50
II.3.4	Special features of the cationic photopolymerization	50
II.3.4.1	Deactivation processes	50
II.3.4.2	Inhibition	50
II.3.4.3	Side reactions	51
II.3.4.4	Living character.....	52
II.3.4.5	Temperature	52
II.4	Conclusion.....	52
III	IPN PHOTOPOLYMERIZATION.....	53
III.1	Different ways of UV cured IPN synthesis.....	53
III.1.1	Simultaneous UV IPNs	53
III.1.2	Sequential IPNs	53
III.2	Photopolymerization process of IPNs	55
III.2.1	Kinetics aspects of photoIPNs.....	55
III.2.2	Characterization of the photocured IPNs	57
III.2.2.1	IPN morphology	57
III.2.2.2	IPN thermomechanical properties.....	59
III.2.2.3	Transparency	60

IV	EXPERIMENTAL STUDY	61
IV.1	Understanding of the IPN formation between a diglycidyl ether epoxide and an acrylate under Huntsman industrial specifications	61
IV.1.1	Context of the study.....	61
IV.1.2	Characterization of the commercial resin Renshape®SL 7870.....	62
IV.1.2.1	Griffin and SLA 7000 trials.....	62
IV.1.2.2	UV spectroscopy measurements.....	65
IV.1.2.3	Kinetics of photopolymerization at 366 nm	66
IV.1.3	Optimization of the IPN kinetics: Enhancement of the cationic photopolymerization by sensitization processes.....	68
IV.1.3.1	Compounds used as sensitizers.....	68
IV.1.3.2	Effect of free radicals from radical photoinitiator photolysis.....	70
IV.1.3.3	Evaluation of the chemical balance between the radical polymerization and the electron transfer reaction.....	76
IV.1.3.4	Effect of the photosensitizers	81
IV.1.3.5	Tests with Griffin	84
IV.1.4	Use of triphenylphosphine for the improvement of the IPN kinetics.....	86
IV.1.4.1	Trials with Griffin.....	87
IV.1.4.2	RT FTIR spectroscopy	88
IV.1.5	Influence of temperature on the photopolymerization process	90
IV.1.5.1	RT FTIR spectroscopy	90
IV.1.5.2	PhotoDSC experiments	95
IV.1.6	Characterization of the final properties	99
IV.1.6.1	Thermomechanical properties	99
IV.1.6.2	IPN morphology	101
IV.2	Academic study on the formation of quasi-simultaneous IPNs between a cycloaliphatic epoxide and a methacrylate.....	103
IV.2.1	Compounds.....	104
IV.2.2	Kinetics study under broadband irradiation.....	105
IV.2.2.1	Photopolymerization of the starting monomers	105
IV.2.2.2	Photopolymerization of the hybrid mixture	107
IV.2.3	Kinetics study at 366 nm exposure.....	109
IV.2.3.1	Photopolymerization of the starting monomers	109
IV.2.3.2	Photopolymerization of the hybrid mixture	110
IV.2.4	Final properties	112
IV.2.4.1	Thermomechanical analysis of the UV cured analysis.....	112
IV.2.4.2	Morphology of the UV cured IPNs	115
IV.2.4.3	Rheological properties of the UV cured analysis	116
V	CONCLUSIONS AND PERSPECTIVES	119
VI	REFERENCES	121

I INTRODUCTION

Interpenetrating Polymer Networks (IPNs) are defined as a special polymer blend in which two or more crosslinked polymers are entangled¹⁻⁵. It implies that one of these polymers crosslinked in the close vicinity of the others. This feature confers on the IPNs some interesting properties as they combine the properties of the different networks⁶. The first IPNs were synthesized in 1914 by Jonas Aylsworth and Thomas Edison⁷. It was a mixture of natural rubber and sulphur with crosslinked phenol-formaldehyde resin so as to get a tougher material^{8,9}. But the term IPN was first employed by Millar¹⁰ in 1960 for the preparation of homo IPNs polystyrene/polystyrene^{2,3,8,11}. Millar wanted to increase the size of the particles for ion exchange resin applications. Afterwards, IPNs with various polymer combinations were synthesized by thermal radical or cationic polymerization and/or polycondensation¹².

However, the aforementioned IPNs frequently display unhomogeneous morphology with more or less phase separation. The latter one mainly depends on the compatibility between the polymers and the curing time and causes damage to the mechanical properties.

Homogeneous IPNs can be straightforwardly synthesized by means of UV curing technology^{13,14}. Indeed, high polymerization rates can be easily reached at room temperature under high light intensities which limits the phase separation and improves the final properties¹². In addition, this method provides the advantage to be solvent free and thus respects the environment^{12,15}. Basically, the UV curable mixture comprises photosensitive multifunctional monomers that polymerize according to different mechanisms^{12,16,17} and independently from each other. Thus, outstanding features can be reached. Their properties are so attractive that UV cured IPNs are more and more employed in various industrial fields such as adhesive industry, stereolithography, holography, dentistry....

This chapter will be divided into two parts. The first part will deal with the general aspects of both the radical and cationic photopolymerization as well as the state of the art of the IPNs photopolymerization. The second part corresponds to the experimental survey. It will be firstly dedicated to the improvement of the performances of an existing commercial hybrid system for given specifications. Finally, we will focus our attention on the comprehension and the control of the simultaneous IPNs formation thanks to a model formulation. Different parameters will be studied such as radical photoinitiator concentration and the light intensity.

II GENERAL ASPECTS OF PHOTOPOLYMERIZATION PROCESSES

II.1 Introduction

Photopolymerization is a chain process in which monomers combine together to form a polymer upon light irradiation. Usually, the monomers do not produce sufficient reactive species owing to their weak absorption above 300 nm and their poor cleavage efficiency. Hence, an additional substance capable of absorbing UV-visible light and inducing the polymerization is needed: the photoinitiator or a photoinitiating system.

Basically, a photosensitive formulation is constituted by mainly three compounds¹⁸⁻²³:

- **A photoinitiating system** which is based either on a photoinitiator or on a mixture of a photoinitiator with a photosensitizer or a photoinitiator with a coinitiator or the combination of the three compounds. It creates under UV radiation free radicals or cations reacting with the oligomer and/or the monomer.
- **A multifunctional oligomer** whose polymerization gives rise to a crosslinked polymer network. Its structure governs the material final properties.
- **A mono or multifunctional monomer which** both copolymerize with the oligomer and acts as a solvent. Its presence allows to reduce or to adjust the formulation viscosity.

In order to improve the final properties of the photopolymer, various additives such as surface active additives, light stabilizers, fillers, dyes...can be added.

Generally speaking, UV curable resins can be classified into two categories according to their polymerization mechanism either radically or cationically. These mechanisms will be discussed in more detail thereafter.

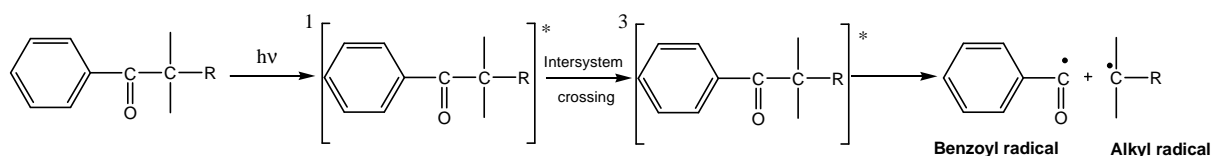
II.2 Radical photopolymerization

II.2.1 Radical photoinitiators

Two types of photoinitiators are commonly used in radical photopolymerization: the α -cleavable type I and the non cleavable type II photoinitiators. Their reactivity in conjunction with the photosensitization mechanism will be described in the following pages.

II.2.1.1 α -cleavable photoinitiators (type I) ^{21,23}

The radical photoinitiators are generally aromatic ketones. At the triplet state, they undergo a Norrish I cleavage process in α of the carbonyl group. The two generated radicals, benzoyl (or a substituted benzoyl) and alkyl, can initiate the reaction. The overall mechanism is pictured in Scheme II. 1.



Scheme II. 1: Mechanism of the α -cleavable photoinitiator photolysis

Commonly, the photoinitiators that belong to this family are benzyl ketal, benzoin ethers, hydroxy alkyl phenyl ketones, dialkoxy acetophenones, acyl phosphine oxides and amino ketones. Their structures are gathered in Figure II. 1.

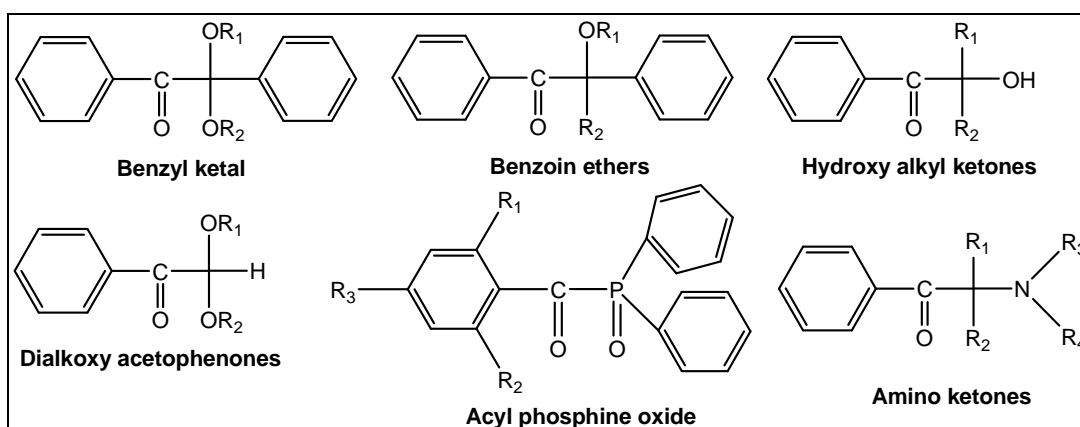
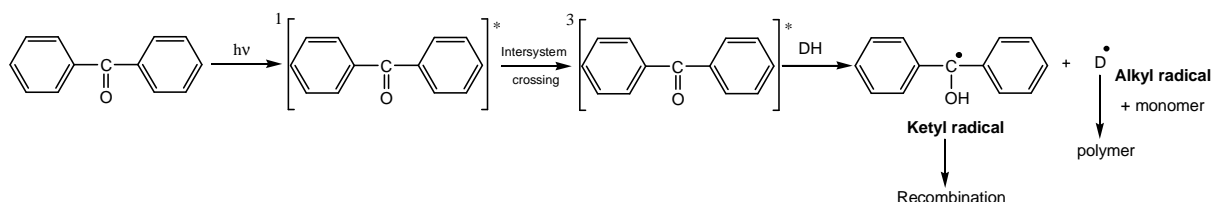


Figure II. 1: Structures of some α -cleavable photoinitiators

Oxime esters are also α -cleavable photoinitiators but they are less used due to the low thermal stability of the simple derivatives. Since some strides have been made in tailoring their structures, the new derivatives display better properties ²⁴.

II.2.1.2 Type II photoinitiators➤ H-abstraction process ^{21,22}

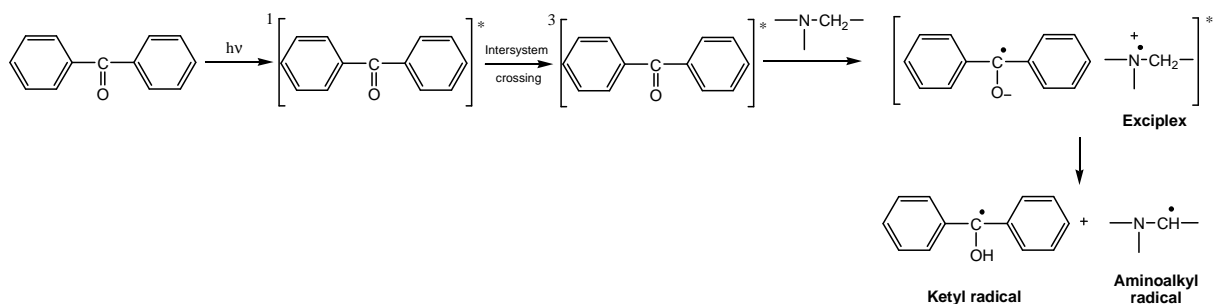
Some diarylketones such as benzophenone and thioxanthone, do not cleave in the excited state but are able to abstract an hydrogen from a H donor (DH) such as alcohols, ethers, thiols. A ketyl radical and an alkyl radical are then formed. The latter one induces the polymerization whereas the ketyl radical is a terminating radical.



Scheme II. 2: Formation of the free radicals by H abstraction process (DH: H donor)

➤ Electron transfer followed by a proton transfer ^{21,22}

These photoinitiators can also be associated to tertiary amines to produce the initiating species. Under irradiation, the amine and the triplet excited photoinitiator form an exciplex in which an electron of the nitrogen lone pair is transferred to the oxygen of the carbonyl group. The electron transfer reaction is then followed by a proton transfer with the formation of two radicals. The polymerization is induced by the generated α -amino alkyl radicals.

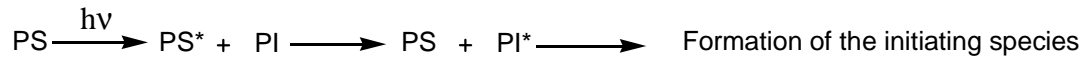


Scheme II. 3: Formation of the free radicals by electron and proton transfer reactions

The products formed are similar to the ones obtained with an H-abstraction process but the reaction rate is much faster.

II.2.1.3 Photosensitization process ²¹

In some cases, the photoinitiators can not absorb directly the UV light either because their UV absorption spectrum does not overlap the emission spectrum of the light source or their absorption is hampered by the presence of pigments. In order to extend their spectral sensitivity, a photosensitizer (PS) can be used. Its role consists in transferring its energy at the excited state to the photoinitiator. The process is shown in Scheme II. 4.



Scheme II. 4: Energy transfer reaction between a photosensitizer (PS) and a photoinitiator (PI)

To be efficient, the photosensitizer has to fulfil some requirements:

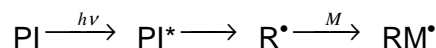
- ✓ The energy level of its excited state is superior to the excited photoinitiator one.
- ✓ Its UV absorption spectrum is not overlapped by the filler or pigment UV absorption spectrum.
- ✓ The photosensitizer is chemically and photochemically inert.

II.2.2 Kinetics of radical photopolymerization ^{25,26}

The kinetics of radical photopolymerization take place in three steps: i) the **initiation** corresponding to the creation of the reactive species, followed by ii) the **propagation** with the growing of the polymer chains and finally iii) the **termination** pointing out the end of the active chain ends.

II.2.2.1 Initiation

This is the only step induced by light. By a photochemical process, the photoinitiator (PI) at the excited state reacts to produce free radicals (R•) that will add on the monomer (M) to initiate the polymerization.



Initiation rate can be defined by:

$$\boxed{R_i = \phi_i * I_{abs}} \quad (\text{II.1})$$

with

ϕ_a , the initiation quantum yield, mol.Einstein⁻¹

I_{abs} , the absorbed photon flux, Einstein.L⁻¹.s⁻¹

In the case of a monochromatic light source, I_{abs} is expressed by:

$$I_{abs} = I_0 * (1 - 10^{-A_\lambda}) \quad (II.2)$$

with

I_0 , the incident light intensity, Einstein.L⁻¹.s⁻¹

A_λ , the absorbance of the sample at the wavelength λ

By virtue of the Beer's law, the expression of the absorbance is:

$$A_\lambda = \epsilon_\lambda * l * C \quad (II.3)$$

ϵ_λ , the molar absorption coefficient of the photoinitiator at λ , L.mol⁻¹.cm⁻¹

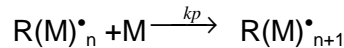
l , irradiated sample thickness, cm

C , photoinitiator concentration, mol L⁻¹

For a polychromatic light source, the I_{abs} calculation must take into account the light source emission spectrum.

II.2.2.2 Propagation

During the propagation, the polymer chains are growing up. The addition of a monomer to a macroradical yields to a larger one.



The polymerization rate is defined as follows:

$$R_p = k_p [R(M)_n^\bullet] [M] \quad (II.4)$$

With

k_p , propagation rate constant, L.mol⁻¹.s⁻¹

$[R(M)_n^\bullet]$ radical species concentration, mol.L⁻¹

$[M]$, monomer concentration, mol.L⁻¹

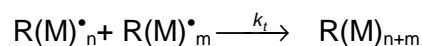
II.2.2.3 Termination

At this stage, the propagating polymer chains stop growing. Various termination modes can occur depending on the viscosity of the medium.

1) *At low viscosity, bimolecular reactions can take place.*

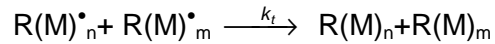
a) Recombination

Two propagating radicals react with each other to form a polymer.



b) Disproportionation

A β -hydrogen from one radical is transferred to another radical. Thereby, one polymer with a saturated end and a polymer with an unsaturated end are produced.



In the case of a bimolecular termination, if we assume that the concentration in radical species is constant during the reaction according to the stationary state approximation then the initiation rate is equal to the termination rate.

The polymerization rate can finally be expressed by this formula:

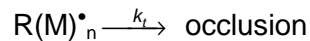
$$R_p = \frac{k_p}{\sqrt{k_t}} [M] \sqrt{\phi I_{abs}} \quad (II.5)$$

With

k_t , the bimolecular termination rate constant, $L \cdot mol^{-1} \cdot s^{-1}$

2) *At high viscosity, monomolecular reaction occurs.*

If the medium becomes too viscous, the monomers can hardly diffuse within the medium in order to react with the reactive species. The polymerization stops because the compounds are trapped.



Herein, if we apply the stationary state approximation, the polymerization rate formula can be written:

$$R_p = \frac{k_p}{k_t} [M] \phi I_{abs} \quad (II.6)$$

II.2.3 Monomers: acrylic and methacrylic resins ²¹

Monomers that undergo photoinduced free-radical photopolymerizations are commonly unsaturated monomers comprising a reactive carbon-carbon double bond. Thiol-ene, unsaturated polyester and methacrylate/ acrylate systems are the most used resins. But in our case, we will only consider the methacrylate and acrylate systems because quite a few investigations on UV cured IPNs employ these latter.

Acrylic monomers are the most widely used in UV curing because of their high reactivity, their low volatility, their availability and their moderate costs. Typically, the liquid resin is converted into a solid in few seconds. Moreover, a large range of telechelic monomers with different structures such as epoxy, polyether, polyester, urethane and silicone are commercially available which allows to tailor the material final properties (cf Figure II. 2)

23,26

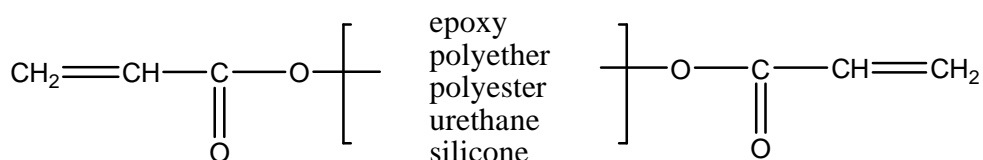


Figure II. 2: Structure of the common acrylate terminated oligomers

For instance, epoxy-acrylated resins give rise to UV cured materials displaying good adhesion, good mechanical properties, high curing rate in air, high chemical and weathering resistance. By contrast, the polyester acrylates have a poor hydrolysis resistance because of the presence of the ester group. Generally, flexible materials are obtained with aliphatic monomers while hard and glassy polymers are obtained with aromatic acrylates. Since some oligomers are highly viscous, monofunctional and difunctional monomers such as isobornyl acrylate (IBOA) and 1,6-hexanediol diacrylate (HDDA) are added in order to reduce the viscosity. The monomer functionality plays an important role in acrylate polymerization as it influences not only the curing speed but also the crosslinking density. The increase in the monomer functionality yields to an increase in the polymerization rate, the crosslinking density, better mechanical strength and solvent resistance but at the expense of the degree of cure, the flexibility and the adhesion properties. Acrylates exhibit outstanding properties nevertheless they have some drawbacks. They are irritant, toxic and their polymerization causes important shrinkage. As regards to methacrylates, they display similar features to the acrylates except that the polymerization reaction is slower owing to a less important propagation rate constant.

II.2.4 Special features of the radical photopolymerization

II.2.4.1 Side reactions^{21,25}

When the radical photoinitiator (PI) is at the excited states, various deactivation processes can take place and diminish the initiation quantum yield. There are two types of processes:

➤ Radiation processes

Fluorescence: ${}^1\text{PI}^* \longrightarrow \text{PI} + h\nu'$

Phosphorescence: ${}^3\text{PI}^* \longrightarrow \text{PI} + h\nu''$

➤ Radiationless processes

Internal conversion (IC): ${}^1\text{PI}^* \longrightarrow \text{PI} + \text{heat}$

${}^3\text{PI}^* \longrightarrow \text{PI} + \text{heat}$

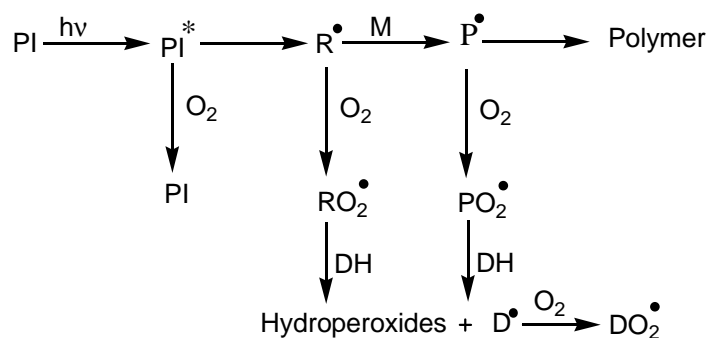
Monomer quenching (M): $\text{PI}^* + \text{M} \longrightarrow \text{PI} + \text{M}^*$

Oxygen quenching (O_2): $\text{PI}^* + {}^3\text{O}_2 \longrightarrow \text{PI} + {}^1\text{O}_2$

The detrimental action of oxygen towards the radical polymerization takes place during the different steps of the polymerization. Consequently, we have decided to point out this phenomenon.

➤ Sensitivity towards oxygen^{20,23,27}

O_2 is known to inhibit radical polymerization because of its high reactivity towards excited states and radical species like initiating radicals. Indeed, O_2 adds on radicals to generate peroxy radicals that are not efficient to initiate the polymerization but they can abstract an H from a H donor (DH) to form an hydroperoxide. Therefore, O_2 leads to a decrease in both the polymerization rate and degree of cure and tacky surfaces can be obtained. The oxygen scavenging mechanism is depicted in Scheme II. 5.



Scheme II. 5: Influence of the oxygen on the radical photopolymerization process²⁰

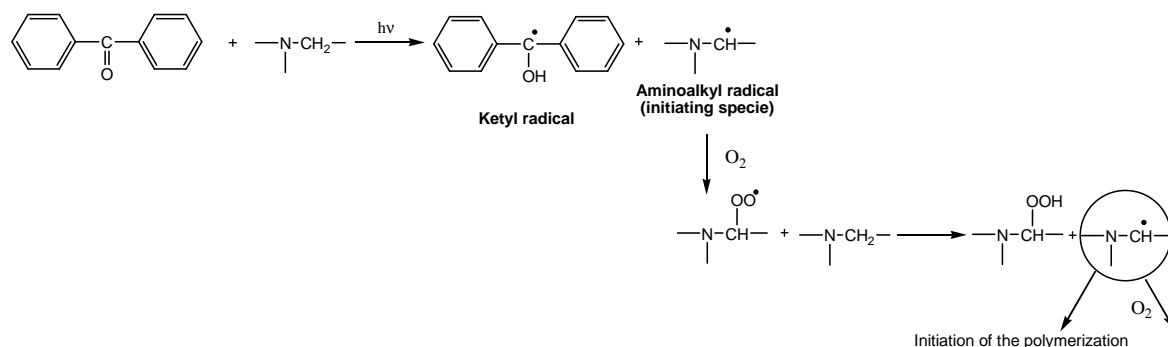
To limit the oxygen detrimental effect, different physical and chemical methods have been proposed:

➤ Physical routes

- 1) The use of high light intensities allows to generate sufficient initiating species able to counterbalance the oxygen inhibition.
- 2) Work under inert atmosphere or under laminated conditions prevents the atmospheric oxygen from diffusing
- 3) The increase in sample thickness also limits the diffusion of the atmospheric oxygen through the sample.

➤ Chemical routes

- 1) The increase in photoinitiator concentration contributes to tackle the oxygen effect by generating a significant amount of initiating species.
- 2) The increase in formulation viscosity slows down the diffusion of oxygen into the film.
- 3) The addition of molecules such as amines or thiols²⁸ that provide labile H atoms. Their reaction with oxygen during the peroxidation mechanism leads to the formation of initiating species. Scheme II. 6 reports the scavenging action of a tertiary amine used as a coinitiator on oxygen²¹. An alternative of this method is to incorporate easily abstractable H within the monomer backbone such as N-vinylamides, acrylates with thioether groups.



Scheme II. 6: Mechanism of the oxygen consumption by a tertiary amine

- 4) The last method consists in using photoinitiating system that consumes the dissolved oxygen before the polymerization process. This photoinitiating system comprises a singlet oxygen generator coupled with a singlet oxygen scavenger.

II.3 Cationic photopolymerization

One of the limiting factors in the development of the cationic UV curing was the lack of stable cationic photoinitiators. Indeed, in the early 70, Schlessinger *et al*²⁹ had demonstrated the great potential of aryldiazonium salts to induce the cationic ring opening polymerization of epoxides. However, these compounds were not thermally stable and the gaseous nitrogen evolved during aryldiazonium salts photolysis had detrimental impacts on the mechanical properties of the final material. The commercialization of suitable cationic photoinitiators merged from the important work of Crivello *et al*^{30,31 32} on the synthesis of certain onium salts diaryliodonium and triarylsulfonium salts. These crystalline compounds exhibit a high photosensitivity and thermal stability. They act as efficient photoinitiator for the commonly used monomers in cationic photoinitiators.

II.3.1 Cationic photoinitiators

II.3.1.1 Diaryliodonium salts and triarylsulfonium salts

Diaryliodonium and triarylsulfonium salts are the most widely used onium salts. The structure of these salts consists of a cationic moiety for which a positively charged atom is bonded to several alkyl or aromatic groups and an anion such as BF_4^- , PF_6^- , AsF_6^- ... Figure II. 3 gives an example of an iodonium and sulfonium salt^{21,33,34}.

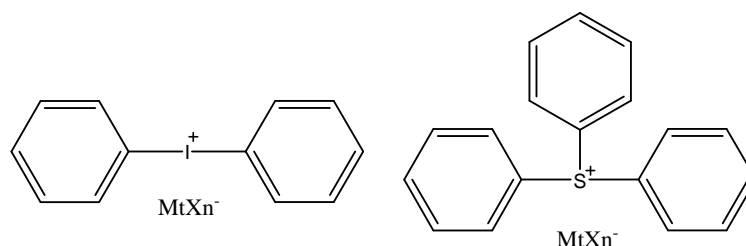
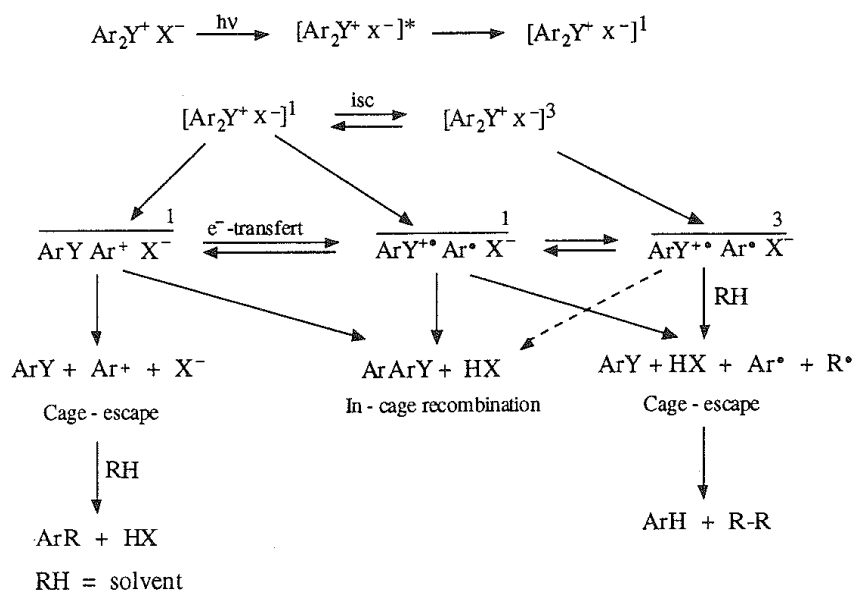


Figure II. 3: Chemical structure of a diaryliodonium and a triarylsulfonium salt with MtX_n^- , the counter ion

➤ Direct photolysis mechanism

Upon UV irradiation, these photoinitiators undergo a complex photolysis involving both the excited singlet and triplet states and in cage and cage-escape reactivity, as it is described in Scheme II. 7^{35,36}. At the excited state, the C-onium atom bond cleaves both homolytically and heterolytically. The interactions between the photolysis products and an H donor (typically monomer, solvent, impurities) result in the formation of Brönsted acid initiating species.



Scheme II. 7: General trends of the photolysis mechanism for an onium salt ($\text{Ar}_2\text{Y}^+\text{X}^-$), $\text{Y}=\text{I}, \text{S} \dots$ ²¹

It is noteworthy to say that the photolysis mechanism for the triarylsulfonium salts slightly differs from Scheme II. 7. It was demonstrated that the heterolytic cleavage route was predominant in comparison with the homolytic cleavage route^{21,37}.

➤ Features of the onium salts

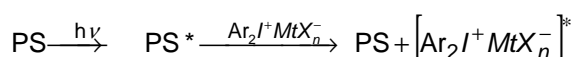
Their UV absorption capacity deeply depends on the structure of the cation moiety. Indeed, the cation whose structure governs the UV absorption characteristics, the quantum yield of photolysis, the photosensitization and the thermal stability of the corresponding onium salts. It was found that the introduction of chromophores in the aromatic rings enables to broaden the intensity and the wavelength absorption of the iodonium salts ³¹.

The anion moiety rather influences the initiation efficiency and the propagation rate constant. The nature of the counter ion is of prime importance in the polymerization process because it may react with reactive cationic species and thus slow down or even inhibit the reaction of polymerization ³¹. Consequently, a non-nucleophilic anion with an important delocalisation volume of its electronic charge should be employed so that the monomer can easily penetrate into the ion pair and then prevents any quenching of the polymerization. Hence, the classification of the suitable anions by growing order of reactivity has been established as follows: $\text{BF}_4^- < \text{PF}_6^- < \text{AsF}_6^- < \text{SbF}_6^-$ ³⁸.

These photoinitiators are very efficient since they exhibit an high quantum yield photolysis of about 0.5 to 0.7 ³⁸. Nevertheless, these compounds do not significantly absorb the light above 300 nm (their main UV absorption is located between 220 and 250 nm) which limits their uses when long wavelength sources are employed ³⁸. One way to broaden the UV absorption spectrum of onium salts is to incorporate chromophores onto their aromatic rings. However, the synthesis process is time-consuming and the achievement is uncertain ³⁹. Therefore, several indirect acting initiating systems have been described to overcome this problem. The main mechanism will be described hereafter.

➤ Sensitization process by energy transfer ²¹

As for radical photoinitiators, a photosensitizer (PS) that readily absorbs the light, transfers its energy to the onium salts. The process mainly occurs in the triplet state provided that the energy of the excited state PS* is higher than the excited onium salts one. Scheme II. 8 is an example of energy transfer reaction with an iodonium salt.



Scheme II. 8: Energy transfer mechanism between a photosensitizer (PS) and an iodonium salt

➤ Sensitization process by electron transfer ^{39,40}

These two approaches involve an electron transfer reaction between the onium salt and either a photoexcited sensitizer or free radicals. The efficiency of the electron transfer is strongly linked to the redox potentials of both entities. The higher is the reduction potential of the onium salt, the most efficient is the sensitization reaction.

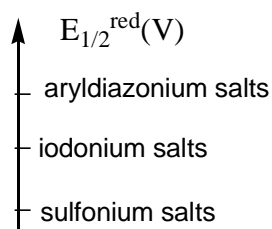
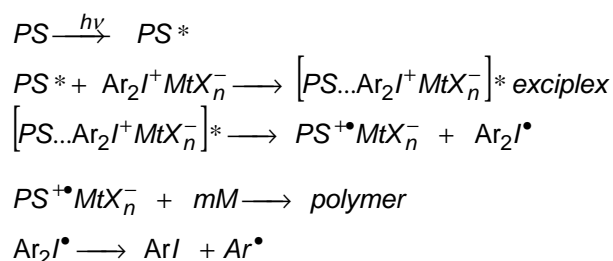


Figure II. 4: Classification of the aryldiazonium, iodonium and sulfonium salts by growing reduction potential

As it is shown in Figure II. 4, aryldiazonium salts are the most powerful oxidizing agents. Nonetheless, they are not thermally stable. In comparison to iodonium salts, triarylsulfonium salts display a lower reduction potential so they will be less easily photosensitized. The mechanisms for the electron transfer reactions are the same for both the triarylsulfonium and the iodonium salts. Since the iodonium salts are more straightforwardly sensitized, they will be taken as example for the following mechanisms.

Photosensitizers ⁴⁰⁻⁴⁵

Some aromatic hydrocarbons (anthracene, perylene, pyrene...) can photosensitize the onium salts through an electron transfer reaction. The overall process between the photoexcited sensitizer (PS) and an iodonium salt is described in Scheme II. 9.



Scheme II. 9: Photosensitized cationic polymerization mechanism via the formation of an exciplex,

M stands for monomer

The mechanism involves the formation of an exciplex between the photosensitizer and the ground state onium salt. An electron is transferred from the sensitizer to the onium salt and leads to the production of sensitizer radical cations that initiate the cationic polymerization either directly or indirectly by abstracting an H from the monomer, solvent or others species present within the formulation.

The ability of polynuclear aromatic compounds to transfer an electron depends on several parameters.

1. The photosensitizer must greatly absorb in the wavelengths of interest.
2. The energy of the photosensitizer excited state must be high.
3. The lifetime of the excited state must be long so the photosensitizer can possibly encounter the onium salt.

The occurrence of the electron transfer reaction can be given by the extended Rehm-Weller equation:

$$\Delta G = F \left[E_{1/2}^{ox}(PS) - E_{1/2}^{red}(On^+) \right] - E(PS^*) \quad (II.7)$$

With

ΔG , the Gibbs free energy

F , the Faraday constant

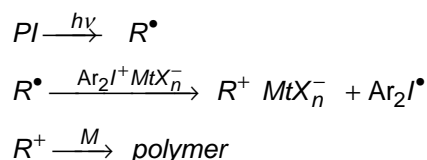
$E(PS^*)$, the energy of the photosensitizer excited state (singlet or triplet)

$E_{1/2}^{red}(On^+)$, the reduction potential of the onium salt, On^+

It has been admitted that the electron transfer reaction takes place if ΔG value is lower than 10 kcal.mol^{-1} ⁴².

Free radicals ⁴⁶

Another route to enhance the initiation step of the cationic polymerization is to introduce a radical photoinitiator whose free radicals generated from its photolysis are able to sensitize the onium salt. The mechanism lies in the oxidation of the photochemically formed radicals by a suitable onium salt. The generated cations are the initiating species for the cationic polymerization (cf Scheme II. 10) ³⁹.

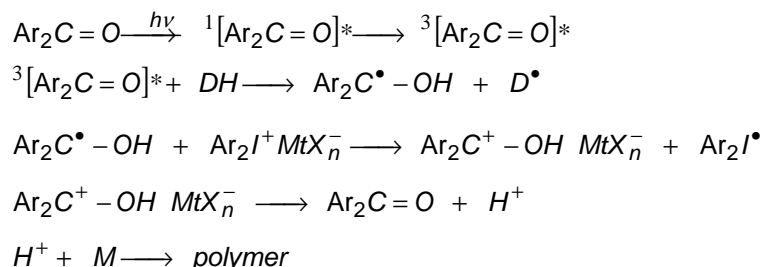


Scheme II. 10: Mechanism of a photosensitized cationic photoinitiator using a cleavable radical photoinitiator (PI) in presence of an iodonium salt and a monomer M

Radical photoinitiators such as benzoin and its derivatives, acylphosphine oxides, etc...can be involved in the sensitization process⁴⁷⁻⁵⁰. As previously, according to the formula II.8, it can be assessed for a given onium salt whether or not it can oxidize a free radical⁴⁰.

$$\Delta G = F[E_{1/2}^{Ox}(R^\bullet) - E_{1/2}^{red}(On^+)] \quad (II.8)$$

Free radicals from the hydrogen abstraction reaction of photoexcited aromatic carbonyl compounds can be also used to reduce the onium salts (see Scheme II. 11). The triplet photoexcited sensitizer abstracts an H from an H donor to generate electron donor ketyl radicals. These species are then oxidized by the onium salts. It gives rise to Brönsted acids which initiate the cationic polymerization. Benzophenone, thioxanthone, camphorquinone, benzil and anthraquinone derivatives are usually employed for sensitization^{39,48}.

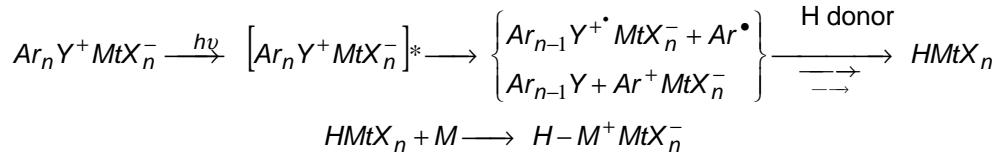


Scheme II. 11: Mechanism of a photosensitized cationic photoinitiator using a hydrogen abstraction type radical photoinitiator (PI) in presence of an iodonium salt, monomer (M) and an H donor (DH)

II.3.2 Kinetics of cationic photopolymerization

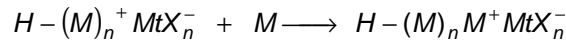
II.3.2.1 Initiation ^{31,38,51}

Initiation with an onium salt ($Ar_nY^+MtX_n^-$) is characterized by the generation of Brönsted acids which are reactive towards the monomer (M).



II.3.2.2 Propagation ^{31,38,51}

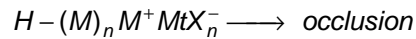
The addition of monomers to growing macromolecular chains leads to the formation of the polymer.



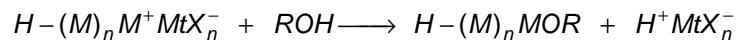
II.3.2.3 Termination ⁵²

Given that the cationic species can not recombine, the termination takes place either by occlusion or by reaction with impurities present in the environment including water and compounds containing hydroxyl group or by transfer reactions (reaction with the counter ion, cyclization...)

a) Occlusion

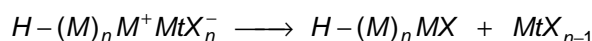
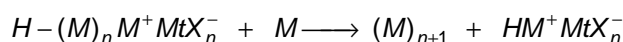
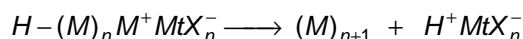


b) Reaction with impurities (example with an alcohol ROH)



If we suppose that the chain transfer is negligible and that the expressions of the propagation R_p and termination rates R_t are: $R_p = k_p[M][H-M^+MtX_n^-]$, $R_t = k_t[N][H-M^+MtX_n^-]$ with N electroneutral nucleophiles present in the formulation with a concentration superior to the ions concentration. According to the steady state approximation, the relation between the initiation rate (R_i) rate of polymerization would be given by: ⁵³

$$\boxed{R_p = \frac{k_p}{k_t[N]} [M]R_i} \quad (II.9)$$

c) Reaction with counter ion (MtX_n^-)d) Reaction with the monomere) Spontaneous chain transfer reaction

II.3.3 Cationic monomers and oligomers

Numerous monomers such as vinyl or heterocyclic resins can be polymerized by a cationic mechanism. Vinyl ethers and epoxides are in fact the most prominent classes of cationically photopolymerizable monomers since they possess really reactive functions and are commercially available³¹. Herein, we will be particularly interested in the epoxides because all the experiments were carried out with the epoxidized hydrogenated bisphenol A and 4-epoxycyclohexylmethyl-3',4'-epoxycyclohexylcarboxylate monomers.

II.3.3.1 Epoxide monomers

Epoxides are attractive monomers. Indeed, contrary to unsaturated monomers such as acrylates and vinyl ethers, the polymerization displays less shrinkage as the propagation step is achieved by opening the epoxide ring⁵⁴. Nevertheless, they are sensitive to humidity and the polymerization rate is clearly lower than for acrylate monomers because of the low propagation rate constant k_p ¹⁹. The most used epoxide resins in UV curing are diglycidyl ether epoxides and cycloaliphatic epoxides (cf Figure II. 5). Some attempts about structure-reactivity relationships for epoxides have been carried out. It turned out that glycidyl ethers and glycidyl esters were less reactive than monomers bearing epoxycyclohexane groups³¹. This could be explained by the fact that the epoxide bond was not as strained and not as reactive as in small ring cycloaliphatic epoxides. In addition, even though, the epoxy groups were terminal and relatively unhindered, the flexible chains can adopt conformations which sterically disturb the approach of the epoxide oxygen to the activated chain end³⁸.

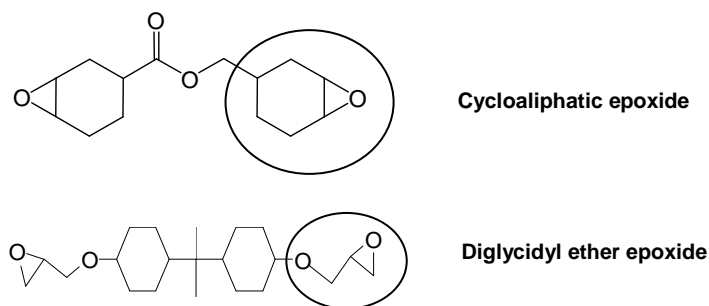


Figure II. 5: Chemical structures of the commercial resins 4-epoxycyclohexylmethyl-3',4'-epoxycyclohexylcarboxylate and epoxidized hydrogenated bisphenol A

II.3.3.2 Vinyl ether monomers

Vinyl ethers have demonstrated a great reactivity in cationic photopolymerization due to the high electronic density of the C=C double bond and the stabilization of the carbocation by resonance. They undergo a fast and complete polymerization. The versatility of this family leads to a broad range of polymers with outstanding solvent resistance and mechanical properties^{18,23,55}. Vinyl ethers terminated telechelic oligomers typically comprise ether, ester, urethane or siloxane moieties. Nevertheless, their high cost and the hazards due to their preparation limit their use³¹. An example of commercial vinyl ether resin is depicted in Figure II. 6.

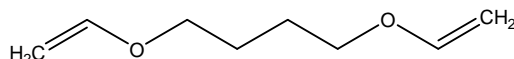


Figure II. 6: Chemical structure of 1,4-butanedioldivinyl ether

II.3.4 Special features of the cationic photopolymerization

II.3.4.1 Deactivation processes

As for the radical photoinitiator, the cationic photoinitiator is submitted to the radiative and radiationless deactivation processes.

II.3.4.2 Inhibition

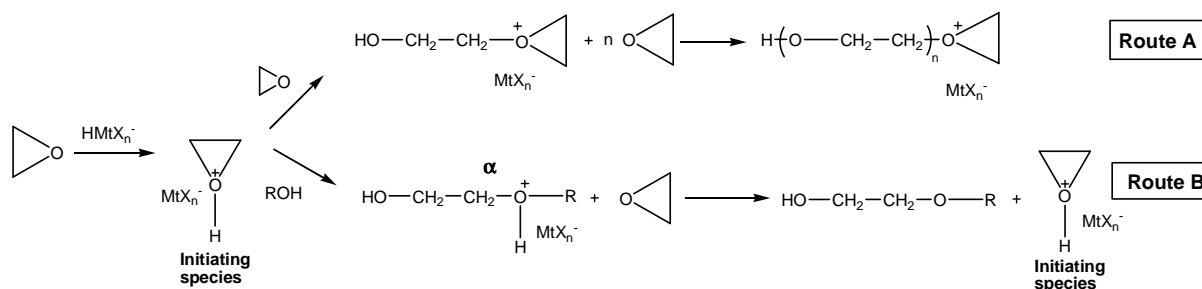
Contrary to radical photopolymerization, the cationic photopolymerization is not sensitive towards oxygen but it can be delayed or even inhibited by transfer reactions in presence of nucleophile or basic compounds. Therefore, it is advised neither to work with amines

and some alcohol additives, nor under a high rate of humidity^{56,57} and nor with monomers bearing nucleophile or basic moieties within their backbone²¹.

II.3.4.3 Side reactions

As seen for termination step, various transfer reactions can occur during the cationic polymerization. They lead to the termination of a growing polymer chain but also to the formation of a reactive specie capable of initiating a new chain. Penczek and Kubisa⁵⁸ have pointed out that in presence of alcohol compounds a different polymerization mechanism named Activated Monomer (AM) can take place in addition to the conventional cationic ring opening polymerization named Active Chain End polymerization (ACE). Indeed, an ACE polymerization corresponds to a nucleophilic attack of the monomer on the tertiary oxonium ion active species (cf route A Scheme II. 12).

By contrast, in AM polymerization, the oxonium ions of the growing chains undergo a nucleophilic attack by the alcohol to produce protonated ether (α). Afterwards, another proton transfer might occur between (α) and the monomer. The created oxonium ions can induce new cationic photopolymerization (cf route B Scheme II. 12). This mechanism might keep occurring until there were not any more terminal hydroxyl groups. It is important to underline that transfer reactions take place during normal cationic polymerization because of the formation of terminal hydroxyl groups. The two polymerization mechanisms will compete during the UV curing process.



Scheme II. 12: Mechanisms of Active Chain End mechanism polymerization (ACE), Route A and Activated Monomer polymerization (AM), Route B

The chain transfer reaction yields to the formation of UV cured materials with shorter chain lengths. Consequently, the final mechanical properties might be affected.

II.3.4.4 Living character³³

As mentioned before, the reactive species can not interact from each other. Therefore, once the initiating species are produced during the photochemical process, the propagation step can continue in the dark. On one hand, this unique feature allows to reduce the irradiation exposure time. On the other hand, it is more difficult to control the polymer formation since the polymer properties keep developing over time.

II.3.4.5 Temperature³³

Whilst the initiation is a photochemical process, the propagation step for a cationic photopolymerization is temperature sensitive. Therefore, the increase in temperature can improve the polymerization rate of a cationic system or extend the final degree of cure by a thermal post curing treatment.

II.4 Conclusion

The description of the radical and cationic photopolymerization mechanisms has highlighted not only the advantages of both processes but also their drawbacks.

On one hand, acrylic monomers are the most widely used materials in UV curing owing to their high reactivity, their low volatility and their moderate costs. In addition, a large choice of radical photoinitiators and acrylate monomers are commercially available. Nevertheless, these compounds are really sensitive to the atmospheric oxygen and the shrinkage is important (up to 15%)¹⁵. The increase in density can yield to stress, distortions and even cracks. On the other hand, to a lower extent, epoxide monomers are also employed: they display lower shrinkage phenomenon due to the ring opening process and the reactive species are particularly stable. Indeed, these species are not sensitive towards oxygen and the polymerization continues even in the dark. Furthermore, as cationic photoinitiators, the onium salts can potentially polymerize all the common cationically polymerizable monomers. But only some of them are synthesized in industrial scale and their maximum UV absorption is rather around 300 nm than in UVA range. Additionally, the epoxide low polymerization rate as well as their sensitivity to humidity turn out to be shortcomings for some industrial applications.

To overcome the limitations of both acrylate and epoxy polymerizations, these systems can be mixed together in order to synthesize Interpenetrating Polymer Networks (IPNs)

2,8,59

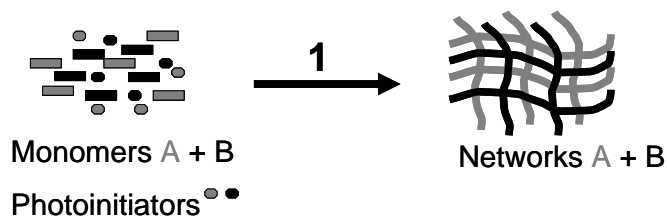
III IPN PHOTOPOLYMERIZATION

This part will deal with UV interpenetrating polymer networks. Their preparation, their kinetics of polymerization as well as the characterization of their final properties will be reviewed.

III.1 Different ways of UV cured IPN synthesis

III.1.1 Simultaneous UV IPNs

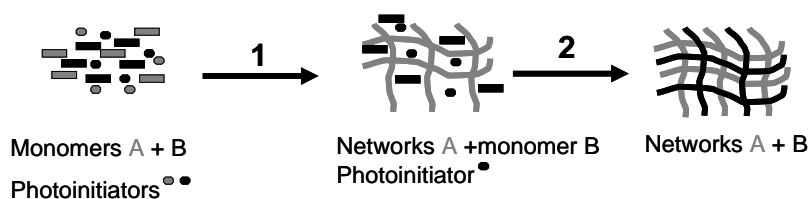
The multifunctional monomers are photopolymerized at the same time but independently from each other. The process is depicted in Scheme II. 13. Although, the polymerizations occur together, the polymerization rate of the different mechanisms can be different ¹³.



Scheme II. 13: Synthesis of simultaneous IPNs

III.1.2 Sequential IPNs

After the mixture of the components, a first network is formed and leads to a highly viscous medium in which a second network is built (cf Scheme II. 14). The formation of the second network modifies the properties of the first one ^{4,14,60}.



Scheme II. 14: Synthesis of sequential IPNs

The final properties of the IPNs depend on number factors such as the order of the sequence (the cationic and the radical photopolymerizations can be inverted), the timing of the sequences and the monomer structures ⁶¹.

There are different ways to control the order and the timing of IPN formation. First, a cationic photoinitiator and a radical photoinitiator absorbing at different wavelengths can be successively excited by either changing the light source or by removing a band pass filter^{6,18,20,62}. As depicted in Figure II. 7, a first exposure 365 nm led to the formation of the acrylic network. Then a second irradiation at 325 nm initiated the cationic polymerization⁶³.

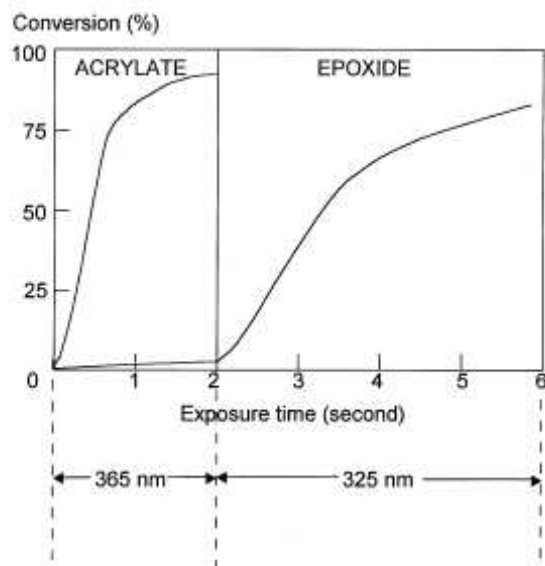


Figure II. 7: Kinetic profiles of a dual cure in laser imaging (an acrylate/epoxide mixture in presence of phosphine oxide and sulfonium photoinitiators)

This method allows an excellent temporal control of the two polymerization steps. However, illuminating twice the sample can be time consuming for some applications.

A second method involves two photoinitiators active at the same wavelengths but the sequential stage is chemically controlled by the production of the reactive species. For example, according to the ratio between the photoinitiator concentrations, the sequence of the network formation could be modified in methacrylate/vinyl ether systems. Under a large excess of radical photoinitiator or in presence of cationic photopolymerization inhibitors like amine additive or water, the radical polymerization can be promoted over the cationic reaction. Light irradiation also plays a crucial role in the sequence order since at low intensities vinyl ether monomer can act as diluent¹⁶.

A third method relies on a single initiator system which is able to generate both free radicals and cations via electron and proton transfer reactions. Oxman *et al*⁶⁴ have presented a three-component initiator system a photosensitizer (camphorquinone)/an electron donor (amine)/an iodonium salt) inducing a sequential free radical/cationic hybrid photopolymerization. A judicious choice of the amine in terms of thermodynamic

properties and basicity considerations proved that the cationic polymerization could be delayed in comparison to the acrylate polymerization.

For three dimensional object manufacturing or curing of paints, UV IPNs show limitations due to the presence of uncured shadow areas within the resulting photopolymer. Consequently, dual UV and thermal curing could be implemented as reported by some authors⁶⁵⁻⁶⁷.

III.2 Photopolymerization process of IPNs

This part relies on methacrylate or acrylate/ epoxide systems that have been more extensively studied. The comprehension of the formation mechanism is difficult because IPNs are multicomponent systems in which each system depends on the processing conditions and can be affected by the presence of the other system. Therefore, the major trends will be declined in this part.

III.2.1 Kinetics aspects of photoIPNs

Real Time Infra Red (RTIR) spectroscopy method has been shown to be particularly suitable for following the kinetics of hybrid systems. Indeed, it is possible to monitor separately the disappearance of IR absorption vibration bands of characteristic reactive functions for each system. It provides some interesting information about the reactivity and the influence of some experimental parameters on the monomer conversion¹³.

Authors such as *Decker, Lecamp and Sangermano et al*^{12,13,15} have investigated the simultaneous acrylate and epoxide photopolymerizations. They have clearly evidenced that the polymerization of the two different networks occurred on similar time scale but independently from each other. More precisely, the acrylate monomer has been found to polymerize faster and more extensively than the epoxide one. Its cure proceeds in much greater extent than for the homopolymerization process.

The importance of the radical photopolymerization in terms of polymerization rate and degree of cure is explained by several factors. First, owing to the slowness of the cationic polymerization, the epoxide can act as plasticizer for radical polymerization and thus extend the radical polymerization by delaying the vitrification phenomenon. The diluent effect is all the more pronounced than the delay between the formation of the two networks increases. The extreme case corresponds to the formation of sequential IPNs for which the polymerization extent of the second monomer rests on the first network glassy state^{4,5,14}. Secondly, the acrylate polymerization is less sensitive towards oxygen in hybrid system because the viscosity greatly increases with the concomitant build up of

acrylate and epoxide networks^{13,15}. This phenomenon might considerably reduce atmospheric oxygen from diffusing within the mixture and from scavenging radical polymerization. This assumption was corroborated by *Cai et al*⁶⁸. They have demonstrated by means of Raman spectroscopy combined with Raman confocal microscopy that the conversion for both acrylate double bond and epoxide ring was nearly the same at the coating surface and in the bulk. Besides, the film-air interface of UV cured epoxide/methacrylate hybrid materials has been observed by scanning electronic microscopy (SEM). Actually, it has pointed out that the surface for an oxygen sensitive resin such as neat acrylic formulation is rough whilst the surface of UV cured hybrid material is rather smooth⁶⁹.

Finally, *Lecamp et al*¹² has evidenced that the free radicals from the photolysis of the UVI 6976 cationic photoinitiator were capable of inducing the radical polymerization and hence might contribute to increase the radical polymerization rate. Sometimes, this synergist effect on the acrylate polymerization can be weakened owing to possible free radical recombinations or reactions between both photoinitiators.

To overcome the difference in reactivity between the methacrylate/acrylate polymerization and the epoxide photopolymerization, some authors have undertaken investigations to substantially speed up the cationic photopolymerization. *Lecamp et al*¹² has proved that the increase in medium temperature from 30°C to 90° C tremendously improved the cationic polymerization rate compared to the radical one. At 90°C, the degree of cure reached by the cycloaliphatic epoxide was even more prominent than for the methacrylate. Another way to “tune up” the cationic polymerization is via a sensitization process using photosensitizers or free radicals as mentioned before⁷⁰. This method not only enhances the cationic polymerization rate in the hybrid system but also the Persoz hardness, the solvent resistance as well as the surface curing properties¹³.

The prediction of the kinetics of IPN formation turns out to be very complex because numerous chemical and physical parameters are involved. They influence not only the formation of each network but also the final properties.

III.2.2 Characterization of the photocured IPNs

III.2.2.1 IPN morphology

Basically, the polymer morphology describes the spatial organization of the macromolecular chains and their microscopic ordering⁷¹. The prediction and the control of the polymer morphology turns out to be complicated for IPNs because of their multicomponent composition⁷². In fact, the IPN morphology is governed not only by the kinetics of photopolymerization of the components contained in the IPN but also by the miscibility of those components^{14,72,73}. At first glance, one can expect that the physical interpenetration between the two networks should avoid the phase separation but it was shown in literature that the phase separation can take place⁷⁴. The degree of polymer miscibility is thermodynamically assessed by the Gibbs free energy of mixing (ΔG_M). According to the Flory-Huggins theory, ΔG_M is defined as follows³:

$$\Delta G_M = \Delta H_M - T\Delta S_M \quad (\text{II.10})$$

with

ΔH_M : the enthalpy of mixing term

T: the temperature

ΔS_M : the entropy of mixing term

The polymers are miscible provided that ΔG_M is negative. If the increase in molecular weight of the polymers becomes too high, the entropy of mixing becomes very low and ΔG_M become positive (for high ΔH_M). Consequently, the polymers are immiscible³.

The former equation can be also expressed as a function of the total volume system V, the volume fraction ϕ_i , the molar volume V_i and the solubility parameters δ_i of each component i⁷².

$$\Delta G_M = \phi_1\phi_2V(\delta_1 - \delta_2)^2 + RT\left(\frac{\phi_1}{V_1}\ln\phi_1 + \frac{\phi_2}{V_2}\ln\phi_2\right) \quad (\text{II.11})$$

As a matter of fact, the closer are the solubility parameters, the more stable will be the mixture. Hence, the degree of mixing relies on the balance between the thermodynamics and kinetics of cure because at the glassy state, the diffusion of the components and the subsequent phase separation are prevented.

If a high degree of crosslinking density is achieved in the IPNs before the components can diffuse then a very limited phase separation and a high degree of mixing would be observed.

Phase separation in IPNs occurs according to mainly the spinodal decomposition mechanism and to a less extent to the nucleation and growth mechanism^{73,75,76}. As regards to the nucleation and growth mechanism, during the phase separation, the volume of nodules containing a constant amount of one of the two components increases. In addition, the nodules merge. As a consequence, the morphology is characterized by dispersed regular domains within the matrix. Adversely, for the spinodal decomposition mechanism, interconnected cylinders of the second phase within the matrix of the first phase are generally produced from the phase separation and tend to grow by increasing their wave amplitude. Coarsening and coalescence phenomena subsequently occur modifying to a certain extent the morphology. The phases are co-continuous.

The morphology of IPNs can be determined by scanning electronic microscopy (SEM)⁷⁷ and transmission electronic microscopy (TEM)¹¹. Various investigations have been carried out for thermal IPNs. The factors influencing morphology were shown to be the polymerization methods, the sequence orders¹⁴, IPN composition^{2,3,78,79}, the compatibility between the polymers and the crosslinking density⁸. However, few experiments have been done on the morphology of UV cured IPNs especially epoxide/acrylate mixtures. Lately, Nowers *et al*⁵ have exploited the flexibility of the dual process thermal cured epoxide polymerization/photoinduced acrylate polymerization in order to examine both the effect of the curing sequence and the composition on the morphology. The SEM micrographs of rupture surfaces disclose that the brittleness increases with the epoxy content and for the samples for which the epoxide polymerization occurred first (named epoxide first samples). In addition, the epoxy first samples display no apparent microstructure whereas the acrylate first samples up to 0.25 exhibit a growing coarse morphology. As regards to the morphology of UV simultaneous IPNs, the study will be even more difficult because it will rely on the time sequence of three events: the gelation of the polymer 1, the gelation of the polymer 2 and the phase separation of these two polymers. The final physical and mechanical properties of the material will be completely different according to the order of the three phenomena. If the gelation of one of the component takes place before the phase separation, then the morphology will be more continuous. Adversely, if the phase separation happens before gelation, then the morphology will be unhomogeneous⁸.

III.2.2.2 IPN thermomechanical properties

The phase morphology is an important parameter because it is responsible for the subsequent final properties^{14,72}. The existence and the distribution of domains within the cured material are merely analyzed by using SEM and TEM. Nevertheless, these devices give information neither about the polymer fraction in the different phases nor the degree of phase separation. Differential Scanning Calorimetry (DSC) and Dynamic Mechanical Analysis (DMA) are two techniques that give an idea about the degree of interpenetration through the shift and the broadening of the glass transition temperatures (T_g s) of the homopolymers and hybrid systems.

If the hybrid system is homogeneous at least at the macromolecular scale then only one broad T_g located between the two homopolymers is detected. Sangermano *et al*¹⁵ have managed to synthesize an interphase material as it is illustrated in Figure II. 8. The hybrid mixture possesses a large and broad $\text{Tan}\delta$ curve. This special feature confers to the system some interesting damping properties.

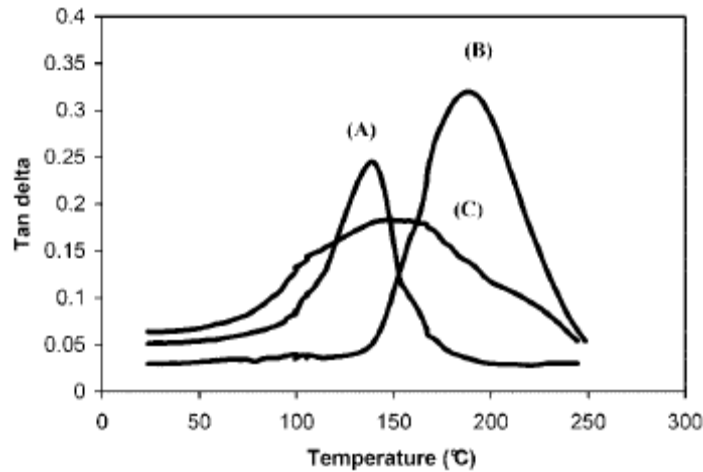


Figure II. 8: $\text{Tan}\delta$ from DMA analysis of pure 1,6-hexanediol diacrylate (HDDA) (curve A) and 3,4-epoxycyclohexylmethyl-30,40-epoxycyclohexyl carboxylate (UVacure 1500) (curve B) and the HDDA/UVacure 1500 50/50 mol% hybrid mixture (curve C)¹⁵

In this case, the resultant T_g of the hybrid material can be expressed according to the Fox-Flory equation⁷⁹:

$$\frac{1}{T_g} = \frac{w_1}{T_{g1}} + \frac{w_2}{T_{g2}} \quad (\text{II.12})$$

with

w_i , the composition by weight of each component i

T_{gi} , the T_g of each component i

If the degree of interpenetration is low then two glass transition temperatures are measured corresponding to the two individual polymer T_g s.

III.2.2.3 Transparency

The sample transparency might evidence the great interpenetration of the networks^{13,15}. Indeed, opacity is attributed to the diffusion of the visible light by domains whose size is superior to 100-400 nm. However the relevance of this criterion has to be taken with caution because some cured materials were transparent despite the presence of phase separated domains. It was account for the good matching between the polymers index of refraction⁸⁰.

This bibliography survey revealed that many papers dealt with the field of UV cured IPNs. The effect oxygen, humidity, temperature and photoinitiator concentration on the kinetics of photopolymerization of this hybrid mixture was extensively studied. Thermomechanical as well as the structural properties of IPNs were highlighted. The conclusions drawn from this bibliography study will be first employed for the optimization of an industrial hybrid mixture and then to understand of the formation of IPNs between a cycloaliphatic epoxide and a methacrylate (1:1 weight ratio) under specific experimental conditions, also try to establish some relations between the material morphology, the mechanical properties and the processing conditions.

IV EXPERIMENTAL STUDY

IV.1 Understanding of the IPN formation between a diglycidyl ether epoxide and an acrylate under Huntsman industrial specifications

IV.1.1 Context of the study


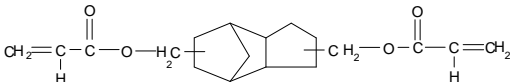

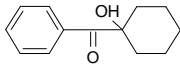
The aim of this study is to compare the UV curing performances between two technologies using different irradiation sources: Araldite®Digitalis developed by Huntsman and Stereolithography (SLA) developed by 3D systems. On one hand, for Araldite®Digitalis, the light source is a conventional UV lamp whose main emission wavelengths are 366 nm, 405 nm and 413 nm. The 366 nm wavelength has been taken as the actinic wavelength for the following experiments. The light intensity varies from 15-30 mW/cm² and the variation of the temperature in situ during the building process is negligible. On the other hand, the stereolithography machine SLA 7000 functions with a laser emitting at 355 nm. The light intensity is about 800 mW/cm² and the elevation of the temperature in situ is prominent.

The first comparative experiments consisted in curing Huntsman commercial resins optimized for SLA process with Araldite®Digitalis demonstrator named Griffin, and see if the resulting photopolymer exhibited sufficient mechanical properties (green strength) for handling the post-curing treatment⁸¹. It turns out that the commercial resin Renshape®SL 7870 (70 wt% epoxide + 30 wt% acrylate) fulfilling all the requirements in SLA process such as rapid curing and low shrinkage, did not reach the green strength at the Araldite®Digitalis optimum exposure speed. Therefore, the first part of this study will be dedicated to the understanding of this underachievement. Then, the second part will deal with the optimization of this hybrid commercial mixture.

IV.1.2 Characterization of the commercial resin Renshape®SL 7870

Renshape®SL 7870 is a liquid resin that is formulated for the production of three-dimensional objects by SLA. It contains various components but the most important are the monomers epoxidized hydrogenated bisphenol A (E5000) and tricyclodecane dimethanol diacrylate (SR 833S) and the photoinitiators triarylsulfonium hexafluoroantimonate mixture salts (TAS) and 1-hydroxycyclohexyl benzophenone (I 184). For convenience sake, we will only consider these components within Renshape®SL 7870. Their chemical structures and their weight percentages are reported in Table II. 1.

Table II. 1: Weight percentage and chemical structure of the main components present in Renshape® SL 7870

wt%	Role	Chemical name	Chemical structure
67.2	cationic monomer	mainly epoxidized hydrogenated bisphenol A (E5000)	
28.8	radical monomer	mainly tricyclodecane dimethanol diacrylate (SR 833S)	
2	cationic photoinitiator	triarylsulfonium hexafluoroantimonate mixture salts (TAS)	
2	radical photoinitiator	1-hydroxycyclohexylphenyl ketone (I 184)	

The mixture also contains additives such as stabilizer but they will be neglected in this study.

IV.1.2.1 Griffin and SLA 7000 trials

In order to understand the differences in reactivity of Renshape®SL 7870 with Griffin and SLA 7000 machine, the resulting UV cured materials were examined by IR spectroscopy to determine the degree of cure reached by both epoxide and acrylate monomers.

The experiments lie in drawing strand specimens with both Griffin and SLA 7000 machines. To facilitate the fabrication of single strands, the large resin vat of the conventional Griffin and SLA 7000 machines were removed and a platform was inserted

in its place. This platform was used to support an aluminium dish filled to the rim with Renshape®SL 7870. The dish was placed at a given position so that the focal point of the light source irradiates the resin surface. Due to the complex geometry of the machines, it was not possible to measure with a conventional device the light intensity of both the UV lamp and the laser.

However, we report here the irradiation conditions that allowed the commercial resin to reach the green strength with each device. As regards to Griffin, the strand was obtained by performing 2 passes at an exposure speed 3 mm.s^{-1} (minimum scanning exposure) whereas for SLA machine, the curing energy was set up at 13 mJ/cm^2 .

Given that the specimen thicknesses are $\geq 0.27 \text{ mm}$, Near Infra Red (NIR) spectroscopy in transmission mode was employed for the conversion determination. This spectroscopy is particularly suitable for studying thick samples as the extinction coefficient of the functional groups between the visible and the middle IR regions (between $12\,500 \text{ cm}^{-1}$ and 4000 cm^{-1}) is much lower. In this range, combination bands (averaged vibrations of two adjacent molecular motions) and first overtone bands determined from fundamental absorption bands in the middle IR can be identified⁸². Therefore, the NIR absorption bands that were selected are the absorption band at 4738 cm^{-1} assigned to acrylate =C-H absorption⁸² and the large band at 4525 cm^{-1} related to a combination of the epoxide C-H fundamental band at 3050 cm^{-1} and CH_2 fundamental band at 1460 cm^{-1} ⁸³. The final conversion for both acrylate C=C double bond and epoxide ring was determined according to this formula:

$$\boxed{\text{Conversion} = \frac{A_0 - A_t}{A_0} \times 100} \quad (\text{II.13})$$

with

A_0 , corresponding to the area of IR absorption band of reactive function before the curing

A_t , corresponding to the area of IR absorption band of reactive function at the time $t(\text{s})$

The calculation of the final conversion can be influenced by our experimental procedure. Some approximations that we made are depicted below:

1. The shrinkage phenomenon was not taken into account. It was assumed that the sample thickness remained unchanged before and after the polymerization in order to determine the area of the characteristic NIR absorption bands of the reactive functions at $t=0 \text{ s}$. Therefore, calibration curve of IR absorbance of the liquid Renshape®SL 7870 resin versus its thickness were established.

2. The NIR analysis were performed at DPG 19 hours after UV curing at Huntsman for practical reasons (the experiments at Huntsman were carried out in the afternoon and the ones at DPG in the following morning). In consequence, just the final conversion ratio of epoxide was evaluated. The living character of the cationic polymerization could not be highlighted.
3. Moreover, the cured sample surface was supposed to be flat.
4. The samples were dried with tissues before the NIR analysis. It was assumed most of the uncured liquid resin was taken away during this dryness process.

Consequently, the data given in Figure II. 9 have to be taken with caution, only general observations can be made. It seems that under Griffin cure, the E5000 conversion is inexistent or very limited. The green strength is only ensured by the SR 833S (the minor monomer component in Renshape®SL 7870 cf Table II. 1). On the contrary, with the SLA machine, both the acrylate (SR 833S) and the epoxide (E5000) readily polymerize. The resulting photopolymer is thus made of both polyether and polyacrylate networks. It can be more easily handled than the strand cured with Griffin machine.

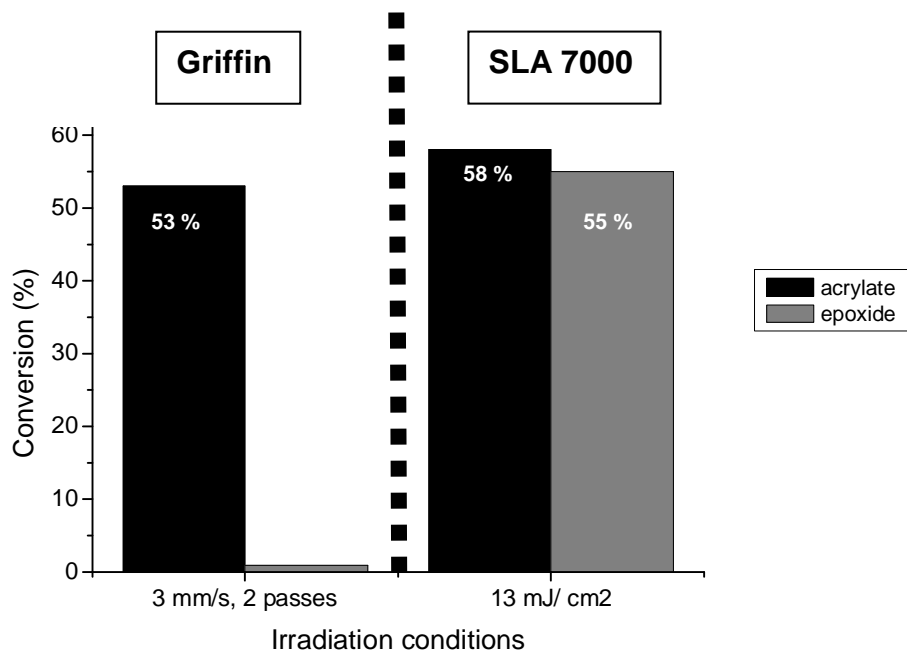


Figure II. 9: Determination of the degree of cure reached by both acrylate and epoxide monomers contained in Renshape®SL 7870 under Griffin curing (3 mm/s, 2 passes, sample thickness~0.7 mm) and SLA 7000 curing (curing energy= 13 mJ/cm², sample thickness~0.27 mm)

Since the photoinitiating system remains unchanged on both devices, the lower efficiency of the cationic photoinitiator under Griffin cure might be explained by a lower absorption of the light at 366 nm compared to 355 nm for TAS.

IV.1.2.2 UV spectroscopy measurements

In order to confirm the previous hypothesis, both the molar extinction coefficients and the UV absorbance contribution of each photoinitiator were evaluated. To calculate the UV absorbance, we set up the sample thickness at 100 μm corresponding to the standard layer thickness in stereolithography process. In practice, as seen before the layer thickness can vary depending on the irradiating conditions. Table II. 2 gathers all the information.

Table II. 2: Calculation of the molar concentration, the molar extinction coefficient and the UV absorbance of the cationic photoinitiator TAS and the radical photoinitiator I 184

Photoinitiator name	Molar concentration (mol.L ⁻¹) (a)	Molar extinction coefficient (L. mol ⁻¹ . cm ⁻¹) (b)		UV absorbance (c)	
		355 nm	366 nm	355 nm	366 nm
TAS	1.5×10^{-2}	712	109	0.11	0.02
I 184	1.2×10^{-1}	65	27	0.08	0.03

- (a) The molar concentration of each photoinitiator within the mixture: 67.2 wt% E5000+ 28.2 wt% SR 833S+ 2wt% TAS+ 2 wt% I 184
 (b) In acetonitrile
 (c) Calculated from Beer law: $A=\epsilon lC$, with ϵ molar extinction coefficient, l the sample thickness equal to 100 μm , typical layer thickness in SLA and C the molar concentration of each photoinitiator

According to Table II. 2, both photoinitiators exhibit a more important absorption at 355 nm than at 366 nm. The molar absorption coefficients of both TAS and I 184 are respectively 7 and 4 times higher at 355 nm than at 366 nm. In addition, TAS exhibits a greater UV absorbance than I 184 at 355 nm (1.4 times) that is why both radical and cationic polymerization can take place at 355 nm. By contrast, at 366 nm, both UV absorbance of TAS and I 184 are weak. The TAS UV absorbance value was divided by a factor 5 in comparison with the value calculated at 355 nm. This low absorption of the cationic photoinitiator can account for the sluggish cationic polymerization at 366 nm. The UV absorbance of I 184 is in the same range than for TAS at this wavelength but the high quantum yield and the reactivity of the generated free radicals might lead to an efficient initiation of the radical polymerization ($\Phi_{\alpha} \sim 0.8$ quantum yield of the bond cleavage in α ^{24,84} and the rates constant of addition of benzoyl and isopropyl ketyl radical onto acrylates are high ($2.7 \times 10^5 \text{ M}^{-1} \cdot \text{s}^{-1}$ and $1.3 \times 10^7 \text{ M}^{-1} \cdot \text{s}^{-1}$ on butylacrylate, respectively ⁸⁵)) and explain the high conversion reached by SR 833S under Griffin cure.

To supplement the characterization study about Renshape®SL 7870, it is very important to evaluate the reactivity of both acrylate and epoxide monomers and distinguish their individual contribution to the overall photopolymerization process under Griffin curing. It was achieved by investigating their kinetics of photopolymerization by RT FTIR spectroscopy at 366 nm.

IV.1.2.3 Kinetics of photopolymerization at 366 nm

The RT FTIR principle and the experimental conditions are thoroughly explained in Annex I.1 and Annex II.1. The degree of cure versus time for both E5000 and SR 833S were assessed by monitoring the decrease of the typical vibration absorption bands at 910 cm^{-1} for the epoxide ring (stretching vibration) and at 1407 cm^{-1} (deformation vibration) for the acrylate double bond⁸⁶. First of all, it is important to underline that the results presented in Figure II. 10 are different from the results obtained with Griffin because the light dose received by the samples was different. However, the actinic wavelength is the same so the photoinitiator efficiency should be conserved.

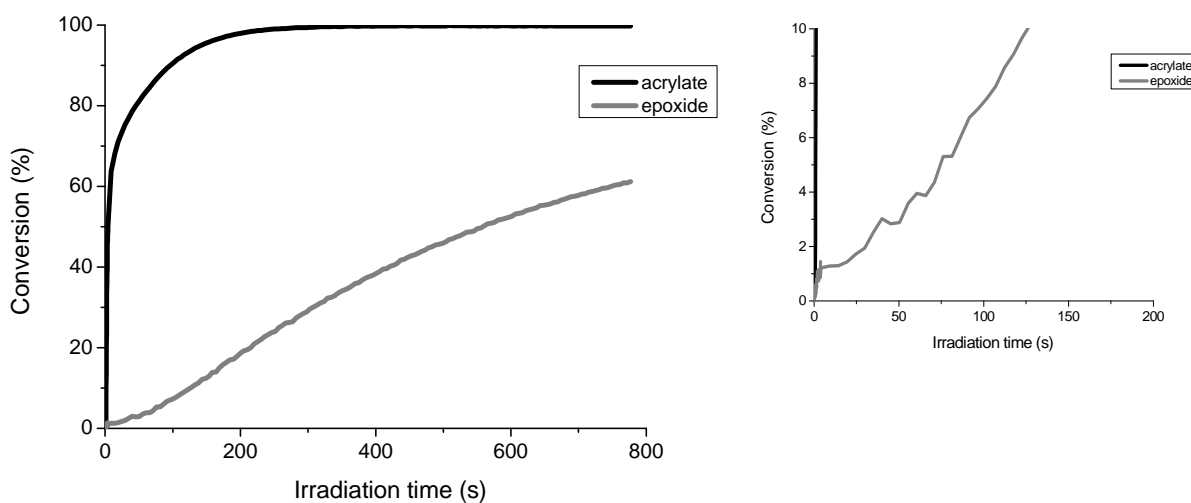


Figure II. 10: Photoinitiated polymerization of the hybrid epoxide/acrylate Renshape®SL 7870 resin containing 67.2 wt% E5000, 28.8 wt% SR 833S; photoinitiators: 2 wt% TAS, 2 wt% I 184; Hg-Xe Hamamatsu lamp at 366 nm; light intensity $\sim 17\text{ mW/cm}^2$; sample thickness $\sim 35\text{ }\mu\text{m}$

As seen in Figure II. 10, under such experimental conditions, SR 833S undergoes a nearly complete polymerization (~100% of conversion) meanwhile the E5000 conversion reaches 61%. This difference could be explained by considering the diepoxide monomer as a plasticizer during the acrylate polymerization since the polymerization rate of the radical system is 180 times higher (cf Table II. 3). E5000 presence might increase the mobility of the macroradicals and contribute to the extent of the radical polymerization^{12,13,15}. Some experiments not reported here with the neat E5000 system disclosed that the cationic system is slightly affected by the earlier formation of the polyacrylate network. A sharp increase in the polymerization rate was even so noticed at the very beginning of the polymerization (4s) as seen in the insert in Figure II. 10.

Table II. 3: Determination of the ratio maximum polymerization rate to the monomer initial concentration ($R_{p_{max}}/[M]_0$) and the conversion at 780 s for the commercial resin Renshape®SL 7870; same experimental conditions than in Figure II. 10


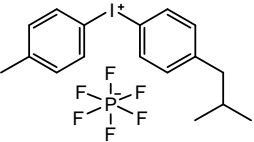
Formulation name	Function	$R_{p_{max}}/[M]_0$ * 100 (s ⁻¹)	Conversion (%)
Renshape®SL 7870	Acrylate	20.5	~100
	Epoxide	0.11	61

To conclude, these few experiments led to a better understanding of the Renshape®SL 7870 photopolymerization on both SLA 7000 and Griffin devices. The green strength can be easily reached with SLA machine because both radical and cationic photoinitiators are efficient enough at this wavelength to ensure the polymerization of both reactive functions. On the contrary, Griffin machine could not properly cure Renshape®SL 7870 because TAS exhibits a too low absorption at 366 nm and the cationic polymerization is significantly slower than the radical one. The radical polymerization alone might not be enough to ensure the green strength at high speed cure as required from Huntsman. For these reasons, if we want to keep using IPN chemistry with Griffin, it is necessary to speed up the cationic polymerization of Renshape®SL 7870. As seen previously in the literature study, iodonium salts are more suitable than sulfonium salts for the sensitization process owing to their high reduction potential. As a consequence, the sensitization of both TAS and the iodonium salt, iodonium, (4-methylphenyl)[4-(2-methylpropyl) phenyl]-, hexafluorophosphate(1-) Irgacure®250 (I 250) will be investigated in the following paragraphs in conjunction with the influence of an oxygen scavenger.

IV.1.3 Optimization of the IPN kinetics: Enhancement of the cationic photopolymerization by sensitization processes

As described in the literature and in the section II.3.1, the onium salts spectral sensitivity can be enhanced to the visible range via an electron transfer reaction with photoexcited sensitizers and via free radicals generated from radical photoinitiator photolysis. Their photosensitivity efficiency towards TAS and I 250 will be straightforwardly evaluated by RT FTIR spectroscopy. Their structures and their molar absorption coefficients are given in Table II. 4. The analysis will be performed at 366 nm in the experimental conditions described in Annex I.1 and Annex II.1.

Table II. 4: Chemical structures and molar absorption coefficients of TAS and I 250

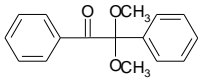
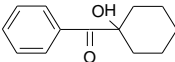
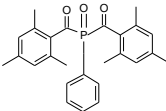
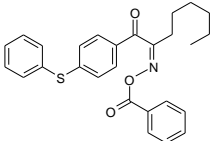
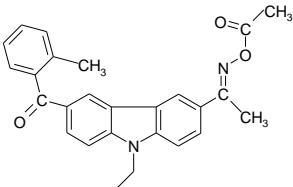
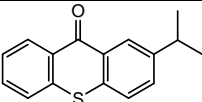
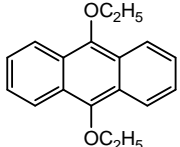
Chemical name	Chemical structure	Molar absorption coefficient at 366 nm (L.mol ⁻¹ .cm ⁻¹) (a)
Triarylsulfonium hexafluoroantimonate mixture salts (TAS)		109
Iodonium, (4-methylphenyl)[4-(2-methylpropyl) phenyl]-, hexafluorophosphate(1-) (I 250)		6

(a) determined in acetonitrile

IV.1.3.1 Compounds used as sensitizers

A large range of radical photoinitiators is commercially available. In order to assess the beneficial or the detrimental effect of the free radicals produced upon their photolysis on the cationic polymerization, radical type I photoinitiators from CIBA Chemicals were selected: Irgacure®651, a benzoin ether, Irgacure®184, an hydroxyl alkyl phenyl ketone, Irgacure®819, a phosphine oxide and finally Irgacure®OXE01 and Irgacure®OXE02, oxime esters. Additionally, the role of the photosensitizers isopropylthioxanthone (ITX) and 9,10-diethoxyanthracene (910) were also studied. Their chemical structures, molecular weight and molar absorption coefficient at 366 nm are reported in Table II. 5.

Table II. 5: Chemical structures, molecular weights and molar absorption coefficients at 366 nm of the selected radical photoinitiators and photosensitizers

RADICAL PHOTOINITIATORS			
Chemical name	Chemical structure	Molecular weight (g.mol⁻¹)	Molar absorption coefficient at 366 nm (L.mol⁻¹.cm⁻¹) (a)
2,2-dimethoxy-1,2-diphenylethan-1-one Irgacure®651 (I 651)		256	121
1-hydroxycyclohexyl phenyl ketone Irgacure®184 (I 184)		204	17
Bis(2,4,6-trimethylbenzoyl)-phenylphosphineoxide Irgacure®819 (I 819)		419	884
1,2-octanedione,1-[4-(phenylthio)phenyl]-, 2-(O-benzoyloxime) Irgacure®OXE01 (I OXE01)		446	2807
1-[9-ethyl-6-(2-methylbenzoyl)-9H-carbazol-3-yl]-, 1-(O-acetyloxime)-ethanone Irgacure®OXE02 (I OXE02)		409	3269
PHOTOSENSITIZERS			
Isopropylthioxanthone (ITX)		254	4500
9,10-diethoxyanthracene (910)		266	5800

(a) determined in acetonitrile

These sensitizers display different molecular weights and molar absorption coefficients. All these distinct features will play a role in the sensitization of the cationic system. To assess their impact, we will only consider here the cationic system. First, we will focus on the influence of the free radicals from radical photoinitiator photolysis.

IV.1.3.2 Effect of free radicals from radical photoinitiator photolysis

Mixtures containing 96 wt% of Epalloy®5000 (E5000) + 2 wt% of either TAS or I 250 + 2 wt% of one radical type I photoinitiators were prepared and tested by RT FTIR spectroscopy. Their kinetics profiles were compared to the ones obtained for the reference formulations comprising only 98 wt% of E5000 + 2 wt% either TAS or I 250. All the information about the relevant kinetics parameters are summarized in Figure II. 11.

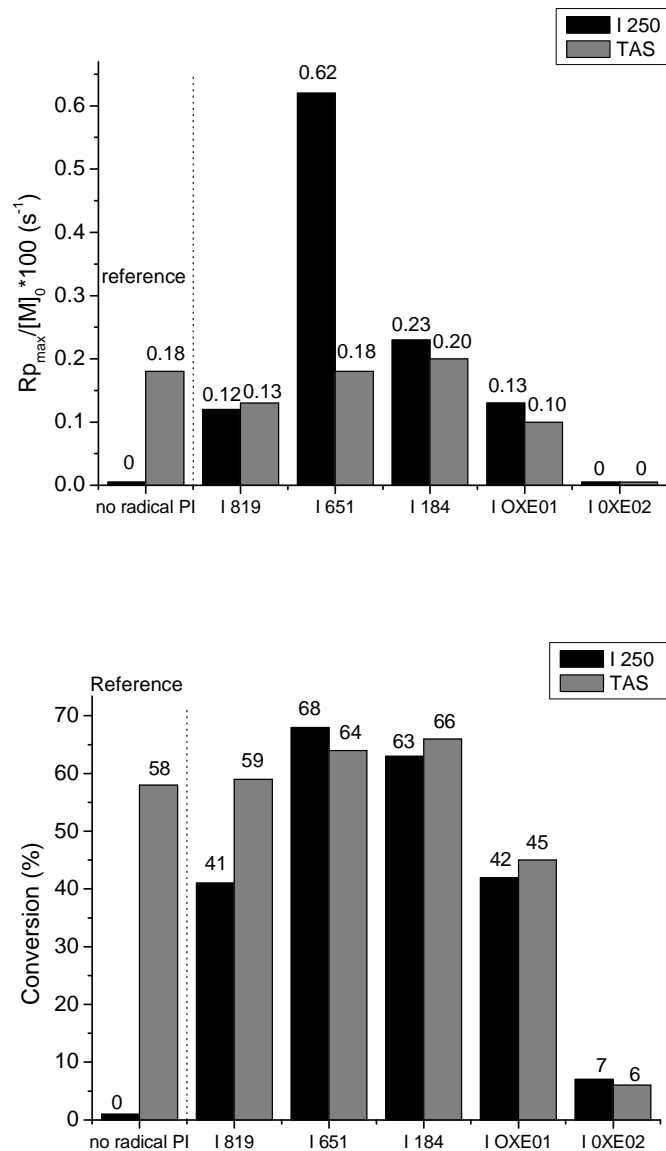


Figure II. 11: $R_{p,max}/[M]_0$ and conversion at 780 s for the different formulations containing 96 wt% E5000; photoinitiators: 2 wt% TAS or 2 wt% I 250 and 2 wt% radical photoinitiator: I 819, I 651, I 184, I OXE01 and I OXE02; Hg-Xe Hamamatsu lamp at 366 nm, light intensity ~ 17 mW/cm²; sample thickness ~ 35 μ m

The data from Figure II. 11 show that in absence of radical photoinitiator TAS is clearly more efficient than I 250 at 366 nm. There is no polymerization for the system E5000/I 250 whereas the system E5000/TAS undergoes a slow polymerization (a degree of cure of 63% after 430 s of irradiation and with a $R_{p_{max}}/[M]_0$ of about $0.18 \cdot 10^{-2} \text{ s}^{-1}$). This difference is explained by the very low molar absorption coefficient of I 250 at 366 nm, 20 times less than the TAS (cf Table II. 4). Therefore, I 250 needs to be sensitized.

➤ TAS

In sensitized experiments, as illustrated in Figure II. 11, for the systems with TAS, the addition of the different radical photoinitiators only leads to a slight improvement of both the polymerization rate and the degree of cure of the epoxide function. A detrimental impact was noticed with the oxime esters photoinitiators. To our knowledge, no enquiry has been carried out so far about the ability of the free radicals formed during the photolysis of I OXE01 and I OXE02 to sensitize an iodonium and a sulfonium salt. According to Figure II. 11, the presence of I OXE01 had a negative impact on the E5000/TAS system. The polymerization rate was divided by 2 and the final conversion by 1.4. This decrease can be attributed to an internal filter phenomenon since the absorption coefficient of I OXE01 is roughly 25 times higher than the molar absorption coefficient of TAS (cf Table II. 5). Furthermore, it should be underlined that the presence of nitrile, a low basicity group, in I OXE01 structure might interact with the reactive species and thus slow down the polymerization (cf Scheme II. 16). The measurements of the UV absorbance of the coating during the photopolymerization revealed that I OXE01 photobleaches (the UV absorbance was divided by 6) and gives rise to photoproducts more transparent which allowed the cationic polymerization to occur (cf Table II. 6).

Table II. 6: UV absorbance at 366 nm of the formulation comprising 96 wt% E5000, photoinitiators: 2 wt% TAS and 2 wt% I OXE01 during the polymerization; Hg-Xe Hamamatsu lamp at 366 nm, light intensity $\sim 17 \text{ mW/cm}^2$, sample thickness $\sim 35 \mu\text{m}$

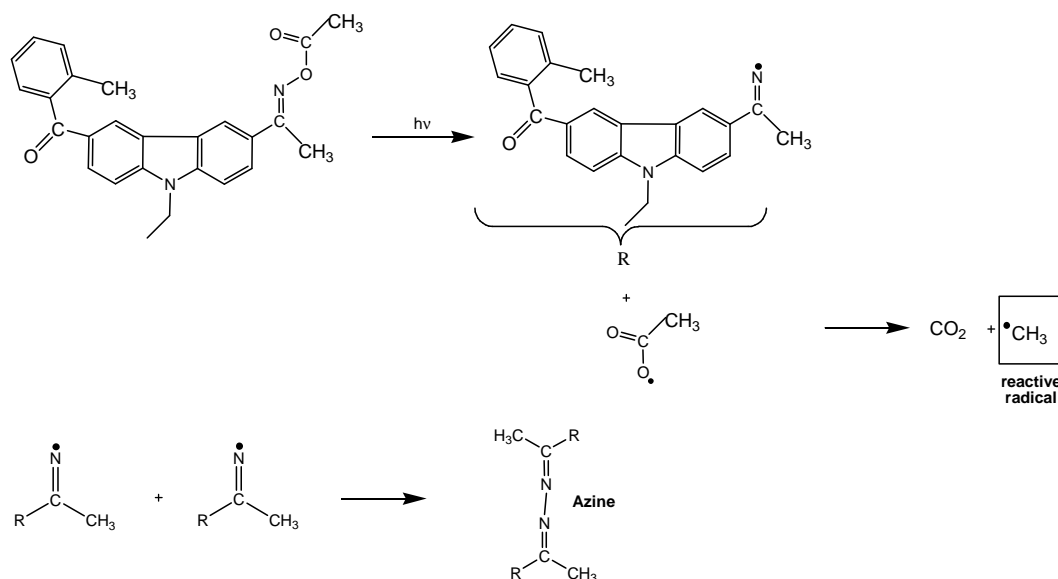
	t=0s	t=50s	t=100s	t=200s	t=500s	t=777s
UV absorbance at 366 nm	0.75	0.22	0.22	0.16	0.14	0.13

Concerning I OXE02, its introduction totally inhibits the cationic polymerization. The molar absorption coefficient of I OXE02 outweighs the TAS one by a factor of 26. In addition, the UV absorbance of the formulation tremendously increases during the polymerization, as pointed out in Table II. 7. Thus, the polymerization is hampered by the inner filter effect.

Table II. 7: Determination of the UV absorbance of the formulation comprising 96 wt% E5000, photoinitiators: 2 wt% I 250 and 2 wt% I OXE02 during the polymerization; at 366 nm; same experimental conditions than in Table II. 6

	t=0s	t=50s	t=100s	t=200s	t=500s	t=777s
UV absorbance at 366 nm	0.63	2.17	2.02	2.13	1.78	1.45

When I OXE02 undergoes the homolytic cleavage into iminyl radicals and acetoxy radicals (see Scheme II. 15)^{24,87,88}, iminyl radicals recombine to give rise to conjugated compounds, presumably azines, whose UV absorption at long wavelengths is broader.

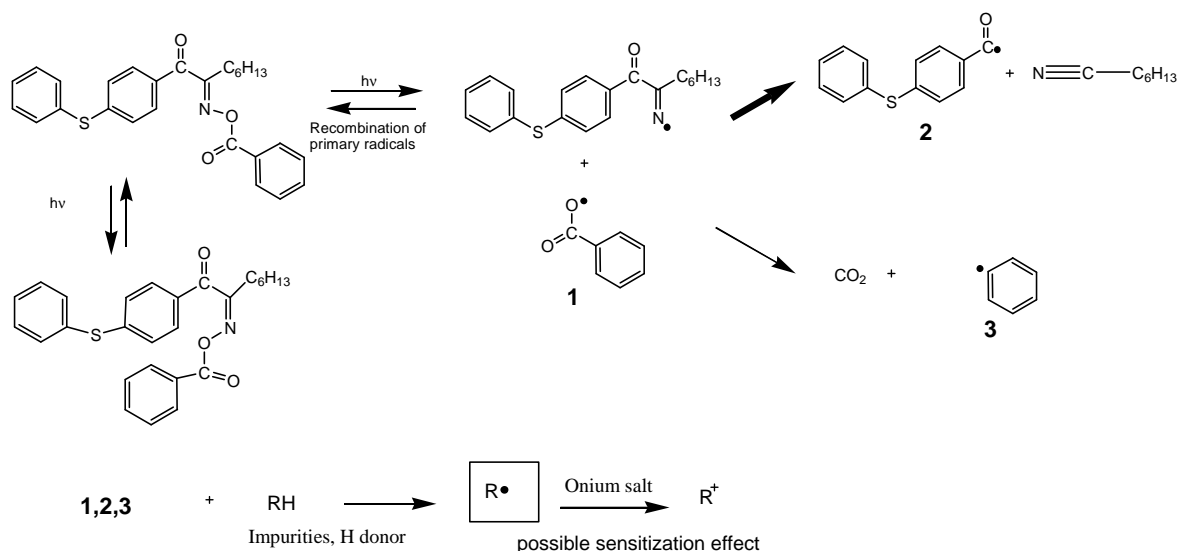


Scheme II. 15: Mechanism of formation of I OXE02 photoproducts

➤ I 250

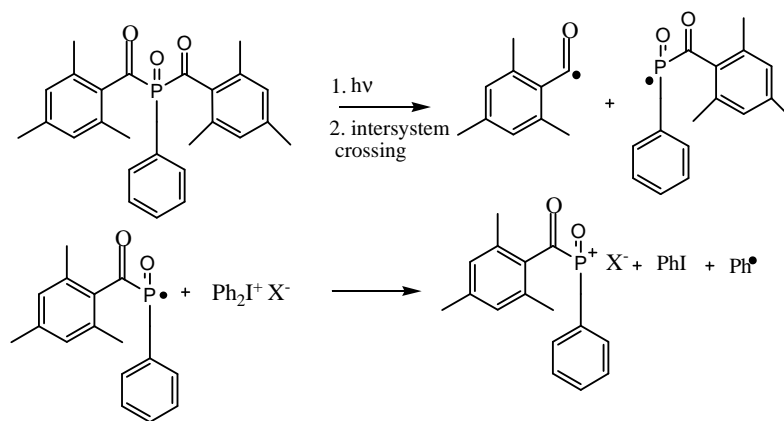
As regards to the effect of the oxime esters on the system containing E5000 and I 250, both $R_{p_{max}}/[M]_0$ and the final conversions were similar to the ones found for the system E5000 and TAS. It seems that the inner filter effect due to both oxime ester absorption and the sensitization reaction of I OXE01 on TAS prevail on the direct UV absorption of TAS. The ability of the free radicals generated from I OXE01 photolysis to photosensitize I 250 is very interesting. We proposed that during I OXE01 photolysis, the carboxyl (1), phenylthiobenzoyl (2) and phenyl (3) radicals might react with impurities and might abstract an H to generate electron donating radicals (see Scheme II. 16). Additionally, if these radicals present a low oxidation potential, they might reduce the iodonium salt.

UV cured Interpenetrating Polymer Networks (IPNs)



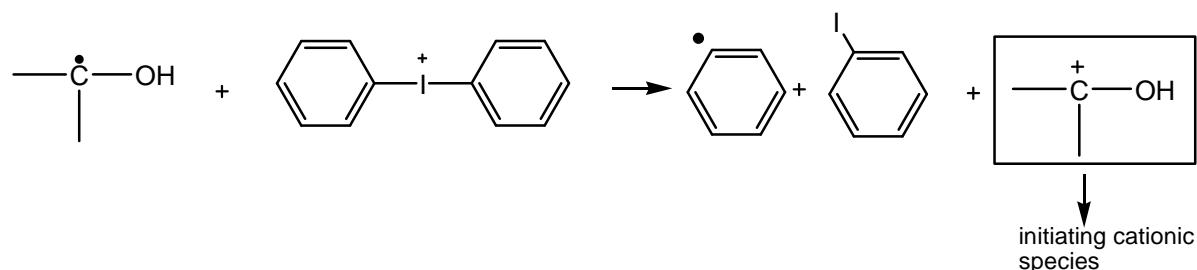
Scheme II. 16: Proposition for the sensitization process involving I OXE01

The use of the other sensitizers with I 250 yielded to striking results since it displays a higher reduction potential than TAS. The elucidation of the sensitization mechanism with a few radical photoinitiators has been reported in literature. The stronger is the electron donor radical, the better is the sensitization. For instance, the ability of free radicals from I 819 photolysis to sensitize I 250 is in great accordance with the results found by Degirmenci *et al*⁷⁰, the phosphinoyl radicals generated via I 819 photocleavage are capable of reducing I 250 in order to form phosphonium cations. These species may participate to the initiation process. The sensitization process is pictured in Scheme II. 17.



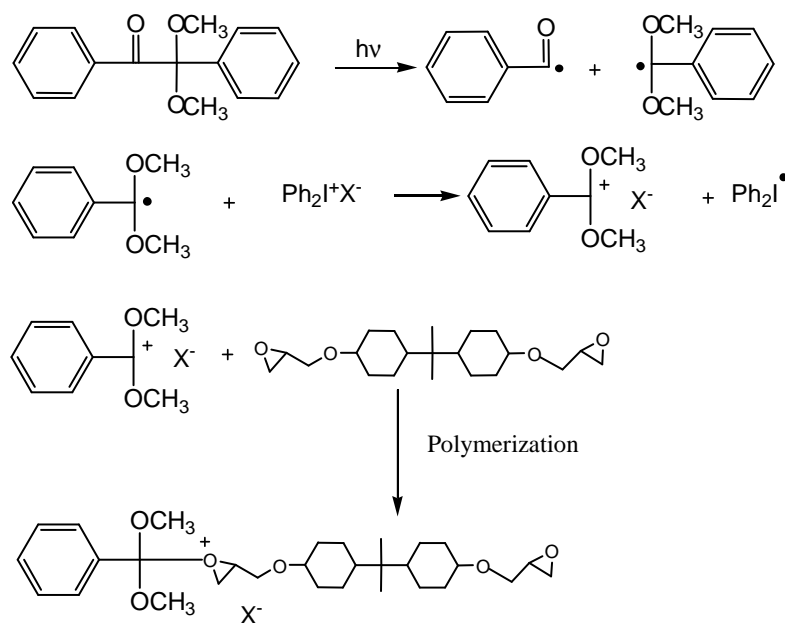
Scheme II. 17: Sensitization mechanism by bisacylphosphine oxides

The cationic polymerization of the system E5000/I 250 is also greatly improved by the presence of I 184. In comparison with the formulation comprising I 819, the rate of polymerization was multiplied by 2 and the final conversion by 1.6. This could be explained by the production in both cases of α -hydroxyl radicals. These free radicals are known to readily reduce the iodonium salt according to the reaction in Scheme II. 18⁴⁰.



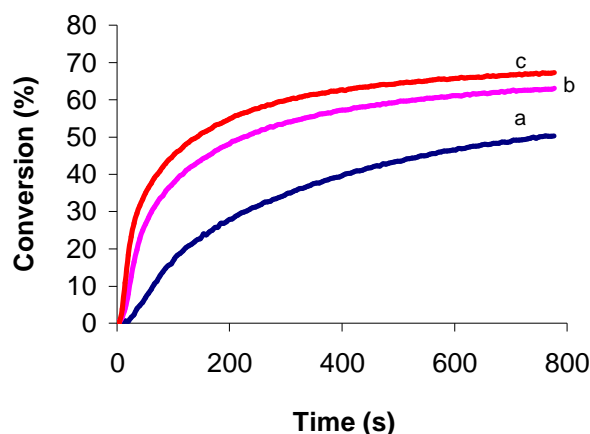
Scheme II. 18: Sensitization mechanism by hydroxyl alkyl phenyl ketones

The most efficient sensitization effect towards I 250 was noticed for the formulation containing I 651. The $R_{p_{max}}/[M]_0$ was about $0.62 \cdot 10^{-2} \text{ s}^{-1}$. In terms of cationic polymerization, this value is particularly important. This enhancement may stem from the participation of strong electron donor alkoxybenzyl radicals from I 651 photolysis in the electron transfer reaction with I 250⁴⁰. The overall mechanism is depicted in Scheme II. 19.



Scheme II. 19: Sensitization mechanism in presence of alkoxybenzyl radicals^{49,50}

Given this promising result, some additional experiments were performed in order to evaluate the effect of the I 651 concentration on the kinetics parameters.



	$Rp_{max}/[M]_0 \cdot 100$ (s^{-1})	Final conversion (%)
0.5% wt I 651	0.22	50
2% wt I 651	0.77	63
5% wt I 651	1.27	67

Figure II. 12: Epoxide conversion versus time profiles and $Rp_{max}/[M]_0$ and conversion at 780 s for the different formulations containing 98 wt% E5000; photoinitiators: 2 wt% I 250 and I 651, a) 0.5 wt%, b) 2 wt% and c) 5 wt%; Hg-Xe Hamamatsu lamp at 366 nm, light intensity ~ 17 mW/cm²; sample thickness ~ 35 μ m

The kinetic profiles in Figure II. 12 point out that an increase in I 651 concentration contributes to produce more initiating species and thus improve greatly the epoxide polymerization. Both rate of polymerization and final conversion are enhanced. The UV absorbance of the formulations before and after polymerization were determined by UV spectroscopy with the Agilent 8453E spectroscopy system (Agilent Technologies) in order to check if an internal filter phenomenon can interfere in the cationic polymerization. It appears from Table II. 8 that even at 5 wt% I 651 concentration, the UV absorbance during the polymerization is low. So, the penetration of the light through the sample is still good. However, a too high content of radical photoinitiator may decrease the radical photoinitiator efficiency because the numerous generated free radicals might tend to recombine. The increase in UV absorbance after polymerization might be attributed to the formation of benzil. It corresponds to the recombination of two benzoyl moieties which shifts the absorption to the visible range^{89,90}. The latter are also capable of absorbing the light and cleaving.

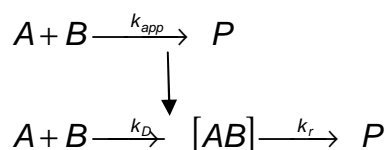
Table II. 8: Evolution of the UV absorbance at 366 nm of the formulations containing 98 wt% E5000; photoinitiators: 2 wt% I 250 and I 651, a) 0.5 wt% I 651, b) 2 wt% I 651 and c) 5 wt% I 651 before and after the polymerization; same experimental conditions than in Figure II. 12

	UV absorbance at 366 nm (before polymerization)	UV absorbance at 366 nm (after polymerization)
a	0.006	0.026
b	0.037	0.094
c	0.103	0.294

Heretofore, only the cationic system has been considered. The addition of both an acrylic compound and a radical photoinitiator into the formulation might affect the photosensitization effect. The generated free radicals might react either with the monomer (radical polymerization) or with the cationic photoinitiator (electron transfer reaction). In order to assess the chemical balance of these reactions, calculations of the ratio of their rate constants versus the viscosity of the medium were conducted.

IV.1.3.3 Evaluation of the chemical balance between the radical polymerization and the electron transfer reaction

Both reactions between free radicals with either the radical monomer or the cationic photoinitiator are bimolecular reactions. Two steps are involved: the two reacting species A and B have first to diffuse in the medium in order to come closer together and form an encounter complex ([AB]) and then the molecules react to form the products (P) (cf Scheme II. 20)



Scheme II. 20: Different steps of a bimolecular reaction

Thus, the apparent rate constant is a contribution of the diffusion controlled bimolecular rate (k_D) and the unimolecular rate constant (k_r) at which the reaction occurs.

The formula of the apparent rate constant is given below ²⁵:

$$\frac{1}{k_{app}} = \frac{1}{k_r} + \frac{1}{k_D} = \frac{k_r + k_D}{k_r * k_D} \quad (II.14)$$

It is noteworthy to say that we neglected the complex dissociation reaction.

There are two extreme cases

If $k_r > k_D$, $k_{app} \sim k_D$ the reaction is diffusion controlled

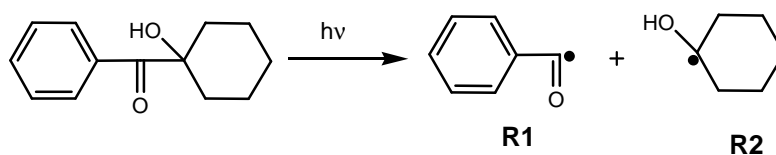
If $k_D > k_r$, $k_{app} \sim k_r$ the reaction is chemically controlled

1. Calculations of apparent rate constants of addition for some free radicals onto the acrylate monomer

We chose among the radical photoinitiators previously tested (cf Table II. 5) Irgacure®184 (I 184) and Irgacure®651 (I 651) because during their dissociation not only a benzoyl radical is formed (R1) but also an α -hydroxyl radical (R2) for I 184 and a methyl radical for I 651 (R3) having different reactivities towards the acrylate monomer. The methyl radical has a low rate constant of addition onto an acrylate ($\sim 10^5$ on methyl acrylate ²⁴). This rate constant is 100 times lower with regard to the rate constant involving α -hydroxyl radical on an acrylate ($\sim 10^7$ on butyl acrylate ²⁴).

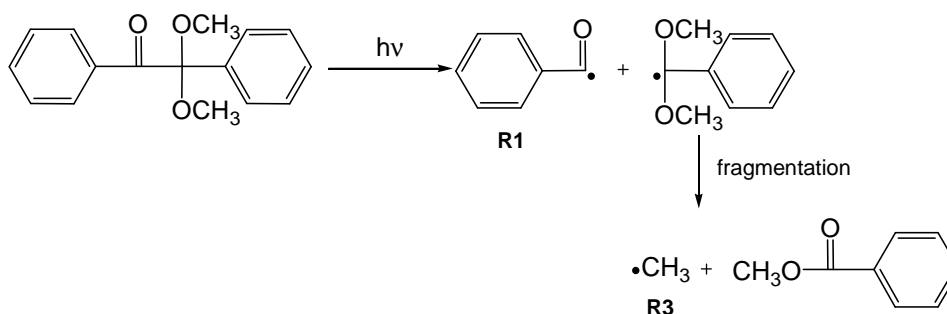
The photolysis mechanisms of I 184 and I 651 are depicted below.

I 184 undergoes an α -cleavage reaction at its excited triplet state. As depicted in Scheme II. 21, its photolysis leads to the formation of a benzoyl radical (R1) and an α -hydroxyl radical (R2).



Scheme II. 21: Formation of the benzoyl and the α -hydroxyl radicals through the I 184 photolysis

During the photolysis of I 651 photoinitiator at the triplet state, the benzoyl and the dimethoxybenzyl radicals are formed. The latter one undergoes a subsequent fragmentation that generates a methyl radical and methyl benzoate²⁴. The mechanism is illustrated in Scheme II. 22.



Scheme II. 22: Photolysis mechanism of I 651

The addition rate constants of benzoyl and ketyl radicals onto butylacrylate (BA) in acetonitrile and the addition rate constants of methyl radical onto methylacrylate (MA) are available in literature. The values are given in Table II. 9.

Table II. 9: Addition rate constants of benzoyl and ketyl radicals onto butyl acrylate (BA)^{24,85}

Structure	k_r (L.mol ⁻¹ .s ⁻¹) (a)
 (R1)	$2.7 \cdot 10^5$ (BA)
 (R2)	$2.5 \cdot 10^7$ (BA)
$\cdot\text{CH}_3$ (R3)	$3.1 \cdot 10^5$ (MA)

(a) determined in acetonitrile

These values demonstrate that the addition of the radicals onto the acrylic monomer can readily occur.

Herein, the final apparent rate constant ($k_{app(\text{radical photoinitiator})}$) corresponds to the sum of the addition apparent rate constants of both radicals generated during the radical photoinitiator photolysis. The results can be found in Table II. 10.

Table II. 10: Calculations of the apparent addition rate constants k_{appi} , final apparent rate constants $k_{app(\text{radical photoinitiator})}$ from the addition rate constants of the free radicals generated from I 184 and I 651 photolysis

Radical photoinitiator	Radical	Addition rate constants k_{ri} (i=1,2,3) (L.mol ⁻¹ .s ⁻¹)	Apparent addition rate constant k_{appi} (i=1,2,3) ($k_{appi} = \left(\frac{k_{ri} * k_D}{k_{ri} + k_D} \right)$) (L.mol ⁻¹ .s ⁻¹)	Final apparent rate constant $k_{app(\text{radical photoinitiator})}$ ($k_{app1} + k_{appi}$) (i=2,3) (L.mol ⁻¹ .s ⁻¹)
I 184	R1	2.7*10 ⁵	2.27 *10 ⁵	1.59 *10 ⁶
	R2	2.5 *10 ⁷	1.36 *10 ⁶	
I 651	R1	2.7*10 ⁵	2.27 *10 ⁵	4.82*10 ⁵
	R3	3.1*10 ⁵	2.55*10 ⁵	

2. Evaluation of the electron transfer rate constant between the free radicals and the onium salt

In this case, it is hypothesized that the electron transfer rate constant is controlled by diffusion. The reaction might occur at each encounter. The reaction rate named $k_{app(TAS)}$ depends on the diffusion of the free radicals and the onium salts towards each other through the resin. The utilization of the Stokes-Einstein equation leads to the determination of the diffusion rate constant according to this formula:

$$k_{app(TAS)} = k_D \approx \frac{4RT}{3\eta} \quad \text{with } \eta \text{ the medium viscosity}$$

3. Calculation of the ratio between the rate constant of addition of the radical on the acrylate monomer and the addition rate constant of the sensitization process

Finally, we tried to generalize this calculation and see how evolves the ratio between the rate constant concerning the radical polymerization and the electron transfer reaction according to the viscosity of the formulation.

The plot of $\frac{k_{app(radicalphotoinitiator)}}{k_{app(TAS)}}$ versus η shows that viscosity can influence the ratio between the reaction rates (cf Figure II. 13).

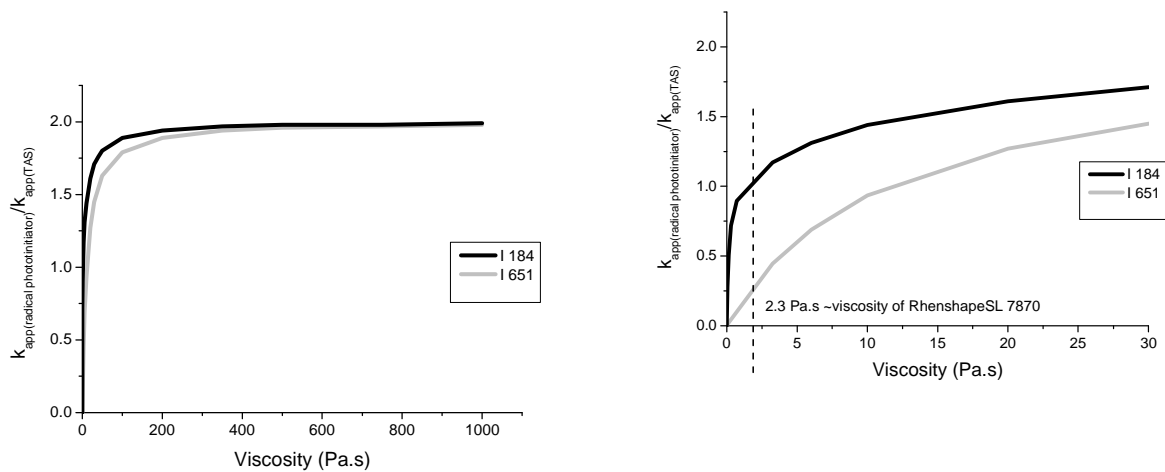


Figure II. 13: Plot of the ratio between the final addition apparent rate constant of the free radicals onto an acrylate double bond on the electron transfer rate constant between the free radicals and the onium salt as a function of the viscosity for the photoinitiators I 184 and I 651

Figure II. 13 clearly shows that according to the nature of the free radicals generated from the photolysis of the radical photoinitiator, the evolution of the ratio between the final apparent rate constants versus viscosity changes. At very low viscosities, the ratio is inferior to 1 that means that the sensitization process might be promoted with regard to the radical polymerization. The upper limit of viscosity for this area will depend on the reactivity of the free radicals. The lower is the reactivity of the radicals towards the addition onto the double bond the higher the upper limit of viscosity. Indeed, for the formulation containing I 184, the ratio is equal to 1 for a viscosity of roughly 2 Pa.s whereas the viscosity is about 12 Pa.s for the system containing I 651. At this stage, acrylate monomer molecules are in competition with onium salt molecules for reacting with the free radicals. It is noteworthy to say that the viscosity of the hybrid resin

Renshape®SL 7870 is about 2.3 Pa.s ($k_D \sim 1.44 \cdot 10^6 \text{ L.mol}^{-1}.\text{s}^{-1}$). So if we draw a parallel between these results and the photopolymerization process of an UV curable resin whose viscosity is similar to Renshape®SL 7870 one, we understand that at the very beginning of the UV curing, the sensitization process will readily occur for the formulation comprising I 651 whereas it will compete with the radical polymerization for the formulation with I 184. Subsequently, with the increase in the viscosity due to the build-up of the crosslinked networks, the ratio value keeps increasing. The radical polymerization might start prevailing on the sensitization effect. Meanwhile, at high viscosities (from 100-150 mPas) assimilated to the glassy state, all the processes are totally limited by diffusion and the ratio will reach a maximum which corresponds to the ratio 2 ($k_{app(\text{radical photoinitiator})} \sim 2 \cdot k_D$ and $k_{app(\text{TAS})} \sim k_D$). If any reaction can take place at this stage, the radical polymerization is predominant. These results are consistent with the results obtained in RT FTIR experiments showing the highest efficiency of I 651 as the other radicals produced react more with the acrylate monomers (cf Figure II. 11).

Secondly, to complete the previous experiments, the ability of photosensitizers to enhance the cationic photopolymerization will be investigated.

IV.1.3.4 Effect of the photosensitizers

The compounds used for this study are the carbonyl aromatic compound isopropylthioxanthone (ITX) and the aromatic compound 9,10-diethoxyanthracene (named 910). The results of the RT FTIR kinetic surveys of Epalloy®5000 photopolymerization in presence of I 250 and TAS with these compounds are summarized in Figure II. 14. In the previous part, the best sensitization effect was found with the mixture containing I 651+ I 250. So the formulations comprising cationic photoinitiator and I 651 in addition with the formulations containing only each cationic photoinitiator were taken as reference.

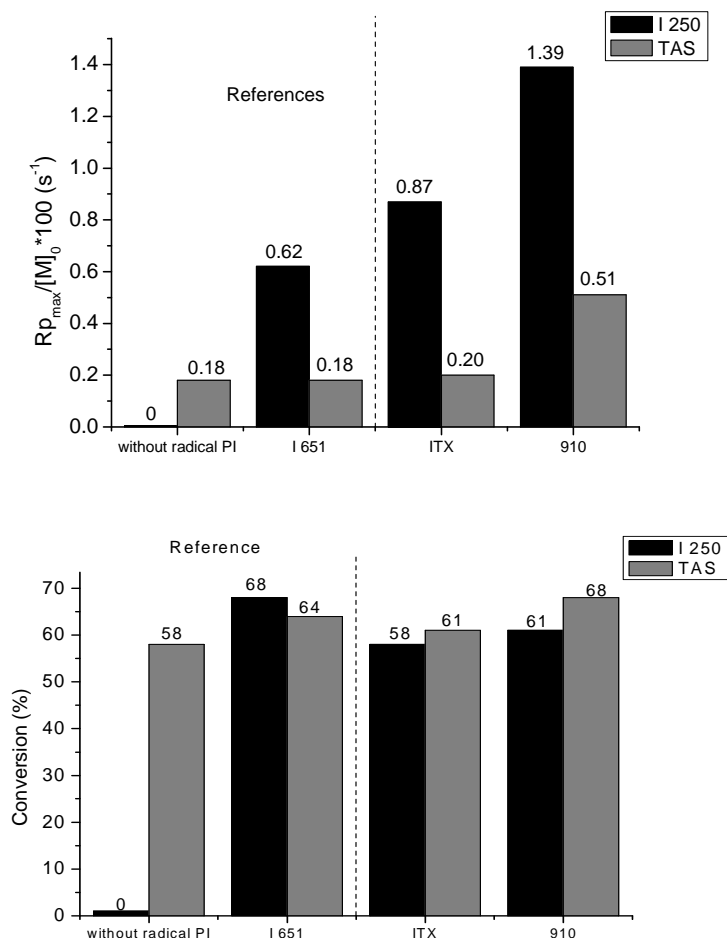
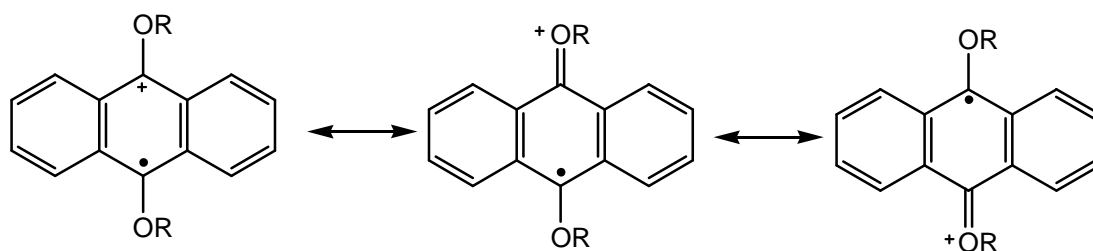


Figure II. 14: $R_{p_{\max}}/[M]_0$ and conversion at 430 s for the different formulations containing 96 wt% E5000, photoinitiators: 2 wt% TAS or 2 wt% I 250, 2 wt% photoexcited sensitizers: ITX and 910; Hg-Xe Hamamatsu lamp at 366 nm, light intensity ~ 17 mW/cm²; sample thickness ~ 35 μ m

The results involving ITX and 9,10-diethoxyanthracene in Figure II. 14 are particularly of interest since the rate of polymerization for the system E5000/I 250 was better than for the formulation with I 651 (the best formulation found previously). The high efficiency of 9,10-diethoxyanthracene can be firstly accounted for its higher absorption at 366 nm in comparison with ITX (1.3 times higher) (cf Table II. 5). Then, it possesses electron donor substituents which may facilitate the transfer of the lone electron and stabilize the cation radical. The stabilization process is represented in Scheme II. 23.



Scheme II. 23: Stabilization of the 9,10-diethoxyanthracene cation radical

Finally, a rough calculation of the Gibbs free energy according to the extended Rehm-Weller equation (cf formula (II.7)) demonstrates that the reaction between the two onium salts and 9,10-diethoxyanthracene are particularly favored which is consistent with the RT FTIR experiments (cf Table II. 11). For the calculations, some approximations have been made. The oxidation potentials and the excited state energy values of ITX and 9,10-diethoxyanthracene are taken as those of thioxanthone and anthracene. It is supposed that the oxidation potential of ITX and 9,10-diethoxyanthracene are lower than those of thioxanthone and anthracene due to respectively alkyl moiety and electron donor substituents. In addition, the reduction potential of I 250 is presumed to be -0.83 V ⁹¹. It corresponds to the value found for the photoinitiator bis(4-tert-butylphenyl)iodonium hexafluorophosphate displaying a similar backbone. The reduction potential for TAS was supposed to be equal to -1.1 V referring to the value measured for triphenylsulfonium salt²¹.

It is important to underline that the sensitization involves respectively the triplet-excited thioxanthone and the singlet-excited anthracene⁹².

Table II. 11: Half wave oxidation potentials $E_{1/2}^{\text{ox}}(\text{S})$ (vs SCE), triplet or singlet excitation energies $E(\text{S}^*)$ of thioxanthone and anthracene, calculation of the Gibbs free energy between respectively I 250, TAS and thioxanthone and anthracene

Sensitizer	$E_{1/2}^{\text{ox}}(\text{S})$ (V)	$E(\text{S}^*)$ (kJ.mol ⁻¹)	$\Delta G_{\text{I 250}}$ (kJ.mol ⁻¹)	ΔG_{TAS} (kJ.mol ⁻¹)
Thioxanthone	1.7 ^{33,40}	277(triplet) ^{21,33}	-32.86	-6.80
Anthracene	1.1 ^{33,40}	319(singlet) ^{21,33}	-132.76	-106.70

To conclude, due to their low reduction potential, triarylsulfonium salts are not easily photosensitized by an electron transfer process. In contrast, a clear evidence of sensitized effect by both free radicals and photosensitizers was noticed for I 250. These results were expected since I 250 is known in literature for its high reduction potential. The alkoxybenzyl radicals from I 651 photolysis are particularly of interest since an $R_{p_{\text{max}}}/[M]_0$ was reached ($0.77 \cdot 10^{-2}\text{ s}^{-1}$). Moreover, to a certain extent, this value can be enhanced by the increase in I 651 concentration. The best performance was obtained with 9,10-

diethoxyanthracene. Its presence allowed to maximize $Rp_{max}/[M]_0$ at $1.39 \cdot 10^{-2} \text{ s}^{-1}$. It is 6 times higher than for the system containing only TAS. However, I 250 is not thermally stable so it is necessary to improve its stability before using it for the fabrication of three dimensional objects.

According to the results obtained previously on the cationic polymerization sensitization, new hybrid formulations have been prepared with the best photoinitiating systems. As for Renshape®SL 7870, they were cured with both Griffin machine.

IV.1.3.5 Tests with Griffin

For these new set of experiments with Griffin, 3 hybrid mixtures were formulated. In the formulation 1 and 3, the cationic photoinitiator TAS was associated to the radical photoinitiator I 651 and the photoexcited sensitizer 9,10-diethoxyanthracene exhibiting the best sensitizing efficiency towards the cationic polymerization. Despite the low thermal stability of I 250, the aforementioned promising results obtained with I 651 conducted us to test this photoinitiating system (formulation 2). The composition of the formulations is detailed in Table II. 12.

Table II. 12: Composition in weight percentage of the formulation 1, formulation 2 and formulation 3

Formulation name	E5000 (wt%)	SR 833S (wt%)	Cationic PI (wt%)	Radical PI or photosensitizer (wt%)
Formulation 1	64.4	27.6	2 (TAS)	4.0 (I 651)
Formulation 2	65.0	28.2	2 (I 250)	4.0 (I 651)
Formulation 3	66.0	28.1	2 (TAS)	1.8 (9,10-diethoxyanthracene)

Their reactivity was compared to the Renshape®SL 7870 one at a speed exposure of 3 mm/s with 2 passes.

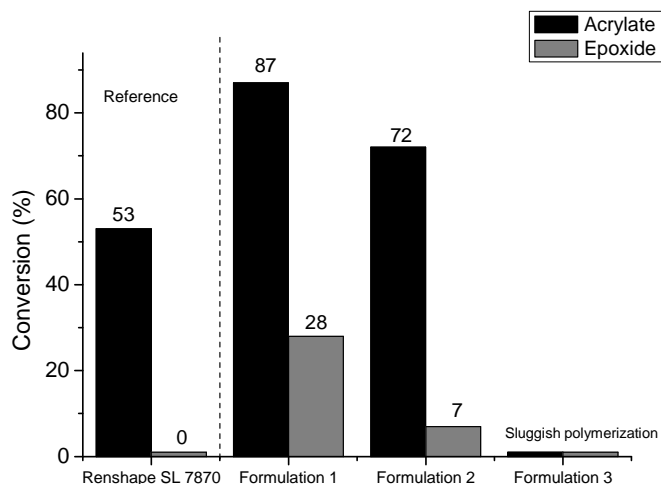


Figure II. 15: Determination of the degree of cure reached by both acrylate and epoxide monomers contained in Renshape®SL 7870 (sample thickness=0.70 mm), in formulation 1 (sample thickness=0.85 mm), formulation 2 (sample thickness=3.98 mm) and formulation 3 under Griffin curing (3 mm/s, 2 passes)

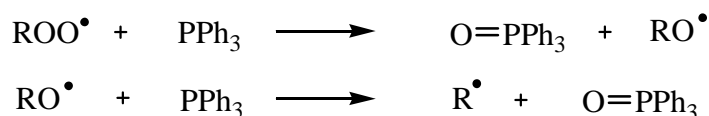
On one hand, the formulation 3 containing I 250 and 9,10-diethoxyanthracene did not reach the green strength even at low speed 3 mm/s and with 2 passes (cf Figure II. 15). This result might stem from a too slow radical polymerization because 9,10-diethoxyanthracene can not induce radical polymerization without the presence of H donor or a tertiary amine. And the phenyl radical produced during the sensitization process are highly reactive radicals that mainly react with impurities through H abstraction reaction. Their ability to induce the radical polymerization is poor. Therefore, to speed up the radical polymerization it is proposed to add a radical photoinitiator. Its triplet energy state should be lower than the 9,10-diethoxyanthracene one otherwise an energy transfer reaction might occur between them and lead to the deactivation of the radical photoinitiator. It is also advised to decrease the 9,10-diethoxyanthracene concentration to prevent any inner filter effect. On the other hand, the formulations 1 and 2 display a better reactivity than Renshape®SL 7870. The sensitization process occurring in these systems (cf in the section IV.1.3.2) is efficient because the degree of cure for the epoxide monomer could be for the first time quantified. A conversion of 30% was even reached by the epoxide in the formulation 1. Additionally, the good efficiency of I 651 quantum yield of the bond cleavage in α at 366 nm ($\epsilon_{366\text{nm}} \sim 121 \text{ L}\cdot\text{mol}^{-1}\cdot\text{cm}^{-1}$ and $\Phi_{\alpha} \sim 0.52$ ²⁴) might explain the significant improvement of the acrylate conversion. It is noteworthy to say that the sample thickness for the formulation 2 is about 4 times greater than for Renshape®SL 7870 and

the formulation 1. This is a good evidence of the efficiency of the photoinitiating system I 250/I 651. Therefore, it is in agreement with the RT FTIR experiments.

However, these enhancements are not sufficient to reach the green strength at 10 mm/s exposure speed. As a consequence, the sensitization process of the cationic photoinitiator is perhaps not the method of choice for improving the reactivity of the hybrid formulation under Griffin curing. Hence, we have decided to speed up even more the radical polymerization in order to reach more rapidly the green strength. In that purpose, an anti-oxidant was added in order to reduce the oxygen inhibitory effect.

IV.1.4 Use of triphenylphosphine for the improvement of the IPN kinetics

Triphenylphosphine (TP) is an efficient oxygen scavenger. It was shown that it might react with peroxy radicals formed by the reaction between the O₂ and the growing chain polymers and generate free radicals capable of inducing the polymerization⁹³⁻⁹⁶.



For these experiments, the concentration of TP was set up at 1.5 wt%.

Two hybrid formulations were prepared having different monomer amounts. The composition of the first formulation (formulation 4) is based on the Renshape®SL 7870 composition, in other words, it is mainly constituted by E5000. By contrast, the second one (formulation 5) mostly comprises the radical monomer SR 833S since the triphenylphosphine acts on the radical polymerization. Their compositions are detailed in Table II. 13. Renshape®SL 7870 will be used as reference.

Table II. 13: Composition in weight percentage of the formulations 4 and 5

Formulation name	E5000 (wt%)	SR 833S (wt%)	TAS (wt%)	I 184 (wt%)	TP (wt%)
Formulation 4	66.3	28.4	1.9	2	1.4
Formulation 5	28.4	66.2	1.9	2	1.5

IV.1.4.1 Trials with Griffin

The reactivity of the two above-mentioned formulations was compared during a trial with the Griffin machine at 3 mm/s speed exposure with 2 passes. The determination of the UV cured single strand final conversion was achieved with the same method described in IV.1.2.1.

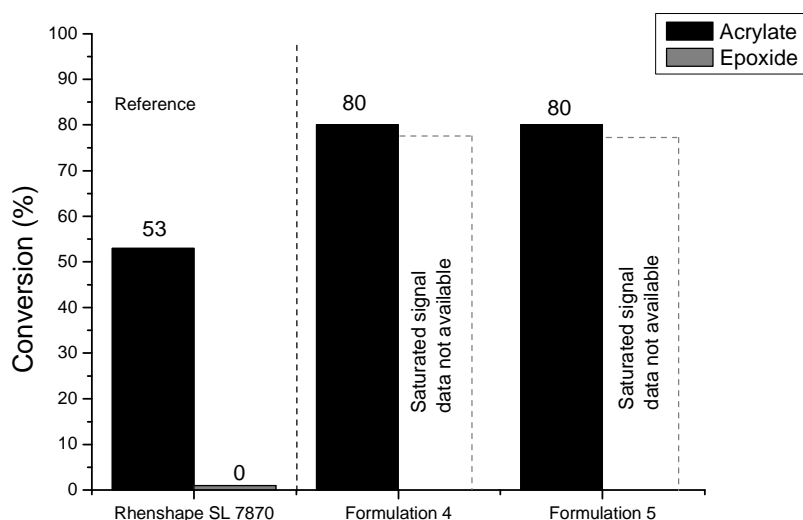


Figure II. 16: Determination of the degree of cure reached by both acrylate and epoxide monomers contained in Renshape®SL 7870 (sample thickness~0.7 mm), formulation 4 (sample thickness~8.4 mm) and formulation 5 (sample thickness~13.2 mm) under Griffin curing (3 mm/s, 2 passes)

As expected, the introduction of the anti-oxidant TP into the formulation 4 contributes to enhance by a factor 1.5 the degree of cure reached by SR 833 S in comparison to Renshape®SL 7870. Even the formulation 5 containing a high amount of SR 833S reaches 80% of conversion (cf Figure II. 16). These new formulations are clearly less sensitive towards oxygen. Almost all the liquid resin present in the aluminium dishes was photopolymerized for the formulations 4 and 5. Due to the high thickness of these samples, it was not possible to quantify the epoxy conversion. The increase in speed exposure up to 10 mm/s allowed to get thinner samples and determine the conversion for both reactive functions. The results are featured in Table II. 14.

Table II. 14: Cured sample thicknesses, and degree of cure reached by both acrylate and epoxide monomers present in the formulation 4 and in the formulation 5 under Griffin curing (10 mm/s, 1 pass)

	Cured sample thickness (mm)	Acrylate conversion (%)	Epoxy conversion (%)
Formulation 1	2.46	75	no polymerization
Formulation 5	6.39	68	no polymerization

These results are interesting because for the first time the green strength was attained for a formulation mainly constituted by epoxide at a speed exposure defined as “optimal” for Griffin applications. The sample thickness is still too important and clearly shows that the light was not enough confined. The optimization of TP concentration is thereby required.

Given the interesting results obtained with the formulations containing TP. It was decided to do some RT FTIR experiments in order to define the TP role in the photopolymerization process.

IV.1.4.2 RT FTIR spectroscopy

The RT FTIR experiments were conducted in the same experimental conditions than in IV.1.2.3. It is important to say that they do not correspond to the real processing conditions. All the details can be found in Annex I.1 and Annex II.1. The kinetics profiles in Figure II. 17 show that TP has an impact not only on the radical polymerization but also on the cationic polymerization.

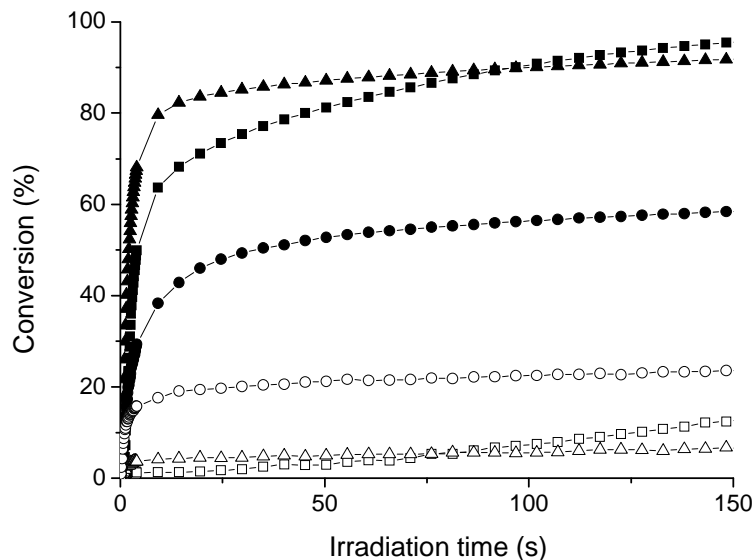


Figure II. 17: Kinetics profiles of the formulations Renshape@SL 7870 (■ acrylate double bond, □ ring epoxide), formulation 4 (▲ acrylate double bond, △ ring epoxide) and formulation 5 (● acrylate double bond, ○ ring epoxide), in air; photoinitiators: 2 wt% TAS and 2 wt% I 184; additive~ 1.5 wt% TP; Hg-Xe Hamamatsu lamp at 366 nm, light intensity=19 mW/cm²; sample thickness~35 μm

According to Table II. 15, the presence of TP greatly improves both the radical and the cationic polymerization rates of the formulation 4 compared to the Renshape®SL 7870 ones. However, this high reactivity leads to an important decrease in the epoxide conversion owing to an earlier vitrification. In addition, at high SR 833S concentration (cf formulation 5), the radical and the cationic polymerizations are almost concomitant. It seems that the increase in the reactivity of the radical polymerization impacts the cationic polymerization rate. We could assume that the heat released during the radical photopolymerization might induce the cationic polymerization.

Table II. 15: Determination of $R_{p_{max}}/[M]_0$ and the conversion at 780 s for Renshape®SL 7870, formulation 4 and formulation 5; same experimental conditions than in Figure II. 17

Formulation name	Function	$R_{p_{max}}/[M]_0$ * 100 (s ⁻¹)	Conversion (%)
Renshape®SL 7870	Acrylate	20.5	~100
	Epoxide	0.11	61
Formulation 4	Acrylate	30.8	99
	Epoxide	2.56	11
Formulation 5	Acrylate	14.5	68
	Epoxide	12.5	32

The effect of temperature must be considered with caution because during SLA building, considerable heat is released due to the exothermicity of the polymerization and the direct heating effect of the laser. The temperature in situ can reach 120°C. This result can be related to the experiments done by Crivello *et al*^{97,98} dealing with hybrid systems. They have disclosed by optical pyrometry (OP) that a local stimulus was sufficient to thermally induce the cationic polymerization and propagate the reaction within the entire sample. As a result, this temperature increase will influence not only the kinetics of polymerization but also the final properties. Therefore, we have decided to investigate on the influence of temperature on the photopolymerization process.

IV.1.5 Influence of temperature on the photopolymerization process

IV.1.5.1 RT FTIR spectroscopy

Usually, the photopolymerization process is performed at ambient temperature. But in the case of fast photopolymerization, an important amount of heat is evolved in a very short timescale which may lead to a drastic sample temperature rise⁹⁹. RT FTIR spectroscopy was found to be the most suitable technique to monitor in situ the temperature of high speed photopolymerizations of neat resins and monomer mixtures. The analyses lie in laminating the UV curable mixture between two polypropylene (PP) films used as a temperature probe^{100,101}. Indeed, the vibration band at 842 cm^{-1} ¹⁰² (rocking (r) CH_2 + stretching $\nu\text{C-CH}_3$) is sensitive to heat and decreases linearly between 20 and 110°C . During the photopolymerization process, the heat evolved is partly transferred to the PP films thereby producing a temperature change in the PP films. Assuming that the calorific capacity of the sample and the PP films are similar, the variation of the temperature of the PP film is expected to be close to the sample temperature itself. This corresponds to the quasi-adiabatic conditions. Taking into account the PP and the resin film thickness, it is possible to assess the temperature variation of the resin (ΔT_{resin}) after establishing an IR absorbance calibration curve of the 842 cm^{-1} vibration bond as a function of temperature. ΔT_{resin} can be calculated from this formula¹⁰³:

$$\Delta T_{PP} = \Delta T_{\text{resin}} \times \frac{e_{\text{resin}}}{e_{\text{resin}} + e_{PP}} \quad (\text{II.15})$$

with

ΔT_{resin} : temperature variation underwent by the resin (in $^\circ\text{C}$)

ΔT_{PP} : temperature variation underwent by PP (in $^\circ\text{C}$)

e_{resin} : cured film thickness (μm)

e_{PP} : PP thickness (μm)

By means of Decker's method, the heat released during the photoinitiated polymerization of each monomer E5000 and SR 833S has been first examined before monitoring the exothermicity during the photopolymerization of the hybrid mixture. The composition of the hybrid mixture is almost the same than for Renshape®SL 7870 (cf Table II. 16) except that the radical photoinitiator I 184 was replaced by I 819 exhibiting a better absorption at 366 nm. Therefore, this formulation will become the reference for the end of this study.

Table II. 16: Weight percentage of the different components contained in SR 833S (I 819), E5000 (TAS) and 7030 (I 819) formulations

Formulation name	E5000 (wt%)	SR 833S (wt%)	TAS (wt%)	I 819 (wt%)
SR 833S (I 819)	0	98	0	2
E5000 (TAS)	98	0	2	0
7030 (TAS+I 819)	67.2	28.8	2	2

The experiments were performed at room temperature and at 366 nm. The only difference with the previous RT FTIR experiments was that the kinetics were conducted under laminated conditions between 2 PP films. As the 842 cm^{-1} band described in literature overlaps with the one of the epoxy resins another band at 2720 cm^{-1} (C-H deformation) was taken as reference. The corresponding IR calibration curve versus temperature was established (cf Figure II. 18).

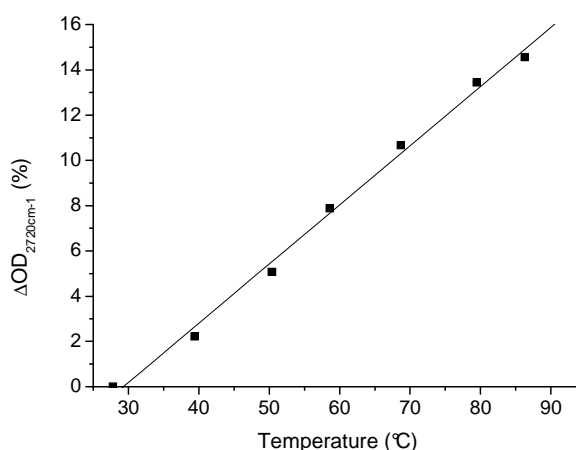


Figure II. 18: Variation of the PP absorbance at 2720 cm^{-1} as a function of temperature recorded by RT FTIR spectroscopy

➤ SR 833S (I 819)

In absence of the diffusion of atmospheric oxygen within the film, SR 833S undergoes a very fast polymerization in a very short time scale. All the kinetics data are shown in Table II. 17.

Table II. 17: $R_{p_{max}}/[M]_0$ and conversion at 450 s for the formulation SR 833S (I 819), laminated conditions; photoinitiator: 2 wt% I 819; Hg-Xe Hamamatsu lamp at 366 nm, light intensity=19 mW/cm²; sample thickness~35 μ m

Formulation name	Function	$R_{p_{max}}/[M]_0 \cdot 100 \text{ (s}^{-1}\text{)}$ *	Conversion (%)
SR 833S (I 819)	Acrylate	69	60

This high polymerization rate is responsible for a sharp increase in PP temperature (cf Figure II. 19).

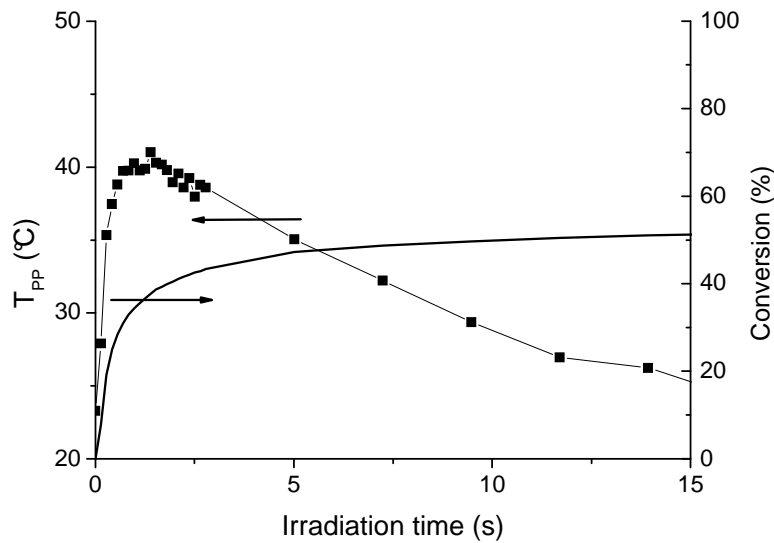


Figure II. 19: Temperature and conversion profiles monitored by RT FTIR spectroscopy of the formulation SR 833S (I 819); same experimental conditions than in Table II. 17

At the beginning of the photopolymerization, the temperature is drastically increasing until a maximum. According to the formula (II.13), the temperature reached by the resin is around 70°C. Then the temperature of PP is slightly decreasing because of vitrification and the predominance of air cooling over the heat emitted at the end of the reaction. This reaction is highly exothermic which is consistent with the experiments performed on the acrylic systems hexanediol diacrylate/polyurethane acrylate by Decker *et al*¹⁰⁰.

➤ E5000 (TAS)

The IR vibration band used for recording the epoxide polymerization was not the IR band at 910 cm^{-1} because there is an overlay between this latter and a PP IR band. As a consequence, we work with the band at 760 cm^{-1} corresponding to the symmetric epoxide stretching vibration. As shown in Figure II. 20, a slight PP temperature elevation (only a few Celsius degrees) was measured during the polymerization. The maximum temperature attained by the epoxide monomer was about 46°C .

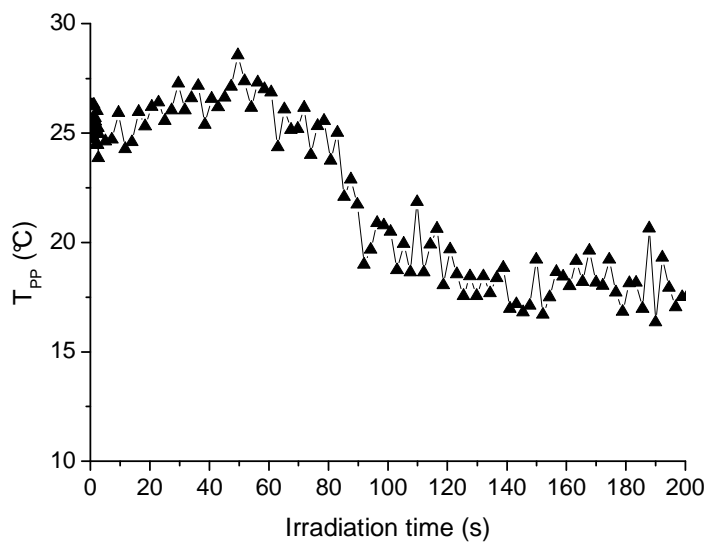


Figure II. 20: Temperature profile monitored by RT FTIR spectroscopy of the formulation E5000 (TAS); same experimental conditions than in Table II. 17

This results from the low reactivity of E5000. A $R_{p_{\max}}/[M]_0$ of $0.34 \cdot 10^{-2}\text{ s}^{-1}$ was determined (cf Table II. 18).

Table II. 18: Determination of $R_{p_{\max}}/[M]_0$ and the conversion at 450 s for the formulation E5000 (TAS), laminated conditions; photoinitiator: 2 wt% TAS; Hg-Xe Hamamatsu lamp at 366 nm, light intensity= 19 mW/cm^2 ; sample thickness= $35\text{ }\mu\text{m}$

Formulation name	Function	$R_{p_{\max}}/[M]_0^*$ $100\text{ (s}^{-1}\text{)}$	Conversion (%)
E5000 (TAS)	Epoxide	0.34	46

➤ 7030 (TAS+I 819)

The experiment was also achieved with the hybrid system 7030 (TAS+I 819). Despite a SR 833S concentration of only 30wt%, the temperature profile looked like the one of the acrylic resin SR 833S (I 819) (cf Figure II. 21). From the temperature profile in Figure II. 19, it was calculated that the hybrid formulation temperature reached the maximum value of nearly 73°C during the photopolymerization process.

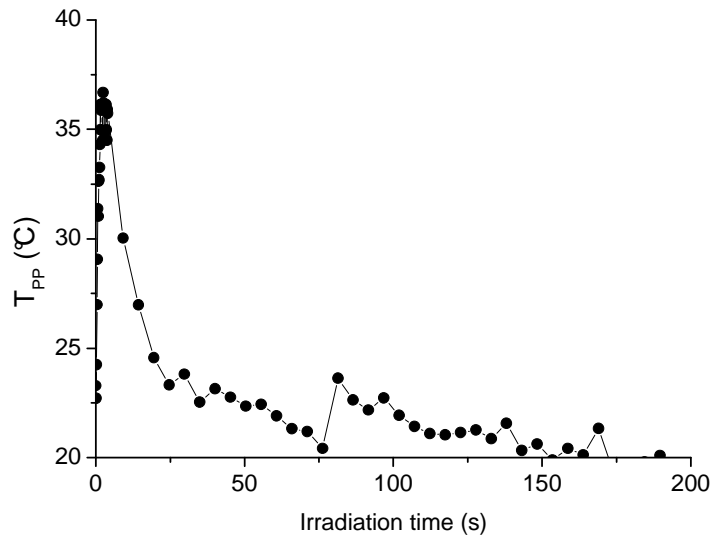


Figure II. 21: Temperature profile monitored by RT FTIR spectroscopy of the formulation

7030 (I 819); same experimental conditions than in Table II. 18

It was proved from these experiments that an elevated temperature could be reached by the hybrid resin during the photopolymerization. Therefore, this exothermicity might be responsible for the slight rise in the cationic $R_{p_{max}}/[M]_0$ in the hybrid system as regards to the result obtained in the neat epoxide resin (cf. Table II. 18 and Table II. 19). This local heat stimulus seems to play a role only at the very beginning of the cationic photopolymerization process because the fast formation of the high crosslinked acrylic network might limit its effect.

Table II. 19: Determination of $R_{p_{max}}/[M]_0$ and the conversion at 450 s for the formulation 7030 (TAS+I 819), laminated conditions; photoinitiators: 2 wt% I 819+ 2wt% TAS; Hg-Xe Hamamatsu lamp at 366 nm, light intensity=19 mW/cm²; sample thickness~35 μm

Formulation name	Function	$R_{p_{max}}/[M]_0$ * 100 (s ⁻¹)	Conversion (%)
7030 (TAS+I 819)	Acrylate	56	92
	Epoxide	0.5	39

Previously, we put forward that a non negligible heat was evolved during the photopolymerization of the hybrid system. However, the effect of the heat stimulus was limited by the glassy state of the polyacrylate network. In order to study the influence of the temperature on the IPN formation kinetics, we performed by means of photo Differential Scanning Calorimetry (photoDSC) a set of isotherm experiments at different temperatures.

IV.1.5.2 PhotoDSC experiments

The samples were photocured with DSC Q200 equipped with a photocalorimetry accessory from TA instruments under nitrogen atmosphere (50 mL/min). The description of this technique is given in Annex II.2. They were placed in uncovered aluminium hermetic pans. The sample weight was about 10 mg. A special attention was paid to the sample preparation to get a flat surface to optimize the heat transfer with the pan. The experiments could not be performed at 366 nm as previously. The samples were irradiated by a broadband Hamamatsu lamp whose light intensity was about 21 mW/cm².

The temperature effect was assessed by performing the epoxide photopolymerization over a range of temperature isotherms (25°C, 45°C and 65°C). The conversion was calculated from the formula (II.14) corresponding to the ratio between the reaction enthalpy (ΔH_t) and the theoretical total heat of reaction ($\Delta H'_{\text{theoretical}}$)¹⁰⁴.

$$X_t = \frac{\Delta H_t}{\Delta H'_{\text{theoretical}}} \times 100 \quad (\text{II.16})$$

$\Delta H'_{\text{theoretical}}$ was calculated according to this relation:

$$\Delta H'_{\text{theoretical}} = \frac{f \times E \times x_M}{M} \quad (\text{II.17})$$

with

f, the monomer functionality

E, the energy necessary to open the diglycidyl ether ring was taken as 76 kJ/mol⁻¹

x_M , the monomer fraction within the formulation

M, the monomer molecular weight

➤ E5000 (TAS)

Figure II. 22 presents the evolution of the E5000 conversion versus the irradiation time and the medium temperature.

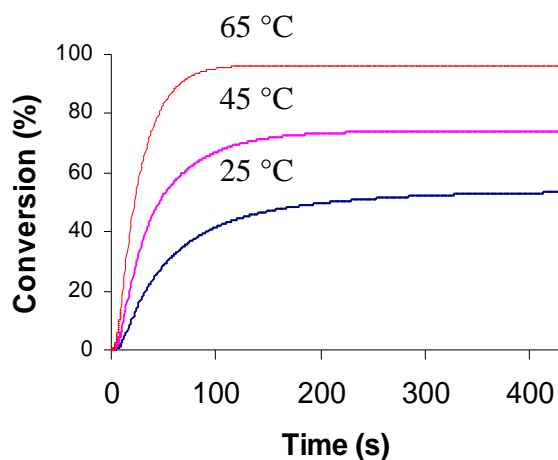


Figure II. 22: Kinetics of photopolymerization of E5000 (TAS) formulation versus irradiation time at 25°C, 45°C and 65°C; N₂ atmosphere, sample weight~10 mg, Hg-Xe Hamamatsu lamp, 21 mW/cm²

As shown in Figure II. 22 and in Table II. 20, the higher the temperature, the better both $R_{p_{max}}/[M]_0$ and conversion at 450 s. A nearly complete polymerization is achieved at the isotherm 65 °C ($R_{p_{max}}/[M]_0$ was multiplied by 3.6 and the degree of cure by 1.8 regarding the values found at room temperature). In fact, the increase in temperature decreases the viscosity of the system and thereby promotes the mobility of the reactive species and also the cleavage reaction.

Table II. 20: Variation of $R_{p_{max}}/[M]_0$ and conversion at 450 s for the formulation E5000 (TAS), according to isotherm temperature; same experimental conditions than in Figure II. 22

	$R_{p_{max}}/[M]_0 \cdot 100 \text{ (s}^{-1}\text{)}$ *	Conversion (%)
Isotherm at 25°C	0.80	53
Isotherm at 45°C	1.64	74
Isotherm at 65°C	2.91	96

With the kinetic profiles previously found at different reaction temperatures, it was possible to calculate the activation energy of the cationic polymerization. The calculation is based on the Arrhenius law:

$$k = Ae^{-\frac{E_a}{RT}} \quad (\text{II.18})$$

with

k , the cationic polymerization rate constant, $\text{L}\cdot\text{mol}^{-1}\cdot\text{s}^{-1}$

A , the pre-exponential factor, $\text{L}\cdot\text{mol}^{-1}\cdot\text{s}^{-1}$

E_a , the activation energy, $\text{J}\cdot\text{mol}^{-1}$

R , the gas constant, $\text{J}\cdot\text{mol}^{-1}\cdot\text{K}^{-1}$

T , the absolute temperature, K

To simplify this calculation, an Arrhenius plot was constructed from the logarithm of the maximum cationic polymerization rates, $\ln R_{p_{\max}}$ as a function of $1/T$. As shown in Figure II. 23, the plot is linear that is to say the system obeys to the Arrhenius equation. The activation energy corresponds to the slope of the straight line. It was found to be equal to $27 \text{ kJ}\cdot\text{mol}^{-1}$. This value is reasonably close to the one reported by Abadie *et al*¹⁰⁵ for the polymerization of the diglycidyl ether of bisphenol A cured under UV light in presence of Cyacure UVI-6974 ($33 \text{ kJ}\cdot\text{mol}^{-1}$). This implies that the maximum polymerization rate is multiplied by about 2 when the temperature rise is about 20°C .

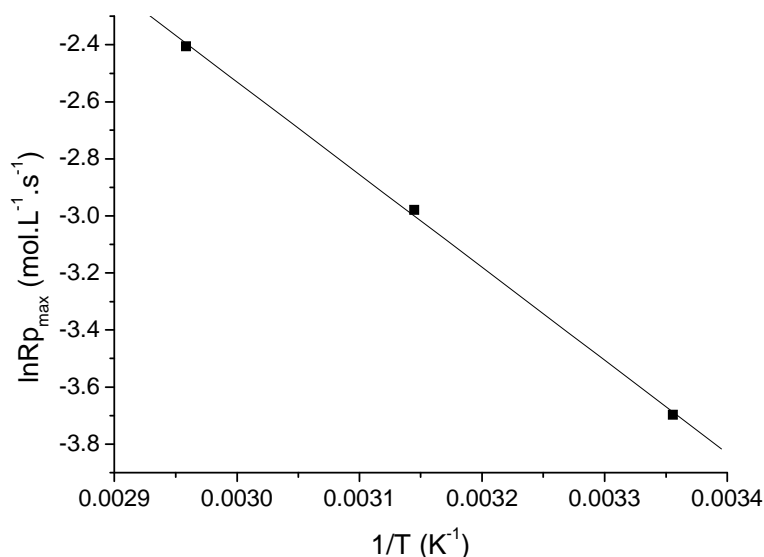


Figure II. 23: Arrhenius plot $\ln R_{p_{\max}}$ versus $1/T$ for the cationic system E5000 (TAS) cured at 3 different temperatures 25°C , 45°C and 65°C

➤ SR 833S (I 819)

The effect of the reaction temperature on the kinetics of photopolymerization for the neat radical system SR 833S (I 819) was also evaluated. As shown in Figure II. 24, the system seems to be less sensitive towards temperature than the epoxide system.

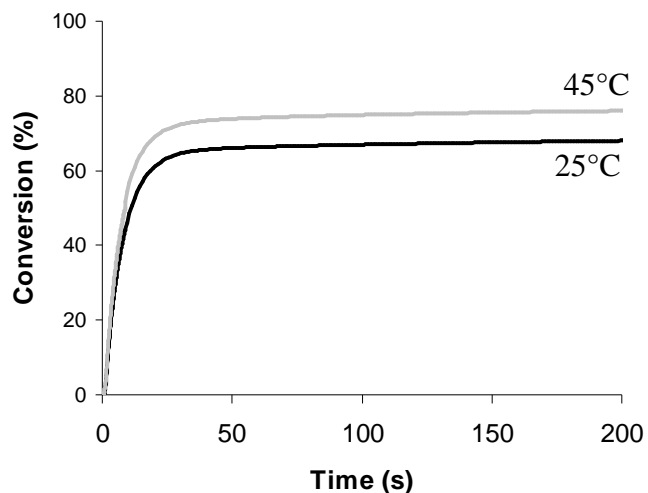


Figure II. 24: Kinetics profiles of SR 833S (I 819) formulation versus irradiation time at 25°C and 45°C; N₂ atmosphere; sample weight~10 mg; Hg-Xe Hamamatsu lamp, 21 mW/cm²

Only a slight increase in both $R_{p_{max}}/[M]_0$ and the final conversion (1.2 times higher for both kinetics parameters) was observed at 45°C. These results are consistent with the experiments performed by *Decker et al*¹⁰⁶ at room temperature and at 70°C. The kinetics profiles were almost the same at these two temperatures. These similarities were explained by the fact that the acrylate systems undergo such a fast polymerization that the thermal runaway might occur after the beginning of the polymerization process and therefore might not influence the kinetics of photopolymerization.

Table II. 21: Variation of $R_{p_{max}}/[M]_0$ and conversion at 230 s for the formulation SR 833S (I 819), according to isotherm temperature; same experimental conditions than in Figure II. 24

	$R_{p_{max}}/[M]_0 \cdot 100 \text{ (s}^{-1}\text{)}$ *	Conversion (%)
Isotherm at 25°C	7.89	68
Isotherm at 45°C	9.36	76

➤ 7030 (TAS+I 819)

We were not able to carry out the experiments for the hybrid formulation 7030 (TAS+I 819) because the photoDSC device measures the total reaction enthalpy without distinguishing the polymerization enthalpy of each monomer. As a result, it was not possible to follow separately the conversion of each monomer according to the time at a given temperature. The ideal would be to use the RT FTIR spectrometer, the tool of choice for monitoring the conversion in hybrid system, under a controlled temperature. A Linkam accessory that allows a temperature control has been purchased very recently by the DPG and it would be interesting to combine it with the RT FTIR spectrometer and see how the temperature can affect both the kinetics and the sequence order of the radical and the cationic photopolymerizations. Subsequently, the effect of humidity on the IPN formation could be also investigated.

We have seen that the temperature could affect the kinetics of photopolymerization in particular for the epoxide system. The temperature rise could not only enhance the cationic polymerization rate but also promote the molecular mobility and yield to higher final conversion. It will be interesting now to see how these changes in the kinetics of photopolymerization for the neat and the hybrid systems can impact the final properties of the material such as T_g and their morphology.

IV.1.6 Characterization of the final properties

IV.1.6.1 Thermomechanical properties

After the UV curing with the photoDSC (cf experimental conditions in IV.1.5), the pans were hermetically sealed. The determination of the photopolymer glass transition temperature (T_g) of each individual monomer and the hybrid formulation was carried out with the same apparatus but with the Modulated Differential Scanning Calorimetry option (MDSC) from TA instruments. The principle of MDSC is described in detail in Annex III.2. The temperature was ramped at 2°C/min from -50°C to 250°C and modulated at \pm 2°C/min every 60s. The DSC traces were exploited with the Universal Analysis program from TA instruments.

➤ E5000 (TAS)

During the first MDSC run, two T_g s were detected for the samples cured at 25°C and 45°C whereas only one T_g was determined for the sample cured at 65°C (cf Table II. 22). These differences can be ascribed to the final conversion reached by the material after the photoDSC experiments. Indeed, the sample cured at 65°C has undergone a nearly complete polymerization (96 % of conversion). By contrast, the other samples are partially cured. The increase in temperature enhances the mobility of the unconverted monomer which results in higher conversion ratio and a structural rearrangement. To confirm this assumption a second run was performed under the same experimental conditions. As presented in Table II. 22, no matter the reaction temperature, after the second run, only a single T_g was measured at a lower temperature range than for the first trial. In fact, the first temperature ramp was used to achieve a complete reaction and the second run to properly determine the T_g . According to the data obtained during the 2nd run in Table II. 22, by increasing the curing temperature, the degree of cure is enhanced as well as the T_g s to a certain extent.

Table II. 22: Determination of the conversion at 430 s and the glass transition temperatures after 2 runs at 25°C, 45°C and 65°C for the formulation E5000 (TAS)

	Conversion (%)	T_g (°C) 1 st run	T_g (°C) 2 nd run
Isotherm at 25°C	53	50 79	45
Isotherm at 45°C	74	59 78	46
Isotherm at 65°C	96	76	52

➤ SR 833S (I 819)

Similar investigations were carried out for SR 833S monomer. The samples cured under inert atmosphere reached prominent degree of cure as seen in Table II. 23. Despite several attempts, it was not possible to determine a T_g . As a matter of fact, the reversing signal keeps decreasing but the slope does not sharply change. The weak mobility of the polymer chains even under high temperature could be attributed to the high crosslinking density of the material and to the presence of the rigid and bulky tricyclodecane group within the SR 833S backbone.

Table II. 23: Determination of the conversion at 230 s and the glass transition temperatures after 2 runs at 25°C and 45°C for the formulation SR 833S (I 819)

	Conversion (%)	T _g (°C) 1 st run	T _g (°C) 2 nd run
Isotherm at 25°C	68	Not available	Not available
Isotherm at 45°C	76	Not available	Not available

➤ 7030 (TAS+I 819)

The assessment of the T_g value for the hybrid system 7030 (TAS+I 819) was difficult to obtain because the decrease in the MDSC signal occurs in a large temperature range. For the reasons previously mentioned, SR 833S might be taken as responsible.

The previous experiments confirmed the sensitivity of epoxides towards the temperature. Indeed, the increase in temperature led to a more crosslinked material. MDSC allowed the evaluation of the T_g of pure cationic system. By this way, we have demonstrated that the control of the curing temperature during the build-up of a part is of prime importance because it influences both the kinetics process and the final conversion. However, it was not possible to determine the T_gs for pure acrylic and for the hybrid systems. The presence of bulky and rigid tricyclodecane moieties of SR833 S reducing the motions of the polymer chains during the temperature ramp might account for these results. As a complement, SEM was used to study the morphology of the hybrid materials. It may be possible to quantify the phase segregation phenomenon.

IV.1.6.2 IPN morphology

The investigation of IPN morphology was carried out for different E5000/SR 833S ratios 70/30 and 30/70 in order to underline the influence of each component on the internal structure of the hybrid system. The composition of these two formulations can be found in Table II. 24.

Table II. 24: Weight percentage of the components within the formulations 7030 (TAS+I 819) and 3070 (TAS+I 819)

Components	E5000 (wt%)	SR 833S (wt%)	TAS (wt%)	I 819 (wt%)
7030 (TAS+I 819)	67.2	28.8	2	2
3070 (TAS+I 819)	28.8	67.2	2	2

The samples were cured under broadband irradiation with the UV belt conveyor. Transparent tacky free films of respectively 37 μm for 7030 (TAS+I 819) sample and 39 μm for 3070 (TAS+I 819) were obtained. Their morphology was analyzed by SEM by viewing the fracture surface at a magnification of 25000 x. The details concerning the sample preparation and the curing are described in Annex IV.1.

The micrographs in Figure II. 25 reveal that the morphology of IPNs differs with the composition. For the sample 7030 (TAS+I 819), the micrograph in Figure II. 25a indicates the presence of 1 μm -diameter nodules which is a clear evidence that the phase separation phenomenon occurs. Given that E5000 is the major component, one can suppose that the matrix is made with the polyether network and the dispersed phase is the polyacrylate network. According to the kinetics profiles obtained at 366 nm, we could assume that the first network formed under broadband irradiation might be the polyacrylate one and this latter might be not miscible in the cationic system or the phase separation phenomenon might occur before the completion of the polyether network. By contrast, for the sample 3070 (TAS+I 819), no phase segregation was identified in the micrograph in Figure II. 25b. In that case, the main component is the acrylate system. As it polymerizes faster than the epoxide monomer, it might constitute a continuous phase.

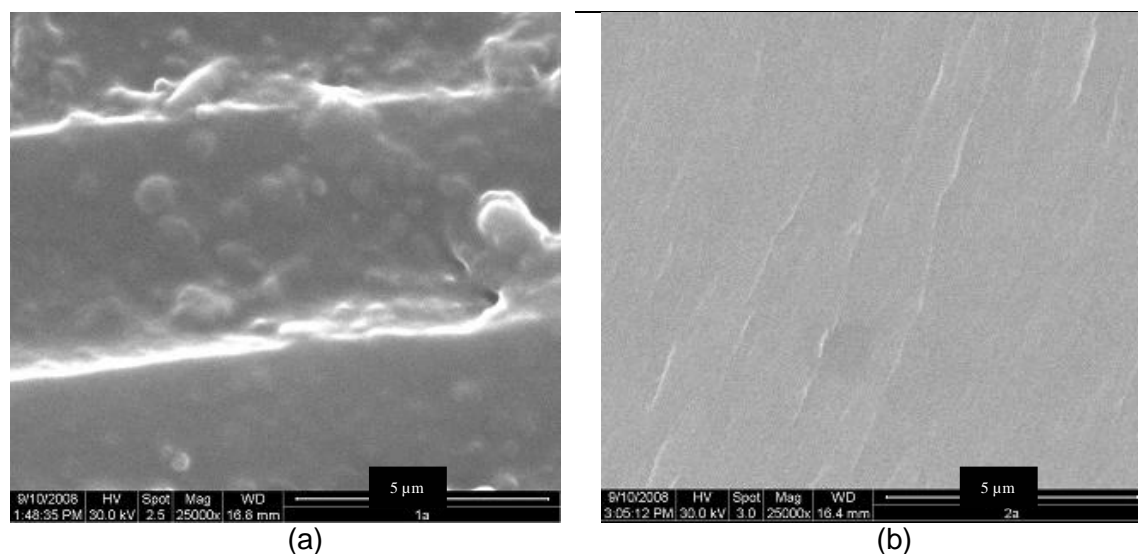


Figure II. 25: SEM micrographs of the formulation 7030 (TAS+I 819) at a thickness of 36.5 μm (a) and of the formulation 3070 (TAS+I 819) at a thickness of 38.6 μm (b); broadband irradiation under UV belt conveyor, 1.2 J/cm²

The visualization of the ruptures surfaces by SEM can also give some indications about the mechanical properties. In Figure II. 26a, the micrograph of the UV cured sample with a high epoxide content (7030 (TAS+I 819)) shows brittle failure with important crack lines whilst at high acrylate monomer concentration, the micrograph in Figure II. 26b exhibits a clean fracture typical of a ductile material.

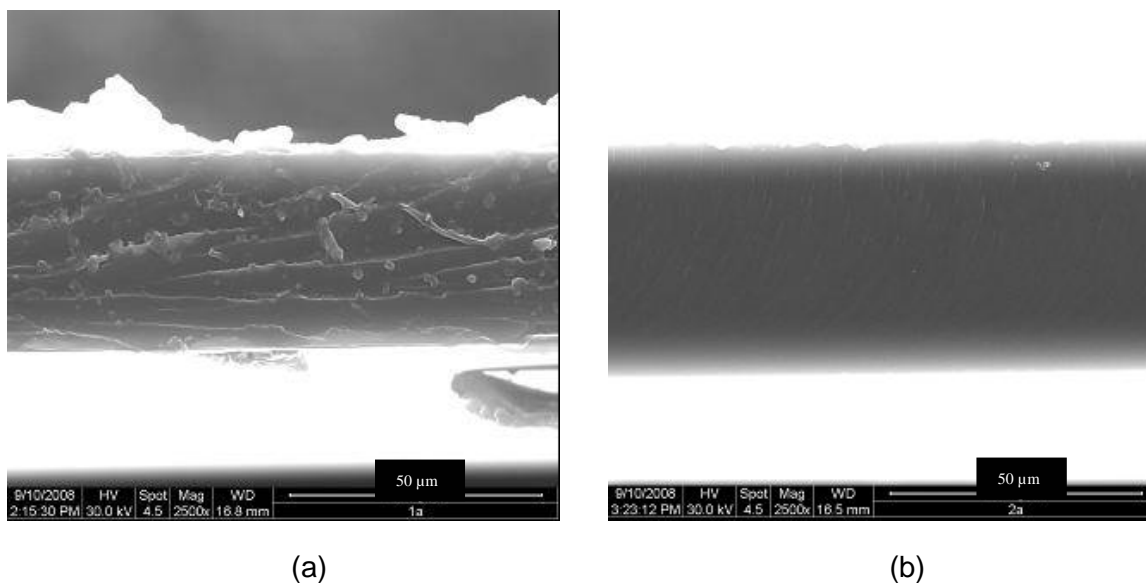


Figure II. 26: Micrographs of the rupture surfaces of the formulation 7030 (TAS+I 819) at a thickness of 36.5 μm (a) and of the formulation 3070 (TAS+I 819) at a thickness of 38.6 μm (b), broadband irradiation under UV belt conveyor, 1.2 J/cm²

Besides the Huntsman project, an academic study was performed in the laboratory which gave results that are interesting to be reported here.

IV.2 Academic study on the formation of quasi-simultaneous IPNs between a cycloaliphatic epoxide and a methacrylate

In this part, we will try to understand how the relative radical and cationic polymerization rates influence the network formation and therefore the mechanical properties of the created IPNs. To the best of our knowledge, a clear picture relating the relative kinetics formation of the networks and the IPN network structures for simultaneous UV cured IPNs has not been evidenced, and the corresponding effect on the final properties was not discussed. The aim of this study is to control the kinetics of formation of IPNs. Therefore, monomers have been selected in order to increase the cationic polymerization rate and to reduce the radical polymerization rate: a cycloaliphatic epoxide and a methacrylate ((1:1) weight ratio). It is worth noting that a methacrylate was employed instead of an acrylate because methacrylates are known to have a lower reactivity than the acrylates. Besides, cycloaliphatic epoxides are known to be more reactive than diglycidyl ether epoxides. As a consequence, the difference in reactivity between the dimethacrylate and the cycloaliphatic diepoxide will be minimized. The influence of the kinetics of IPN formation on the morphology, the phase separation and the composition of the final material were studied for different experimental conditions.

IV.2.1 Compounds

The monomers selected for this study are an ethoxylated (3) bisphenol A dimethacrylate from Sartomer (DAC, viscosity=550-1700 mPa.s at 25°C), and a 3,4-epoxycyclohexylmethyl-3',4'-epoxycyclohexylcarboxylate from Dow Chemical (DEP, viscosity=350-450 mPa.s at 25°C). The radical photo initiator 2-hydroxy-2-methyl-1-phenyl-propan-1-one (D 1173) was obtained from Ciba and the cationic photoinitiator triarylsulfonium hexafluoroantimonate salts (TAS) was purchased from Aldrich. All these compounds were used without any further purification. Their chemical structures are shown in Table II. 25.

Table II. 25: Chemical structures of the methacrylate, the cycloaliphatic epoxide, the radical photoinitiator and the cationic photoinitiator

Chemical name	Chemical structure
Ethoxylated (3) bisphenol A dimethacrylate (DAC)	
3,4-epoxycyclohexylmethyl-3',4'-epoxycyclohexylcarboxylate (DEP)	
2-hydroxy-2-methyl-1-phenyl-propan-1-one (D 1173)	
Triarylsulfonium hexafluoroantimonate mixture salts (TAS)	

The composition of all the tested mixtures in this part is summarized in Table II. 26.

Table II. 26: Composition in weight percentage of the different runs

Run	DAC concentration (wt%)	D 1173 concentration (wt%)	DEP concentration (wt%)	TAS concentration (wt%)
1; 7	99.5	0.5	-	-
2; 8	-	-	99	1
3	98.5	0.5	-	1
4; 9	49.5	0.5	49	1
5; 10	49	1	49	1
6; 11	48	2	49	1

This part of the study will be performed with a broadband irradiation source in order to ensure that both photoinitiating systems would absorb efficiently the light. Then, a monochromatic irradiation will be employed in order to modulate the relative reactivity of the epoxide and methacrylate functions.

IV.2.2 Kinetics study under broadband irradiation

At first, IPN formations were performed under broadband exposure using an Hg-Xe light source. In that case, one can expect the formation of simultaneous UV cured IPNs, the polymerization of both monomers occurring at the same time, limiting the phase separation. As a consequence, homogeneous material may be formed, enhancing the miscibility between the polymer blends and leading to better mechanical properties.

IV.2.2.1 Photopolymerization of the starting monomers

The kinetics of photopolymerization were studied by RT FTIR spectroscopy for each monomer as mixtures comprising respectively 0.5 wt% of D 1173 in DAC (Run 1) and 1 wt% TAS in DEP (Run 2), respectively. The conversion data were obtained by monitoring the decay of the IR absorption bands at 1637 cm^{-1} for the methacrylate ($\text{C}=\text{CH}_2$ stretching vibration mode)¹² and the IR absorption bands from 768 cm^{-1} to 805 cm^{-1} for the epoxide (symmetrical stretching of the epoxide ring)¹⁷. The samples were exposed to the polychromatic light of a Hamamatsu Hg-Xe lamp with a selected intensity reduced to 70 mW/cm^2 (cf Annex I.1 and Annex II.1).

As can be seen from Figure II. 27 and Table II. 27, both the neat methacrylate (Run 1) and the neat epoxide (Run 2) lead to a low final conversion. The final conversion of the methacrylate monomer hardly reaches 40 % after 630 s of exposure, and the corresponding value for the neat epoxide is 60% after 630 s of exposure. This effect might be attributed to the vitrification of the medium, as the photopolymerization reaction is known to stop when the material is at the glassy state. The radical photopolymerization proceeds at a slower rate (20 times slower than for the acrylate polymerization in Renshape®SL 7870) with a more important inhibition time due to the presence of oxygen. Indeed, it is well known that oxygen strongly inhibits free radical photopolymerization by scavenging the photoinitiator triplet state and both the initiating and the propagating radicals. The quantity of initiating species generated through the photolysis of only

0.5 wt% of D 1173 is so low that most of the initiating radicals are involved in oxygen scavenging rather than initiation process.

Although the $R_{p_{max}}/[M]_0$ value for the cationic system is 5 times higher than the value found for the radical one (cf Table II. 27) and at least 10 times higher than for the diglycidyl ether epoxide E5000, the epoxy function are not fully cured. The reaction rate slow down after a few second, but the polymerization continues to evolve in the dark.

As the photolysis of the cationic photoinitiator is responsible for both the formation of a strong acid and radical, the presence of TAS in a formulation containing a methacrylate can participate to the photopolymerization of the later. In order to check the impact of the cationic photoinitiator on the radical polymerization an experiment (Run 3) focusing on the free radical photopolymerization of the methacrylate in the presence of both D 1173 and TAS was performed (cf Figure II. 27). It appears from Table II. 27 that the free radicals from the TAS photolysis only slightly contributes to an increase in the $R_{p_{max}}/[M]_0$ and the final conversion.

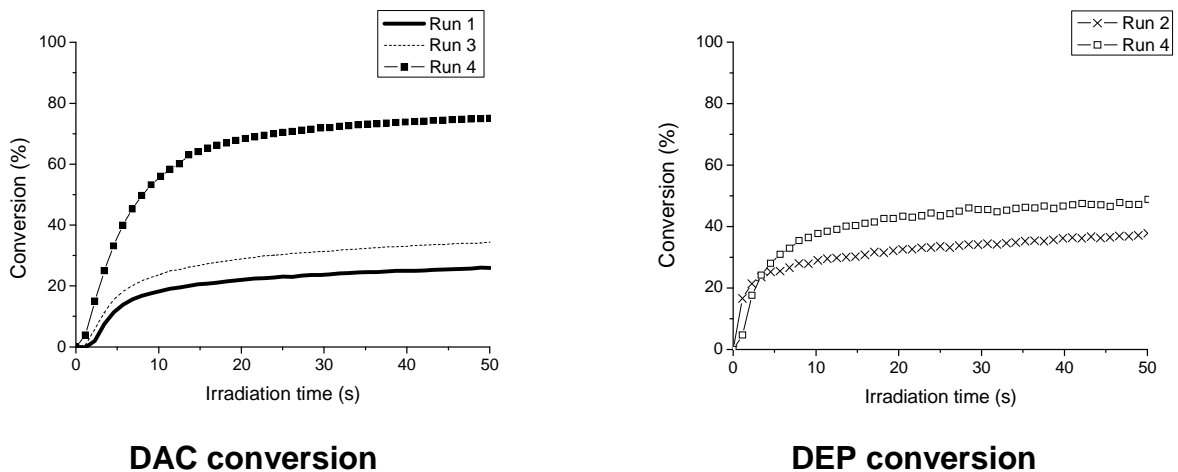


Figure II. 27: Conversion profiles of the neat resins (Runs 1 to 3) and the hybrid mixture (Run 4) under broadband exposure, light intensity $\sim 70 \text{ mW/cm}^2$, sample thickness $\sim 35 \mu\text{m}$

Table II. 27: $R_{p_{max}}/[M]_0$ and conversion at 630s for the neat resins and the hybrid formulations; same experimental conditions than in Figure II. 27

Run	$R_{p_{max}}/[M]_0 * 100 \text{ (s}^{-1}\text{)}$		Conversion (%)	
	DAC	DEP	DAC	DEP
Run 1	3	-	39	-
Run 2	-	15	-	60
Run 3	4	-	48	-
Run 4	10	11	85	62
Run 5	14	13	87	64
Run 6	19	13	97	66

IV.2.2.2 Photopolymerization of the hybrid mixture

When both monomers are mixed in equiweight ratio in presence of 0.5 wt% of D 1173 and 1 wt% of TAS (Run 4), the photopolymerization kinetics of both methacrylate and epoxide resins were found to occur simultaneously as shown by the similar $R_{p_{max}}/[M]_0$ value (cf Table II. 27). Moreover, a good conversion for the methacrylate was achieved in this mixture, with a final conversion of 85% after 630 seconds of exposure compared to the 40% for the neat resin in the same conditions. This result is mainly explained by the fact that the photopolymerization process takes places for both methacrylate and epoxide, the viscosity of the medium increases rapidly, thereby limiting the effect of oxygen inhibition of the free radical photopolymerization by decreasing the diffusion of oxygen. This phenomenon has already been observed in confocal Raman spectroscopy⁶⁸.

In the meantime, the epoxide polymerization is barely affected by the presence of the radical system as it was the case for the acrylate in the first part of this Chapter.

These experiments show that the photopolymerization of the methacrylate resin in the hybrid mixture is much more effective than the photopolymerization of the neat resins with the corresponding photoinitiators leading to a comparable polymerization rate for DAC and DEP. A variation of the radical photoinitiator content in the formulation will be done in order to modify the radical polymerization and to increase the DAC final conversion.

➤ Effect of radical photoinitiator concentration

Some attempts were made to affect the IPN formation by changing the concentration of one photoinitiator with respect to the other one. It is expected that the absorption of the light will be different affecting the relative polymer kinetics of both radical and cationic systems. Therefore, the radical photoinitiator amount was varied from 0.5 wt% to 2 wt%, keeping constant the cationic photoinitiator concentration to 1 wt% Table II. 26. The impact of this variation on the kinetics profiles of both reactive functions is shown in Figure II. 28.

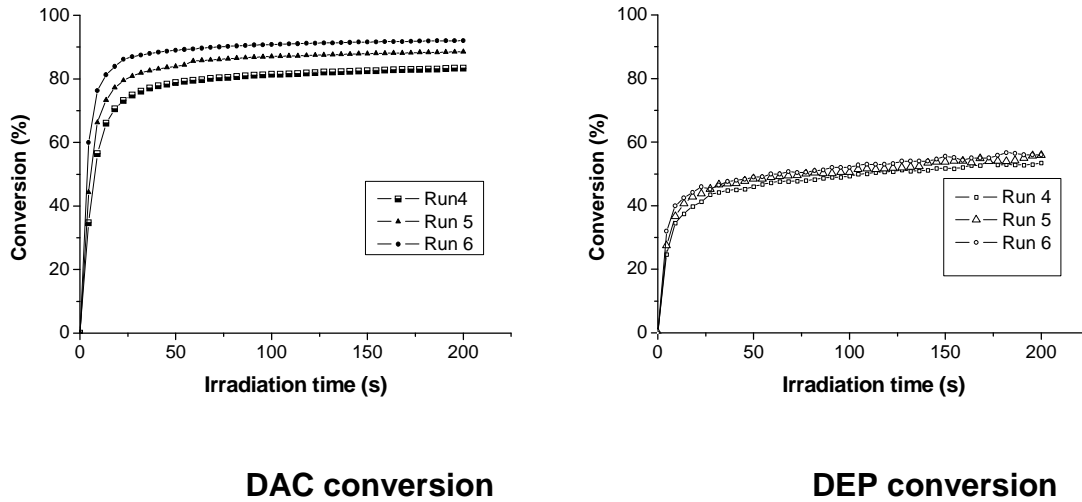


Figure II. 28: Influence of the concentration of the radical photoinitiator on the photopolymerization kinetics of DAC and DEP under a broadband exposure, light intensity $\sim 70 \text{ mW/cm}^2$

From the results collected in Table II. 27, it can be seen that the increase in D 1173 concentration contributed to improve noticeably both $R_{p_{\max}}/[M]_0$ as well as the final conversion for the methacrylate. This effect is merely attributed to the increase of the absorbed light with increasing the D 1173 concentration, thereby resulting in increasing the initiating rate R_i (cf formula II.1 and II.2). Therefore, the enhancement of the polymerization extent arises from the increasing formation of initiating species. By contrast, the variation of the radical photoinitiator concentration has only a slight impact on the kinetics of the epoxide photopolymerization increasing slightly both $R_{p_{\max}}/[M]_0$ and conversion probably due to the exothermicity of the radical polymerization (cf Table II. 27). From these experiments, it can be concluded that whatever the radical photoinitiator content (between 0.5 wt% and 2 wt%), the epoxide polymerization proceeded quite as fast as the methacrylate one, and the photopolymerization of the later is noticeably affected. In order to increase the difference in reactivity between the cationic and the radical photopolymerization in UV cured IPNs, a monochromatic irradiation was selected. By adjusting the radical photoinitiator content, the sequence order of the two systems can be changed.

IV.2.3 Kinetics study at 366 nm exposure

As seen above, broadband exposure does not affect strongly the photopolymerization kinetics. Therefore, it was decided to study the formation of IPNs under monochromatic exposure at 366 nm (the light intensity is about 15 mW/cm²) for which the two photoinitiators exhibit very different absorption properties (cf Annex I.1 and Annex II.1).

IV.2.3.1 Photopolymerization of the starting monomers

Again, the photopolymerization of each individual monomer and of the hybrid methacrylate/epoxide mixture were monitored. Results are collected in Table II. 28.

Table II. 28: $R_{p_{max}}/[M]_0$ and conversion at 630s for the neat resins and the hybrid formulations; at 366 nm, light intensity~15 mW/cm², 35 μ m

Run	$R_{p_{max}}/[M]_0 * 100 (s^{-1})$		Conversion (%)	
	DAC	DEP	DAC	DEP
Run 7	0.01	-	8	-
Run 8	-	1.3	-	61
Run 9	1.1	1.6	45	85
Run 10	1.6	1.7	56	88
Run 11	4.1	2.3	72	82

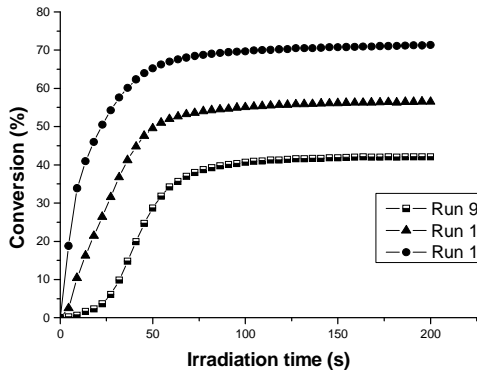
Again at 366 nm with a reduced light intensity and in presence of air, the $R_{p_{max}}/[M]_0$ of the methacrylate resin was low and the final degree of cure hardly reached 8% (Run 7). This lack of efficiency can be explained as before by the effect of oxygen which is quite pronounced due to the thin sample thickness (~35 μ m), the low photoinitiator concentration (0.5 wt%), the low light intensity and the value of the extinction coefficient of D 1173 which was measured to be about 10 L. mol⁻¹.cm⁻¹ at 366 nm in acetonitrile.

As regards to the polymerization of the neat epoxide (Run 8), it was observed to take place more rapidly than for the methacrylate Run 7. The polymerization rate is 100 times higher and the degree of cure reached after 630 s of illumination is 61%. DEP readily polymerizes since the TAS extinction coefficient value is relatively important: the value for TAS is 109 L.mol⁻¹.cm⁻¹ at 366 nm in acetonitrile. In addition, the system is not inhibited by oxygen, and the presence of an induction period rather depends on the presence of moisture (few seconds).

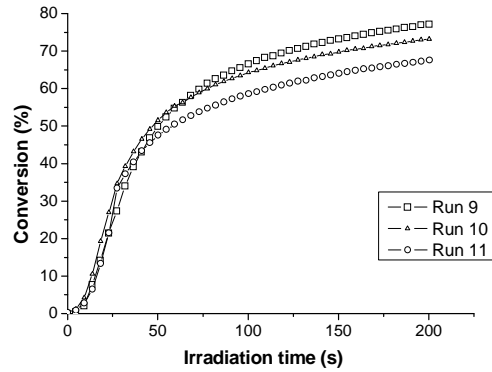
IV.2.3.2 Photopolymerization of the hybrid mixture➤ Effect of radical photoinitiator concentration

Turning now to the curing of the hybrid system, the effect of the concentration in radical photoinitiator on the kinetics profiles of both the methacrylate and the epoxide photopolymerizations is illustrated in Figure II. 29.

1)



DAC conversion



DEP conversion

2)

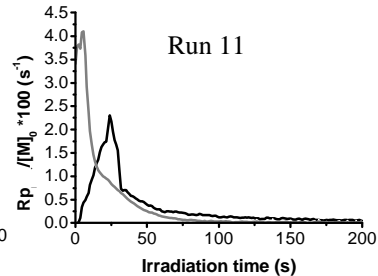
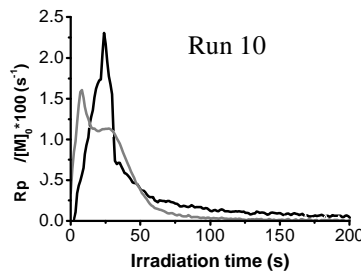
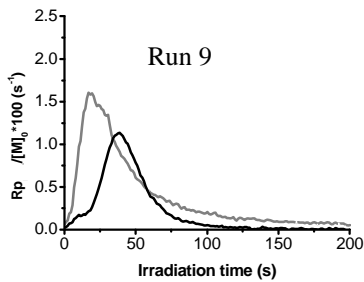


Figure II. 29: 1) Influence of the radical photoinitiator concentration on the kinetics of photopolymerization of DAC (SR 348C) and DEP (UVR 6110) at 366 nm, 15 mW/cm². 2) $R_p/[M]_0$ versus time curves: black for DAC, grey for DEP at 366 nm, 15 mW/cm²

The plots of the $R_p/[M]_0$ vs irradiation time have been calculated from the slope of the conversion curve at each time. It allows us to follow the evolution of the polymerization rate with time and with the evolving networking formation. This leads to a different approach of the polymerization process which can be divided into three steps. The first step is the autoacceleration process. The increase in the medium viscosity increases the efficiency of the propagation reaction until a maximum is reached (Trommsdorff effect). Then, the $R_p/[M]_0$ value is levelled off to a maximum value during a short time interval because the propagation starts to be diffusion controlled. Finally, the polymerization rate drops down due to the vitrification phenomenon which finally stops the reaction.

From Run 9, it can be seen that the presence of the epoxide greatly improves both the methacrylate $R_{p_{max}}/[M]_0$ and the final conversion compared to the one of the neat methacrylate formulation for the same reason as above-mentioned. As before, for the cationic system, neither the polymerization rate nor the final conversion are noticeably affected by the presence of DAC.

Obviously, the increase in D 1173 concentration increased both the maximum rate of polymerization and the final conversion of the methacrylate system. This is clear when looking at the rate profiles, on which can be seen that the maximum rate of polymerization is shifting to shorter times when the D 1173 concentration increases. In the meantime, a sharp decrease in the inhibition time is noted. Very interestingly, the DEP polymerization is barely affected by the kinetic of formation of the polymethacrylate network. The DEP kinetics profiles are very similar from Run 9 to 11, and the maximum of the rate profiles are very similar as shown in Figure II. 29.

Focusing on the relative reaction of the two monomers leads to a picture of the IPN formation. In the case of Run 9, the epoxide reacts prior to the methacrylate. The polymerization of the latter exhibits an important inhibition period. When the epoxide conversion is high enough, the radical polymerization starts due to a gelification of the medium which decreases the inhibition by oxygen. However, the same effect limits the final conversion of the methacrylate to a relatively low value. Run 10 exhibits a different behaviour. Indeed, the formation of the two networks occurs simultaneously, as can be seen from the rate profiles. This would lead to a real simultaneous IPNs. As a consequence, the final conversion of the methacrylate is higher than in the previous case. Finally, for Run 11 the D 1173 concentration is high enough to make the photopolymerization of the methacrylate much faster than the epoxide one leading to a higher final conversion of the polymethacrylate network.

Therefore, the two networks are formed in different time scales depending on the D 1173 concentration. Besides, we succeeded by modifying the radical photoinitiator concentration, to influence the sequence of formation of each polymer network and ultimately one can expect to end up with different morphologies and final properties for the different materials. As a result, we will study the thermomechanical properties of most of the UV cured IPNs studied in this academic study.

IV.2.4 Final properties

IV.2.4.1 Thermomechanical analysis of the UV cured analysis

Mechanical properties of some selected systems were performed by DMA analysis (cf Annex I.1, Annex I.2 and Annex III.1) for the principle of this technique and the experimental conditions), with the aim to obtain glass transition temperature (T_g) and to eventually observe phase separation phenomena. All these materials possess only one T_g meaning that phase separation was either avoided or very limited. The presence of only one peak is an evidence of a good interpenetration and compatibility between the two networks within the final material, showing that homogeneous UV cured IPNs have been synthesized. The T_g values referring to the different samples are given in Table II. 29.

Table II. 29: Determination of the T_g of the different selected formulations

Run	T_g (°C)
Run 1	109 ^a
Run 2	t.b. ^a
Run 3	n.m. ^a
Run 4	154 ^a
Run 5	153 ^a
Run 6	157 ^a
Run 7	n.m. ^b
Run 8	t.b. ^b
Run 9	t.b. ^b
Run 10	t.b. ^b
Run 11	127 ^b

n.m.: not measured; t.b.: too brittle to be measured

^a samples cured under UV belt conveyor with a fusion lamp type H, 10 m/min, light intensity: UVA: 440 mJ/cm², UVB: 430 mJ/cm², UVC: 90 mJ/cm², UVV: 480 mJ/cm², 4 passes done, sample thickness~85 μ m

^b samples cured with polychromatic light of a Hamamatsu Hg-Xe lamp at 366 nm with a light intensity~15 mW/cm², sample thickness~85 μ m

The T_g value for the pure methacrylic resin photopolymerized with a broadband lamp was found at 109°C, showing that in these conditions, the photopolymerization of dimethacrylate is high enough (final conversion of 39%), allowing to perform a DMA analysis. On the contrary, the brittleness of the UV cured epoxy resin (Run 2) prevented us from determining the T_g value for this compound, but it is probably high.

In the case of hybrid mixtures Run 4 to 6, nice films were obtained as a consequence of the IPN formation. Meanwhile, the T_g values of these hybrid formulations were more important than the neat methacrylic sample (about 154°C for the hybrid formulations and 109°C for the neat methacrylic resin) due to the higher conversion degree of the methacrylate function and the presence of the polyether network. The striking point is that for the hybrid blends, the T_g values are similar despite the variation of the radical photoinitiator amount. This similarity might account for the nearly complete polymerization achieved by the dimethacrylate in all the cases and the use of a broadband light source leads to a methacrylate first polymerization according to the reaction rates obtained earlier. The properties of the photo-IPNs seem to depend mainly on the first network

formed. The second network has a lower impact on the mechanical properties in absence of postcuring.

Under exposure at 366nm, it was not possible to determine the T_g values for the samples obtained from the neat methacrylate (Run 7), the sample being only slightly converted (final conversion of 8%). This effect was due to the low light intensity of the Hg-Xe lamp and the oxygen inhibitory effect. The neat epoxide sample Run 8 was as previously found to be too brittle to be tested in tension mode. This was also the case for Run 9 and 10 for which the IPNs are mainly composed from polyether network, i.e. a final conversion higher than 85% for epoxide and less than 56% for methacrylate. In these cases, the epoxide network is formed first or simultaneously with the methacrylate one. By contrast, Run 11 exhibits the highest final conversion (72%) of methacrylate and a slightly lower final conversion of epoxide (82%), leading to a more flexible IPNs. In that case again, the methacrylate network is formed first and the T_g is close to the one obtained for the pure methacrylate photopolymer at 39% of conversion (broadband irradiation). The damping properties are conserved in that sample as in the one photopolymerized under a broadband irradiation even if the DAC conversion is lower and the DEP conversion is higher. The dimethacrylate contributes to the toughness of the UV cured material.

According to the experimental results, T_g values for IPNs are close to the one of the first network photopolymerized when the polymerization rates of epoxide and methacrylate are different.

IV.2.4.2 Morphology of the UV cured IPNs

The aim of these experiments is to try to identify domains inside the IPNs that could correspond to the 3D organization of the networks inside the coating. Figure II. 30 displays the SEM photos of the selected formulations depending on the nature of the light source (cf Annex I.1, Annex I.2 and Annex IV.1).

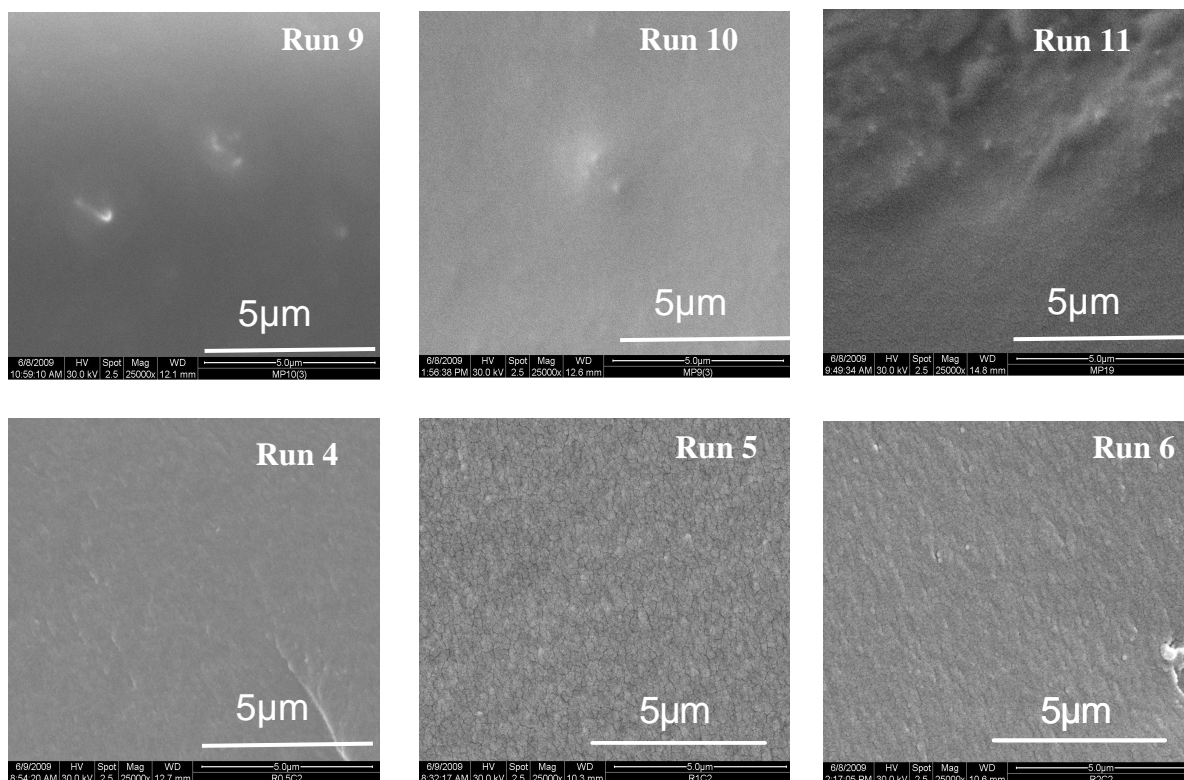


Figure II. 30: SEM micrographs of the IPN samples cured at 366 nm; light intensity, 15 mW/cm² (Run 9, Run 10 and Run 11) and at broadband irradiation (Run4, Run 5, Run 6); with an H type lamp (Fusion) associated to a conveyor belt; speed=10 m/min; UVA: 440 mJ/cm², UVB: 430 mJ/cm², UVC: 90 mJ/cm², UVV: 480 mJ/cm²); four passes were done

Unfortunately, for the samples cured at 366 nm, it is not possible to properly conclude on the presence of any domains owing to the presence of liquid resin remaining in the samples (mainly methacrylate). This observation is in line with the results from the RT-FTIR experiments, showing that upon UV exposure at 366 nm and at a light intensity of 15 mW/cm², the dimethacrylate does not fully cure.

On the contrary, for the samples cured with the broadband exposure setup, a slight phase separation with undefined boundaries between the phase domains of the two polymers was noticed. The domain size ranges from 80 nm to 160 nm and 250 nm, with the increase in the radical photoinitiator concentration. The domains size is lower than 400 nm (visible wavelengths) which suggests a good interpenetration between the networks.

These results are consistent with the single T_g found for the UV cured hybrid mixtures with the DMA analysis. The evidence of the radical PI on the domain size show that the microscale network properties will strongly depend on the relative rate of polymerization of DAC and DEP even if the T_g value does not strongly vary. Unfortunately, it was not possible to chemical identify the two networks. Complementary experiments with AFM in order to characterize the local hardness should therefore be performed to have a better knowledge of the final IPN morphology.

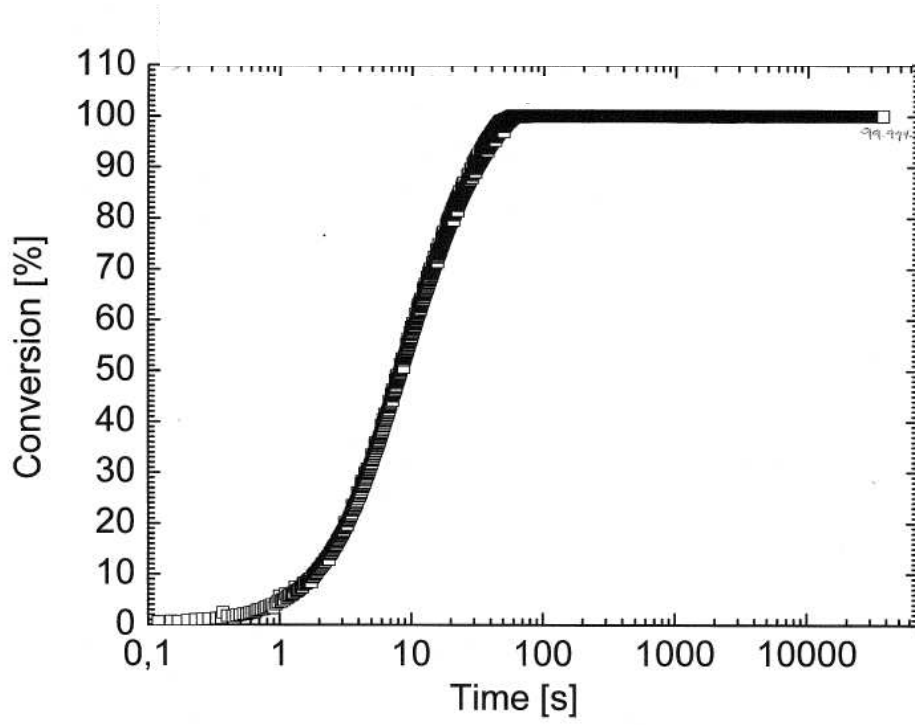
An insight on the evolution of the mechanical properties like the shear modulus could be important to have more details about the network formation. It has been done through a collaboration with Deutsches Kunststoff-Institut, in Darmstadt, Germany with a home made real-time ultrasound reflectometry RTUR combined with near-infrared spectroscopy.

IV.2.4.3 Rheological properties of the UV cured analysis

Changes in rheological properties, and particularly shear modulus, of the resin during photopolymerization process can be probed by means of real-time ultrasound reflectometry RTUR combined with near-infrared spectroscopy used to follow the conversion of the reactive functions as a function of time ^{107,108}. One of the main advantages of RTUR is the possibility to monitor the properties even at high vitrification levels. This technique is described in Annex V.1.

The formulation used in Run 4 was cured in the device during 300 s. The conversion of the methacrylate, as followed by near-infrared spectroscopy, is fully completed within 100s (Figure II. 31a).

a)



b)

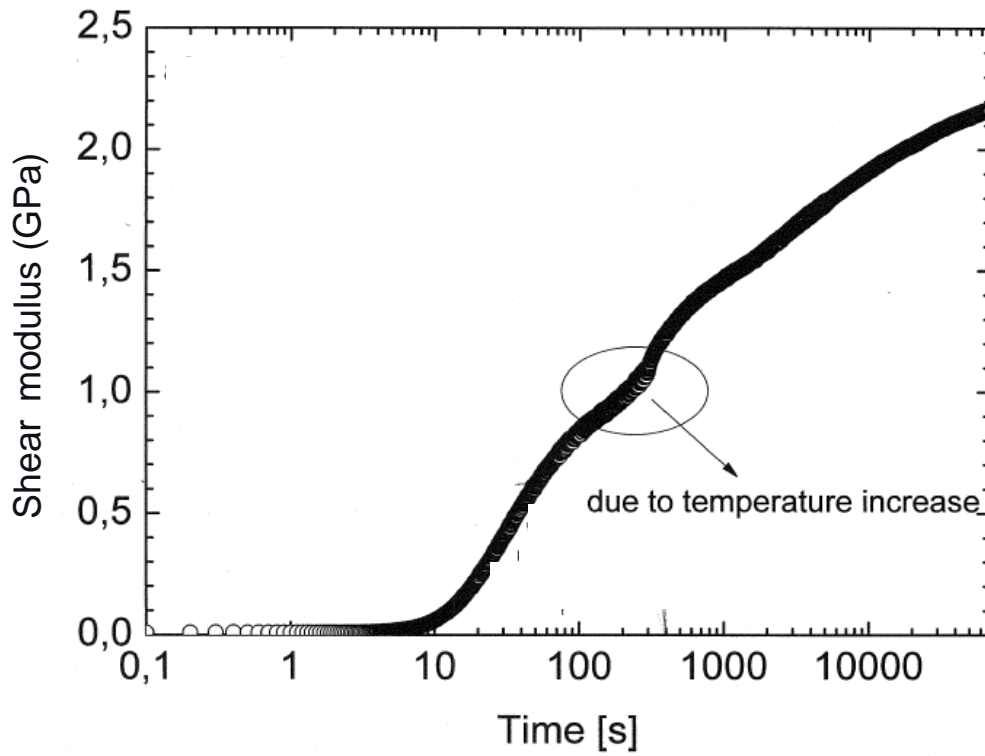


Figure II. 31: Real-time near-infrared spectroscopy (a) and ultrasound reflectometry (b) of Run 4

Although the conversion of the epoxide cannot be followed in-situ because there is no characteristic vibration band of the cycloaliphatic ring in the NIR, one can assess that the photopolymerization occurs in the same time scale as the one of methacrylate, as discussed above (see Figure II. 27).

Figure II. 31b shows that the shear modulus increases as the photopolymerization proceeds and reaches about 0.5-0.7 GPa. Very interestingly, it can be seen that the shear modulus continues to increase after the completion of the photopolymerization a change in the slope of the curve around 300 s is explained by a change of the sample temperature as a consequence of the switch off of the lamp.

The continuous increase in the shear modulus is attributed to the increase in the polyether network formation, due to the living character of the cationic polymerization. This is confirmed by DSC experiments that show the presence of unreacted monomer after exposure. 10000 s after exposure, the value of the shear modulus was found 4 times higher than the one obtained after the switching off of the lamp. It can also be seen that the shear modulus keeps growing after 7h of monitoring. This shows clearly how the IPNs strengthen after the photogenesis.

V CONCLUSIONS AND PERSPECTIVES

This chapter dealt with the comparison of the curing properties of a commercial hybrid resin Renshape®SL 7870 under a stereolithography set up SLA 7000 and a new rapid manufacturing device developed by Huntsman. These techniques mainly differ from their actinic wavelengths, their curing speed and the temperature reached by the resin at the focal point during the building process. The criterion of comparison was the achievement of the green strength for the UV cured materials. The green strength corresponds to an overall of mechanical properties (modulus of elasticity, fracture strength...) that the UV cured material must have in order to withstand the handling and the post-curing steps. The curing kinetics were studied in DPG to understand why the Renshape®SL 7870 resin undergoes a sluggish polymerization at high speed exposures with Griffin machine but it is readily cured by SLA machine. This difference in reactivity was found to be strongly dependent on the actinic wavelength. Indeed, on one hand, at 355 nm, both radical and cationic photoinitiators absorb light and the green strength is ensured by both radical and cationic systems. On the other hand, at 366 nm, the cationic photoinitiator exhibits a very low absorption. No epoxide conversion was evidenced by NIR spectroscopy. Therefore, the green strength could not be reached. Some attempts have been made to broaden the spectral sensitivity of the triarylsulfonium salt used as a cationic photoinitiator at 366 nm. A radical photoinitiator or a photosensitizer was added to the formulation so that it sensitizes the cationic photoinitiator through an electron transfer reaction. However, owing to the low reduction potential of the sulfonium salt, only a slight enhancement was noticed. The same experiments were performed with the iodonium salt Irgacure®250 (I 250) known for its high reduction potential. In presence of only I 250, the epoxide monomer does not polymerize but with the alkoxybenzyl radicals from Irgacure®651 photolysis, the polymerization rate was found to be 4 times greater than for the system containing exclusively the epoxide monomer and the sulfonium salt. Besides, the most striking result was obtained with the polynuclear aromatic compound 9,10-diethoxyanthracene in combination with I 250, the polymerization rate was 7 times higher. However, the iodonium salt is not thermally stable which can be detrimental for the rapid prototyping process. To overcome this shortcoming, it could be interesting to add into the formulation a stabilizer.

Another alternative to enhance the curing speed was to introduce into the hybrid formulation the anti-oxidant triphenyl phosphine. Its presence tremendously speeded up the radical polymerization and therefore the resulting heat evolved might induce the cationic polymerization and increase the initial polymerization rate.

Aware of the complexity of the interpenetrating polymer networks systems, we decided to investigate by an academic approach the formation of another hybrid system based on a cycloaliphatic epoxide and a methacrylate as a function of different exposure conditions and relative amount of photoinitiators. By controlling the exposure conditions, it was found possible to control the formation of the two networks and to evidence the effect on the final properties. On this basis, real time ultrasonic reflectometry demonstrated that the shear modulus of the IPNs increases up to more than 7h after exposure, as a consequence of the living character of the cationic polymerization.

Despite all the efforts made in order to understand and to optimize the commercial hybrid resin, it was not possible to increase the cure speed under Griffin. As a consequence, it was decided to move on different chemistries and to investigate new routes for the development of photopolymerizable formulations more adapted to the Griffin device.

VI REFERENCES

1. Kayaman-Apohan, N.; Demirci, R.; Cakir, M.; Gungor, A. *Radiation Physics and Chemistry* **2005**, *73*, 254-262.
2. Sperling, L. H.; Mishra, V. *Polymers for Advanced Technologies* **1996**, *7*, 197-208.
3. Suthar, B.; Xiao, H. X.; Klempner, D.; Frisch, K. C. *Polymers for Advanced Technologies* **1996**, *7*, 221-233.
4. Nowers, J. R.; Narasimhan, B. *Polymer* **2006**, *47*, 1108-1118.
5. Nowers, J. R.; Costanzo, J. A.; Narasimhan, B. *Journal of Applied Polymer Science* **2007**, *104*, 891-901.
6. Decker, C. *Pigment & Resin Technology* **2001**, *30*, 278-286.
7. Aylsworth, J. W. 1111284, 1914.
8. Sperling, L. H.; Hu, R. *Polymer Blends Handbook* **2002**, *1*, 417-447.
9. Simic, S.; Dunjic, B.; Tasic, S.; Bozic, B.; Jovanovic, D.; Popovic, I. *Progress in Organic Coatings* **2008**, *63*, 43-48.
10. Millar, J. R. *Journal of the Chemical Society* **1960**, 1311-1317.
11. Athawale, V. D.; Kolekar, S. L.; Raut, S. S. *Journal of Macromolecular Science, Polymer Reviews* **2003**, *C43*, 1-26.
12. Lecamp, L.; Pavillon, C.; Lebaudy, P.; Bunel, C. *European Polymer Journal* **2005**, *41*, 169-176.
13. Decker, C.; Nguyen Thi Viet, T.; Decker, D.; Weber-Koehl, E. *Polymer* **2001**, *42*, 5531-5541.
14. Dean, K.; Cook, W. D. *Macromolecules* **2002**, *35*, 7942-7954.
15. Sangermano, M.; Carbonaro, W.; Malucelli, G.; Priola, A. *Macromolecular Materials and Engineering* **2008**, *293*, 515-520.
16. Lin, Y.; Stansbury, J. W. *Polymer* **2003**, *44*, 4781-4789.
17. Benfarhi, S.; Decker, C.; Keller, L.; Zahouily, K. *European Polymer Journal* **2004**, *40*, 493-501.
18. Decker, C. *Progress in Polymer Science* **1996**, *21*, 593-650.
19. Decker, C. *Techniques de l'ingénieur* **2000**, *Doc AM 3044*
20. Decker, C. *Macromolecular Rapid Communications* **2002**, *23*, 1067-1093.
21. Fouassier, J.-P., *Photoinitiation photopolymerization and photocuring fundamentals and applications*. 1995.
22. Fouassier, J.-P.; Rabek, J. F., *Radiation Curing in Polymer Science and Technology, Fundamentals and Methods*. Elsevier, Applied Science: 1993; Vol. I.
23. Schwalm, R., *UV coatings, Basics, Recent Developments and New Applications*. Elsevier: 2007.
24. Dietliker, K., *A compilation of photoinitiators commercially available for UV today*. Edinburgh and London, 2002.
25. Andrzejewska, E. *Progress in Polymer Science* **2001**, *26*, 605-665.
26. Fouassier, J.-P.; Rabek, J. F., *Radiation Curing in Polymer Science and Technology, Practical Aspects and Applications*. Elsevier, Applied Science: 1993; Vol. IV.
27. Gou, L.; Opheim, B.; Scranton, A. B. *Photochemistry and UV Curing* **2006**, 301-310.
28. Andrzejewska, E. *Photochemistry & UV Curing: New trends 2006* **2006**, *Research Signpost*.
29. Schlesinger, S. I. *Photographic Science and Engineering* **1974**, *18*, 387-393.
30. Crivello, J. V.; Lam, J. H. W. *Macromolecules* **1977**, *10*, 1307-1315.
31. Crivello, J. V. *Journal of Polymer Science Part A: Polymer Chemistry* **1999**, *37*, 4241-4254.

32. Crivello, J. V.; Lam, J. H. W. *Journal of Polymer Science, Polymer Chemistry Edition* **1979**, *17*, 977-999.
33. Crivello, J. V.; Dietliker, K., *Photoinitiators for Free Radical Cationic & Anionic Photopolymerization*. 2 nd ed.; John Wiley & Sons Ltd in association with SITA Technology Ltd: 1998; Vol. III.
34. Devoe, R. J.; Sahyun, M. R. V.; Serpone, N.; Sharma, D. K. *Can. J. Chem.* **1987**, *65*, 2342-2349.
35. Dektar, J. L.; Hacker, N. P. *Journal of Organic Chemistry* **1990**, *55*, 639-647.
36. Lebel, A.; Couve, J.; Abadie, M. J. M. *Comptes Rendus de l'Academie des Sciences - Series IIC - Chemistry* **1998**, *1*, 201-207.
37. Dektar, J. L.; Hacker, N. P. *Journal of the American Chemical Society* **1990**, *112*, 6004-6015.
38. Crivello, J. V. *Nuclear Instruments and Methods in Physics Research Section B: Beam Interactions with Materials and Atoms* **1999**, *151*, 8-21.
39. Yagci, Y. *Macromolecular Symposia* **2004**, *215*, 267-280.
40. Yagci, Y.; Reetz, I. *Progress in Polymer Science* **1998**, *23*, 1485-1538.
41. Aydogan, B.; Gacal, B.; Yildirim, A.; Yonet, N.; Yuksel, Y.; Yagci, Y. *Photochemistry and UV Curing* **2006**, 187-201.
42. Crivello, J. V.; Jang, M. *Journal of Photochemistry and Photobiology A: Chemistry* **2003**, *159*, 173-188.
43. Hua, Y.; Crivello, J. V. *Macromolecules* **2001**, *34*, 2488-2494.
44. Crivello, J. V.; Jiang, F. *Chemistry of Materials* **2002**, *14*, 4858-4866.
45. Yildirim, T. G.; Hepuzer, Y.; Hizal, G.; Yagci, Y. *Polymer* **1999**, *40*, 3885-3890.
46. Ledwith, A. *Polymer* **1978**, *19*, 1217-1219.
47. Dursun, C.; Degirmenci, M.; Yagci, Y.; Jockusch, S.; Turro, N. J. *Polymer* **2003**, *44*, 7389-7396.
48. Kahveci, M. U.; Tasdelen, M. A.; Yagci, Y. *Polymer* **2007**, *48*, 2199-2202.
49. Bulut, U.; Crivello, J. V. *Macromolecules* **2005**, *38*, 3584-3595.
50. Sangermano, M.; Yagci, Y.; Rizza, G. *Macromolecules* **2007**, *40*, 8827-8829.
51. Crivello, J. V. *Radiation Physics and Chemistry* **2002**, *63*, 21-27.
52. Fouassier, J.-P., Rabek, J.F, *Radiation Curing in polymer Science and Technology, Polymerizations mechanisms*. Elsevier applied science: 1993; Vol. Vol III
53. Mehnert, R.; Pincus, A.; Janorsky, I.; Stowe, R.; Berejka, A., In *UV & EB Curing Technology & Equipment*, Sons, J. W., Ed. Sita Technology Limited: 1998.
54. Sipani, V.; Scranton, A. B. *Journal of Photochemistry and Photobiology A: Chemistry* **2003**, *159*, 189-195.
55. Decker, C.; Bianchi, C.; Decker, D.; Morel, F. *Progress in Organic Coatings* **2001**, *42*, 253-266.
56. Hartwig, A. *International Journal of Adhesion and Adhesives* **2002**, *22*, 409-414.
57. Hartwig, A.; Schneider, B.; Lühring, A. *Polymer* **2002**, *43*, 4243-4250.
58. Penczek, S.; Kubisa, P.; Szymanski, R. *Makromolekulare Chemie, Macromolecular Symposia* **1986**, *3*, 203-220.
59. Sperling, L. H. *Advances in Chemistry Series* **1994**, *239*, 3-38.
60. Widmaier, J.-M.; Nilly, A.; Chenal, J.-M.; Mathis, A. *Polymer* **2005**, *46*, 3318-3322.
61. Ficek, B. A.; Magwood, L.; Coretsopoulos, C.; Scranton, A. B.: *Photochemistry and UV Curing* **2006**, 293-300.
62. Decker, C. *Polymer International* **2002**, *51*, 1141-1150.
63. Decker, C. *Nuclear Instruments & Methods in Physics Research, Section B: Beam Interactions with Materials and Atoms* **1999**, *151*, 22-28.

64. Oxman, J. D.; Jacobs, D. W.; Trom, M. C.; Sipani, V.; Ficek, B.; Scranton, A. B. *Journal of Polymer Science, Part A: Polymer Chemistry* **2005**, *43*, 1747-1756.
65. Decker, C.; Masson, F.; Schwalm, R. *Macromolecular Materials and Engineering* **2003**, *288*, 17-28.
66. Maag, K.; Lenhard, W.; Loffles, H. *Progress in Organic Coatings* **2000**, *40*, 93-97.
67. Studer, K.; Nguyen, P. T.; Decker, C.; Beck, E.; Schwalm, R. *Progress in Organic Coatings* **2005**, *54*, 230-239.
68. Cai, Y.; Jessop, J. L. P. *Polymer* **2006**, *47*, 6560-6566.
69. Cho, J.-D.; Hong, J.-W. *Journal of Applied Polymer Science* **2004**, *93*, 1473-1483.
70. Degirmenci, M.; Y.Hepuzer; Y.Yagci. *Journal of Applied Polymer Science* **2002**, *85*, 2389-2395.
71. Keller, A. *Pure and Applied Chemistry* **1992**, *64*, 193-204.
72. Chen, F.; Cook, W. D. *European Polymer Journal* **2008**, *44*, 1796-1813.
73. Lipatov, Y. S.; Alekseeva, T. T. *Polymers for Advanced Technologies* **1996**, *7*, 234-246.
74. Chenal, J.-M.; Widmaier, J.-M. *Polymer* **2005**, *46*, 671-675.
75. Vincent, D. Thesis, Université de Paris XII, Paris, 2005.
76. Sperling, L. H. *American Chemical Society* **1994**.
77. Chakrabarty, D. *Polymer Gels and Networks* **1998**, *6*, 191-204.
78. Hua, F. J.; Hu, C. P. *European Polymer Journal* **1999**, *36*, 27-33.
79. Das, B.; Chakraborty, D. *Polymer Gels and Networks* **1995**, *3*, 197-208.
80. Yang, J.; Winnik, M. A.; Ylitalo, D.; DeVoe, R. J. *Macromolecules* **1996**, *29*, 7047-7054.
81. Bernhard, P.; Hofmann, M.; Hunziker, M.; Klingert, B.; Klingert, B.; Schulthess, A.; Steinmann, B., Three-Dimensional Laser Polymerisation. In *Radiation Curing In Polymer Science and Technology Practical Aspects and Applications*, Fouassier, J. P.; Rabek, J. F., Eds. Elsevier Applied Science: London and New York, 1993; Vol. IV.
82. Stansbury, J. W.; Dickens, S. H. *Dental Materials* **2001**, *17*, 71-79.
83. Varley, R. J.; Heath, G. R.; Hawthorne, D. G.; Hodgkin, H. H.; Simon, G. P. *Polymer* **1995**, *36*, 1347-1355.
84. Allonas, X.; Lalevee, J.; Fouassier, J.-P. *Journal of Photochemistry and Photobiology, A: Chemistry* **2003**, *159*, 127-133.
85. Lalevee, J.; Allonas, X.; Jradi, S.; Fouassier, J.-P. *Macromolecules* **2006**, *39*, 1872-1879.
86. Colthup, N.; Daly, L. H.; Wiberley, S. E., *Introduction to Infrared and Raman spectroscopy*. 2 nd ed.; Academic Press Inc: London, 1975.
87. Hwang, H.; Jang, D. J.; Chae, K. H. *Journal of Photochemistry and Photobiology, A: Chemistry* **1999**, *126*, 37-42.
88. Lalevee, J.; Allonas, X.; Fouassier, J. P.; Tachi, H.; Izumitani, A.; Shirai, M.; Tsunooka, M. *Journal of Photochemistry and Photobiology, A: Chemistry* **2002**, *151*, 27-37.
89. Miyata, K.; Koyanagi, M. *Bulletin of the Chemical Society of Japan* **1988**, *61*, 3813-3817.
90. Liska, R.; Schuster, M.; Infuehr, R.; Turecek, C.; Fritscher, C.; Seidl, B.; Schmidt, V.; Kuna, L.; Haase, A.; Varga, F.; Lichtenegger, H.; Stampfl, J. *Journal of Coatings Technology and Research* **2007**, *4*, 505-510.
91. Allonas, X.; Obeid, H.; Fouassier, J.-P.; Kaji, M.; Ichihashi, Y.; Murakami, Y. *Journal of Photopolymer Science and Technology* **2003**, *16*, 123-128.

92. DeVoe, R. J.; Sahyun, M. R. V.; Schmidt, E.; Serpone, N.; Sharma, D. K. *Canadian Journal of Chemistry* **1988**, *66*, 319-324.
93. Morgan, C. R.; Kyle, D. R. *Journal of Radiation Curing* **1983**, *10*.
94. Zadok, E.; Eitan, A.; Tamir, I. *Thermochimica Acta* **1989**, *148*, 387-393.
95. Adair, P. C. *RadTech'94 North America: 4th International UV/EB Conference* **1994**, *1*, 564-570.
96. Kuang, W.; Hoyle, C. E. *Rad Tech 2002 Technical Conference Proceedings* **2002**.
97. Crivello, J. V. *Journal of Polymer Science, Part A: Polymer Chemistry* **2007**, *45*, 3759-3769.
98. Crivello, J., V. *Journal of Polymer Science Part A: Polymer Chemistry* **2007**, *45*, 4331-4340.
99. Decker, C.; Moussa, K. *Journal of Coatings Technology* **1990**, *62*, 55-61.
100. Decker, C.; Decker, D.; Morel, F. *ACS Symposium Series* **1997**, *673*, 63-80.
101. Decker, C. *Journal of Polymer Science, Part A: Polymer Chemistry* **1992**, *30*, 913-928.
102. Arruebarrena de Baez, M.; Hendra, P. J.; Judkins, M. *Spectrochimica Acta, Part A: Molecular and Biomolecular Spectroscopy* **1995**, *51A*, 2117-2124.
103. Morel, F. Thesis, Université de Haute-Alsace, Mulhouse, 1998.
104. Bayou, S.; Mouzali, M.; Abadie, M. J. M. *Comptes Rendus Chimie* **2005**, *8*, 903-910.
105. Abadie, M. J. M.; Chia, N. K.; Boey, F. *Journal of Applied Polymer Science* **2002**, *86*, 1587-1591.
106. Decker, C.; Decker, D.; Morel, F. *Polymeric Materials Science and Engineering* **1996**, *74*, 350-351.
107. Alig, I.; Steeman, P. A. M.; Lellinger, D.; Dias, A. A.; Wienke, D. *Progress in Organic Coatings* **2006**, *55*, 88-96.
108. Alig, I.; Oehler, H.; Lellinger, D.; Tadjbach, S. *Progress in Organic Coatings* **2007**, *58*, 200-208.

Chapter III: Alternatives to IPN chemistry

I	INTRODUCTION.....	127
II	LITERATURE SURVEY	129
II.1	Basics of thiol-ene chemistry	129
II.1.1	History	129
II.1.2	The reactants	129
II.1.2.1	Thiol compounds.....	129
II.1.2.2	Ene compounds	130
II.1.2.3	Kinetics of photopolymerization.....	131
II.1.2.4	Properties of thiol-ene chemistry	133
II.2	Silane-ene	135
II.3	Maleimide chemistry.....	137
II.3.1	Donor/acceptor copolymerization	138
II.3.1.1	Definition	138
II.3.1.2	Polymerization mechanism: Description of the different steps	139
II.3.2	Maleimide/vinyl ether system	142
III	STUDY OF MALEIMIDE /VINYL ETHER MIXTURES IN PRESENCE OF RADICAL PHOTOINITIATOR.....	146
III.1	Chemicals	146
III.2	Variation of the proportions between N-tertbutylmaleimide and Tris[4-(vinyloxy)butyl] trimellitate	147
III.3	Variation of vinyl ether nature	150
III.4	Variation of MI structure.....	151
III.5	Influence of the photoinitiator system.....	153
III.5.1	Addition of a cationic photoinitiator to the formulation BMI-2300@2575 DIVE	153
III.5.2	Modification of the radical photoinitiator in presence of the cationic photoinitiators TAS and I 250.....	155
III.6	Influence of the post-curing treatment	158
III.7	Thermomechanical properties	160
III.8	Determination of the volumetric shrinkage and linear deflection.....	162
IV	INVESTIGATIONS ON THE POLYMERIZATION OF MALEIMIDE / NORBORNENE MIXTURES IN PRESENCE OF RADICAL PHOTOINITIATOR	164
IV.1	Introduction	164
IV.2	Thermomechanical properties	168
IV.3	Volumetric shrinkage and linear deflection	169
V	CONCLUSIONS AND PERSPECTIVES.....	170
VI	REFERENCES.....	172

I INTRODUCTION

Due to their commercial availability and their high reactivity, UV curable acrylate monomers have been widely used in various industrial fields ¹⁻⁶. Nevertheless, their sensitivity towards oxygen during photopolymerization and the important shrinkage within the final material are particularly detrimental ⁶⁻⁸. One way to overcome most of these drawbacks is to use Interpenetrating Polymer Networks (IPNs). Indeed, these hybrid systems combine the advantages of both radical and cationic photopolymerizations. However it was demonstrated in Chapter II that they have shown limits for applications under Araldite®Digitalis.

Another approach is to investigate alternative or new chemistries capable of replacing acrylate-based systems. The chemistries that were selected are thiol-ene, silane-ene and maleimide chemistries. Some literature studies have highlighted both their high reactivity and degree of cure with the advantage of being less sensitive towards oxygen ⁹⁻¹¹. In terms of fast response, these chemistries may fulfill the Huntsman specifications for Araldite®Digitalis but the resulting UV cured materials have also to meet some mechanical properties requirements (flexural green strength~40 MPa, high T_g , high tensile modulus (1400-1500 MPa) and low shrinkage). Therefore, this chapter will consider all these parameters. The first part of this chapter starts with a literature review of these three chemistries in order to understand the basics and fundamental aspects of each chemistry and determine their assets and also the associated problems.

In the light of this bibliography survey, our interest then will focus on the maleimide chemistry despite the lack of commercial monomers. In addition to the commercial N-tertbutylmaleimide, we chose to synthesize a liquid bismaleimide since these monomers display outstanding features. They can for instance act as comonomer in charge transfer photoinduced polymerization ^{12,13}. The process is based on the copolymerization between an electron acceptor monomer and an electron donor monomer ¹⁴⁻¹⁹. This chemistry is versatile since manifold combinations have been examined but we decided to inquire on one of the most reactive and promising combination, maleimide (MI)/vinyl ether (VE). Therefore, the second part of this chapter deals with the study of the kinetics of photopolymerization of different systems as well as the characterization of the final properties of the cured materials in order to optimize the performances of the formulations in comparison with some commercial SL resins. Finally, due to the high shrinkage exhibited by the vinyl ether monomers, they were replaced by norbornene monomers. These latter are known to be highly reactive in thiol-ene chemistry and they give rise to

high crosslinked materials ¹¹. Unfortunately, a few norbornenes are commercially available so for our survey we synthesized 3 compounds. To our knowledge, the association maleimide/ norbornene has never been examined before so the results obtained from the kinetics and from the thermomechanical analysis were compared to the MI/VE systems.

II LITERATURE SURVEY

II.1 Basics of thiol-ene chemistry

II.1.1 History

An interesting alternative to the common acrylate, epoxy and IPN photopolymerizations is thiol-ene chemistry that combines not only the outstanding features of acrylate photopolymerization but also their insensitivity towards oxygen²⁰⁻²³. Different aspects of this chemistry have already been reported by numerous researchers such as Morgan *et al*²⁴, Bowman *et al*^{20-23,25-35}, Hoyle *et al*^{11,36-39}, Jonsson *et al*^{36,39}...The most important features will be presented in the following pages. The thiol-ene polymerization lies in the reaction between a thiol functional group and an ene functional group²².

II.1.2 The reactants

II.1.2.1 Thiol compounds

Basically, alkyl thiols, thiol glycolate esters and thiol propionate esters are employed in thiol-ene polymerization¹¹. The typical structures are represented in Figure III. 1.

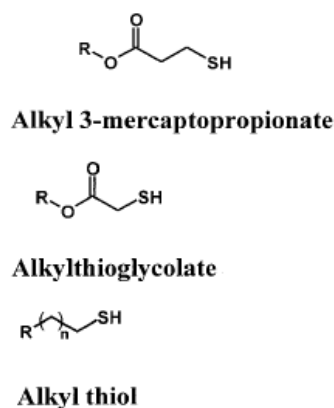


Figure III. 1 : Typical chemical structures of thiols used in thiol-ene chemistry

Thiol glycolate esters and thiol propionate esters were shown to be more reactive. Indeed, the H bonding between the thiol function and the ester carbonyl might facilitate the cleavage of S-H bonds. Wutticharoenwong *et al*⁴⁰ have demonstrated that the thiyl radicals reactivity also depends on the structure of the thiols. They have demonstrated that, for a same structure, the cycloaliphatic thiol was the less reactive than the aromatic thiol. The steric hindrance and the ring strain of cyclohexane cycle might explain this result.

II.1.2.2 Ene compounds

It was reported that polythiols were capable of copolymerizing with various multifunctional enes such as norbornene, vinyl ether, allyl ether, acrylate, etc...¹¹ The structures of the enes commonly used in thiol-ene chemistry are depicted in Figure III. 2.

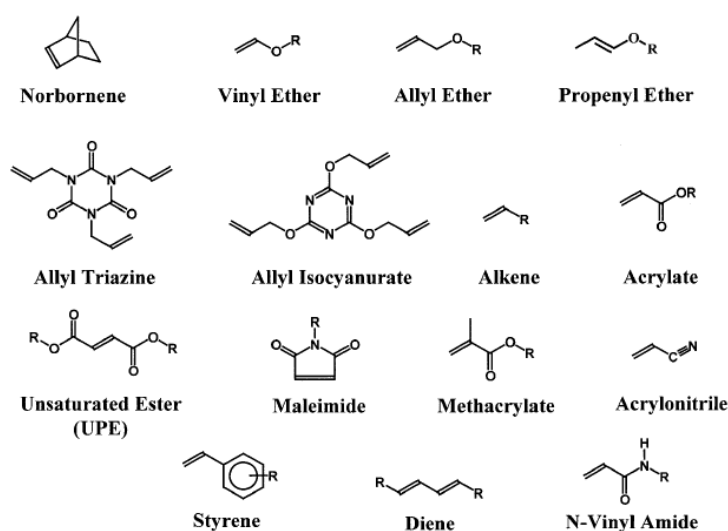


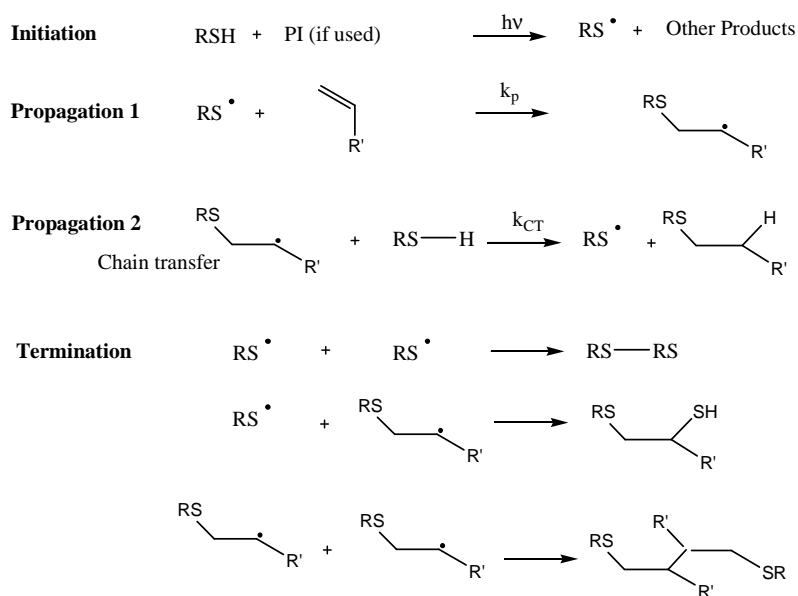
Figure III. 2 : Typical chemical structures of enes used in thiol-ene chemistry

Their reactivity was shown to be strongly linked to the nature of double bond substituent groups. Hoyle *et al*¹¹ have classified these compounds according to their reactivity. It tends to diminish in the case they are electron poor monomers: Norbornene > Vinyl ether > Propenyl > Alkene \approx Vinyl ester > N-Vinyl amides > Allyl ether \approx Allyl triazine > Allyl isocyanurate > Acrylate > Unsaturated ester > N-substituted maleimide > Acrylonitrile > Methacrylate > Styrene > Conjugated dienes. Norbornenes, methacrylates, styrenes, and conjugated dienes exhibit particular behaviours. The exceptional reactivity of the norbornenes compounds is related to the release of the ring strain during the addition of the thiyl radical on the double bond and the ease of the hydrogen abstraction reaction of the thiol hydrogen by the carbon centered radical. Methacrylates, styrene or conjugated dienes are among the less reactive enes because of the stability of the carbon centered radicals formed after the addition of the thiyl radical on to the ene double bond. Besides

this, the generated radicals (methacrylic, benzylic, allylic) undergo an hydrogen abstraction reaction with low rate constants.

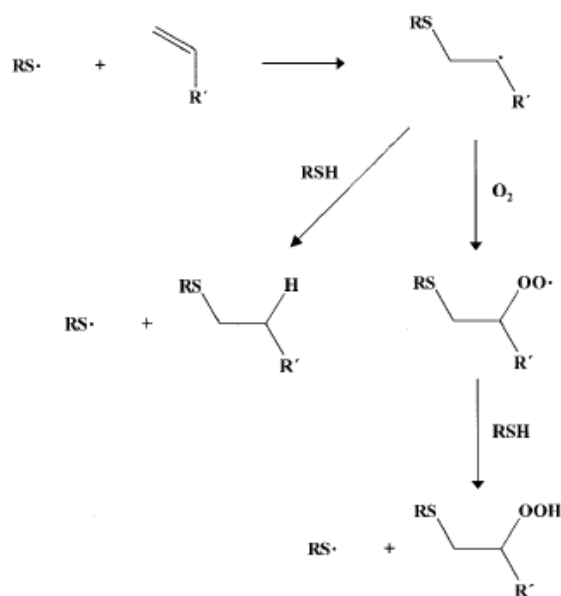
II.1.2.3 Kinetics of photopolymerization

Thiol-ene photopolymerization is based on a step growth addition between an olefin and a thiol. The first step consists in forming thiyl radicals by using benzophenone derivatives, or cleavable photoinitiators (PI) or directly exciting thiol compounds. Subsequently, these radicals react with ene double bonds to produce carbon centered radicals that abstract an H from thiol groups to form again thiyl radicals via a chain transfer reaction (CT) (the rate constant for the chain transfer reaction is k_{CT}). Finally, the thiyl radicals continue the propagation step (the rate constant for the propagation step is k_p). Generally, termination involves a recombination process¹¹. The overall mechanism is illustrated in Scheme III. 1 for a monofunctional thiol and a monofunctional ene. Usually, a multifunctional ene and a multifunctional thiol are used to get a crosslinked network (average functionality is greater than two).



Scheme III. 1 : Different steps of thiol-ene photopolymerization involving monofunctional thiol and ene. k_p and k_{CT} stand for the propagation and chain transfer rate constants respectively

Contrary to acrylates, thiol-ene system is much less sensitive towards oxygen since in presence of oxygen, the thiyl radicals which are insensitive towards oxygen are generated. Indeed, first, molecular oxygen reacts with the carbon centered radicals to produce peroxy radicals. Afterwards, the peroxy radicals are scavenged by thiols via an hydrogen abstraction reaction to form thiyl radicals capable of participating to the propagation step¹¹. The mechanism is described in Scheme III. 2.



Scheme III. 2 : Effect of oxygen on the thiol-ene polymerization

According to Scheme III. 1, in a stoichiometric thiol-ene mixture, both thiol and ene are consumed in the same proportions unless the ene compound has the ability to homopolymerize. For instance, in a stoichiometric thiol/acrylate mixture, the acrylate undergoes a nearly complete polymerization whereas the thiol conversion is levelling off at 50%^{23,25}. Cramer *et al*²³ have performed some experiments between a tetrafunctional thiol and different enes (respectively acrylate, norbornene, vinyl ether and vinyl silizane) by means of DSC and RT FTIR spectroscopy in order to investigate the kinetics mechanisms. The results outlined the changes in the kinetics mechanisms according to the nature of the ene monomers. The polymerization rate can be expressed as a function of thiol and ene concentrations with n and m the reaction order for each reactant ($R_p \propto [SH]^n [C=C]^m$) (III.1). n and m were shown to be dependent on the ratio of the rate constant of propagation (k_p) to the rate constant of chain transfer (k_{CT}): (k_p/k_{CT}). The value of the ratio might be related to the olefin electron density and the carbon centered stability. For instance, for thiol-allyl ether and thiol-acrylate, the ratio value was found to be very high so the polymerization rate depends only on the thiol concentration with a first order dependency. This means that the chain-transfer hydrogen abstraction process is the limiting step. Meanwhile, for thiol-norbornene and thiol vinyl ether, both k_p and k_{CT} values were similar. In other words, neither the propagation step nor the chain-transfer step is rate-determining. As a consequence, both thiol and ene concentrations displayed 0.5 reaction order. As regards to vinyl silizane, the ratio value was low, below unity. The

polymerization rate was first order according to only the ene concentration. In this case, the propagation step 1 is the limiting step.

II.1.2.4 Properties of thiol-ene chemistry

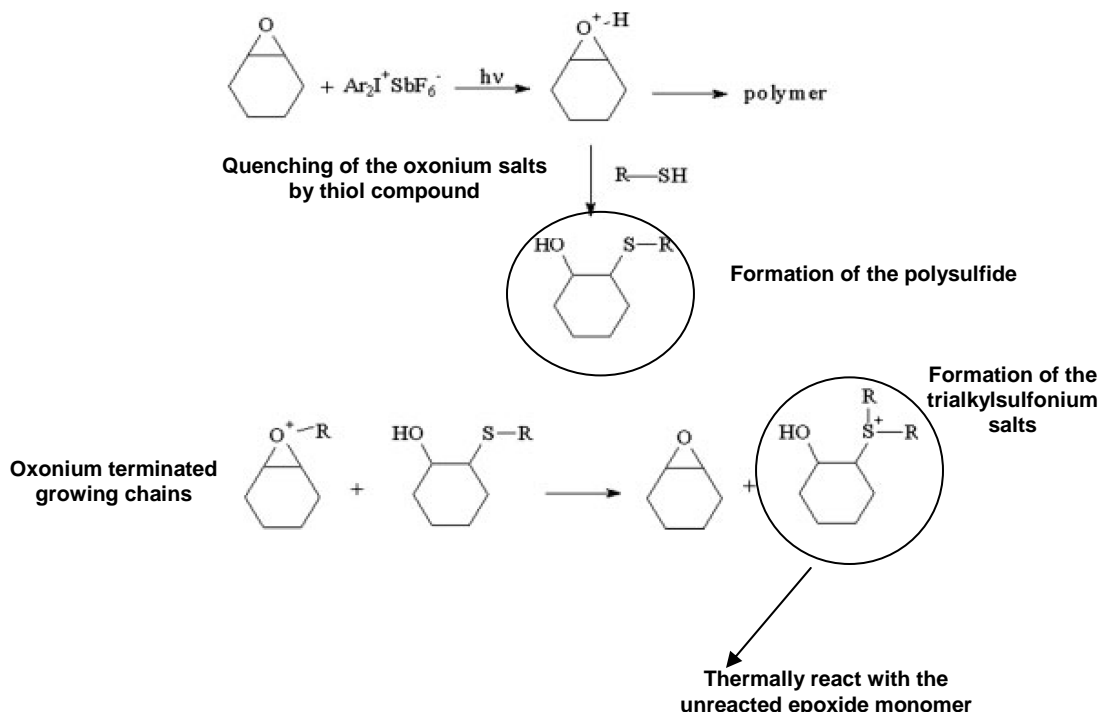
Thiol-ene based photopolymers display outstanding properties such as good adhesion and oxidative stability due to the presence of thioether bonds, homogeneous crosslinked network, water absorption resistance and excellent color stability ¹¹. Furthermore, the onset of the gel formation is delayed in thiol-ene system compared to the traditional acrylate systems owing to the step-growth process. As a consequence, a higher polymerization conversion might be reached for the thiol-ene polymerization and combined with a lower volume shrinkage contribute to alleviate the shrinkage stress within the cured material ¹¹.

Nevertheless, thiol-ene chemistry often gives rise to tough materials with low glass transition temperature. The flexural strength and modulus was shown to be lower than the ones of the dimethacrylate resins ²⁷. However, for some distinct applications, hard materials are often required. These mechanical properties can be improved by adding fillers into the formulations or by achieving different combinations between multifunctional thiols and enes. Indeed, it is possible to get stiff material by mixing thiols with norbornenes. The presence of rigid moieties such as norbornene aromatic cycle increases the T_g value ^{11,31}.

Instead of synthesizing new rigid thiol and ene monomers, a third component, a vinyl monomer can be added to the formulation ³³. The advantage of a ternary system thiol/vinyl 1/vinyl 2 is the possibility to both control and tailor the final properties of the material. Work ³⁰ has been done about the determination of the kinetic parameters of such complex system. When the vinyl monomers do not homopolymerize, typical step growth polymerization takes place between the thiol and the vinyl monomers (e.g. thiol/vinyl ether/norbornene, thiol/allyl ether/norbornene). The relative conversion of the reactive functions depends on the ratio between the propagation rate constants. Whilst, in the case where one vinyl monomer homopolymerizes (e.g. thiol/ene/acrylate), the copolymerizations between the thiol and the vinyl monomers simultaneously happen with the vinyl homopolymerization. The degree of cure of each monomer is related to both the propagation and chain transfer kinetic parameters. In addition the morphology of these ternary systems has been examined. Wei and al ³⁹ have worked on the photopolymerization of a ternary system containing trithiol and triallyl ether (ratio 1:1) and a 16-functional acrylate based monomer. The increase in acrylate amount not only raised the T_g value but also broadened this transition range. The polyacrylate presence might harden the final material and might bring some heterogeneity within the cured material.

The presence of nanodomains rich in polyacrylate were inferred from AFM analysis. Modifying the component proportions might enable to control thermal properties of the photopolymerized material. The DMA measurements along with the Perzoz hardness experiments on different thiol-ene/acrylate ternary systems shed on light the relation between the ability to absorb energy during an impact and the T_g value. The impact absorption seems to grow in the vicinity of the glass transition. Additionally, the nature of the acrylate monomer strongly influenced the impact resistance of the cured material. Ternary systems that contained acrylates with bisphenol A moiety possesses outstanding impact energy absorption at room temperature.

Another alternative is to form an hybrid material by introducing a cationic monomer such as an epoxide monomer. The action of polysulfide generated according to a thiol-ene polymerization on epoxide monomers, was investigated by Ortiz *et al*^{41,42}. They have shown that their inherent nucleophilicity had a detrimental effect on the cationic polymerization. They partially or totally inhibit the polymerization by reacting with the oxonium ions. However, the sulfides could afterwards quickly react with the oxonium terminated growing polyether chains to form sulfonium salts capable of inducing thermally polymerization of the remaining epoxy functions, as referring to Scheme III. 3. The thermal treatment consisted in heating the samples at 100°C for 1 h⁴¹.



Scheme III. 3 : Effect of thiol compound on the cationic photopolymerization for a hybrid system containing cyclohexene oxide with pentaerythritol tetrakis (3-mercaptopropionate) (RSH) in presence of 1% of (4-n-decyloxyphenyl)phenyliodonium hexafluoroantimonate⁴¹

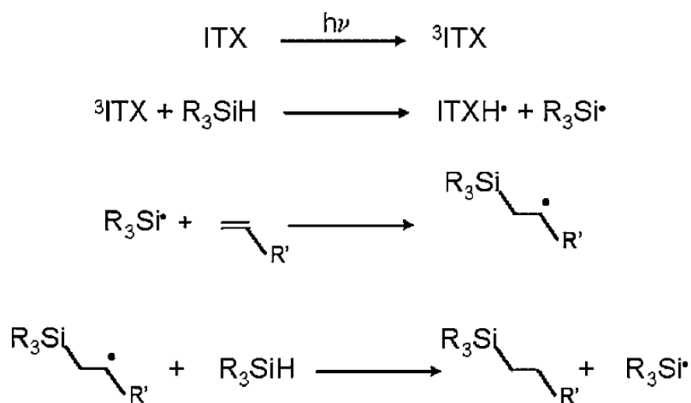
The DMA analysis of the resulting postcured photopolymers indicated an important shift of the polymer T_g to higher values in comparison to the T_g of the thiol-ene based photopolymers. As a consequence, the introduction of epoxy provides better mechanical strength. The morphology of the cured materials was also studied. The TEM micrographs pointed out the material homogeneity which was consistent with the single peak found for the loss modulus results. Carioscia *et al*³² have also worked on the development of interpenetrating polymer networks based on thiol/ene/epoxy formulations but herein the epoxide polymerized anionically. The hybrid system comprised two different mixtures (mixture 1: thiol (50 molar %) /ene (50 molar %) and the mixture 2: thiol (50 molar %) /epoxide (50 molar %)). The thiol-epoxide polymerization lies in the reaction between the thiol and a tertiary amine in order to generate a thiol anion capable of addition with the epoxide group. The variation of the ratio of the mixture concentration had a drastic impact on both conversion and mechanical properties. The highest T_g and the lowest polymerization stress were obtained with the 50/50 w/w thiol-ene/thiol-epoxy mixture. The mechanical properties of the different mixtures were found to be comparable with the ones of dimethacrylate dental restorative resins.

Despite these exceptional properties, this chemistry displays some drawbacks that are not negligible such as thiol odor and the instability of the formulations. Fortunately, they can be partially circumvented by respectively using masking agents, modifying the synthesis process and using thermal stabilizers¹¹.

Although the thiol-ene chemistry was found interesting to study, we were asked to look at alternative chemistry not yet reviewed.

II.2 Silane-ene

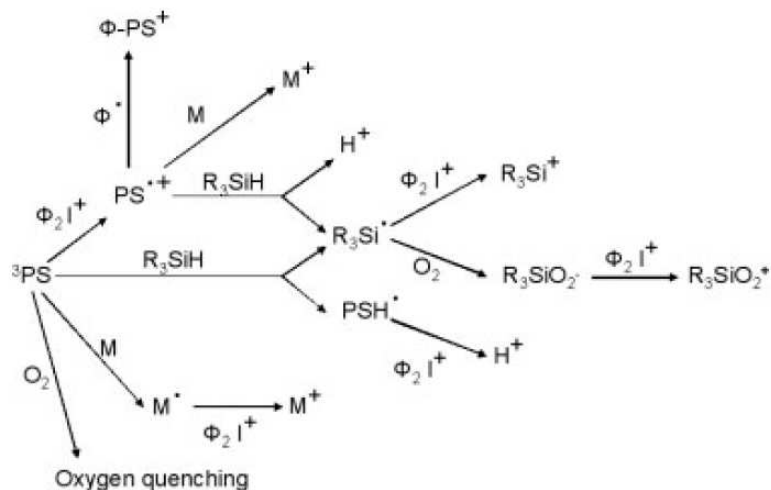
Recently, a new free radical photopolymerizable system based on the association between silanes and ene was presented by Lalevée *et al*⁴³. Very similar in the principle to the thiol-ene polymerization, silyl radicals are the initiating species. They could be generated either by a homolytic cleavage of the Si-Si bond or by hydrogen abstractions on the silane. Afterwards, they react with the ene double bond to produce carbon centered radicals that regenerate silyl radicals via hydrogen abstraction reaction, as illustrated in Scheme III. 4.



Scheme III. 4 : Mechanism of the silane-ene chemistry⁴³

Like thiol-ene, silane-ene polymerization is not sensitive towards oxygen inhibition. This new reaction process was investigated not only with multifunctional acrylates but also with vinylacetates, divinyl ethers and allylbutylethers. The silane-ene mechanism was evidenced by RT FTIR spectroscopy. The high reactivity of the silyl radical towards both electron rich and poor alkenes was pointed out. The addition rate constant was greater than the initiation rate found for benzoyl, phosphinoyl or aminoalkyl radicals formed from the photolysis of type I cleavable photoinitiators. Despite the variation of the ene nature, the diphenylsilane exhibits a low degree of cure in comparison with thiols (in thiol-ene chemistry). The Bond Dissociation Energy (BDE) of Si-H function is higher than for S-H so the hydrogen transfer between the silane and the radical may not be promoted. This drawback can be overcome by using silanes with a low BDE. But only a few silanes are commercially available.

In view of expanding the silane chemistry to the cationic UV polymerization, Lalevée *et al*⁴⁴ have proposed a new three component initiator system composed by a photoinitiator or a dye (camphorquinone (CQ) or Isopropylthioxanthone (ITX) or eosin), a silane and a diphenyl iodonium salt capable of enhancing iodonium UV spectral sensitivity to the visible range. Generally, these systems were more efficient under air than the commonly systems used to promote the cationic polymerization (CQ/amine (Ethyl-4-dimethylaminobenzoate (EDB) or N-methyldiethanolamine (MDEA))/ iodonium salt). Both cationic polymerization rate and final conversion were significantly improved. These results might arise from the different involvements of the silyl radicals on the polymerization process. It was found out that they could be oxidized by the iodonium salts and lead to the propagation of the reaction. They have the propensity to interact with O₂ and thus decrease its concentration within the medium. The possible interactions between the three components are depicted in Scheme III. 5.



Scheme III. 5 : The different interactions of the silyl radicals with oxygen, the iodonium salt ($\Phi_2\text{I}^+$) and the photosensitizer (PS) ⁴⁴

The same might hold true for the sulfonium salts except that they are less effective than the iodonium salts because of their lower reduction potential.

Due to the lack of commercial silanes, preliminary experiments with RT FTIR spectroscopy and DMA analysis were only carried out with diphenylsilane. The study consisted in introducing a growing amount of diphenylsilane into the ethoxylated bisphenol A diacrylate resin. The acrylate polymerization rate was shown to decrease because the copolymerization process is slower than the acrylate homopolymerization. Additionally, the presence of a high concentration of unconverted diphenylsilane after the polymerization results in a decrease in the T_g value from 99°C to 45°C. For now, this chemistry gives rise to materials with thermomechanical properties that are not suitable for our project.

II.3 Maleimide chemistry

For a long time, maleimides have been used as monomers, crosslinking agents or matrix components in organic chemistry. It was also proved that these compounds could be useful in the UV curing field. Indeed, they can act as both photoinitiators for acrylates and comonomers in photoinduced donor acceptor copolymerization ⁴⁵.

II.3.1 Donor/acceptor copolymerization

II.3.1.1 Definition

The process lies in the copolymerization between electron acceptor monomers and electron donor monomers and can lead to the formation of an alternating copolymer¹⁴⁻¹⁹. Basically, the acceptor monomers (A) used are functional substituted ethylenes containing primary carboxyl, anhydride, ester, amide, imide, nitril moieties like maleic anhydride, dimethylfumarate and maleimide monomers. An important variety of donor monomers (D) with electron rich functions is also available such as N-vinylpyrrolidone, styrene ethers and vinyl and propenyl ethers^{18,19}. Examples of donor and acceptor monomers suitable for this chemistry are given in Figure III. 3.

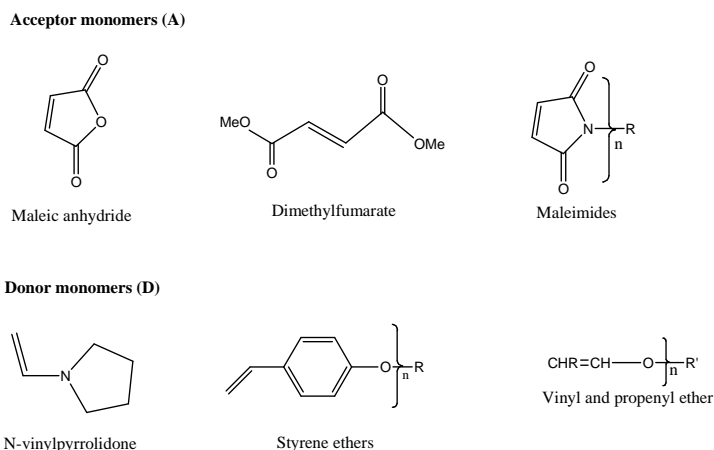


Figure III. 3 : Few examples of acceptor and donor monomers

The choice of multifunctional acceptor and donor monomers is important so as to get a crosslinked material with good properties¹².

These associations exhibit interesting features such as:¹²

- A lower sensitivity to oxygen than the traditional acrylate UV chemistry.
- The disappearance of the chromophore during the polymerization that allows to cure thick samples with high degree of cure.
- The improvement of scratch and adhesion properties (formation of covalent bond during H-abstraction reaction)
- The fact that polymerization can occur without photoinitiator. The maleimides can act as photoinitiators. All the coloration and degradation problems due to photoinitiator byproducts in the cured material are alleviated.

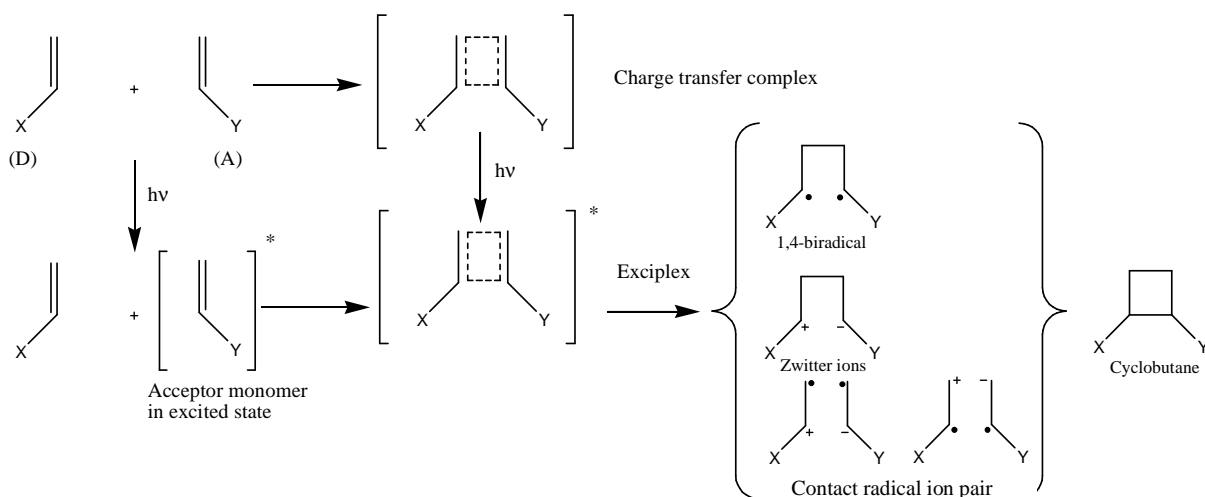
Although the reactivity of this system has been clearly evidenced by photocalorimetry and IR spectroscopy, the polymerization mechanism is still not clear. Some investigations have been made and are reported hereafter.

II.3.1.2 Polymerization mechanism: Description of the different steps

a) *Initiation*

✓ **Initiation via the formation of an excited state charge transfer complex**

Initiation step is generally explained through the formation of an excited state charge transfer complex which can be formed from ground state charge transfer complexes or from an association between the excited acceptor (A) and the donor (D) and *vice et versa*,⁹ as presented in Scheme III. 6.

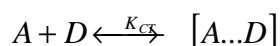


with X: electron donor moiety

Y: electron acceptor moiety

Scheme III. 6 : Two routes for the formation of the exciplex^{9,12}

The formation of the charge transfer complex at the ground state results from dispersion forces between the donor (D) and the acceptor (A) monomers. The equilibrium of the reaction is written as follows⁴⁶:



Basically, the nature of charge transfer complex depends on the strength of intermolecular interactions between the two monomers. According to the Mulliken theory⁹, the charge

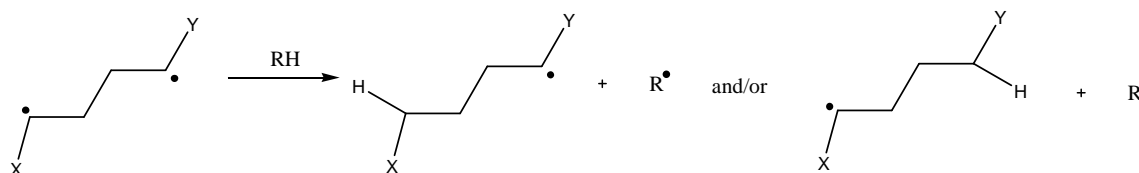
transfer complex will be particularly stable if the overlap between the donor HOMO orbital and the acceptor LUMO orbital is maximal. In this case, the complex will display a high electronic coupling and will be highly colored. Consequently, these complexes can be observed by UV-Visible spectroscopy. Indeed, for some donor/acceptor couples, the presence of the complex will not only induce a bathochromic shift of the UV absorption spectra compared to the addition of the different components but also leads to the creation of new absorption bands. Sometimes, the wavelength shift can be superior to 100 nm.

Whatever the synthesis route chosen for the exciplex formation, the generated species are photochemically identical. As a matter of fact, under the irradiation of a broadband emission source, the two mechanisms might occur at the same time. The decay of the exciplex subsequently yields to the production of several transient species: biradicals, zwitter ions and contact radical ion pair. All the structures are summarized in Scheme III. 6.

The nature of the intermediates is strongly related to the nature of the monomers⁹ as well as the character and the polarity of the medium. If the 1,4 biradical is formed, radical copolymerization will be promoted whereas the zwitter ions will participate to an ionic polymerization. When the contact radical ion pair is formed, the two kinds of copolymerization take place. It is interesting to note that these species can recombine in order to form the stable cyclobutane ring via 2+2 cycloaddition.

Since we are interested in radical induced polymerization, the formation of the 1,4 biradical should be privileged. Lee *et al*⁹ have shown that the combination of respectively strong/weak or weak/strong donor and acceptor monomers could promote the radical process. As a consequence, these complexes exhibit low ionic character and a weak UV absorbance.

Once formed, the 1,4 biradical can generate the initiating species by abstracting a hydrogen from an H-donor (RH) according to the mechanism in Scheme III. 7.

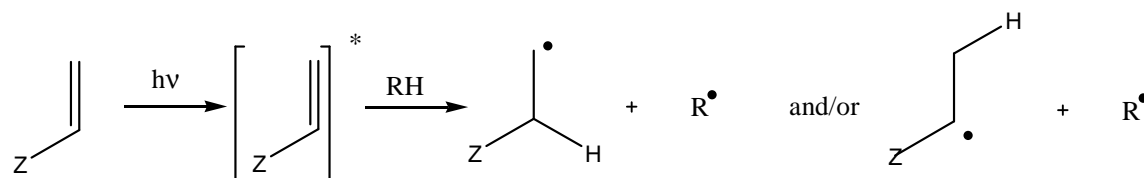


Scheme III. 7: Formation of the initiating species from the biradical 1,4 with the H donor

The H donor can be added to the formulation or be one of the monomers. Therefore, the monomer structures play a key role in the efficiency of donor/acceptor system.

✓ **Initiation by one of the monomers**

Herein, the initiation step proceeds without an exciplex formation^{10,46}. The initiating species are formed via inter (RH, an H donor) or intra molecular H-abstraction from a monomer excited state (cf Scheme III. 8). H-abstraction will predominantly take place in systems where easily abstractable hydrogens are present or in case the concentration of the charge transfer complex is particularly low.

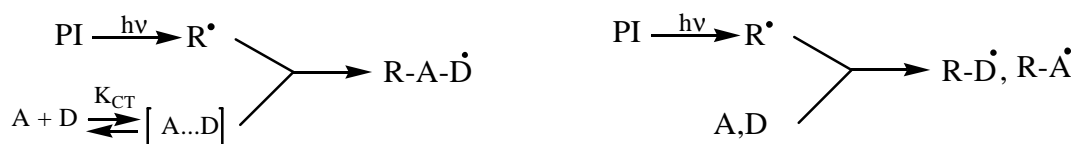


with Z: chromophore moiety

Scheme III. 8 : Formation of the initiating species from one of the monomers in an excited state⁴⁶

✓ **Initiation by a radical photoinitiator**

In the cases where the UV absorption of the charge transfer complex or of the monomer is too low to generate enough initiating species, the introduction of a photoinitiator is essential in order to enhance the overall polymerization process and reach both high polymerization rate and final conversion. Several authors have worked on the investigation of the mechanism⁴⁷⁻⁵⁰. As it is drawn in Scheme III. 9, they have suggested that the free radicals generated from the radical photoinitiator photolysis might either react with the charge transfer complex or with one of the monomer.



Scheme III. 9 : Initiation mechanism using a radical photoinitiator⁴⁶

b) *Propagation*

The propagation step will occur according to two mechanisms either by a cross-over process or by the homopolymerization of the charge transfer complex^{10,13,47,51,52}. The description of the mechanisms is given in Scheme III. 10.

Thus, they have the ability to act as photoinitiator for free radical polymerization^{45,57,63-70}. They can undergo an easy homopolymerization in presence of labile H on the N-alkylchain. At the triplet excited state, the maleimide might abstract an H according to both intermolecular and intramolecular reactions so as to produce the initiating species. These latter react with the maleimide monomer in the propagation step to form the polymer.

Incidentally, the maleimide excited state involved in initiation step might be different depending on the maleimide concentration. In other words, for low maleimide concentration, only the maleimide in the triplet state undergoes self quenching reaction and hydrogen abstraction reaction. By increasing the maleimide concentration, the likelihood for the participation of the maleimide singlet state to the electron/proton transfer sequence rises. The same holds true if an important amount of hydrogen donor is introduced within the formulation. Due to the relative short singlet lifetime, the reactions involving these species have not been clearly ensured but they have to be taken into account in the event of some species able to react with the singlet⁴⁵.

Usually, the polymeric material obtained after the copolymerization between a donor and an acceptor monomer is an alternating copolymer. But, the maleimide can homopolymerize so a statistical copolymer with isolated vinyl ether units might also be produced. Both the maleimide homopolymerization and the vinyl ether/maleimide copolymerizations processes are in competition which yields to a more complex analysis of the mechanism involved between these two monomers. To clarify the mechanism, investigations have been carried out especially by means of NMR analysis, laser flash photolysis and RT FTIR spectroscopy.

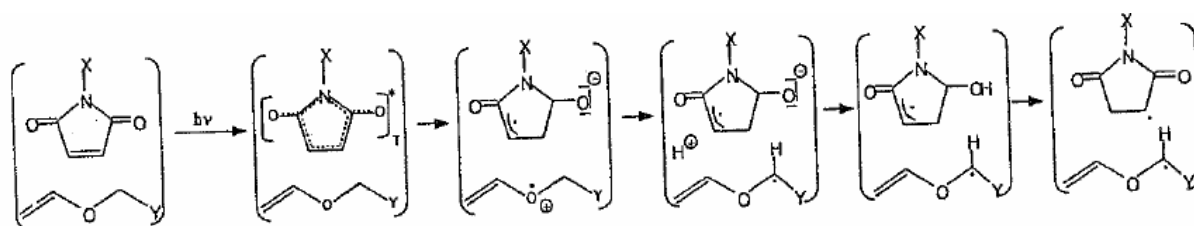
b) Mechanism of the kinetics of photopolymerization

✓ **Initiation**

As mentioned before on the basis of the donor and acceptor copolymerization process, the initiation of the system maleimide/vinyl ether can proceed either via the direct excitation of the maleimide or via the formation of an exciplex. The first hypothesis that the excited maleimides initiate the photopolymerization by intramolecular or intermolecular H abstraction was emitted because the existence of transfer complex between the maleimide and the vinyl ether was not confirmed by UV spectroscopy⁹. However, there are some indications that are in favor of the participation of the charge transfer complex during initiation. Some NMR measurements performed on maleimide/vinyl ether copolymer prepared with an excess of vinyl ether at ambient temperature support the

hypothesis of the complex formation. Indeed, the stereochemistry of the resulting copolymer was constituted by cis succinimide units. However, according to Mulliken theory, if the reaction had involved free monomers, the succinimide units should have adopted the thermodynamically stable conformation trans¹⁶.

Another pathway for initiation step was evidenced by Jonsson by means of laser flash photolysis measurements⁶⁰. It was pointed out that the maleimide in the triplet state was quenched by the vinyl ether monomer via an electron transfer reaction. The initiating radicals were subsequently generated through the transfer of a proton from the vinyl ether radical cation to the maleimide radical anion. An overall process is proposed in Scheme III. 11.



Scheme III. 11 : Electron/proton transfer reactions as initiation step for maleimides and vinyl ether mixtures⁷¹

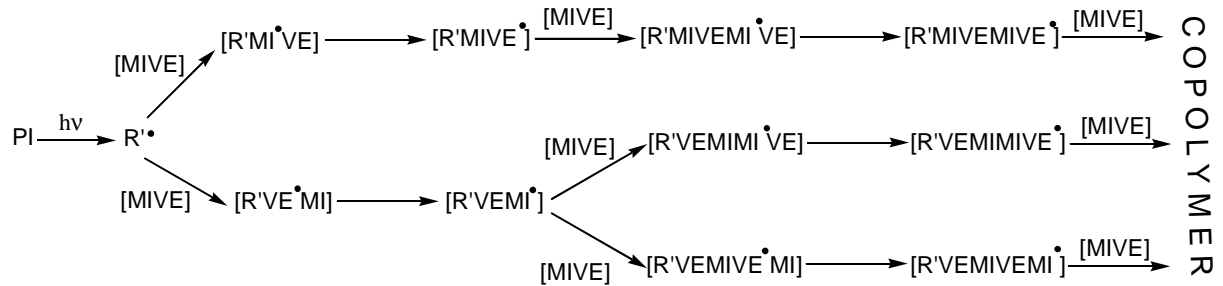
This pathway seems to be the more likely but the initiation via the formation of an exciplex can also happen particularly under high light intensity.

✓ **Propagation**

The elucidation of the propagation step was achieved by Decker with IR spectroscopy by studying the influence of the monomer concentrations on both the maleimide and the vinyl ether polymerization rates in presence of a radical photoinitiator at a wavelength superior to 385 nm^{13,51}. The determination of the kinetics mechanism is easier with a radical photoinitiator because the initiation step is dissociated from the propagation step since the same amount of initiating species is produced for all the formulations. By contrast, in a photoinitiator free system, the initiation rate depends on the maleimide concentration. It decreases with the disappearance of maleimide double bond upon UV irradiation. Therefore, the study would have been more difficult.

The results have demonstrated that when the vinyl ether monomer is in excess, no maleimide homopolymerization occurs because all the maleimide monomers are associated to the vinyl ether monomers. Under these conditions, the copolymerization is very effective and gives rise to an alternating copolymer. As the polymerization rate is not related to both the maleimide and the vinyl ether concentrations but varies linearly with the maleimide concentration, Decker & al^{13,51} have concluded that the acceptor-donor

complex participates to the chain reaction. Broadly speaking, the polymerization mechanism of the maleimide/vinyl ether monomer with an excess of vinyl ether can be described as follows:



Scheme III. 12 : Polymerization mechanism of the system maleimide/vinyl ether when vinyl ether is in excess and in presence of a radical photoinitiator

According to Scheme III. 12, the propagating vinyl ether radicals only react with the maleimide monomer (because the vinyl ether monomer can not homopolymerize) whereas the initiating radicals R• and the propagating maleimide radicals can react with both monomers. So the copolymer formed is not a pure alternating copolymer. When the maleimide is in excess, the copolymerization process is hindered by the homopolymerization process. The obtained polymer is a statistical copolymer with isolated vinyl ether units.

c) Properties

The researches done on MI/VE systems mainly concern the kinetics of photopolymerization.

Morel *et al*⁴⁸ have conducted a prospective study about the final properties of the resulting crosslinked networks for some photoinitiator free MI/VE systems. They have shown that the UV cured materials are not only chemically resistant to chloroform but also highly crosslinked. Their viscoelastic properties might be modulated by acting on the monomer chemical structures.

Few investigations have been made into this field and need to be continued in order to get a good insight of the photopolymer engineer properties (heat resistance, hardness...) and consider the photopolymer practical applications. Consequently, the influence of the monomer structures on the thermomechanical properties and on the extent of shrinkage will be explored.

III STUDY OF MALEIMIDE /VINYL ETHER MIXTURES IN PRESENCE OF RADICAL PHOTOINITIATOR

III.1 Chemicals

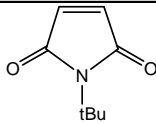
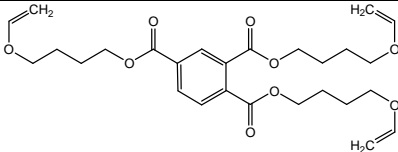
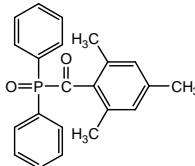
At the beginning of this study, we encountered some difficulties due to the limited choice of commercial maleimide monomers. The name of the available compounds is summarized in Table III. 1. Most of them were in solid form. Except for BMI-2300®, the attempts to dissolve them into vinyl ether resins or in organic solvents such as acetone or THF were not fruitful. Lumicure MIA 200 and Q-Bond are liquid bismaleimides but they are not commercialized any more. N-tertbutylmaleimide (NTMI), a monofunctional monomer, was chosen for this study because it was the only liquid maleimide commercially available.

Table III. 1 : List of the available commercial maleimides

Physical state	Chemical name	Remark
solid	4,4-bismaleimidodiphenylmethane (Matrimid 5292 A)	Problems of solubility
	N-cyclohexylmaleimide	
	N-benzylmaleimide	
	1,6'-bismaleimide-(2,2,4-trimethyl)hexane (BMI-TMH®)	
	phenylmethane maleimide (BMI-2300®)	ok
liquid	polyether-based bismaleimide acetic ester (Lumicure MIA 200)	No longer commercialized
	Bismaleimide 36 carbon cycloaliphatic branched structure (Q-Bond)	
	N-tertbutylmaleimide (NTMI)	ok

Owing to the irritancy of NTMI, it was mandatory to wear suitable respiratory equipment and to perform experiments in well-ventilated rooms. It was associated to the trifunctional vinyl ether monomer tris[4-vinyloxy)butyl)trimellitate (TRIVE) in order to get a high crosslinked UV cured material. 2,4,6-trimethylbenzoyl-diphenyl-phosphineoxide (TPO) was used as radical photoinitiator since it displays a great efficiency and absorption up to 400 nm. Its concentration was set up at 5 wt% after a prescreening study. The overall chemical structures of these compounds are depicted in Table III. 2.

Table III. 2 : Chemical structures of the maleimide, vinyl ether and radical photoinitiator present in the reference formulations

Chemical name	Chemical structure
N-tertbutylmaleimide (NTMI)	
Tris[4-(vinylloxy)butyl] trimellitate (TRIVE)	
2,4,6-trimethylbenzoyl-diphenyl-phosphineoxide (TPO)	

III.2 Variation of the proportions between N-tertbutylmaleimide and Tris[4-(vinylloxy)butyl] trimellitate

Three formulations with different molar proportions of NTMI and TRIVE were prepared. The proportions were calculated with respect to the reactive functions. The details of the three formulations are given in Table III. 3.

Table III. 3: Composition of the different NTMI/TRIVE formulations

Formulation name	Composition		
	mol% of NTMI double bond function	mol% of TRIVE double bond function	wt% of TPO
NTMI 3070 TRIVE	30	70	5
NTMI 5050 TRIVE	50	50	5
NTMI 7030 TRIVE	70	30	5

The experimental conditions are described in Annex I.1 and Annex II.1. The decrease of the characteristic IR absorption bands at 693 cm^{-1} corresponding to C-H maleimide double bond and at 1637 cm^{-1} assigned to the stretching vibration of vinyl ether double bond have been used to compute the respective conversion of these functions^{13,72}. The kinetics profiles are shown Figure III. 4. Herein, the commercial acrylic resin Renshape®SL Y-C 9500 is taken as reference. Its reactivity is compared to the reactivity of the tested formulations. The composition of MI/TRIVE mixture was found to have drastic effect on both the polymerization rate and the final conversion.

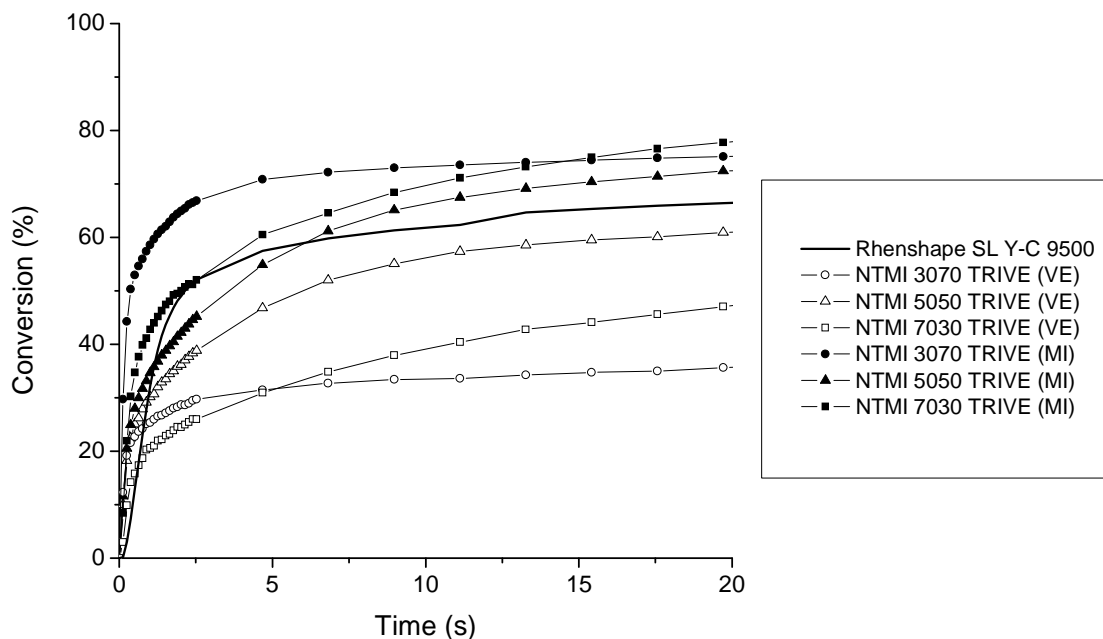


Figure III. 4 : Influence of the molar percentage of monomer reactive functions on the kinetics of photopolymerization of the 3 MI/TRIVE mixtures; 5 wt% TPO; kinetics profile of Renshape®SL Y-C 9500 as reference; in air; Hg-Xe Hamamatsu lamp at 366 nm, light intensity=19 mW/cm²; sample thickness~35 μm

Table III. 4 reports information about some kinetics parameters, $R_{p_{max}}/[M]_0$ (s⁻¹), the conversion reached by the system after 430 s of irradiation and the amount of converted maleimide and vinyl ether double bond reactive functions. Interestingly, these systems are highly reactive as they display higher $R_{p_{max}}/[M]_0$ values than the Renshape®SL Y-C 9500. When TRIVE is in excess (formulation NTMI 3070 TRIVE), the $R_{p_{max}}/[M]_0$ value for the maleimide monomer is about 2.4 times higher than for the vinyl ether. At first glance, the high polymerization rate for the maleimide in comparison with the vinyl ether was assigned to the maleimide homopolymerization that concomitantly occurs with the copolymerization process. Nonetheless, the calculation of the molar percentage of the polymerized reactive functions discloses that the value for maleimide compound is surprisingly slightly lower than for TRIVE. The plasticizing effect of the unreacted vinyl ether molecules (38 mol% of unreacted vinyl ether double bond) might partially contribute to the high values found for the $R_{p_{max}}/[M]_0$. The higher molar percentage of converted vinyl ether double bonds is unexpected because it is known from literature that the vinyl ether monomer can only radically copolymerize so the molar percentage of polymerized vinyl ether double bond should be inferior or at maximum equal to the molar percentage of cured maleimide double bond. The additional disappearance of vinyl ether monomer during the photopolymerization can not be attributed to the vinyl ether monomer volatility

since its boiling temperature is 95°C at 20 mmHg. The difference observed might arise from possible side reactions. Decker *et al*¹³ have demonstrated that in presence of an excess of vinyl ether, TPO radicals reacted with the vinyl ether monomer to generate extra vinyl ether initiating radicals. These species might presumably abstract an H from the medium.

By contrast, when the maleimide concentration is equal or superior to the vinyl ether concentration, the $R_{p_{max}}/[M]_0$ values for NTMI decrease in comparison with the values found for TRIVE and the molar percentage of converted maleimide double bonds increase becomes larger than for vinyl ether double bonds. In the equimolar mixture, both $R_{p_{max}}/[M]_0$ and extent of cure for NTMI are higher than for TRIVE. If pure copolymerization process occurred, these values should be similar. Thus, the maleimide homopolymerization has also to be taken into consideration. Both processes take place. When NTMI is in excess, the proportion of converted maleimide double bond is superior to the proportion of vinyl ether. So the homopolymerization process seems to occur concomitantly with the copolymerization process. The NTMI homopolymerization is sluggish which could explain the decrease in the polymerization rate for the maleimide system.

These experiments underline the complexity of the photopolymerization between NTMI and TRIVE in presence of a radical photoinitiator. It involves not only NTMI homopolymerization, NTMI/TRIVE copolymerization but also side reactions that were not clearly identified.

Table III. 4 : Determination of $R_{p_{max}}/[M]_0$, the conversion at 430 s and the mol% of converted reactive functions, same experimental conditions than Figure III.4

Formulation name	Function	$R_{p_{max}}/[M]_0$ * 100 (s ⁻¹)	Conversion (%)	mol% of converted reactive functions
Renshape® SL Y-C 9500	AC*	38	77	n.d**
NTMI 3070 TRIVE	VE	98	45	32
	MI	236	80	24
NTMI 5050 TRIVE	VE	60	69	35
	MI	81	83	42
NTMI 7030 TRIVE	VE	82	95	29
	MI	44	70	49

*stands for acrylate double bond function

**No information on the exact composition of this commercial resin

III.3 Variation of vinyl ether nature

The experiments consisted in preparing equimolar mixtures containing NTMI with different difunctional vinyl ether monomers in presence of 5 wt% TPO in order to study the influence of the VE structure on both the kinetics of photopolymerization and on the thermomechanical properties. The vinyl ethers have different backbones. Their chemical structure is given in Table III. 5. 1,4-butanedioldivinyl ether (BDVE) and 1,4-cyclohexanedimethanol divinyl ether (CDDVE) respectively possess an aliphatic chain and a cyclohexane ring in their backbone. As regards to bis[4-(vinylloxy)butyl]isophthalate (DIVE), its backbone is the same than TRIVE. For this survey the reference formulation is NTMI 5050 TRIVE.

Table III. 5 : Chemical structures and viscosities of the selected vinyl ether monomers

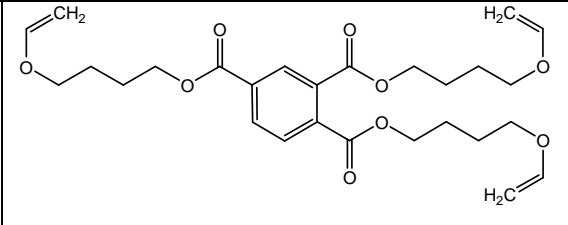
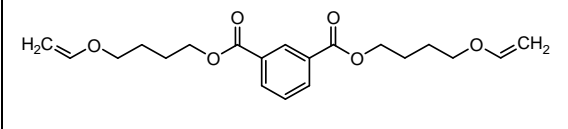
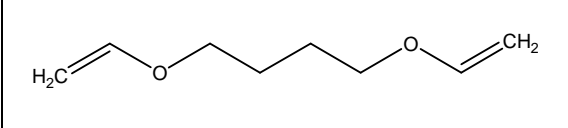
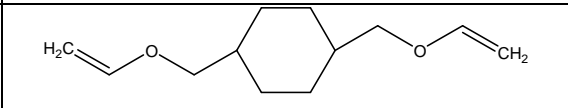
Chemical name	Chemical structure	Viscosity (mPa.s)
Tris[4-(vinylloxy)butyl] trimellitate (TRIVE)		253 mPa.s at 22°C
Bis[4-(vinylloxy)butyl] isophthalate (DIVE)		85 mPa.s at 22°C
1,4-butanedioldivinyl ether (BDVE)		1.3 mPa.s at 22°C
1,4-cyclohexanedimethanol divinyl ether (CDDVE)		4.4 mPa.s at 22°C

Table III. 6 indicates the influence of the vinyl ether monomer on the kinetics parameters. First of all, except for the formulation NTMI 5050 BDVE, the quantity of reacted MI double bonds and the $R_{p_{max}}/[M]_0$ are slightly greater than for vinyl ether monomers. The general trend observed is in full line with the fact that contrary to vinyl ether monomer that can only radically copolymerize, NTMI undergoes both copolymerization and homopolymerization processes. Interestingly, the ratio between $R_{p_{max}}/[M]_0$ for NTMI and $R_{p_{max}}/[M]_0$ for VE monomer is almost the same for all the formulations about 1.2. As expected, the decrease in the vinyl ether functionality led to a decrease in reactive function concentration and thus, the rate of polymerization is lower. However, the final conversion for the formulation NTMI 5050 DIVE is better because the vitrification phenomenon is delayed. Furthermore, Table III. 6 clearly outlines the higher reactivity of

both TRIVE and DIVE compared to BDVE and CDDVE monomers. For the mixture NTMI/TRIVE, the polymerization rate is on average 23 times higher and the induction period time is roughly 10 times smaller. In fact, these formulations are more viscous so the atmospheric oxygen can not readily diffuse into the sample and affect the radical polymerization by scavenging the triplet excited TPO molecules and the initiating radicals generated from TPO photolysis.

Table III. 6 : Determination of the induction period, the $R_{p_{max}}/[M]_0$, the conversion at 430 s and the mol% of converted reactive functions as a function of vinyl ether nature for formulations containing 50 mol% of NTMI reactive functions and 50 mol% of various VE (DIVE, BDVE and CDDVE); same experimental conditions than Figure III.4

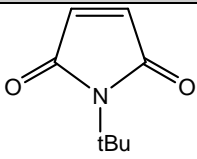
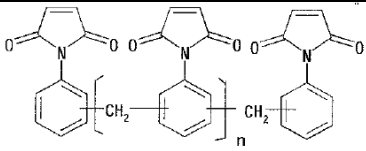
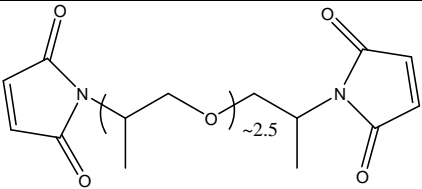
Formulation name	Function	Induction time period (s)	$R_{p_{max}}/[M]_0 * 100 (s^{-1})$	Conversion (%)	mol% of converted reactive functions
NTMI 5050 TRIVE	VE	0.1	60	69	35
	MI		81	83	42
NTMI 5050 DIVE	VE	0.1	69	79	40
	MI		77	95	48
NTMI 5050 BDVE	VE	1.4	2.3	84	42
	MI		1.8	67	34
NTMI 5050 CDDVE	VE	2.3	3.2	83	42
	MI		3.6	88	44

III.4 Variation of MI structure

In order to investigate the influence of the maleimide functionality and structure on the photopolymerization process with DIVE, a solid maleimide oligomer, the phenylmethane maleimide, was used despite the solubility and crystallisation problems encountered with a solid. Its molecular weight is unknown so some approximations were made. Its molar percentage was calculated as a function of the polymer unit. It was dissolved in DIVE by heating at 70°C according to this composition 25 mol% BMI-2300®+75 mol% DIVE+5 wt% TPO. Due to solubility problem, it was not possible to investigate the variation of monomer proportions. As the choice of maleimide compound was really limited, it was decided to synthesize one liquid bismaleimide at the end of this PhD thesis, the poly(propylene glycol) bismaleimide compound (PPGBMI), to confirm some hypothesis and fill out this survey. It is noteworthy to say that by lack of time, all the experimental data have not been collected for the system PPGBMI/DIVE. The synthesis of PPGBMI is thoroughly described in Annex VI. Vásquez *et al*⁷³ has shown that PPGBMI was particularly reactive. Its photopolymerization rate in absence of photoinitiator was close to

the photopolymerization rate for the system tripropylene glycol diacrylate with 3 wt% of D 1173. The chemical structures of these compounds are depicted in Table III. 7.

Table III. 7 : Chemical structures of selected maleimides

Chemical name	Chemical structure
N-tertbutylmaleimide (NTMI)	
Phenylmethane maleimide (BMI-2300®)	
Poly(propylene glycol) bismaleimide (PPGBMI)	

The composition of the different tested formulations is specified in Table III. 8.

Table III. 8 : Composition detail of NTMI 3070 DIVE, BMI-2300®2575 DIVE and PPGBMI 3070 DIVE

Formulation name	Composition		
	mol% of MI double bond function	mol% of DIVE double bond function	wt% of TPO
NTMI 3070 DIVE	30	70	5
BMI-2300®2575 DIVE	25	75	5
PPGBMI 3070 DIVE	30	70	5

According to Table III. 9, under our experimental conditions, the $R_{p_{max}}/[M]_0$ value for the maleimide monomer is about 2-3 times higher than for the vinyl ether depending on its nature and its viscosity. The difference is all the more noticeable than the formulation is less viscous. The formulations are ranked in descending order of viscosity as follows: NTMI 3070 DIVE > PPGBMI 3070 DIVE > BMI-2300®2575 DIVE. These results are consistent with the results found for the formulation NTMI 3070 TRIVE. Therefore, the same arguments can be used herein for the interpretation of the kinetics parameters.

BMI-2300® possesses a higher functionality and a lower irritancy than NTMI so we will continue our study with the system BMI-2300®2575 DIVE. For convenience sake, the use of PPGBMI/DIVE mixture would have been more suitable but at that time, PPGBMI had

not been synthesized. In the BMI-2300®2575 DIVE formulations in which VE reactive functions are in excess, an important amount of residual vinyl ether insaturations is present which can possibly modify the physical properties of the material in long term. One solution to increase the degree of cure of vinyl ether monomer is to introduce into the formulation a cationic photoinitiator to promote the vinyl ether homopolymerization.

Table III. 9 : Determination of $R_{p_{max}}/[M]_0$, the conversion at 430 s and the mol% of converted reactive functions according to the maleimide nature; in air; Hg-Xe Hamamatsu lamp at 366 nm, light intensity=19 mW/cm²; sample thickness~35 μ m

Formulation name	Function	$R_{p_{max}}/[M]_0$ * 100 (s ⁻¹)	Conversion (%)	mol% of converted reactive functions
NTMI 3070 DIVE	VE	38	36	25
	MI	113	97	29
BMI-2300®2575 DIVE	VE	10	59	44
	MI	19	93	23
PPGBMI 3070 DIVE	VE	43	58	41
	MI	105	94	28

III.5 Influence of the photoinitiator system

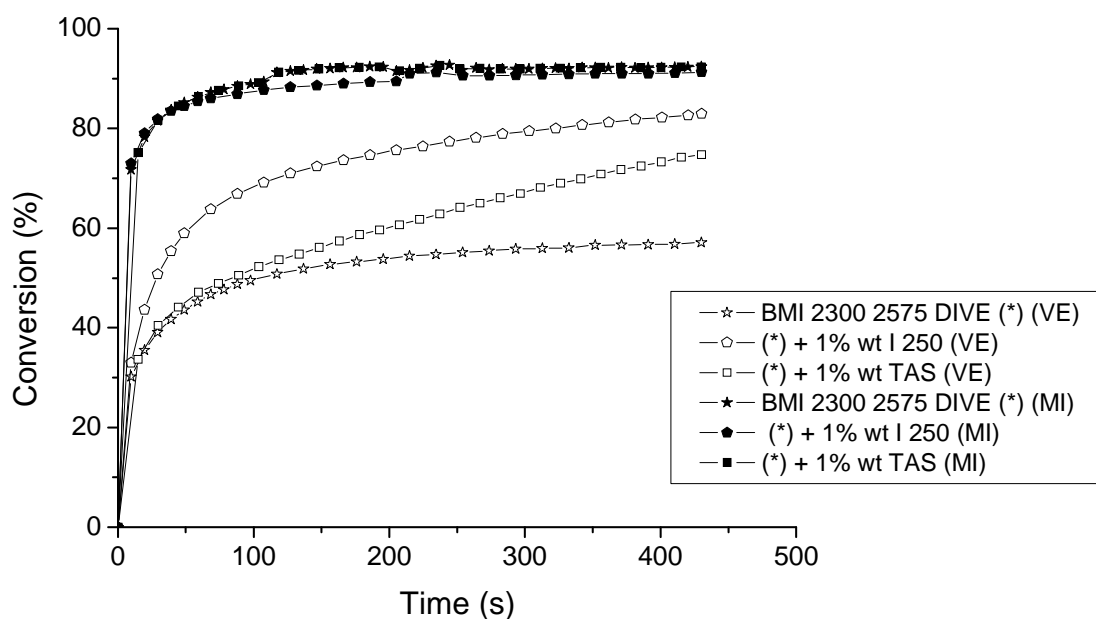
III.5.1 Addition of a cationic photoinitiator to the formulation BMI-2300® 2575 DIVE

For this study, two kinds of onium salts were chosen: the iodonium, (4-methylphenyl)[4-(2-methylpropyl) phenyl]-, hexafluorophosphate(1-) (I 250) and the mixture triarylsulfonium hexafluoroantimonate salts (TAS). They are known to be highly efficient photoinitiators for cationic polymerization. Their structure is drawn in Table III. 10. Mixtures containing 25 mol% BMI-2300® + 75 mol% DIVE+ 5 wt% TPO (BMI-2300®2575 DIVE) and 1 wt% of each cationic photoinitiator were prepared. The name of the formulations is respectively BMI-2300®2575 DIVE +1 wt% I 250 and BMI-2300®2575 DIVE +1 wt% TAS. They were prepared and tested by RT FTIR spectroscopy. Their kinetics profiles were compared to the formulation named BMI-2300®2575 DIVE in which just TPO is present.

Table III. 10 : Chemical structures of the selected cationic photoinitiators

Chemical name	Chemical structure
Iodonium, (4-methylphenyl)[4-(2-methylpropyl) phenyl]-, hexafluorophosphate(1-) (I 250)	
Triarylsulfonium hexafluoroantimonate salts (TAS)	

As it is pointed out in Figure III. 5, the presence of the cationic photoinitiator has no influence on the maleimide kinetics profiles but has a great impact on the vinyl ether conversion. The introduction of TAS and I 250 allow to increase the vinyl ether conversion.



* For an easier reading of the legend, the composition of the formulation BMI-2300@2575 DIVE is written (*)

Figure III. 5 : Effect of the cationic photoinitiator on the kinetics profiles of the formulations BMI-2300@2575 DIVE; BMI-2300@2575 DIVE + 1 wt% I 250; BMI-2300@2575 DIVE + 1 wt% TAS; in air; Hg-Xe Hamamatsu lamp at 366 nm, light intensity=19 mW/cm²; sample thickness~35 μm

Table III. 11 outlines the nearly complete maleimide conversion despite the variation of vinyl ether conversion. The effect of cationic photoinitiator is not preponderant at the beginning of the process. Indeed, similar $R_{p_{max}}/[M]_0$ was found for the formulations with and without the cationic photoinitiators. It seems that first the copolymerization process occurs and is predominant compared to the cationic homopolymerization. After, the copolymerization process slows down showing only the cationic homopolymerization. The improvement is more significant for the formulation containing I 250 than TAS. Indeed, according to the literature, I 250 is more easily sensitized than TAS by the phosphinoyl radicals generated during TPO cleavage owing to its higher reduction potential. This result is also in good accordance with the results presented in Chapter II.

Table III. 11 : Determination of $R_{p_{max}}/[M]_0$, the conversion at 430 s and the mol% of converted reactive functions for the formulations BMI-2300®2575 DIVE; BMI-2300®2575 DIVE + 1 wt% I 250; BMI-2300®2575 DIVE + 1 wt%TAS; same experimental conditions than in Figure III. 5

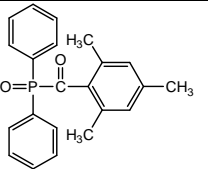
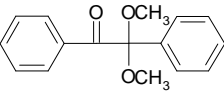
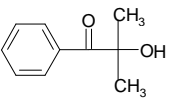
Formulation name	Function	$R_{p_{max}}/[M]_0$ * 100 (s ⁻¹)	Conversion (%)	mol% of converted reactive functions
BMI-2300® 2575 DIVE	VE	10	59	44
	MI	19	93	23
BMI-2300® 2575 DIVE + 1 wt% I 250	VE	10	85	64
	MI	20	91	23
BMI-2300® 2575 DIVE + 1 wt% TAS	VE	10	73	51
	MI	19	93	23

This experiment has demonstrated that an increase in vinyl ether conversion is feasible with a cationic homopolymerization sensitized by the free radicals produced upon radical photoinitiator photolysis. A large choice of radical photoinitiators with distinct absorption features is commercially available. Hence, by a proper choice of the radical photoinitiator, it might be possible to greatly improve the vinyl ether conversion.

III.5.2 Modification of the radical photoinitiator in presence of the cationic photoinitiators TAS and I 250

Based on the best results shown in Chapter II for the cationic polymerization sensitization, TPO was replaced by the benzoin ether photoinitiator 2,2-dimethoxy-1,2-diphenylethan-1-one (Irgacure®651) and the hydroxyl alkyl phenyl ketone 2-hydroxy-2-methyl-1-phenylpropan-1-one (Darocur®1173). Their structure, their molar and weight concentrations and the extinction molar coefficient are gathered in Table III. 12.

Table III. 12 : Chemical structures, weight and molar concentrations and molar extinction coefficients of the selected radical photoinitiators

Name	Chemical structures	Concentration (wt%)	Concentration (mol.L ⁻¹)	$\epsilon_{366nm}^{(*)}$ (L.mol ⁻¹ .cm ⁻¹)
2,4,6-Trimethylbenzoyl-diphenyl phosphine oxide (TPO)		5	0.22	442
2,2-Dimethoxy-1,2-diphenylethan-1-one (I 651)		5	0.30	105
2-Hydroxy-2-methyl-1-phenylpropan-1-one (D 1173)		5	0.51	10

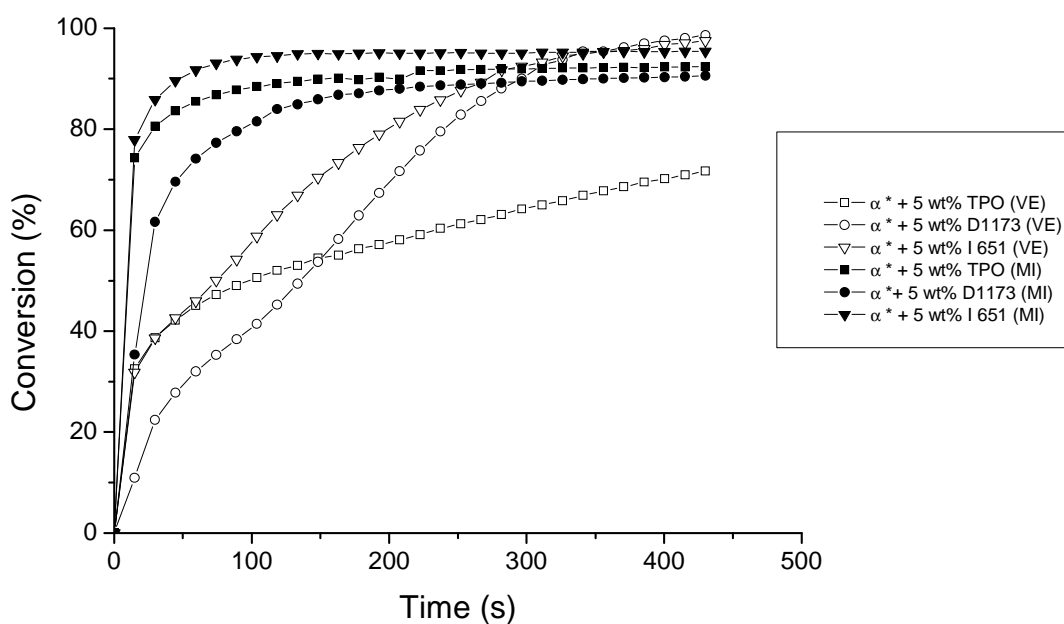
(*) in acetonitrile

For convenience sake, the mixture 25 mol % BMI-2300® + 75 mol % DIVE + 1 wt % TAS will be named α for the next experiments. For instance, the formulation containing 25 mol % BMI-2300® + 75 mol % DIVE + 5 wt% TPO +1 wt % TAS will be named $\alpha + 5 \text{ wt\% TPO}$ (same formulation previously called BMI-2300®2575 DIVE +1 wt% TAS). The name and the composition of the tested formulations are presented in Table III. 13.

Table III. 13 : Name and composition of the different formulations

Formulation name	Composition			
	mol% of BMI-2300® double bond function	mol% of DIVE double bond function	wt% of radical photoinitiator	wt% of TAS (wt%)
$\alpha + 5 \text{ wt \% TPO}$	25	75	5	1
$\alpha + 5 \text{ wt \% I 651}$	25	75	5	1
$\alpha + 5 \text{ wt \% D 1173}$	25	75	5	1

The formulation $\alpha + 5 \text{ wt \% TPO}$ is taken as reference. The kinetics profiles obtained by RT FTIR spectroscopy are represented in Figure III. 6. The difference in reactivity is significant. According to the nature of the radical photoinitiator, the polymerization rate for both reactive functions and the final conversion for vinyl ether monomer can be modified.



* α represents the mixture 25 mol % BMI-2300® + 75 mol % DIVE +1 wt % TAS

Figure III. 6 : Influence of the radical photoinitiator on the kinetics profile of the different formulations α + 5 wt % I 651 and α + 5 wt % D 1173; in presence of 1 wt% TAS; reference formulation: α + 5 wt % TPO; in air; Hg-Xe Hamamatsu lamp at 366 nm, light intensity=19 mW/cm²; sample thickness~35 μ m

The polymerization rate for both reactive functions was found to be higher for the formulation α + 5 wt % TPO than for the formulations α + 5 wt % I 651 and α + 5 wt % D 1173. According to Table III. 12, TPO exhibits a higher molar extinction coefficient than I 651 and D 1173 which promotes the production of radicals and leads to a larger polymerization rate. By contrast, in Table III. 14, the degree of cure reached by vinyl ether monomer for the formulations α + 5 wt % I 651 and 5 wt % D 1173 is nearly total whereas the degree of cure is levelling off at 73% for the formulation α + 5 wt % TPO. This incomplete vinyl ether conversion might be explained by the premature vitrification of the medium due to a higher polymerization rate for the later system. Additionally, the initial concentration of both D 1173 and I 651 are slightly higher than for TPO. In Chapter II, we have demonstrated that alkoxybenzyl and α -hydroxyl radicals from I 651 and D 1173 photolysis respectively were more efficient photosensitizers than phosphinoyl radicals towards TAS.

As it is shown in Table III. 14, the replacement of TAS by I 250 does not influence the $R_{p_{max}}/[M]_0$ of the different systems but contributes to increase the degree of cure. For

formulations comprising both I 250 and a radical photoinitiator, the mixture 25 mol % BMI-2300® + 75 mol % DIVE + 5 wt% TPO + 1 wt % I 250 is written down β .

The compositions of the formulations are similar to the one reported in Table III. 13 replacing α by β and TAS by I 250.

Table III. 14 : Determination of $R_{p_{max}}/[M]_0$ and the degree of cure for different formulations $\alpha + 5$ wt % TPO, $\alpha + 5$ wt % I 651 and $\alpha + 5$ wt % D 1173 (in presence of 1 wt% TAS); $\beta + 5$ wt % TPO, $\beta + 5$ wt % I 651 and $\beta + 5$ wt % D 1173 (in presence of 1 wt% I 250); reference formulation: BMI-2300®2575 DIVE; same experimental conditions than in Figure III. 6

Formulation name	Function	$R_{p_{max}}/[M]_0$ *100 (s ⁻¹)		Conversion (%) at 430 s	
		α	β	α	β
α or β + 5 wt% TPO	Vinyl ether (1637 cm ⁻¹)	10	11	73	85
	Maleimide (697 cm ⁻¹)	19	24	93	91
α or β +5 wt% I 651	Vinyl ether (1637 cm ⁻¹)	5	3	98	88
	Maleimide (697 cm ⁻¹)	14	13	95	92
α or β +5 wt% D 1173	Vinyl ether (1637 cm ⁻¹)	1	0.9	99	100
	Maleimide (697 cm ⁻¹)	3	2.6	91	88

Another possibility to increase the degree of cure of both reactive functions is by performing a post-curing treatment. This process is currently used in stereolithography in order to reach the required mechanical properties. Usually, an UV oven with broadband UV lamps is used to thoroughly polymerize the laser cured part. It will be compared to thermal post-curing.

III.6 Influence of the post-curing treatment

To perform these experiments, we decided to work with formulations undergoing an incomplete photopolymerization process such as the formulations NTMI/TRIVE.

After RT FTIR experiments at 366 nm, the photopolymers obtained from NTMI/TRIVE mixtures were subjected to UV and thermal post curing treatments. The UV curing post treatment lied in curing the samples with a fusion lamp type H associated to a conveyor belt speed of 10 m/min. Four passes were done. Conversely, for the thermal post cure process, the samples were maintained in an oven at a temperature of 110°C during 1 and 2 hours.

The final conversion was determined by RT FTIR spectroscopy before and after they had been post cured under UV and thermal exposure. The characteristic IR absorption bands for monitoring the disappearance of both reactive functions were the same than previously. Nonetheless, an internal standard band was chosen in order to compensate

the eventual change in sample thickness owing to the post curing treatments. The absorption band at 750 cm^{-1} ascribed to =C-H aromatic ring was used as internal standard⁷² band for the calculation.

The corrected conversion is determined according to this formula:

$$\text{Corrected conversion} = \frac{\frac{A_{0_{c=c}}}{A_{0_{ref}}} - \frac{A_{t_{c=c}}}{A_{t_{ref}}}}{\frac{A_{0_{c=c}}}{A_{0_{ref}}}} \times 100 \quad (\text{III.2})$$

With

$A_{0_{c=c}}$ corresponding to the area of IR absorption band of reactive double bond at $t=0$ s

$A_{0_{ref}}$ corresponding to the area of the reference IR absorption band of =C-H aromatic ring at $t=0$ s

$A_{t_{c=c}}$ corresponding to the area of IR absorption band of reactive double bond at t s

$A_{t_{ref}}$ corresponding to the area of the reference IR absorption band of =C-H aromatic ring at t s

Table III. 15 reports the evolution of the degree of cure as a function of UV and thermal post-curing treatment for the different formulations NTMI 3070 TRIVE, NTMI 5050 TRIVE and NTMI 7030 TRIVE. The results highlight the fact that for all the formulations, the UV and the thermal post-curing treatment yield to the same final conversion for both reactive functions. One can expect that under the thermal post curing treatment, the mobility of radicals raise due to the increase in temperature which yields to an increase in double bond conversion. Under UV post curing treatment, additional free radicals are produced from the photolysis of maleimide leading also to further double bond conversion.

For formulations NTMI 3070 TRIVE and NTMI 5050 TRIVE, the increase in conversion for both reactive functions is very low because the few unreacted maleimide functions left (between 5 and 8 mol%) might be trapped within the three dimensional polymer networks. Their action might be probably hindered. For the formulation NTMI 7030 TRIVE, a conversion of 100 % is observed for double vinyl ether functions whilst an almost complete polymerization is attained for the maleimide function. The increase in the conversion is more important for the double bond maleimide function than for the double vinyl ether function (+14% for the double bond maleimide function and +9% for the double bond vinyl ether function) because the maleimide homopolymerization occurs

concomitantly with the copolymerization process. The levelling off of the double bond maleimide conversion might stem from the low amount of unreacted maleimide function left and the vitrification phenomenon.

Table III. 15 : Effect of UV and thermal post-curing treatment on the degree of cure of the formulations NTMI 3070 TRIVE, NTMI 5050 TRIVE, NTMI 7030 TRIVE studied in Table III. 4

Formulation name	Function	Conversion after the curing at 366nm (%)	Conversion after the UV post curing (%)				Conversion after the curing at 366nm (%)	Conversion after the thermal post curing (%)	
			1 st (b)	2 nd (b)	3 rd (b)	4 th (b)		1h (c)	2h (c)
		(a)							
NTMI 3070 TRIVE	VE	46	48	48	49	49	41	49	52
	MI	82	81	81	81	81	79	78	79
NTMI 5050 TRIVE	VE	73	75	77	78	78	73	79	81
	MI	85	87	87	88	88	85	89	89
NTMI 7030 TRIVE	VE	91	91	100	100	100	94	100	100
	MI	77	84	87	88	90	74	92	93

Curing conditions:

- Hg-Xe hamamatsu lamp at 366 nm, light intensity~19 mW/cm² during 430 s, sample thickness~35 μ m
- UV belt conveyor with a fusion lamp type H, 10 m/min, light intensity: UVA: 440 mJ/cm², UVB: 430 mJ/cm², UVC: 90 mJ/cm², UVV: 480 mJ/cm², 4 passes done, conversion after each pass
- Sample heated at 110°C in oven during 1h and 2 h

These experiments have demonstrated MI/VE systems are highly reactive systems that can give rise to fully cured materials depending on both the nature of the monomers, the radical and cationic photoinitiators. It will be interesting now to investigate the thermal mechanical properties of the most relevant above-mentioned formulations.

III.7 Thermomechanical properties

The mechanical properties especially the glass transition temperature and the Young's modulus were evaluated for the most relevant above-mentioned formulations by using a DMA equipment in tension mode. The curing and the measurement procedures are explained in detail in Annex I.2 and Annex III.1. The degree of cure reached by the monomers corresponds to the values given in Table III. 15 after the UV post-curing. The glass transition temperature and the Young's modulus values are presented in Table III. 16. The commercial resin Renshape®SL Y-C 9500 was used as reference. From these results, it can be noticed that the monomer proportions within the matrix influences a lot the final mechanical properties. For maleimide double bond concentration above 50 mol%, the formulations exhibit interesting features. Their Young's modulus values are comparable to the value obtained for Renshape®SL Y-C 9500 and their T_g values are

higher. An increase of almost 100°C is observed. This difference can be attributed to the high rigidity of MI combined with the fact that more maleimide double bonds have been converted. These formulations gave rise to highly crosslinked materials.

By contrast, when the vinyl ether monomer is in excess, both Young's modulus and T_g values decrease. The Young's modulus values are divided by a factor 4 to 40 depending on the nature of the formulations. As regards to the T_g values, they are similar to the Renshape®SL Y-C 9500 photopolymer. In the formulations NTMI 3070 TRIVE, NTMI 3070 DIVE, BMI-2300®2575 DIVE, about 30-45 mol% of unpolymerized vinyl ether double bond are still remaining after the curing. They may act as plasticizers which lowers the density of crosslinking and cause a decrease in the T_g value as well as in Young's modulus. The increase in DIVE double bond conversion, as it is the case for the formulation $\alpha + 5$ wt% D 1173 with the introduction of the cationic photoinitiator does not lead to a significant increase in both the Young's modulus and T_g values. On the contrary, both values are lower. It was demonstrated by a few experiments that are not presented here that the presence of DIVE decreased the T_g value probably due to the long chains in the backbone. The structure of the monomer also plays an important role. The increase in functionality improves the degree of crosslinking. Therefore, a rise of 30°C in T_g values was noticed between the formulation with TRIVE and DIVE. The influence of the functionality on the Young's modulus is more important for the mixtures NTMI 3070 TRIVE and NTMI 3070 DIVE where vinyl ether double bond functions are in excess.

Table III. 16 : Determination of the glass transition temperatures and Young's moduli for the reference Renshape®SL Y-C 9500 resin and some MI/VE formulations

	Young's modulus (MPa) (a)	T_g (°C) (a)
SL Y-C 9500	1430 ± 100	92
NTMI 3070 TRIVE	438 ± 65	88
NTMI 5050 TRIVE	1325 ± 87	176
NTMI 7030 TRIVE	1240 ± 91	202
NTMI 3070 DIVE	45 ± 4	53
NTMI 5050 DIVE	1365 ± 295	132
NTMI 7030 DIVE	1685 ± 115	171
NTMI 5050 CDDVE	-	
NTMI 7030 CDDVE	-	260
BMI-2300®2575 DIVE	358 ± 61	84
$\alpha + 5$ wt% TPO	-	92
$\beta + 5$ wt% TPO	-	81
$\alpha + 5$ wt% I 651	Too brittle	
$\alpha + 5$ wt% D 1173	240 ± 37	74

(a) samples cured under UV belt conveyor with a fusion lamp type H, 10 m/min, light intensity: UVA: 440 mJ/cm², UVB: 430 mJ/cm², UVC: 90 mJ/cm², UVV: 480 mJ/cm², 4 passes done, sample thickness~90 μ m

The formulations containing a high content of maleimide display high T_g s and Young's modulus which fulfills a part of the specific properties of SL resins in terms of rigidity and robustness. Another requirement that these resins should meet is a low shrinkage. Shrinkage is a topical issue in stereolithography because the UV curable resins tend to develop a non uniform linear shrinkage during the photopolymerization process which results in residual internal stresses responsible for distortions and changes in the generating part dimensions. As a consequence, the linear shrinkage of these materials has been determined.

III.8 Determination of the volumetric shrinkage and linear deflection

Both volumetric and linear shrinkage were determined for some formulations listed in Table III. 17. The volumetric shrinkage was evaluated by calculating the density of the formulation before and after curing according to the procedure described in Chapter IV. The linear shrinkage was indirectly assessed by straightforwardly measuring the deflection of a coated cantilever upon irradiation (cf Chapter IV). All the data were compared to the values found for the formulation containing 95 wt% trimethylolpropane triacrylate (TMPTA) + 5 wt % TPO (named TMPTA), the commercial acrylic Renshape® SL Y-C 9500 and hybrid acrylate/epoxide Renshape®SL 7800 resins.

Table III. 17 : Determination of the linear deflection for the most relevant formulations

	Average deflection (mm) (a)
TMPTA *	6.8 ± 2
Renshape®SL Y-C 9500 *	0.6 ± 0.25
Renshape®SL 7800	0.3 ± 0.25
NTMI 5050 TRIVE	2.2 ± 0.75
NTMI 7030 TRIVE	0.7 ± 0.25
BMI-2300®2575 DIVE	0.6 ± 0.25
α + 5 wt% TPO	1.0 ± 0.25
β + 5 wt% TPO	0.7 ± 0.25

* The UV cured samples are not tack free

(a) samples cured with a Hg Oriol lamp, light intensity~24 mW/cm², sample thickness~50 μm

Before interpreting the results, it is important to say that some samples are not fully cured so the degree of shrinkage might be undervalued in these cases. For a proper comparative study, all the formulations should reach the same degree of cure upon UV irradiation.

By referring to the data from Table III. 17, we first notice that our reference formulation TMPTA undergoes both high volumetric shrinkage and linear deflection which is in good agreement with literature. The conversion of the vinyl double bonds into short covalent bonds induces an important volume contraction.

Secondly, as presumed, the commercial resins Renshape®SL Y-C 9500 and Renshape®SL 7800 were optimized in order to develop both low volumetric shrinkage and linear deflection. Although, Renshape®SL Y-C 9500 is an acrylic resin, the volumetric shrinkage and the linear deflection values are low because this formulation is a mixture comprising various compounds such as high molecular weight oligomers that contribute to decrease the shrinkage magnitude as the concentration of reactive function within the formulation decreases⁷⁴. The result for the hybrid Renshape®SL 7800 resin is not really surprising. Indeed, this optimized mixture is mainly constituted of epoxide resin (70 wt%) and it is well established that the volumetric shrinkage for epoxides is low (between 2-6%) due to the ring opening process⁷⁵. Indeed, during the ring opening process, the release of ring strain counterbalances the volume contraction due to the conversion of the Van der Waal's interactions into shorter covalent bands⁷⁶.

Finally, concerning the maleimide and vinyl ether monomers formulations, drawing conclusions is not so obvious. It seems that the shrinkage level depends on the vinyl ether reactive function content.

In the equimolar mixture NTMI 5050 TRIVE, the shrinkage magnitude is relatively high. This can be accounted for the presence of vinyl double bonds within the vinyl ether monomers. They are responsible for important volume contraction of these monomers during the polymerization process. The shrinkage level is similar to the acrylate one.

By contrast, if the vinyl ether reactive function content is in default such as NTMI 7030 TRIVE, the formulation is characterized by both low volumetric shrinkage and linear deformation. Moreover, despite an important conversion of DIVE double bonds in the formulations BMI-2300®2575 DIVE in presence of both a radical and a cationic photoinitiators, the linear deformation of these formulations is in the same range than for the formulation NTMI 7030 TRIVE because the rate of polymerizations of these systems are tremendously lower than for the system NTMI/TRIVE. For instance, for the formulation $\alpha + 5$ wt% D 1173 the polymerization rates for vinyl ether and maleimide are respectively 72 and 28 times lower than the polymerization rates for the mixture NTMI 5050 TRIVE. Consequently, the system might have time to relax. Additionally, BMI-2300® is an oligomer with long chains so the shrinkage phenomenon might be limited. The value found for the formulation BMI-2300®2575 DIVE is slightly lower because of the presence of unconverted vinyl ether molecules (cf Table III. 14, 31 mol% of unconverted vinyl ether reactive functions are present after the photopolymerization) acting as plasticizers.

The experiments have not been done for the formulation comprising vinyl ether reactive function content with an excess NTMI 3070 TRIVE but we can suppose that the level of shrinkage might be low as a substantial amount of uncured vinyl ether molecules might partially release the internal stresses.

The mixtures NTMI 5050 TRIVE and NTMI 7030 TRIVE were shown to be very interesting in terms of reactivity, degree of cure and thermomechanical properties. Keeping in mind that no optimization was made, at an equimolar monomer ratio, both volumetric and linear shrinkage are high due to the vinylic polymerization process. However, the formulation NTMI 7030 TRIVE exhibited low shrinkage, in the same range than the one for Renshape®SL 7800 resin, a nearly complete polymerization for both reactive function (completion of the conversion with the post curing treatment) and the UV cured material displays a high T_g value (202 °C).

These systems exhibit final properties close to those required for SLA application justifying deeper investigations in particularly on the nature of maleimide comonomer in order to reduce the shrinkage magnitude.

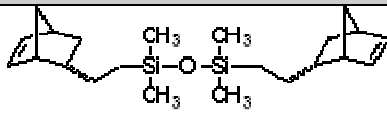
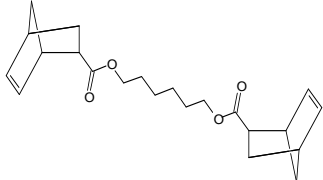
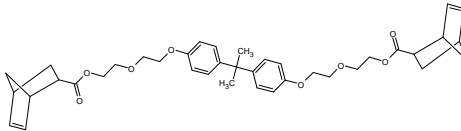
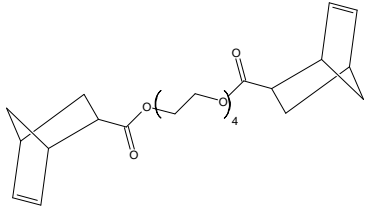
IV INVESTIGATIONS ON THE POLYMERIZATION OF MALEIMIDE / NORBORNENE MIXTURES IN PRESENCE OF RADICAL PHOTOINITIATOR

IV.1 Introduction

Among the available electron rich olefins, norbornenes (NOR) have shown to be promising in thiol-ene chemistry because of their higher reactivity in comparison with vinyl ethers. The fast polymerization of thiol-norbornene is accounted for the alleviation of the ring strain due to the addition of the thiyl radical onto the double bond and the rapidity of the H abstraction reaction between the thiol and the carbon centered radical. Moreover, the UV cured thiol-norbornene materials have high T_g values because of the rigidity of the norbornene structure. It would be now interesting to observe and to understand the influence of norbornene moiety on the maleimide chemistry to see if the backbone chemistry and the norbornene function can impact the polymerization kinetics, the network structure and the shrinkage. Few norbornenes are commercially available. We used the 1,1,3,3-tetramethyl-1,3-bis[2-(5-norbornen-2-yl)ethyl]disiloxane, mixture of endo and exo (TBDNS) from Aldrich. This kind of silicon monomers displays particular features as regards to the surface properties, and thermal resistance. It is not representative of the behaviour of the common norbornenes. Thus, we synthesized 3 norbornenes according to the synthesis procedures presented in Annex VII.

We synthesized the compound 1,6-hexanediol di-(endo,exo-norborn-2-ene-5-carboxylate) (HDDNEC). This compound has already been synthesized by Carioscia³¹. Meanwhile, the norbornenes bis-2,2-[4-(2-[norborn-2-ene-5-carboxylate] ethoxy) phenyl] propane (EBANEC) and polyethylene glycol (200) di-(norborn-2-ene-5-carboxylate) (PEGNEC) were to our knowledge for the first time synthesized. HDDNEC and PEGNEC were chosen for their linear chain within their backbone and the presence of respectively 2 and 8 easily abstractable H in order to study the influence of easily abstractable H on the polymerization mechanism in presence of a radical photoinitiator. Concerning EBANEC, its backbone contains the rigid bisphenol A moiety since it imparts outstanding mechanical properties such as high T_g value, toughness, rigidity and elevated temperature performance. Their chemical structures are reported in Table III. 18.

Table III. 18 : Chemical structures of the tested norbornene monomers

Chemical name	Chemical structure
TBDNS	
HDDNEC	
EBANEC	
PEGNEC	

They were studied with respectively NTMI (cf Table III. 19) and PPGBMI (cf Table III. 20) in equimolar ratio. The typical IR absorption bands at 697 cm^{-1} corresponding to the deformation of maleimide ring plane for =C-H bond and the band at 719 cm^{-1} ²³ attributed to the norbornene out of plane bending C-H vibration⁷⁷ were not selected for this study due to the overlap between the maleimide IR absorption band at 697 cm^{-1} and a neighbouring norbornene IR absorption band. Hence, we worked with the IR bands at 3059 cm^{-1} ⁷⁸ and 3105 cm^{-1} ⁷⁹ which correspond respectively to the norbornene =C-H stretching vibration and maleimide =C-H stretching vibration. Although the intensity of

these IR bands is lower than for the bands 697 cm^{-1} and 719 cm^{-1} , the kinetics profiles are equivalent so these new bands are appropriate for our study. The kinetics curves are plotted in Figure III. 7.

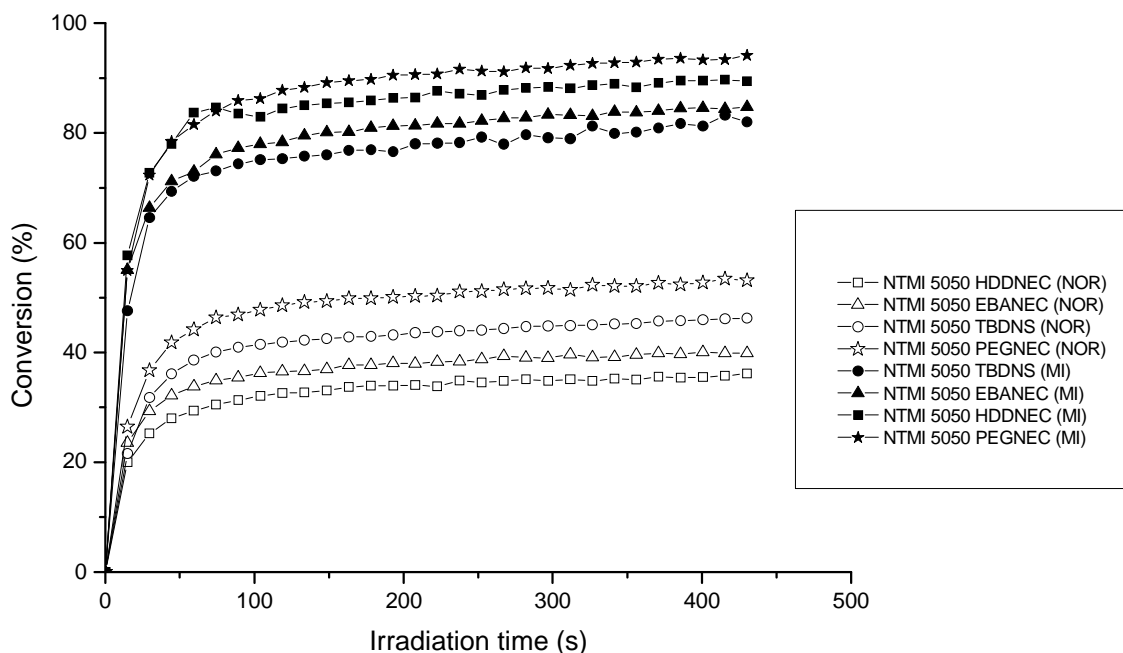


Figure III. 7 : Influence of the norbornene structure on the kinetics of photopolymerization of the mixtures containing 50 wt% of NTMI and 50 wt% of various norbornenes reported in Table III. 18; in air; Hamamatsu lamp at 366 nm , light intensity= 19 mW/cm^2 ; sample thickness $\sim 35\text{ }\mu\text{m}$

The trend is the same for all the formulations no matter the norbornene nature. According to Table III. 19, $R_{p_{\max}}/[M]_0$ for NTMI is about 3 times higher than for the norbornene. Additionally, the conversion of the maleimide double bond is twice greater than the norbornene double bond conversion. Like vinyl ether monomer, the norbornene does not undergo any significant homopolymerization but it can radically copolymerize. So it can be assumed that about half of maleimide double bond functions have participated to the homopolymerization and the other half has reacted with the norbornene double bonds. The reactivity of the MI/NOR systems is significantly less important than for the systems NTMI/TRIVE and NTMI/DIVE but it is better than for the system NTMI/BDVE whose backbone is close to HDDNEC. It should have been interesting to evaluate the reactivity of a norbornene with DIVE backbone but we did not find an acrylate with the same DIVE backbone. Another difference with the system NTMI/VE is the low degree of cure reached by the norbornene between 34 and 50%. The maleimide homopolymerization is promoted at the expense of the copolymerization process.

Perhaps, the free radicals generated during the radical photoinitiator photolysis are not so reactive towards norbornene double bond. The corresponding addition rate constant might be lower than the one between the free radicals and the vinyl ether double bond. We can also assume that the affinity between the maleimide and the vinyl ether is better than between the maleimide and the norbornene. The monomer reactivity ratios could be determined.

The use of a silicon monomer affects mainly the photopolymerization of the maleimide. Both the degree of cure and the polymerization are lower in comparison with the systems using typical norbornene. However, the degree of cure reached by the norbornene is more important in the system NTMI/TBDNS.

Table III. 19 : Determination of $R_{p_{max}}/[M]_0$, the conversion at 430 s and the mol% of converted reactive functions for mixtures containing 50 wt% of NTMI and 50 wt% of various norbornenes reported in Table III. 18; same experimental conditions than in Figure III. 7

Name	Function	$R_{p_{max}}/[M]_0 \cdot 100 \text{ (s}^{-1}\text{)}$	Conversion (%)	mol% of converted reactive functions
NTMI 5050 TBDNS	MI	4.3	78	39
	NOR	1.7	46	23
NTMI 5050 HDDNEC	MI	5.4	94	47
	NOR	2.1	50	25
NTMI 5050 EBANEC	MI	6.6	85	43
	NOR	2.1	37	19
NTMI 5050 PEGNEC	MI	6.8	91	46
	NOR	1.9	34	17

As shown in Table III. 20, the use of PPGBMI instead of NTMI barely affects the kinetics of photopolymerization for the different norbornenes but rather influences the results for the maleimide polymerization. The higher reactivity of PPGBMI contributes to some extent to increase the maleimide polymerization rate sometimes at the expense of the final conversion. It seems that in low viscous PPGBMI 5050 HDDNEC mixture, the difference of reactivity between the maleimide and the norbornene functions is more pronounced because the polymerization rate for the maleimide is 3.7 times higher than for the norbornene.

Table III. 20 : Determination of $R_{p_{max}}/[M]_0$, the conversion at 430 s and the mol% of converted reactive functions for mixtures containing 50 wt% of PPGBMI and 50 wt% of various norbornenes reported in Table III. 18; same experimental conditions than in Figure III. 7

Name	Function	$R_{p_{max}}/[M]_0$ * 100 (s ⁻¹)	Conversion (%)	mol% of converted reactive functions
PPGBMI 5050 HDDNEC	MI	11	99	49.5
	NOR	2.7	48	24
PPGBMI 5050 EBANEC	MI	6.8	77	39
	NOR	1.5	32	16
PPGBMI 5050 PEGNEC	MI	7.8	78	39
	NOR	1.4	30	15

IV.2 Thermomechanical properties

The glass transition temperature for the formulations NTMI with the difunctional norbornene TBDNS was determined in the same experimental conditions than previously. The values are reported in Table III. 21. They are in between the values found for the system NTMI with the difunctional DIVE and the values found for the system NTMI with the trifunctional TRIVE. The rigidity of both maleimide and norbornene functions might account for these results. By lack of time, the thermomechanical properties of the other formulations have not been assessed.

Table III. 21 : Determination of the glass transition temperatures for the Renshape®SL Y-C 9500 reference formulation and some MI/VE and MI/TBDNS formulations

	T_g (°C) (a)
Renshape®SL Y-C 9500	92
NTMI 5050 TRIVE	176
NTMI 7030 TRIVE	202
NTMI 5050 DIVE	132
NTMI 7030 DIVE	171
NTMI 5050 TBDNS	156
NTMI 7030 TBDNS	196

(a) samples cured under UV belt conveyor with a fusion lamp type H, 10 m/min, light intensity: UVA: 440 mJ/cm², UVB: 430 mJ/cm², UVC: 90 mJ/cm², UVV: 480 mJ/cm², 4 passes done, sample thickness~90 μm

Likewise, the volumetric shrinkage and the linear deflection for the formulations NTMI with the difunctional norbornene TBDNS were assessed.

IV.3 Volumetric shrinkage and linear deflection

The data from Table III. 22 disclose that both NTMI 5050 TBDNS and NTMI 7030 TBDNS formulations display a very low linear deformation in comparison with the formulations TMPTA or NTMI/TRIVE. The value is similar to the value for the commercial hybrid mixture Renshape®SL 7800. However, for the same reason as previously mentioned, this value has to be taken with caution because the NTMI 5050 TBDNS and NTMI 7030 TBDNS samples are not fully cured.

Table III. 22 : Determination of the linear deflection for the TMPTA reference formulation, the commercial resins Renshape®SL Y-C 9500 and Renshape®SL 7800, the NTMI/TRIVE and NTMI/TBDNS mixtures

	Average deflection (mm) (a)
TMPTA *	6.8 ± 2
Renshape®SL Y-C 9500 *	0.6 ± 0.25
Renshape®SL 7800	0.3±0.25
NTMI 5050 TRIVE	2.2 ± 0.75
NTMI 7030 TRIVE	0.7 ± 0.25
NTMI 5050 TBDNS *	0.1 ± 0.25
NTMI 7030 TBDNS *	0.3 ± 0.25

* The UV cured samples are not tack free.

(a) samples cured with a Hg Oriel lamp, light intensity~24 mW/cm², sample thickness~50 µm

According to these previous experiments, the MI/NOR systems seem less reactive than MI/VE systems but in compensation the shrinkage level seems lower. Before any optimization, it would be interesting to test the MI/NOR systems under Griffin (Araldite®Digitalis demonstrator) in order to check if the green strength is reached even at high exposure speed.

V CONCLUSIONS AND PERSPECTIVES

Among the potential alternatives to conventional UV curable resins, we selected the MI/VE systems knowing perfectly that we needed to synthesize maleimide monomers owing to their limited commercial availability. Interestingly, these systems almost meet all the Huntsman requirements for Araldite®Digitalis application.

Primarily, as regards to the kinetics of photopolymerization, the RT FTIR experiments pointed out not only their high reactivity in presence of a radical photoinitiator but also the complexity of the photopolymerization process. Indeed, the variation of the monomer concentrations has revealed that side reactions might occur at the same time than the maleimide homopolymerization and the maleimide/vinyl ether copolymerization. In addition, the polymerization rate was shown to be strongly dependent on the formulation viscosity (due to oxygen inhibition and the reactive species mobility) and the nature of the monomers especially the nature of the vinyl ether. Decker has suggested that vinyl ethers are more reactive towards free radicals than N-substituted maleimides¹³. The assessment of this later parameter was particularly difficult owing to the lack of availability of commercial liquid maleimides.

Furthermore, the introduction of an onium salt into the formulation has proved to substantially enhance the conversion of vinyl ether double bond without affecting the maleimide homopolymerization. A nearly complete polymerization was achieved by both functions. This improvement is based on the sensitization of the cationic photoinitiator by free radicals generated during the radical photoinitiator photolysis. Therefore, better results were found for the formulations comprising the iodonium salt than the sulfonium salt because the iodonium salt is more easily sensitized owing to its higher reduction potential. On the contrary, the variation of the radical photoinitiator affects both the maleimide and the vinyl ether kinetics of photopolymerization since the radical photoinitiator plays an important role in the initiation step of the radical polymerization and in the sensitization process of the cationic polymerization.

Secondly, in terms of thermomechanical properties, the DMA analysis demonstrated that these systems led to UV cured materials displaying not only high T_g values but also high tensile modulus, close to the references values (MI double bond functions ≥ 50 mol%). The shrinkage measurements disclosed that low linear deflection could be achieved by decreasing the amount of vinyl ether (VE reactive functions ≤ 30 mol %) within the mixture or by choosing another comonomer. Given these promising results obtained with both RT FTIR spectroscopy and DMA, the most suitable formulation i.e NTMI 7030 TRIVE was tested with Griffin (Araldite®Digitalis demonstrator). Interestingly, the green strength was reached even at high speed such as 10 mm/s (the optimal speed was settled by

Huntsman at 14 mm/s). From these first experiments, this formulation could be used for RP under Araldite® Digitalis. However, as for the commercial resins Renshape® SL Y-C 9500 and Renshape® SL 7800, further investigations have to be done before in order to optimize it.

Finally, the replacement of vinyl ether by norbornene did not tremendously modify the reactivity of the maleimide/ donor monomer system. The prospective study showed that some maleimide/ vinyl ether systems notably NTMI/DIVE and NTMI/TRIVE were more reactive. We have supposed that these differences might lie in the intrinsic norbornene nature and also on the affinity of between the norbornene and the maleimide compounds. Consequently, it would be interesting for the future to investigate for example the effect of norbornene regioselectivity on the photopolymerization process, to elucidate the initiation and the propagation mechanism of this system by using laser flash photolysis and RT FTIR spectroscopy techniques and determine the propagation rate constants of the maleimide homopolymerization and maleimide/norbornene copolymerization. Nonetheless, these systems display interesting features such as high T_g values for the UV cured materials and the low extent of shrinkage. Finally, whatever the studied maleimide/norbornene system, a huge quantity of unreacted norbornene double bond functions was present after the photopolymerization (about 50 mol%). To increase the norbornene double bond conversion, it would be interesting to add a catalyst so the residual norbornene can undergo a ring opening metathesis polymerization during a thermal post-curing treatment.

VI REFERENCES

1. Decker, C. *Macromolecular Rapid Communications* **2002**, *23*, 1067-1093.
2. Decker, C. *Techniques de l'ingénieur* **2000**, *Doc AM 3044*
3. Decker, C. *Progress in Polymer Science* **1996**, *21*, 593-650.
4. Fouassier, J.-P., Rabek, J.F, *Radiation Curing in polymer Science and Technology, Polymerizations mechanisms*. Elsevier applied science: 1993; Vol. Vol III
5. Fouassier, J.-P., *Photoinitiation photopolymerization and photocuring fundamentals and applications*. 1995.
6. Decker, C.; Nguyen Thi Viet, T.; Decker, D.; Weber-Koehl, E. *Polymer* **2001**, *42*, 5531-5541.
7. Kohli, P.; Scranton, A. B.; Blanchard, G. J. *Macromolecules* **1998**, *31*, 5681-5689.
8. Cai, Y.; Jessop, J. L. P. *Polymer* **2006**, *47*, 6560-6566.
9. Jonsson, S.; Sundell, P.-E.; Hultgren, J.; Sheng, D.; Hoyle, C. E. *Progress in Organic Coatings* **1996**, *27*, 107-122.
10. Jonsson, S.; Viswanathan, K.; Hoyle, C. E.; Clark, S. C.; Miller, C.; Morel, F.; Decker, C. *Nuclear Instruments and Methods in Physics Research Section B: Beam Interactions with Materials and Atoms* **1999**, *151*, 268-278.
11. Hoyle C. E; Lee Tai Yeon; Roper Todd. *Journal of Polymer Science Part A: Polymer Chemistry* **2004**, *42*, 5301-5338.
12. Ericsson, J.; Nilsson, M.; Lundmark, S.; Svensson, L.; Joensson, S.; Lindgren, K. *Experience the World of UV/EB, RadTech 2000: The Premier UV/EB Conference & Exhibition, Technical Conference Proceedings* **2000**, 173-195.
13. Decker, C.; Bianchi, C.; Morel, F.; Jonsson, S.; Hoyle, C. *Macromolecular Chemistry and Physics* **2000**, *201*, 1493-1503.
14. Olson, K. G.; Butler, G. B. *Macromolecules* **1984**, *17*, 2480-2486.
15. Olson, K. G.; Butler, G. B. *Macromolecules* **1984**, *17*, 2486-2501.
16. Butler, G. B.; Olson, K. G.; Tu, C. L. *Macromolecules* **1984**, *17*, 1884-1887.
17. Lee, C.; Hall, H. K. *Macromolecules* **1989**, *22*, 21-25.
18. Rzaev, Z. M. O. *Progress in Polymer Science* **2000**, *25*, 163-217.
19. Zhang, X.; Li, Z.-C.; Li, K.-B.; Lin, S.; Du, F.-S.; Li, F.-M. *Progress in Polymer Science* **2006**, *31*, 893-948.
20. Reddy, S. K.; Cramer, N. B.; O'Brien, A. K.; Cross, T.; Raj, R.; Bowman, C. N. *Macromolecular Symposia* **2004**, *206*, 361-374.
21. Cramer, N. B.; Davies, T.; O'Brien, A. K.; Bowman, C. N. *Macromolecules* **2003**, *36*, 4631-4636.
22. Reddy, S. K.; Cramer, N. B.; Bowman, C. N. *Macromolecules* **2006**, *39*, 3673-3680.
23. Cramer, N. B.; Reddy, S. K.; O'Brien, A. K.; Bowman, C. N. *Macromolecules* **2003**, *36*, 7964-7969.
24. Morgan, C. R.; Magnotta, F.; Ketley, A. D. *Journal of Polymer Science, Polymer Chemistry Edition* **1977**, *15*, 627-645.
25. Cramer, N. B.; Bowman, C. N. *Journal of Polymer Science, Part A: Polymer Chemistry* **2001**, *39*, 3311-3319.
26. Bowman, C. N. *RadTech Europe 05: UV/EB--Join the Winning Technology, [Conference Proceedings]* **2005**, *2*, 9-14.
27. Lu, H.; Carioscia Jacquelyn, A.; Stansbury Jeffery, W.; Bowman Christopher, N. *Dental materials : official publication of the Academy of Dental Materials* **2005**, *21*, 1129-1136.
28. Allison K. O'Brien, N. B. C. C. N. B. *Journal of Polymer Science Part A: Polymer Chemistry* **2006**, *44*, 2007-2014.

29. Lee, T. Y.; Bowman, C. N. *Polymer* **2006**, *47*, 6057-6065.
30. Reddy, S. K.; Cramer, N. B.; Bowman, C. N. *Macromolecules* **2006**, *39*, 3681-3687.
31. Carioscia, J. A.; Schneidewind, L.; O'Brien, C.; Ely, R.; Feeser, C.; Cramer, N.; Bowman, C. N. *Journal of Polymer Science Part A: Polymer Chemistry* **2007**, *45*, 5686-5696.
32. Carioscia, J. A.; Stansbury, J. W.; Bowman, C. N. *Polymer* **2007**, *48*, 1526-1532.
33. Lee, T. Y.; Smith, Z.; Reddy, S. K.; Cramer, N. B.; Bowman, C. N. *Macromolecules* **2007**, *40*, 1466-1472.
34. Cook, W. D.; Chausson, S.; Chen, F.; Le Pluart, L.; Bowman, C. N.; Scott, T. F. *Polymer International* **2008**, *57*, 469-478.
35. Johnson, P. M.; Stansbury, J. W.; Bowman, C. N. *Journal of Polymer Science Part A: Polymer Chemistry* **2008**, *46*, 1502-1509.
36. Lee, T. Y.; Roper, T. M.; Jonsson, E. S.; Guymon, C. A.; Hoyle, C. E. *Macromolecules* **2004**, *37*, 3606-3613.
37. Senyurt, A. F.; Wei, H.; Hoyle, C. E.; Piland, S. G.; Gould, T. E. *Macromolecules (Washington, DC, United States)* **2007**, *40*, 4901-4909.
38. Wei, H.; Li, Q.; Ojelade, M.; Madbouly, S.; Otaigbe, J. U.; Hoyle, C. E. *Macromolecules* **2007**, *40*, 8788-8793.
39. Wei, H.; Senyurt, A. F.; Jönsson, S.; Hoyle, C. E. *Journal of Polymer Science Part A: Polymer Chemistry* **2007**, *45*, 822-829.
40. Wutticharoenwong, K.; Soucek, M. D. *Macromolecular Materials and Engineering* **2008**, *293*, 45-56.
41. Ortiz, R. A.; Urbina, B. A. P.; Valdez, L. V. C.; Duarte, L. B.; Santos, R. G.; Valdez, A. E. G.; Soucek, M. D. *Journal of Polymer Science, Part A: Polymer Chemistry* **2007**, *45*, 4829-4843.
42. Ortiz, R. A.; Urbina, B. A. P.; Santos, R. G.; Duarte, L. B.; Valdez, A. E. G.; Soucek, M. D. *Macromolecular Materials and Engineering* **2008**, *293*, 731-739.
43. El-Roz, M.; Lalevee, J.; Allonas, X.; Fouassier, J.-P. *Macromolecular Rapid Communications* **2008**, *29*, 804-808.
44. Lalevee, J.; El-Roz, M.; Allonas, X.; Fouassier, J. P. *Journal of Polymer Science, Part A: Polymer Chemistry* **2008**, *46*, 2008-2014.
45. Hoyle, C. E.; Miller, C. W.; Jonsson, E. S. *Trends in Photochemistry & Photobiology* **1999**, *5*, 149-167.
46. Maugiere-Guyonnet, F., thesis, Université de Haute-Alsace, Mulhouse, 2004.
47. Decker, C.; Morel, F.; Jonsson, S.; Clark, S.; Hoyle, C. *Macromolecular Chemistry and Physics* **1999**, *200*, 1005-1013.
48. Morel, F., thesis, Université de Haute-Alsace, Mulhouse, 1998.
49. Burget, D.; Mallein, C.; Fouassier, J. P. *Polymer* **2003**, *44*, 7671-7678.
50. Decker, C.; Bianchi, C.; Jönsson, S. *Polymer* **2004**, *45*, 5803-5811.
51. Decker, C.; Bianchi, C.; Decker, D.; Morel, F. *Progress in Organic Coatings* **2001**, *42*, 253-266.
52. Jönsson, S.; Sundell, P. E.; Shimose, M.; Clark, S.; Miller, C.; Morel, F.; Decker, C.; Hoyle, C. E. *Nuclear Instruments and Methods in Physics Research Section B: Beam Interactions with Materials and Atoms* **1997**, *131*, 276-290.
53. Decker, C. *Polymer International* **1998**, *45*, 133-141.
54. Decker, C.; Decker, D. *Polymer* **1997**, *38*, 2229-2237.
55. Decker, C.; Bianchi, C.; Decker, D.; Morel, F. *Experience the World of UV/EB, RadTech 2000: The Premier UV/EB Conference & Exhibition, Technical Conference Proceedings* **2000**, 741-753.

56. Ng, L.-T.; Swami, S.; Jönsson, S. *Radiation Physics and Chemistry* **2004**, *69*, 321-328.
57. Jonsson, S.; Viswanathan, K.; Hoyle, C. E.; Clark, S. C.; Miller, C.; Nguyen, C.; Zhao, W.; Shao, L.; Morel, F.; Decker, C. *Journal of Photopolymer Science and Technology* **2000**, *13*, 125-143.
58. Jonsson, S.; Hasselgren, C.; Ericsson, J. S.; Johansson, M.; Clark, S.; Miller, C.; Hoyle, C. E. *RadTech'98 North America UV/EB Conference Proceedings* **1998**, 189-206.
59. Hoyle, C. E.; Clark, S. C.; Jonsson, S.; Shimose, M. *Polymer* **1997**, *38*, 5695-5697.
60. Yang, D.; Viswanathan, K.; Hoyle, C. E.; Jonsson, S.; Hasselgren, C. *Experience the World of UV/EB, RadTech 2000: The Premier UV/EB Conference & Exhibition, Technical Conference Proceedings* **2000**, 221-230.
61. Hoyle, C. E.; Clark, S. C.; Viswanathan, K.; Jonsson, S. *Photochemical & Photobiological Sciences* **2003**, *2*, 1074-1079.
62. Morel, F.; Decker, C.; Jönsson, S.; Clark, S. C.; Hoyle, C. E. *Polymer* **1999**, *40*, 2447-2454.
63. Miller, C. W.; Jonsson, S.; Hoyle, C. E.; Hasselgren, C.; Haraldsson, T.; Shao, L. *RadTech'98 North America UV/EB Conference Proceedings* **1998**, 182-188.
64. Andrzejewska, E. *Progress in Polymer Science* **2001**, *26*, 605-665.
65. Clark, S. C.; Hoyle, C. E.; Jönsson, S.; Morel, F.; Decker, C. *Rad Tech 98 Proceedings, International UV & EB Processing Conference and Exhibition* **1998**.
66. Nguyen, C. K.; Johnson, A. T.; Viswanathan, K.; Cole, M. C.; Cavitt, T. B.; Hoyle, C. E.; Jonsson, S.; Miller, C. W.; Pappas, S. P.; Kottmair, E.; Shao, L. *Experience the World of UV/EB, RadTech 2000: The Premier UV/EB Conference & Exhibition, Technical Conference Proceedings* **2000**, 196-210.
67. Miller, C. W.; Hoyle, C. E.; Valente, E. J.; Zubkowski, J. D.; Jonsson, E. S. *Journal of Chemical Crystallography* **2000**, *30*, 563-571.
68. Miller, C. W.; Jonsson, E. S.; Hoyle, C. E.; Viswanathan, K.; Valente, E. J. *The Journal of Physical Chemistry B* **2001**, *105*, 2707-2717.
69. Hoyle, C. E.; Viswanathan, K.; Clark, S. C.; Miller, C. W.; Nguyen, C.; Joensson, S.; Shao, L. *Macromolecules* **1999**, *32*, 2793-2795.
70. Senyurt, A. F.; Hoyle, C. E. *European Polymer Journal* **2006**, *42*, 3133-3139.
71. Mallein, C., thesis, Université de Haute-Alsace, Mulhouse, 2003.
72. Colthup, N.; Daly, L. H.; Wiberley, S. E., *Introduction to Infrared and Raman spectroscopy*. 2nd ed.; Academic Press Inc: London, 1975.
73. Vázquez, C. P.; Joly-Duhamel, C.; Boutevin, B. *Macromolecular Chemistry and Physics* **2009**, 9999, NA.
74. Bernhard, P.; Hofmann, M.; Hunziker, M.; Klingert, B.; Klingert, B.; Schulthess, A.; Steinmann, B., Three-Dimensional Laser Polymerisation. In *Radiation Curing In Polymer Science and Technology Practical Aspects and Applications*, Fouassier, J. P.; Rabek, J. F., Eds. Elsevier Applied Science: London and New York, 1993; Vol. IV.
75. Sangermano, M.; Carbonaro, W.; Malucelli, G.; Priola, A. *Macromolecular Materials and Engineering* **2008**, *293*, 515-520.
76. Lu, B.; Xiao, P.; Sun, M.; Nie, J. *Journal of Applied Polymer Science* **2007**, *104*, 1126-1130.
77. Arrighetti, S.; Vajna, E.; Cesca, S. U.S. Patent 3676512, 1972.
78. Vainer, A.; Dyumaev, K.; Kovalenko, A.; Mareeva, S.; Tarnopol'skii, A.; Shalatonova, A. *Doklady Chemistry* **2008**, *418*, 1-4.

79. Chen, J.-G.; Liu, K.-Y.; Chen, C.-Y.; Lin, C.-Y.; Huang, K.-C.; Lai, Y.-H.; Wu, C.-G.; Lin, K.-F.; Ho, K.-C. *Journal of Polymer Science Part A: Polymer Chemistry* **2010**, *48*, 4950-4957.

Chapter IV: Linear shrinkage measurement

I	INTRODUCTION.....	179
II	DESCRIPTION OF THE SELECTED METHODS TO MEASURE VOLUMETRIC AND LINEAR SHRINKAGES	181
II.1	Measurement of the volumetric shrinkage	181
II.2	Measurement of the linear shrinkage	182
II.2.1	Principle	182
II.2.2	Experimental set up.....	184
II.2.2.1	Substrate	184
II.2.2.2	Application of the coating	184
II.2.2.3	Light sources	184
II.2.2.4	Deflection measurement.....	184
II.2.3	Assessment of the linear shrinkage technique and its optimization.....	186
II.2.3.1	Nature of the substrate.....	187
II.2.3.2	Sample thickness	187
II.2.3.3	Light intensity	189
III	RESULTS.....	191
III.1	Selected formulations	191
III.2	Comparison of the performances between the two linear methods	193
III.3	Comparison between the volumetric and linear shrinkages.....	194
III.4	Kinetic monitoring of the cantilever deflection	196
IV	CONCLUSIONS	198
V	REFERENCES.....	200

I INTRODUCTION

Among the different raw materials used in Rapid Prototyping (RP), UV curable formulations are well-appreciated as the fabrication process only requires a low amount of energy to be cured and the photopolymerization rate is fast ^{1,2}. Nonetheless, these high polymerization rates reached in a bulk formulation can prevent the system from relaxing ³. So, the liquid UV curable resins tend to shrink whilst they turn into solid upon UV irradiation. Shrinkage ^{1,3-5} results from the replacement of intermolecular bonds (Van der Waals' interactions) between the monomer molecules by shorter covalent C-C bonds, in the polymer during the polymerization process ⁶. Moreover, the heat evolved during this process can lead the curing material to thermally expand and contract after cooling down⁷. Therefore, residual stresses occur which can result in important distortions ^{8,9} even cracks within the cured part. These dimensional changes in the generated object are a major problem for RP techniques such as stereolithography (SLA) where the accuracy and the quality of the piece are essential ¹⁰. Like SLA, Araldite®Digitalis process is based on the photopolymerization process, we can expect that this new technology has also to cope with shrinkage issues. To be more precise, these residual stresses do not only depend on the shrinkage and the degree of cure reached by the monomer but also on the adhesion and the confinement, the Young's modulus of the polymer system and on the processing conditions. Indeed, for unconfined systems such as films, the stress resulting from shrinkage can release and trigger visible distortions in the product whereas for confined systems such as dental restorations, the shrinkage is converted into internal stresses which can engender cracks or delamination and undermine the mechanical and physical properties of the coatings ¹¹.

Numerous research studies have been carried out on shrinkage evaluation and on the accuracy in SLA process ¹²⁻¹⁵. The shrinkage magnitude depends non exhaustively on the polymer T_g, the curing temperature, the light intensity as well as the photoinitiator concentration ¹² and the functionality.

The shrinkage can be evaluated by measuring the change in volume during the conversion of the monomer to the polymer. It corresponds to the volumetric shrinkage. It is related to the concentration of the reactive functions in the monomer and the degree of cure in the polymer ⁶. However, the curl distortion of SLA parts does not really depend on the volumetric shrinkage but rather on the photopolymerized thickness layer ^{10,16}, so the determination of the linear shrinkage is also crucial. Therefore, this chapter will consist in setting up both volumetric and linear shrinkage methods in order to characterize the most interesting formulations studied along this thesis. Various methods can be used for the determination of volumetric shrinkage such as gas or liquid pycnometry ^{17,18}, dilatometry

^{6,19,20}, measure of both liquid monomer and solid polymer densities (use of graduated tube and balance) ²¹, buoyant mass determinations (Archimedes principle) ^{22,23}, optical profilometry ²⁴ and bonded disk technique ²⁵⁻²⁷. As regards to the determination of the linear shrinkage, the commonly employed techniques are laser interferometry ^{7,28,29}, holography ³⁰, microscopy ³¹, profilometry ³¹ and linometer ³².

SLA or Araldite®Digitalis is a layered manufacturing process in which 100 µm-thin layers surrounded by liquid monomer are photopolymerized one layer at a time. As a consequence, in order to assess the extent of shrinkage within the multi-layered part, we can assimilate each layer to a coating. Among the aforementioned techniques allowing the determination of shrinkage for coatings, we have chosen two methods that are easy to implement, to analyze the data and to explain the results. The two methods are the determination of the densities before and after curing for thin coatings with the buoyant mass determination method and the method proposed by Ganahl ³³ based on the cantilever deformation. This latter is normally employed for calculating the stress resulting from shrinkage in thin coatings. But herein, since, we are only interested in performing a qualitative survey, we only measured the cantilever curling in response to stress and for convenience sake we assimilated these data to the linear shrinkage. The description of these two methods is thoroughly described in the following pages. For practical reasons, the experiments were not conducted at the Araldite®Digitalis actinic wavelengths (between 330 nm and 450 nm, the main emission band is at 366 nm) but at broadband irradiation.

II DESCRIPTION OF THE SELECTED METHODS TO MEASURE VOLUMETRIC AND LINEAR SHRINKAGES

II.1 Measurement of the volumetric shrinkage

Volumetric shrinkage (S) was determined by calculating the density of the formulations before the curing (d_L) in liquid state and after the curing (d_p) in solid state (polymer) ⁶. It was calculated as follows:

$$S(\%) = \left(1 - \frac{d_L}{d_p}\right) * 100 \quad (\text{IV.1})$$

1) Determination of the density of the liquid formulations (d_L)

The density of the uncured liquid resin was measured by pycnometry.

A precise amount of liquid resin was introduced in a 1 mL-pycnometer. The sample was weighed with a Sartorius balance with ± 0.00005 g of accuracy.

$$d_L = \frac{m_L}{V} \quad (\text{IV.2})$$

with

m_L : the mass of the liquid resin

V: the exact volume of a 1 mL volumetric flask

The relative incertitude values are defined as the error of the volumetric flask. It is the ratio of volumetric flask accuracy over the volumetric flask volume.

2) Determination of the density of the UV cured resins in solid state

The UV curable resins were coated on a glass substrate by means of a motorized bar coater. They were cured under air with a fusion lamp type H associated to a conveyor belt speed of 10 m/min. The light intensity was measured with to be UVA: 440 mJ/cm², UVB: 430 mJ/cm², UVC: 90 mJ/cm², UVV: 480 mJ/cm²). Four passes were done (cf Annex I.2). The sample thickness was around 100 μm . After stripping a piece of the photopolymer from the substrate, its density was evaluated by using the Sartorius density determination kit comprising a hydrostatic balance ²² (accuracy ± 0.0005 g).

When a solid, whose mass in air is m_{air} , is immersed into a reference liquid such as water, its weight decreases to m_{water} owing to the buoyancy force ($F = m_{\text{air}} - m_{\text{water}}$).

By referring to the Archimedes principle (*The force of buoyancy is equal to the weight of the liquid displaced by the volume of the solid*), the volume (V) of the sample is equal to ²³:

$$V = \frac{F}{d_{water}} \quad (IV.3)$$

By measuring the solid mass in air (m_{air}) and in water (m_{water}) the specific gravity is

$$d_p = \frac{m_{air}}{V} = \frac{m_{air} * d_{water}}{(m_{air} - m_{water})} \quad (IV.4)$$

The relative incertitude for the measurement of d_p corresponds to the incertitude of the balance.

Two measurements were carried out in order to determine the average density of the UV cured formulations.

II.2 Measurement of the linear shrinkage

II.2.1 Principle

Ganahl ³³ has set up a straightforward method for the determination of the polymerization stress due to shrinkage during the photopolymerization process. This technique consists in measuring the deflection of a thin brass coated cantilever under UV irradiation which indirectly gives us information about the extent of shrinkage. The deformation of the cantilever results from the transfer of a stress from the coating to the cantilever during the polymerization as the coating is stuck to the cantilever. A scheme in Figure IV. 1 illustrates this phenomenon. An horizontal stress is at the origin of the vertical deflection.

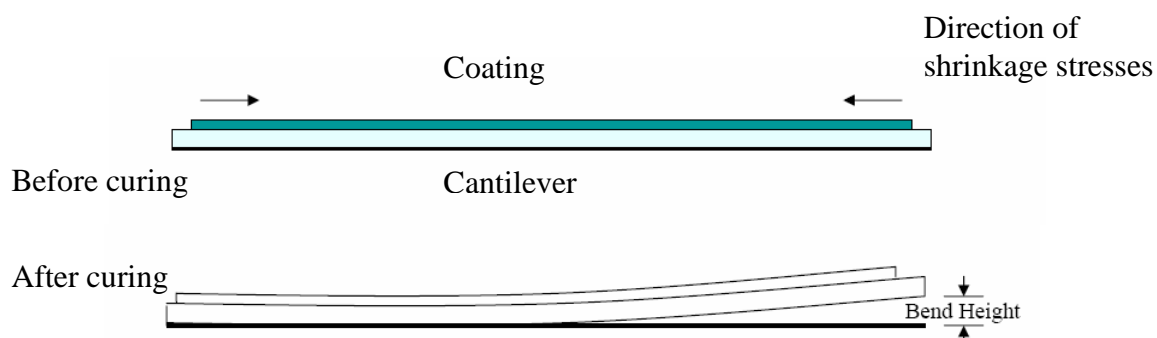


Figure IV. 1 : Scheme of shrinkage stress in the plane of a coating causing a vertical deflection of a cantilever ³³

As it can be expected, the nature of the substrate plays an important role in this technique. In order to facilitate the deflection measurement, the cantilever has to deform with a certain level and meet some requirements: i) the deformation must be elastic, ii) the polymer has to well adhere onto the cantilever, iii) the cantilever must not interfere in the polymerization process by reacting with the monomer or being dissolved by it. Other parameters such as the coating thickness, the chemical nature of the UV curable resin and the light intensity are also at the origin of the cantilever deflection. Their influence will be explained in the following pages.

Herein, we considered that the determination of the cantilever deflection for different formulations was sufficient for a comparative survey. But it is possible with this technique to go further and evaluate the internal stress of the coatings. As a matter of fact, Corcoran *et al*³³ has found in the 1960s a relationship between the cantilever deflection and the internal stresses in the organic coatings. This relationship lies in Stoney's equation and depends on moduli of elasticity and Poisson ratios of the coating and the cantilever. The internal stresses are defined as follows:

$$S = \frac{hE_s t^3}{3L_s L_c c(t+c)(1-Y_s)} + \frac{hE_c(t+c)}{L_s L_c(1-Y_c)} \quad (IV.5)$$

S: the internal stress

h: the deflection of the cantilever

E_s: the modulus of elasticity for the substrate

E_c: the modulus of elasticity for the coating

Y_s: Poisson's ratio of the cantilever substrate

Y_c: Poisson's ratio of the coating

L_s: length of the substrate to the edge point where the deflection is measured

L_c: length of the coating

t: the thickness of the cantilever substrate

c: the thickness of the coating

The first term in the equation deals with the stresses remaining in the coating. By contrast, the second term informs about the stresses evolving during the deflection of the cantilever. This equation is valid if one assumes that the coating is homogeneous along the cantilever length.

II.2.2 Experimental set up

II.2.2.1 Substrate

As depicted by Ganahl³³, we have chosen a brass alloy whose properties fulfil all the aforementioned requirements. It is made of 70% Cu and 30% Zn. The dimensions of the brass cantilevers were 5 cm long, 13 mm wide and 0.05 mm thick. The adhesion between the coating and the cantilever was ensured by washing the cantilever first in water and in soap. Afterwards, the cantilevers were rinsed in deionized water followed by acetone. Finally, they were stored in acetone³³.

II.2.2.2 Application of the coating

The coating thickness was around 30-50 μm . The formulations were applied on the brass cantilever by means of a motorized device for a better reproducibility.

II.2.2.3 Light sources

Two different polychromatic light sources were used. The first one is a Hg Oriel arc lamp whose light intensity was 24 mW/cm^2 . The second one is a Hg Oriel flood exposure light source. Its intensity varies from 15 to 60 mW/cm^2 . The samples were irradiated during 3 min. The emission spectra of both lamps are depicted in Annex I.3 and Annex I.4.

II.2.2.4 Deflection measurement

a. Manual measurement with a ruler

The measurements of the deflection were achieved on both left and right extremities sides of the cantilever with a ruler as some cantilever deformation is not homogeneous. An average value is obtained.

The net deflection is calculated by measuring the cantilever deformation before and after the irradiation. Three experiments were performed in order to determine an average value of the net deflection. For each experiment, the maximum uncertainty value was calculated. It corresponds either to the reading error equal to 0.25 mm which is the half value of the smallest division on the ruler or to the difference between the two extreme values. Figure IV. 2 illustrates this method.

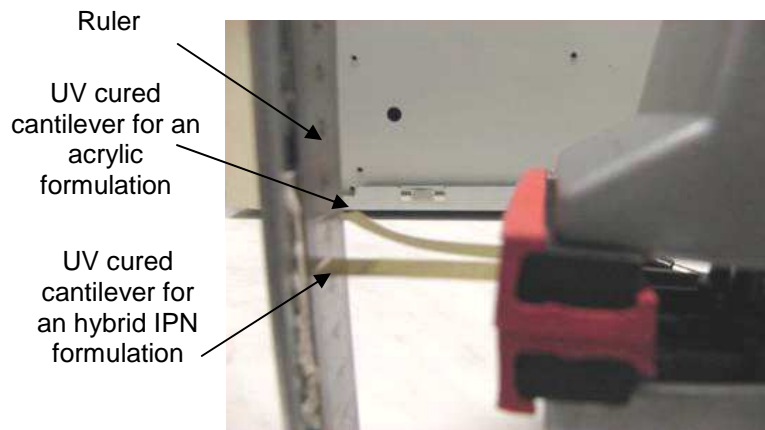


Figure IV. 2 Picture of two coated brass cantilevers after photopolymerization with the Hg Oriel arc lamp, light intensity 24 mW/cm^2

b. Use of a digital micrometer

During the shrinkage study, a digital micrometer was purchased from Keyence in order to achieve an automatic measurement of the deflection. The new experimental set up is shown in Figure IV. 3.

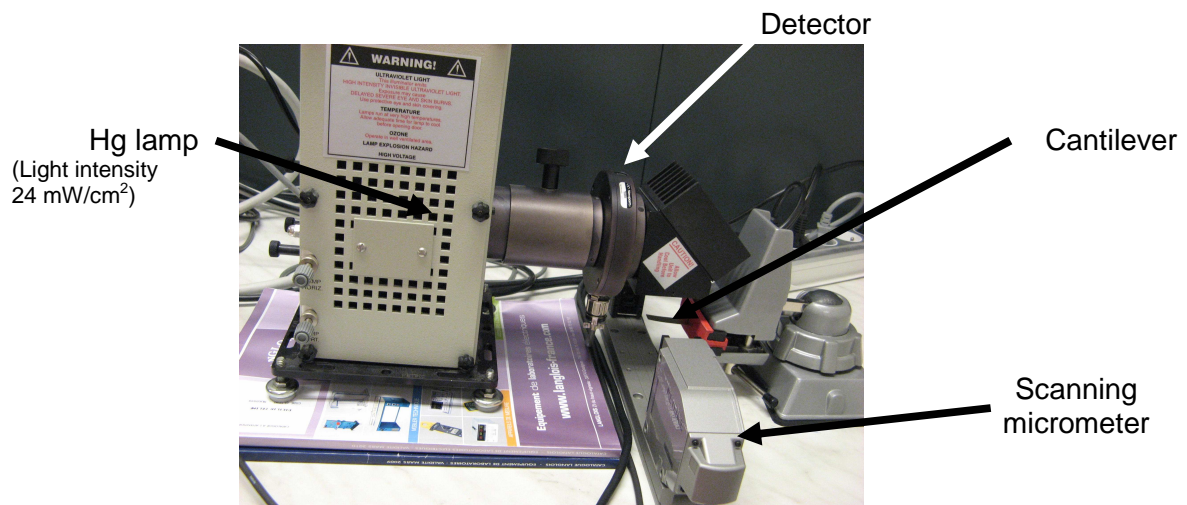


Figure IV. 3 : Picture of the new set-up experiment using a digital micrometer

In this method, the light emitted from a GaN green LED, is first collimated into an uniform parallel light beam (3 cm of width) and then passes through the extremities of the brass cantilever (the target) side. The measurement is achieved in a single point at the middle of the cantilever width. A part of the light is hidden by the target; as a result the high speed linear CCD (HL-CCD) located in the sensor part collects a modulated light intensity with high and low intensity areas.

Afterwards, these data are finally transmitted and processed in the controller unit where the cantilever height is determined and displayed. When the cantilever bends under UV irradiation, the shadow position changes. As a consequence, the height variation can be measured. This device ensures both a high accuracy of $\pm 0.15 \mu\text{m}$ in height and a high-speed measurement (2400 points per second). Thus, besides the accuracy, the possibility to monitor *in situ* the cantilever deflection versus time could also be investigated in order to try to understand the shrinkage stress generation. It is noteworthy to say that the LS 7030M micrometer possesses an imaging camera so it is possible to observe the cantilever deformation. A scheme of the optical micrometer is represented in Figure IV. 4.

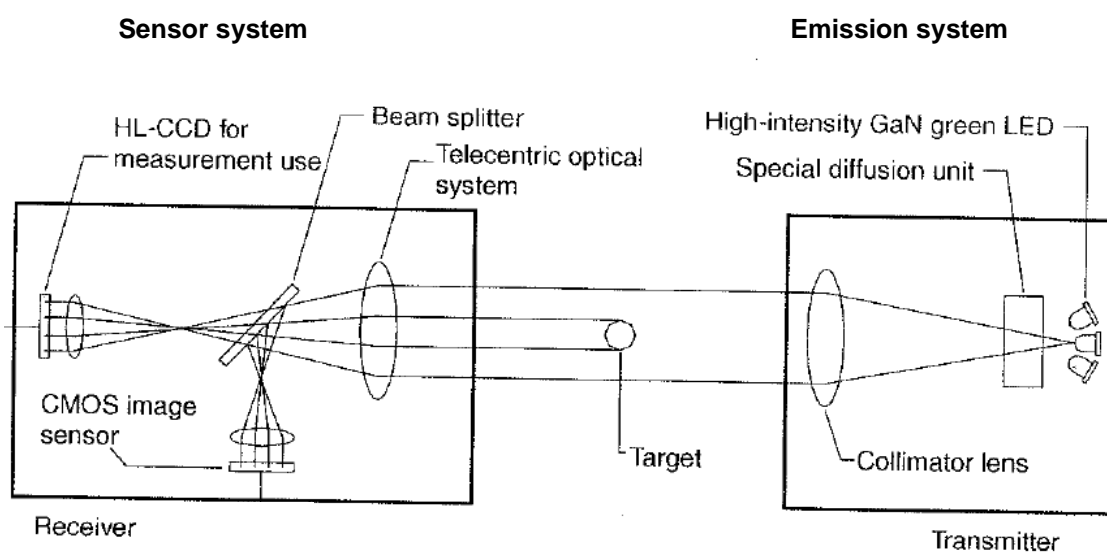


Figure IV. 4 : Scheme of the scanning micrometer

Once again, three experiments were performed in order to determine an average value of the net deflection for each sample. The uncertainty values were calculated according to the difference between the two extreme values.

II.2.3 Assessment of the linear shrinkage technique and its optimization

In order to evaluate the effect of some processing parameters on the manual and digital linear shrinkage methods, we worked with an acrylic resins exhibiting a significant shrinkage. The preliminary experiments were carried out with a formulation named SR 833S comprising a difunctional acrylate monomer SR 833S in presence of 5 wt% of the radical photoinitiator 2,4,6-trimethylbenzoyl-diphenyl-phosphineoxide (TPO). Their chemical structures are represented in Table IV. 1. The influence of the nature of the substrate, the sample thickness and the light intensity was examined.

Table IV. 1 : Chemical structures of SR 833S and the radical photoinitiator TPO

Chemical name	Chemical structure
Tricyclodecane dimethanol diacrylate (SR 833S)	
2,4,6-trimethylbenzoyl-diphenyl-phosphineoxide (TPO)	

II.2.3.1 Nature of the substrate

No matter the method, for quite all the UV cured coated cantilevers, we noticed that the left side was always higher than the right side. We attributed this difference to the manufacturing process of the selected brass alloy.

To confirm this hypothesis, we have carried out few experiments for which the brass alloy substrate was picked out at different areas of the roll that is to say: on the left, in the middle and on the right. The results revealed that the substrate position in the roll greatly influenced the cantilever deformation. A difference was observed between the 3 parts even though the substrates were previously flattened between two metal plates with a 350 bar pressure. The more reproducible experiments were achieved with the substrate cut on the left side. As a consequence, the memory effect of the substrate due to the winding process has to be kept in mind.

II.2.3.2 Sample thickness

The influence of the coating thickness on the cantilever deformation was examined at three different thicknesses (50 μm -70 μm -100 μm) with the two linear shrinkage methods. The cantilever deflection relies on the degree of cure reached at the three sample thicknesses. The extent of cure depends on several physical parameters such as the light penetration, atmospheric oxygen and temperature. Their effect on the polymerization process will be primarily commented and then related to the cantilever deflection as a function of the sample thickness.

First of all, according to the Beer's law, the propagation of the light through the material should decrease exponentially depending on both the nature and the concentration of the photoinitiator as well as the absorption of the monomers.

Herein, despite an important amount of TPO radical photoinitiator, we could assume that the light would penetrate inside the coating and reach the bottom layers and induce the

polymerization process since the photoinitiator photobleaches. As the quantity of monomers increases with the sample thickness, we could suppose that the stress might rise with the sample thickness and result in a prominent deflection.

Secondly, oxygen affects the radical polymerization process by scavenging both the photoinitiator molecules at the excited triplet state and the free radicals³⁴. The effect is particularly pronounced for thin coatings for which the continuous diffusion of oxygen into the coating inhibits the polymerization reaction and leads to a tacky surface. Adversely, it is more difficult for oxygen to reach the bottom layer of the coating because the viscosity increases during polymerization. Thus, there is a gradient of conversion within a coating film. The conversion increases with the depth until a plateau value. Therefore, the samples with high coating thicknesses should be less sensitive towards oxygen and the conversion through the sample might be better owing to the possible migration of the reactive species from the bottom towards the surface.

Finally, owing to the high exothermicity of the acrylate monomer polymerization (about 14-20 kcal.mol⁻¹³⁵), the temperature influence has to be considered too. The heat evolved during the reaction might increase the sample temperature and thus might promote the mobility of the reactive species and extend the degree of cure. By considering the ratio surface to volume, the temperature rise should be more important in thick samples³⁵.

Consequently, all these physical parameters contribute to increase the cantilever deformation with the coating thickness. We have observed that for the 70-100 µm thick samples, the deformation was so important that the cantilever deflection was not homogeneous (the difference between the left and the right side cantilever extremities was important) and not reproducible. The overall data are summarized in Table IV. 2.

Table IV. 2 : Influence of the coating thickness (50 µm -70 µm -100 µm) on the cantilever deflection; measurements performed with the ruler; Hg Oriel lamp, light intensity~24 mW/cm²

	Cantilever	Coating thickness (µm)		
		50 µm	70 µm	100 µm
Trial 1	left side	2.4 ± 0.25	8.7 ± 0.25	6.2 ± 0.25
	right side	2.5 ± 0.25	6.8 ± 0.25	5.3 ± 0.25
Trial 2	left side	2.9 ± 0.25	6.0 ± 0.25	12.5 ± 0.25
	right side	2.6 ± 0.25	3.3 ± 0.25	7.0± 0.25
Trial 3	left side	2.8 ± 0.25	5.0 ± 0.25	13.0± 0.25
	right side	2.7 ± 0.25	2.5 ± 0.25	9.0± 0.25

Typically, the cured layer thickness in SLA process is 100 μm but for a good reproducibility and for accuracy reasons, it is advised to work with a 50 μm coating thickness. The digital method was shown to be particularly sensitive to the extensive cantilever deflection as the substrate deformation is measured at one point and not at two points as it is the case for the manual method. Therefore, the digital method will be only suitable for thin coating thicknesses (maximum 50 μm). By lack of time, we did not have time to check the existence of a gradient of conversion through the samples. Nonetheless, it would be afterwards interesting to use the confocal Raman microscopy in order to determine the conversion profile through the sample.

II.2.3.3 Light intensity

The effect of light intensity on the cantilever deflection was studied. The light intensity ranges from 5 to 70 mW/cm^2 . It appears from Figure IV. 5 that above a threshold light intensity (45 mW/cm^2) a significant increase in cantilever deflection was measured. It could be assumed that a certain amount of energy is required to reach a high degree of cure and subsequently a prominent bending. This result can be related to the influence of light intensity on the overall radical photopolymerization process, since an increase in light intensity allows to increase both the polymerization rate and the final conversion³⁶⁻³⁸. Firstly, at high light intensities, the rise in sample temperature may promote the molecular mobility and yield to higher final conversion³⁸. Then, the use of high light intensities allows to reduce the oxygen inhibition because a sufficient number of free radicals is generated to induce the polymerization and increases the initiation rate². This rate becomes so high that the chemical reaction rate is faster (square root dependence between the polymerization rate and the light intensity for radical photopolymerization³⁹) than the stress relaxation rate which leads to a free volume excess. Under these conditions, the degree of cure achieved by the system increases, hence the shrinkage phenomenon is promoted^{37,40}. As illustrated in Figure IV. 5, the plot is characterized by two well-defined domains that could be modelised by two linear relationships between the cantilever deflection and the light intensity for the difunctional SR 833S monomer.

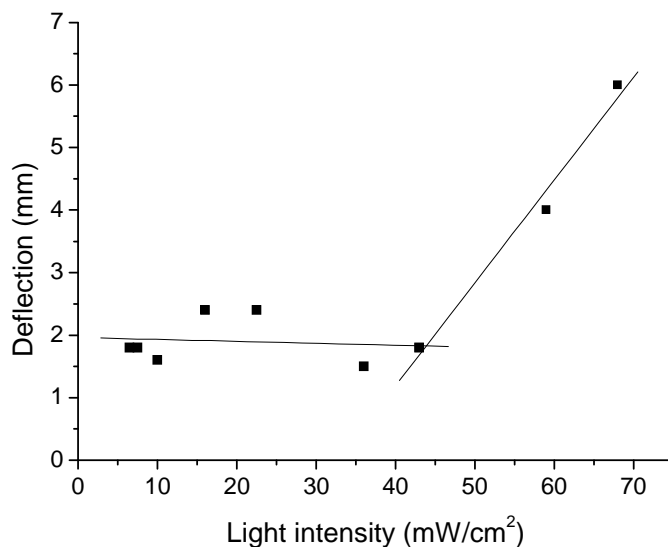


Figure IV. 5 : Plot of the deflection versus light intensity for the SR 833S formulation with the Hg flood exposure light source

In order to confirm this tendency, the same experiment was performed with a trifunctional trimethylolpropane triacrylate (TMPTA). As seen in Figure IV. 6 the same relation than for SR 833S was established. However, the threshold light intensity is reached earlier at about 18 mW/cm² and the cantilever deflection is twice higher. This difference might stem from the increase in monomer functionality. It has been reported that the monomer functionality has a big impact on both the polymerization rate and the degree of cure. As the monomer functionality increases, the initial concentration of reactive functions rises which contributes to tremendously accelerate the polymerization but limits the extent of cure due to the premature vitrification of the medium³⁶⁻³⁸. As a result, the system has no time for relaxation and the shrinkage is higher. We have also noticed that for the TMPTA formulation that some cracks appeared on the coating if the light intensity was superior to 25 mW/cm². The presence of cracks is the evidence that the magnitude of stress within the material has reached a critical value³¹.

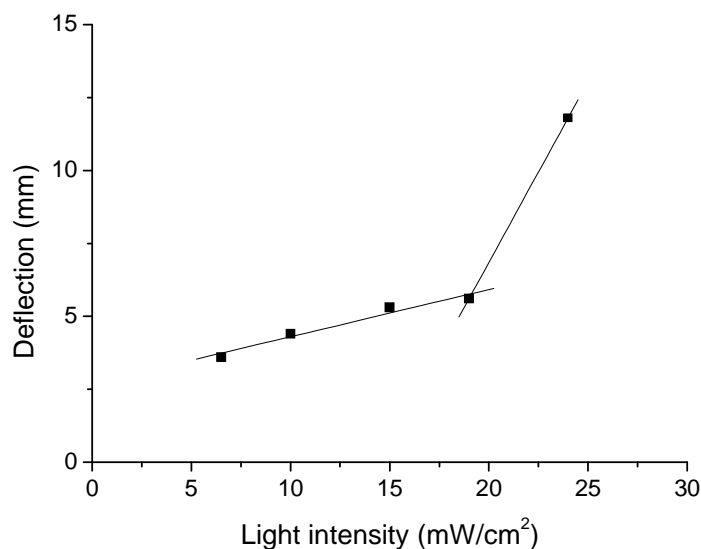


Figure IV. 6 : Plot of the deflection versus light intensity for the TMPTA formulation with the Hg flood exposure light source

To conclude on these preliminary experiments, as the substrate position in the roll can affect the cantilever deformation, for the next experiments, we will always use the left side of the roll to prepare the cantilever. The sample thickness is set up at 50 μm for sake of reproducibility and the Hg Oriel lamp whose light intensity is 24 mW/cm^2 will be selected to prevent any formation of cracks.

III RESULTS

III.1 Selected formulations

For our comparative survey, the acrylic resin named TMPTA exhibiting the higher level of shrinkage for an acrylic based resin was taken as reference. Both the volumetric and the linear shrinkage were determined for this formulation according to the methods presented in the section II.2.2.4. Their magnitudes were first compared to the results obtained with the commercial SL resins Renshape®SL Y-C 9500, a neat acrylic resin and Renshape®SL 7800 an hybrid mixture. Then, the comparison was extended to the systems studied in chapter III displaying a good reactivity and interesting thermomechanical properties. Their chemical composition is reminded in Table IV. 3.

Table IV. 3 : Composition of the selected DPG formulations

Formulation name	Composition			
	mol% of MI double bond function	mol% of DIVE double bond function	wt% of TPO	wt %of cationic photoinitiator
NTMI 5050 TRIVE	50	50	5	-
NTMI 7030 TRIVE	70	30	5	-
BMI-2300® 2575 DIVE	25	75	5	-
BMI-2300® 2575 DIVE + 1 wt% TAS	25	75	5	1
BMI-2300® 2575 DIVE + 1 wt% I 250	25	75	5	1

In order to compare a wide range of chemistries, we have introduced within the commercial acrylic resin Renshape®SL Y-C 9500 30 wt% of NTMI (MDB 7) and 30 wt% of the mixture NTMI 5050 TRIVE (MDB 8) respectively.

For convenience sake, the name of the overall selected formulations was simplified. The shortcut names as well as the detail of the composition of the different mixtures and the chemical structures are given in Table IV. 4.

Table IV. 4 : Shortcut names for the selected formulations

	Shortcut name	Formulation name
Reference	MDB 1	TMPTA
Commercial resins	MDB 2	Renshape®SL Y-C 9500
	MDB 3	Renshape®SL 7800
DPG formulations	MDB 4	NTMI 5050 TRIVE
	MDB 5	NTMI 7030 TRIVE
	MDB 6	BMI-2300® 2575 DIVE
	MDB 7	Renshape®SL Y-C 9500+ 30 wt% NTMI
	MDB 8	Renshape®SL Y-C 9500+ 30 wt% (NTMI 5050 TRIVE)
	MDB 9	BMI-2300® 2575 DIVE+ 1 wt% TAS
	MDB 10	BMI-2300® 2575 DIVE+ 1 wt% I 250

III.2 Comparison of the performances between the two linear methods

The performances of the manual and the digital methods were investigated by means of formulations displaying a different shrinkage magnitude. The comparison is made in Table IV. 5.

Table IV. 5 : Determination of the cantilever deflection by means of the ruler and micrometer methods

	Average deformation manually determined (mm) (a)	Average deformation digitally determined (mm) (a)
SR 833S	2.4 ± 0.4	2 ± 0.4
MDB 1	5.7 ± 2.9	3.5 ± 1.1
MDB 4	3.2 ± 0.5	1.7 ± 0.25
MDB 9	1 ± 0.25	0.92 ± 0.05
MDB 10	0.65 ± 0.3	0.68 ± 0.03

(a) samples cured with a Hg Oriel lamp, light intensity~24 mW/cm², sample thickness~50 µm

As it can be seen in Table IV. 5, for both methods, the error percentage increases for the systems displaying high shrinkage > 2 mm. For the pure acrylic resin MDB 1, the error percentage is about 50 % for the value found manually and 30% for the value found with the micrometer. These huge differences might result from the non uniformity of the coating thickness. If the coating thickness is not homogeneous, the cantilever deformation will be different especially for highly reactive UV curable resins. In addition, the values found with the micrometer were lower than the values found manually because the cantilever height either exceeds the measurement area of the micrometer or is distorted compared to left and the extremities sides (left and right). Adversely, for low cantilever deflection < 2 mm, the results found with the micrometer were similar to the ones obtained with the ruler and the error percentage was lower.

So it is recommended to use the micrometer device only for systems displaying low shrinkage. By contrast, the manual system can be employed for systems exhibiting both high and low cantilever deflections even though its accuracy is lower for the latter case. For the following comparative survey, we will deal with both high and low shrinkable formulations that's why the manual method is selected.

III.3 Comparison between the volumetric and linear shrinkages

Both the volumetric and the linear shrinkages were determined for the formulations reported in Table IV. 6.

Table IV. 6 : Determination of the volumetric and the linear shrinkages for some DPG formulations

Formulations	Volumetric shrinkage (%)	Linear deflection (mm)
MDB 1	11 ± 0.02	6.8 ± 2 *
MDB 2	4 ± 0.02	0.6 ± 0.25 *
MDB 3	2 ± 0.02	0.3 ± 0.25
MDB 4	10 ± 0.02	2.2 ± 0.75
MDB 5	3 ± 0.02	0.7 ± 0.25
MDB 7	8 ± 0.02	$0.85 \pm 0.25^*$
MDB 8	9 ± 0.02	$0.95 \pm 0.25^*$

* not tack free samples

The classification of the formulations by growing volumetric shrinkage in Figure IV. 7 shows almost the same trend than for the linear shrinkage. An inversion was observed between the formulations MDB 2 and MDB 5. This difference might be explained by the fact that the accuracy of both the volumetric and linear method is not the same. Moreover, the volumetric and the linear shrinkage of these two formulations might be very close.

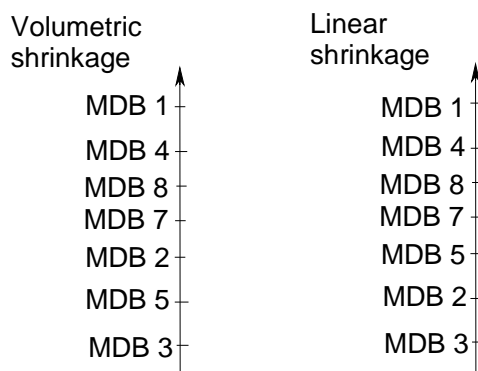


Figure IV. 7 : Classification of the tested formulations according respectively the volumetric and linear shrinkage magnitude

As expected, the acrylate based formulation MDB 1 exhibits both high volumetric and linear shrinkages which is in agreement with the values found in literature^{22,41}. The high exothermicity and the fast formation of the crosslinked network in a very short time results in important shrinkage^{1,7}. Likewise, the commercial resins MDB 2 and MDB 3 optimized for the SL process exhibit low linear shrinkage and reasonable volumetric shrinkage. As regards to the DPG formulations, both volumetric and linear shrinkage values are located in between MDB 1 and MDB 3. Afterwards, the cantilever deflection was plotted as a

function of volumetric shrinkage for the tested formulations in order to establish a relation between them. Ideally, linear shrinkage is proportional to volume shrinkage if the material can freely shrink according to the 3 linear dimensions during the cure. In that case, the linear shrinkage would be equal to one third of volumetric shrinkage⁴² but in practice, the value is not always equal to one third depending on the relaxation characteristics of the material and the effect of orientation⁴³. As it can be seen in Figure IV. 8, in our case, the relation is not linear, we can distinguish 3 areas. The first one corresponds to the formulations exhibiting both low volumetric shrinkage and cantilever deformation (zone 1). The second one gathers the formulations displaying a high volumetric shrinkage and a low cantilever deformation (zone 2). And the last one is formed by the formulations that experiment both high volumetric shrinkage and cantilever deformation (zone 3).

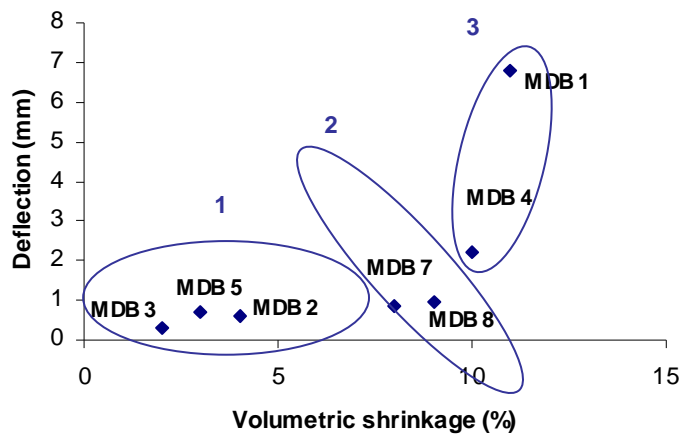


Figure IV. 8 : Linear shrinkage versus volumetric shrinkage

These results might be partially explained by the differences in processing conditions between the two techniques: the light intensity was more important for the sample cured with the UV belt conveyor than with the Oriel Hg lamp. The monomer conversion was assumed to be more important with the conveyor. The affinity between the UV curable resins and the glass substrate might differ from the one with the brass alloy. And for the cantilever method, the UV cured coating thickness varied from 40 to 60 μm whereas the sample coating thickness for the other method was between 80 and 110 μm .

III.4 Kinetic monitoring of the cantilever deflection

One of the interesting point with the digital measurement is the possibility to monitor in real time the cantilever deflection as a function of time. As it is depicted in Figure IV. 9, the cantilever deflection is sharply rising and then it is levelling off due to the vitrification phenomenon.

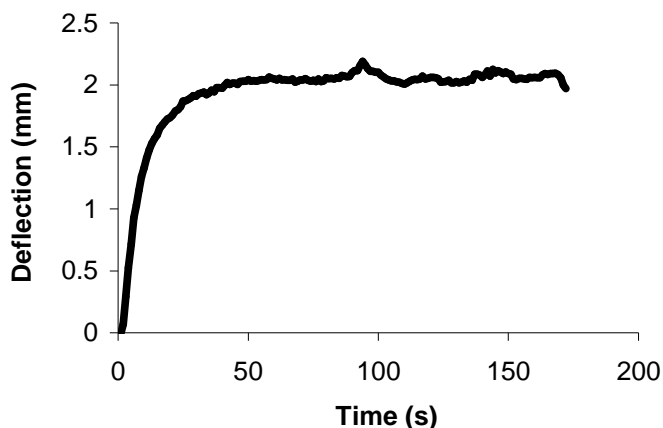


Figure IV. 9 : Example of a typical deflection vs. time curve obtained for the formulation 95 wt% Tricyclodecane dimethanol diacrylate (SR 833S) +5 wt% TPO, coating thickness ~40 μm , light intensity ~24 mW/cm^2

The shape of the curve is comparable to the degree of conversion versus time curve. However, it was not possible to find a correlation between the onset of photopolymerization with the cantilever deflection because we could not follow *in situ* the degree of conversion evolution. The brass alloy is not transparent to IR radiations. Nonetheless, to get an insight of this correlation, we suggest using another substrate and monitoring the kinetics of photopolymerization with a RT FTIR spectrometer under experimental conditions as close as possible to the linear shrinkage measurement conditions.

Taking into account the limitations of the digital micrometer in terms of reading measurements we can observe in Figure IV. 10 an acceptable reproducibility for low shrinkable systems MDB 9 and MDB 10.

Linear shrinkage measurement

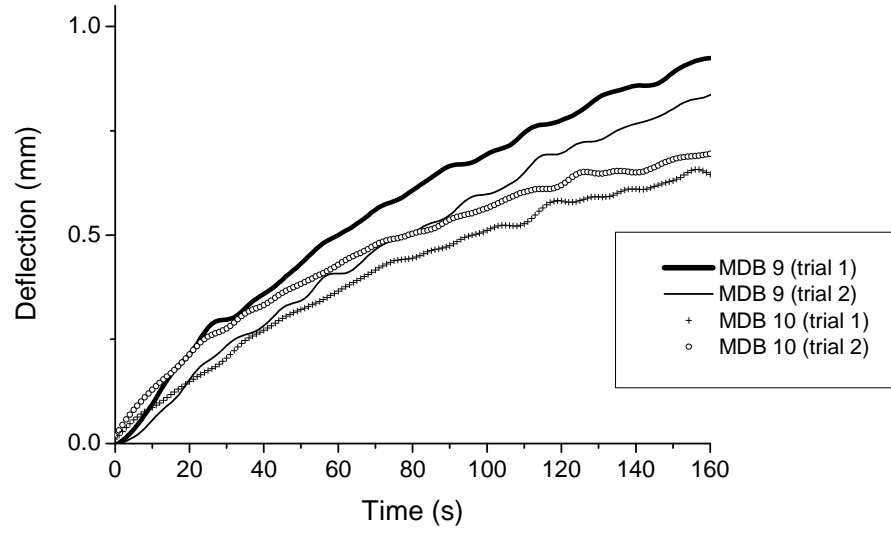


Figure IV. 10 : Superimposition of the kinetics curves for the formulations MDB 9 and MDB 10; coating thickness $\sim 40 \mu\text{m}$, Hg Oriel lamp, light intensity $\sim 24 \text{ mW/cm}^2$

IV CONCLUSIONS AND PERSPECTIVES

Shrinkage has a deleterious effect on the accuracy and on the longevity of the rapid prototyping UV cured part. Hence, the comprehension of shrinkage formation is essential to overcome these problems. To that purpose, the common volumetric shrinkage method based on the variation of density between the monomer and the polymer and a linear shrinkage stress method grounded on the cantilever deflection were used for a comparison of the polymerization shrinkage arising from different UV curable formulations. The experimental conditions for these methods did not correspond exactly to the real processing conditions of Araldite®Digitalis or SLA process. Nonetheless, these methods can inform us about the shrinkage behaviour of some UV cured resins. No significant correlation was found between the volumetric and the deformation methods but quite the same trend for the shrinkage level was observed under our experimental conditions. The DPG formulations display medium volumetric shrinkage and cantilever deformation depending on the monomer natures and their concentration. The influence of these parameters has been inquired in Chapter III.

The techniques used for the linear shrinkage measurement was shown to be effective for the comparative study but they still need to be improved. The replacement of the ruler by the digital micrometer allowed to increase the accuracy of the method but only for systems displaying a low cantilever deformation. The method was still limited by the lack of reproducibility of the coating thickness and by the non homogeneous deflection of the coated substrate. It still needs to be optimized. The application of a precise amount of monomer to the substrate might ensure consistent measurements. As regards to the substrate deflection, the use of sheets instead of rolls might reduce the inhomogeneities due to the winning process otherwise the substrate might be changed. Furthermore, for a better accuracy, the curving angle of the deformed substrate should be calculated for the determination of the exact cantilever deflection. Ideally, the next step would be to implement this method in Araldite®Digitalis or SLA process in order to assess the shrinkage magnitude of built specimens after the process and after the post-curing treatment. We have seen through this chapter that it was important to be closed to the real processing conditions since shrinkage increases with each of these processing parameters: light intensity, monomer functionality and the sample thickness. The results concerning the effect of light intensity was particularly interesting. It descends from our experiments that at relatively low light intensities, the shrinkage is minimized. However, from a given light intensity, the linear shrinkage drastically increases. This would suggest that, for a given dose of radiation, the curing of a sample with a rapid prototyping device should be operated using different passes at high rates and low intensities rather than

using one pass at low rate with a high intensity. Therefore, these experiments should be performed with the Araldite®Digitalis UV conventional lamp or with the SLA laser in smaller reservoirs of photosensitive resin to reproduce the common build-up conditions in the large resin vat. Indeed, the presence of the liquid uncured monomer partially alleviates the extent of stress generated during the formation of the UV cured layers ¹¹. They also should be expanded to multilayers systems to study the additional polymerization shrinkage stemming from the overlay of the freshly cured layer on the former one.

V REFERENCES

1. Lu, B.; Xiao, P.; Sun, M.; Nie, J. *Journal of Applied Polymer Science* 2007, *104*, 1126-1130.
2. Lecamp, L.; Youssef, B.; Bunel, C. *Polymer* **1997**, *38*, 6089-6096.
3. Acham, N.; Crisp, J.; Holman, R.; Kakkar, S.; Kennedy, R. *Rad Tech Europe* **1995**, 71-84.
4. Holst, M.; Schaenzlin, K.; Wenzel, M.; Xu, J.; Lellinger, D.; Alig, I. *Journal of Polymer Science, Part B: Polymer Physics* **2005**, *43*, 2314-2325.
5. Zanchi, C. H.; Carvalho, R. V. d.; Rodrigues Junior, S. A.; Demarco, F. F.; Burnett Júnior, L. H. *Brazilian Oral Research* **2006**, *20*, 137-142.
6. Stansbury, J.; Ge, J. *RadTech Report* **2003**, 56-62.
7. Mucci, V.; Arenas, G.; Duchowicz, R.; Cook, W. D.; Vallo, C. *Dental Materials* **2009**, *25*, 103-114.
8. Huang, Y. M.; Jiang, C. P. *The International Journal of Advanced Manufacturing Technology* **2003**, *21*, 586-595.
9. Huang, Y. M.; Lan, H. Y. *The International Journal of Advanced Manufacturing Technology* **2006**, *27*, 1101-1112.
10. Gan, Z.; Mo, J.; Huang, S.; Xie, H. *Journal of Wuhan University of Technology, Materials Science Edition* **2006**, *21*, 99-101.
11. Ganahl, P. D. Thesis, The Graduate College of the University of Iowa, Iowa, 2007.
12. Karalekas, D.; Aggelopoulos, A. *Journal of Materials Processing Technology* **2003**, *136*, 146-150.
13. Wang, W. L.; Cheah, C. M.; Fuh, J. Y. H.; Lu, L. *Materials & Design* **1996**, *17*, 205-213.
14. Karalekas, D.; Rapti, D.; Gdoutos, E.; Aggelopoulos, A. *Experimental Mechanics* **2002**, *42*, 439-443.
15. Lu, L.; Fuh, J. Y. H.; Nee, A. Y. C.; Kang, E. T.; Miyazawa, T.; Cheah, C. M. *Materials Research Bulletin* **1995**, *30*, 1561-1569.
16. Jacobs, P. F., *Rapid Prototyping and Manufacturing. Fundamentals of Stereolithography*. First ed.; The Society of Manufacturing Engineers 1992.
17. Tarle, Z.; Meniga, A.; Ristic, M.; Sutalo, J.; Pichler, G.; Davidson, C. L. *Journal of oral rehabilitation* **1998**, *25*, 436-442.
18. Cook, W. D.; Forrest, M.; Goodwin, A. A. *Dental materials : official publication of the Academy of Dental Materials* **1999**, *15*, 447-449.
19. Villat, C.; Pradelle-Plasse, N.; Picard, B.; Colon, P. *materials Science and Engineering C* **2008**, *28*, 971-976.
20. Fong, H.; Dickens, S. H.; Flaim, G. M. *Dental Materials* **2005**, *21*, 520-529.
21. Richardson, W. S.; Teggin, J. E. *Journal of Chemical Education* **1988**, *65*, 1013-1014.
22. Sangermano, M.; Carbonaro, W.; Malucelli, G.; Priola, A. *Macromolecular Materials and Engineering* **2008**, *293*, 515-520.
23. Wang, L.; Xian, A.-P. *Journal of Electronic Materials* **2005**, *34*, 1414-1419.
24. Croutxe-Barghorn, C.; Lougnot, D. J. *Proceedings of SPIE-The international Society for Optical Engineering* **1998**, *3417*, 208-215.
25. Watts David, C.; Cash, A. J. *Measurement Science and Technology* **1991**, *2*, 788-794.
26. Watts David, C.; Marouf, A. S.; Al-Hindi, A. M. *Dental Materials* **2003**, *19*, 1-11.
27. Simon, Y.; Mortier, E.; Dahoun, A.; Gerdolle, D. *Polymer Testing* **2008**, *27*, 717-721.

28. Lin-Gibson, S.; Landis, F. A.; Stafford, C. M. *Polymer Preprints* **2006**, *47*, 500-501.
29. Dudi, O.; Grubbs, W. T. *Journal of Applied Polymer Science* **1999**, *74*, 2133-2142.
30. Shelby, R. M.; Waldman, D. A.; Ingwall, R. T. *Optics Letters* **2000**, *25*, 713-715.
31. Francis, L. F.; McCormick, A. V.; Vaessen, D. M.; Payne, J. A. *Journal of Materials Science* **2002**, *37*, 4717-4731.
32. Rosin, M.; Urban, A. D.; Gärtner, C.; Bernhardt, O.; Splieth, C.; Meyer, G. *Dental Materials* **2002**, *18*, 521-528.
33. Ganahl, P. D.; Scranton, A. B.; Coretsopoulos, C. N. *RadTech Report* **2007**, *21*, 10-13.
34. Cai, Y.; Jessop, J. L. P. *Polymer* **2006**, *47*, 6560-6566.
35. Stolov, A. A.; Xie, T.; Penelle, J.; Hsu, S. L. *Macromolecules* **2001**, *34*, 2865-2869.
36. Decker, C. *Progress in Polymer Science* **1996**, *21*, 593-650.
37. Decker, C. *Polymer International* **1998**, *45*, 133-141.
38. Decker, C.; Moussa, K. *Macromolecules* **1989**, *22*, 4455-4462.
39. Decker, C. *Macromolecular Rapid Communications* **2002**, *23*, 1067-1093.
40. Dennison, J. B.; Yaman, P.; Seir, R.; Hamilton, J. C. *The Journal of Prosthetic Dentistry* **2000**, *84*, 499-505.
41. Neo, W. K.; Chan-Park, M. B. *Macromolecular Rapid Communications* **2005**, *26*, 1008-1013.
42. Shoemaker, J., *Moldflow design guide: a resource for plastics engineers*. Hanser Verlag: 2006; Vol. 10, p 178-180.
43. Fogleman, E. A.; Kelly, M. T.; Grubbs, W. T. *Dental Materials* **2002**, *18*, 324-330.

GENERAL CONCLUSION

This thesis comes within the scope of the launch by Huntsman Advanced Materials of Araldite®Digitalis, a new manufacturing machine. The unique feature of this device is its ability to expose in one step a large surface of UV curable resin to conventional UV light thanks to the MicroLightSwitch (MLS) technology, the heart of this invention. Our challenge was to develop for this new device UV curable resins exhibiting outstanding properties. Indeed, the resins have to be quickly cured during the building process, but also the resulting UV cured materials have to display not only good mechanical properties (combination of toughness and hardness properties) but also good surface properties to be easily handled before the post-curing treatment.

At first, we investigated the IPN chemistry that is commonly employed in commercial SLA equipment: the combination of two different polymer networks (epoxide and acrylate) provides complementary physical/mechanical properties such as flexibility and hardness, low shrinkage and high reactivity. It has been demonstrated that the formulations developed for SLA could not be easily used under Araldite®Digitalis: the photosensitive system was not efficient owing to the low absorption of the cationic photoinitiator, a sulfonium salt at the actinic wavelength (366 nm). Hence, it is necessary to increase the reactivity of the cationic system. In that purpose, we have carried out a study about the electron transfer sensitization process. Several radical photoinitiators from Ciba Specialties and aromatic hydrocarbons were tested. Significant improvements were noticed with the free radicals from Irgacure®651 photolysis, the photosensitizer 9,10-diethoxyanthracene, although the increase in reactivity was not sufficient to ensure the green strength at high speed exposures. Besides the sensitization of the cationic photoinitiator, the anti-oxidant triphenylphosphine was introduced into the formulation so as to speed up the radical polymerization. This addition was shown to thermally influence the cationic photoinitiator. By this way, the green strength was even reach at high exposure speeds. Within this framework, we have also carried out an academic study on the IPN chemistry in order to get a better understanding on the IPN formation. We got some relevant information. We have shown that it was possible to control the formation of the two networks by changing the radical photoinitiator content or the nature of the light source. The sequence order of the network formation was found to strongly influence the final thermomechanical properties. Besides, the real time ultrasound reflectometry analysis pointed out that the IPNs keep strengthening even after 7h after the curing due to the living character of the cationic polymerization. Despite the optimization process and a better comprehension of the IPN chemistry, it was not possible to solve the lack of efficiency of the IPN chemistry under Griffin cure by modifying only the photoinitiator system.

As a consequence, new chemistries that could overcome some of the aforementioned shortcomings were investigated.

The association of maleimides with vinyl ether or norbornene monomers (cf Chapter III) for the replacement of IPN chemistry is really promising since these resins fulfil most of the Huntsman expectations. Indeed, RT FTIR experiments revealed higher reactivities than a common commercial acrylic resin. In addition, the vinyl ether conversion can be extended with the additional introduction of a cationic photoinitiator without affecting the complete maleimide polymerization. Furthermore, the final properties of the UV cured materials are very interesting. They display high crosslinking density (high T_g), high tensile modulus and the shrinkage magnitude can be low depending provided that the molar percentage of vinyl ether function is not superior to 30 mol%. Hence, the nature of the comonomer is of prime importance. For the first time, the vinyl ether monomer was replaced by a norbornene monomer, a rich olefin giving rise to materials with high T_g . The reactivity of this new maleimide/norbornene was lower than for some maleimide/vinyl ether formulations and an important amount of norbornene monomer remains unreacted. Nonetheless, UV cured maleimide/norbornene materials are highly crosslinked and the norbornene conversion might be expanded during a post treatment for example by adding a catalyst usually used for ring opening metathesis polymerization. The main encountered problem was the lack of commercial availability of the maleimides and norbornenes. To complete this study, we were obliged to synthesize 3 norbornenes and 1 bismaleimide. For the future, it will be interesting to synthesize various maleimides and norbornenes with different structures in order to characterize their physico-chemical properties and thus get a good insight of the potentiality of this chemistry.

Given the detrimental consequences of linear shrinkage on the piece final properties such as distortions, cracks, the last chapter of this thesis was dedicated to the evaluation of this phenomenon. The shrinkage was measured both volumetrically and linearly. A screening survey was achieved with the formulations tested in Chapter III. Despite the differences in processing conditions, almost the same trends were observed. The implementation of a linear shrinkage method based on the cantilever deflection allowed us to study the influence of some parameters like the nature and the functionality of the monomer, the sample thickness and the light intensity. Interesting conclusions have been drawn. For instance, the variation of the light intensity has pointed out the existence of a threshold value from which the shrinkage value tremendously increases. The experiments have also shown some limitations of this method especially in terms of accuracy and reproducibility. This method still needs to be improved because the final

target is to implement this method directly within the machine in order to carry out the experiments in the real processing conditions.

To conclude, in order to solve an industrial issue, we have conducted a multifacet investigation. We first worked with IPN chemistry. We have highlighted the versatility of this chemistry with the possibility to tailor-made the final properties of the material according to the processing parameters. We have also identified one of its shortcomings which is the low polymerization rate of the cationic polymerization. To overcome this problem, important means have to be found. For instance, it might be interesting to synthesize either more reactive cationic monomers or photoinitiators. Since the end of this thesis, 2 new sulfonium salt photoinitiators from BASF exhibiting a greater absorption in the UVA range have been released on the market. It would be interesting to perform some trials with the latter under Griffin cure. In addition, to increase the stability of the cationic photoinitiator, a stabilizer can be added to the formulation. These innovations might lead to a revival of interest for this chemistry. As regards to the alternative chemistries that we proposed, the features of these chemistries are particularly interesting in terms of reactivity, versatility and final properties. They are worthwhile to go further into investigation particularly for the new maleimide/norbornene system. The mechanism of photopolymerization has still to be elucidated as well as the characterization of the final properties. In addition to these studies dedicated to the formulation chemistry, we were interested in the physical aspect of the shrinkage phenomenon.

ANNEXES

Experimental part.....	211
Annexe I: Irradiation sources.....	212
Annex I.1: Arc mercury-xenon (Hg-Xe) Hamamatsu lamp	212
Annex I.2: UV conveyor belt	213
Annex I.3: Arc Hg Oriel lamp	214
Annex I.4: Hg flood lamp	214
Annexe II: Real time techniques	215
Annex II.1: Real Time Fourier Transform Infra Red (RT FTIR) spectroscopy	215
Annex II.2: Photo Differential Scanning Calorimetry.....	218
Annexe III: Thermoanalytical techniques.....	221
Annex III.1: Dynamic Mechanical Analysis (DMA)	221
Annex III.2: Modulated Differential Scanning Calorimetry (MDSC).....	223
Annexe IV: Electronic microscopy technique.....	226
Annex IV.1: Scanning Electronic Microscopy (SEM)	226
Annexe V: Rheological technique	227
Annex V.1: Combination of Real time dynamic ultrasound reflectometry and time resolved near infrared spectroscopy.....	227
 Synthesis procedures	 229
Annexe VI: Synthesis of liquid bismaleimides.....	230
Annexe VII: Synthesis of norbornenes.....	232
 REFERENCES.....	 234

Experimental part

Annexe I: Irradiation sources

Annex I.1: Arc mercury-xenon (Hg-Xe) Hamamatsu lamp

For the studies of the kinetics of photopolymerization by Real-Time Fourier Transform Infra Red (RT FTIR) spectroscopy, an arc Hg-Xe Hamamatsu lamp (L8222, power=200 W) equipped a reflector optimized for the 366 nm wavelength coupled with a flexible quartz light guide was employed for the irradiation of the sample. This lamp is particularly suitable for the UV region since it presents the best characteristics of both xenon lamps and high-pressure mercury lamp. The spectral distribution of this polychromatic lamp is depicted in Figure 1. It can be converted into a monochromatic source by the addition of an interferential filter at 366 nm. Basically, the light intensity was set up at 17 mW/cm² for the experiments carried out at 366 nm and at 70 mW/cm² under broadband irradiation (cf Chapter II, section IV.2).

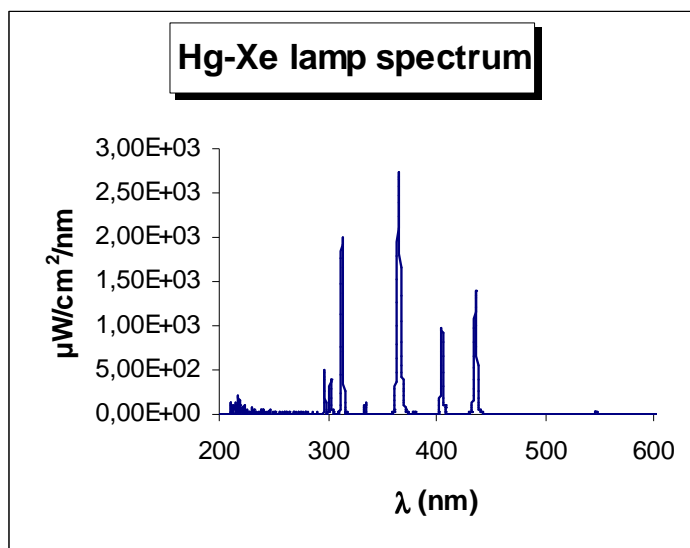


Figure 1: Broadband emission spectrum of the Hg-Xe Hamamatsu lamp

Annex I.2: UV conveyor belt

The preparation of the samples for DMA analysis was performed with a semi-industrial UV conveyor belt from Qurtech.



The samples were exposed to the illumination of a Fusion microwave lamp type H associated to a conveyor belt speed of 10 m/min. The light intensity was measured to be for one pass UVA: 440 mJ/cm², UVB: 430 mJ/cm², UVC: 90 mJ/cm², UVA: 480 mJ/cm². Four passes were done. The emission spectrum is given in Figure 2.

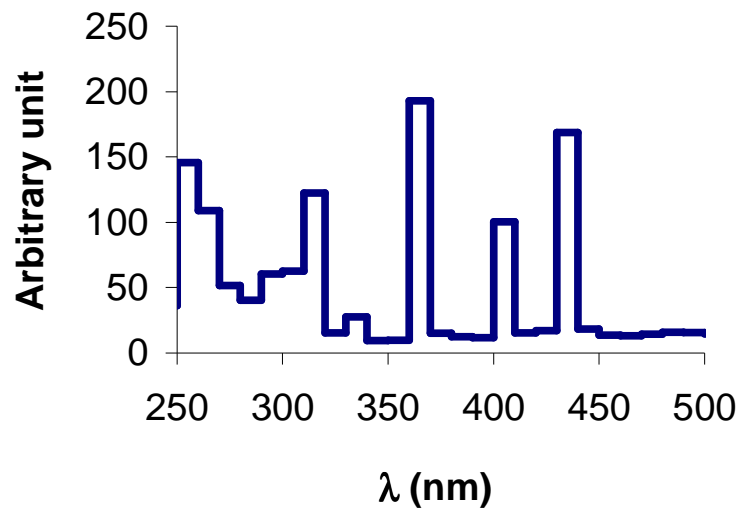


Figure 2: Emission spectrum of the UV conveyor belt

Annex I.3: Arc Hg Oriel lamp

The linear shrinkage measurements were carried out with a 200 W Hg Oriel arc lamp from Newport. The spectrum is shown in Figure 3.

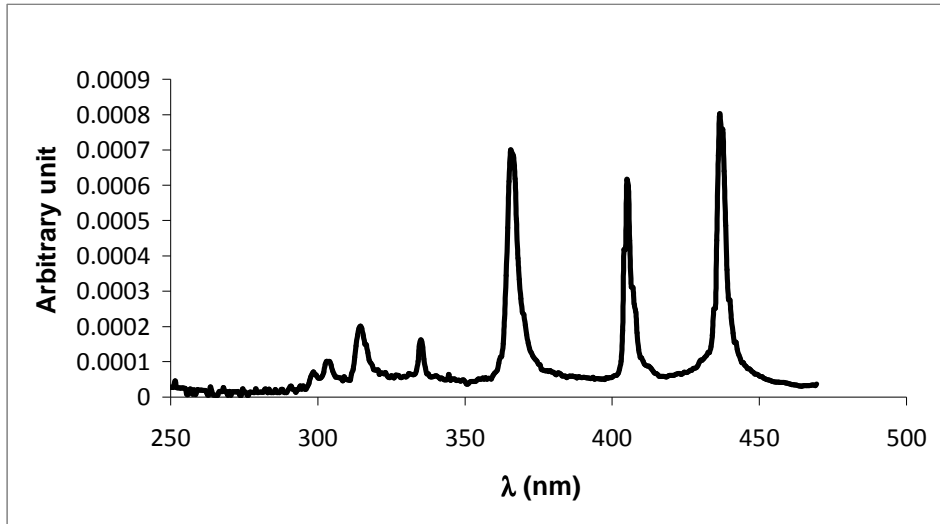


Figure 3: Emission spectrum of the arc Hg Oriel lamp

Annex I.4: Hg flood lamp

The linear shrinkage measurements were also performed with an Hg Oriel lamp (Electric power~300 W) whose spectral distribution is drawn in Figure 4.

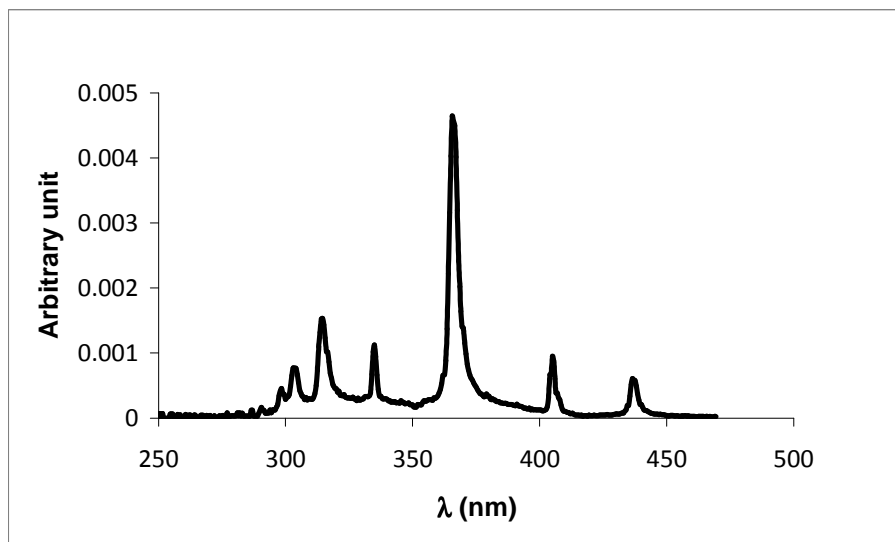


Figure 4: Emission spectrum of the arc Hg flood lamp

Annexe II: Real time techniques

Annex II.1: Real Time Fourier Transform Infra Red (RT FTIR) spectroscopy

VERTEX 70 from Bruker is a digital RT FTIR spectrometer which permits to determine the chemical and molecular composition of inorganic and organic compounds. When a sample is exposed to IR radiation, ($\lambda = 1\text{-}100\ \mu\text{m}$) a part of the radiation will be absorbed by the sample molecules and converted into molecular vibrational energy. The spectral range typically used is the middle infrared (MIR) (from $4000\ \text{cm}^{-1}$ to $400\ \text{cm}^{-1}$) because it corresponds to the range where the fundamental vibrations are typically excited (cf Figure 5) ¹.

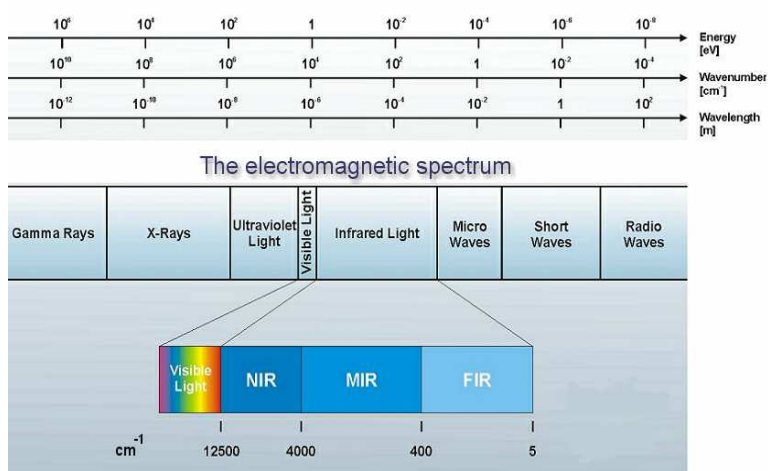


Figure 5: The electromagnetic spectrum

As the vibrational energy depends on the mass of the atoms, the force constant of the bonds, the geometry and environment of the molecule, a FTIR spectrum is characteristic for a complete molecule. The amount of absorption at a specific frequency can be used to quantify the presence of the corresponding bonds.

Generally, the absorbance is calculated according to the Beer-Lambert's law:

$$A = \epsilon l C = -\log\left(\frac{I}{I_0}\right) \quad (\text{A.1})$$

Figure 6: The absorption law

With

ϵ : the extinction absorption, $\text{L}\cdot\text{mol}^{-1}\cdot\text{cm}^{-1}$

I_0 : the intensity of the incident light, $\text{Einstein}\cdot\text{L}^{-1}\cdot\text{s}^{-1}$

I : the transmitted intensity, $\text{Einstein}\cdot\text{L}^{-1}\cdot\text{s}^{-1}$

C : the substance concentration, $\text{mol}\cdot\text{L}^{-1}$

ℓ : the path length or the coating thickness, cm

During the kinetics experiments in RT FTIR spectroscopy ², the sample in Figure 7 is exposed to both the excitation UV beam and the analysis IR beam so the polymerization can be followed in situ. Indeed, a RT FTIR spectrum is recorded at short intervals, one spectrum each 100 ms and collected at a resolution of 4 cm^{-1} thanks to a liquid nitrogen-cooled mercury-cadmium telluride (MCT) detector. The end of the optical guide is placed at a distance of 3 cm from the sample and directed at an incident angle of 90° onto the sample window. The final conversion is evaluated from the changes occurred in the spectrum. For instance, when an acrylate is polymerized the C=C bond at the end of the chain is converted into a C-C bond. This process is clearly visible in the RT FTIR spectra in Figure 7 as the characteristic IR absorption band at 1407 cm^{-1} (deformation of the acrylate double bond) disappears with time.

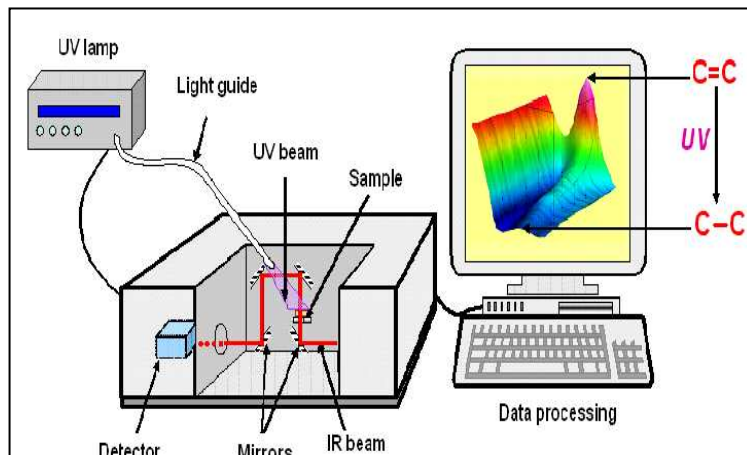


Figure 7: A RT FTIR spectrometer

This technique enables to record directly the conversion versus time. The conversion is calculated according to the formula A.1.

$$\text{Conversion} = \frac{A_0 - A_t}{A_0} \times 100 \quad (\text{A.1})$$

with

A_0 , corresponding to the area of IR absorption band of reactive function before the curing

A_t , corresponding to the area of IR absorption band of reactive function at the time t (s) Figure 8 shows the typical kinetics profile curve recorded by RT FTIR spectroscopy for an UV curable acrylate resin cured upon UV exposure. This profile provides important information about kinetics parameters such as ³:

- The actual polymerization rate (R_p , mol. L⁻¹.s⁻¹) calculated at any time from the slope of the RT FTIR curve and from the initial acrylate double bond concentration $[M]_0$. Its maximum is commonly attained between 10 and 30 % conversion.
- The inhibition period (t_i , s) due to the presence of polymerization scavengers such as oxygen for acrylates
- The final degree of conversion (X_f)

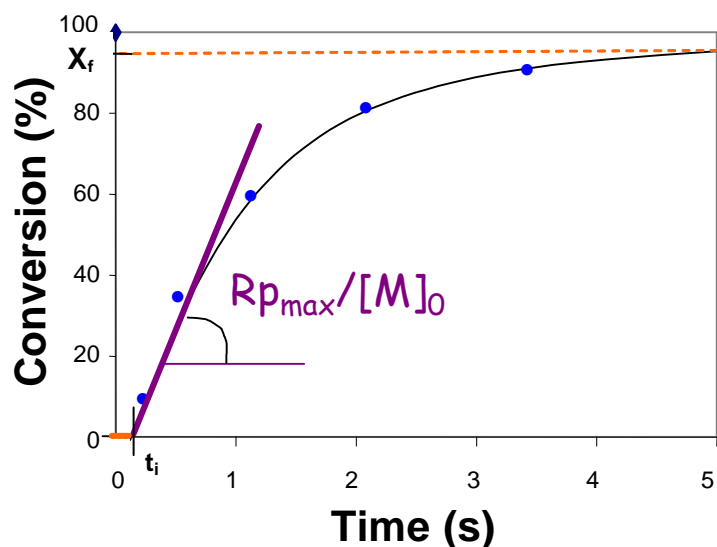


Figure 8: Conversion versus time profile for an UV-curable resin exposed to UV irradiation

These formulations were applied onto a KBr chip with a calibrated bar of 50 μm . The sample thickness was about 35 μm . The analyses were achieved with the IR spectrometer, Vertex70 (Bruker) at room temperature and under air. The samples were exposed to the UV illumination of a broadband Hg-Xe lamp (features in Annex I.1) and a monochromatic light source at 366 nm (features in Annex I.1). The decrease of the typical IR absorption band of the reactive functions was monitored. OPUS software was employed for the integration of the typical IR absorption bands.

Annex II.2: Photo Differential Scanning Calorimetry

Another way to characterize the kinetics of polymerization is to use the photo Differential Scanning Calorimetry (photoDSC). Since the photopolymerization is a highly exothermic reaction, the kinetics parameters can be evaluated by monitoring the evolved heat from the polymerization. The DSC chamber allows to work under isothermal conditions and under inert atmosphere by a constant nitrogen flush. As illustrated in Figure 9, the UV irradiation passes through a transparent quartz window and irradiates both the sample and the reference which is empty.

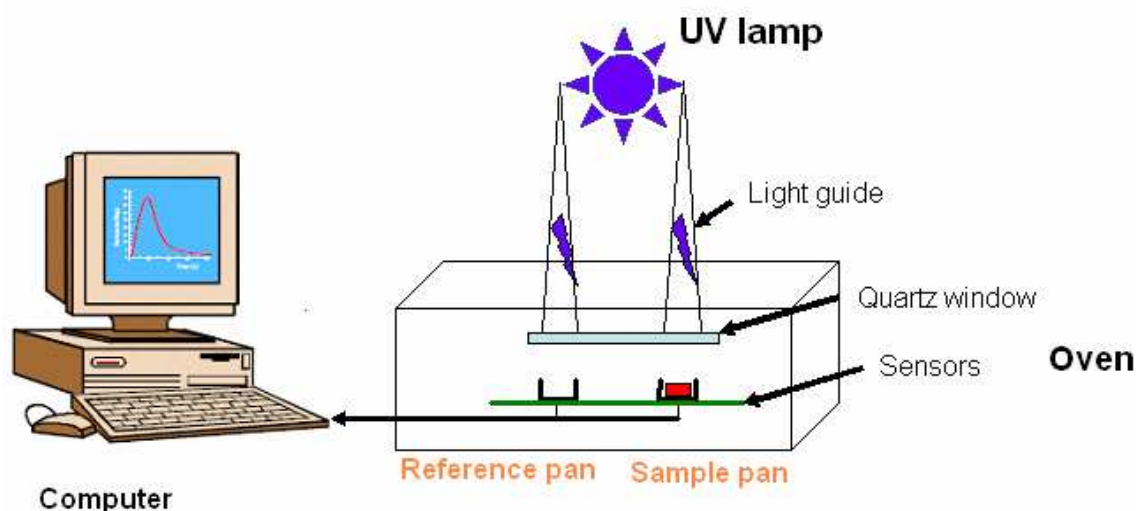


Figure 9: Simplified scheme of the photoDSC principle

Basically, the heat flow between the sample and the reference is recorded according to the time (cf Figure 9).

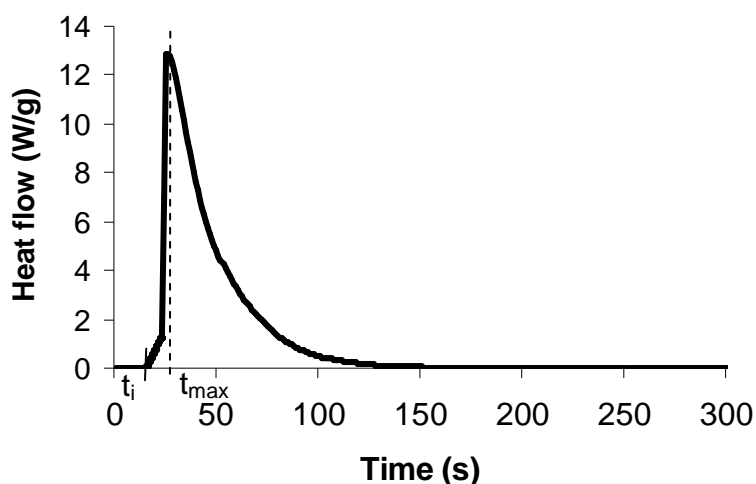


Figure 10: Monitoring of the heat flow evolved during the polymerization by photoDSC

The profile obtained gives access to the kinetics parameters ⁴:

- The enthalpy of the reaction (ΔH_t , J.g⁻¹) corresponds to the area of the curve and is proportional to the number of reactive functions participating to the polymerization.
- The time at the maximum peak (t_{\max} , s) corresponds to the time between the beginning of the exposure and the maximum of the evolved energy of the reaction.
- The induction period (t_i , s) is defined as the time at 1% conversion of the monomer.

The percentage of conversion X (%) and the rate of the polymerization are determined from these formulas.

$$X(\%) = \frac{\Delta H_t}{\Delta H_{theoretical}} \times 100 \quad (A.3)$$

with

ΔH_t , the enthalpy of the reaction at t seconds, J.g⁻¹

$\Delta H_{theoretical}$, the enthalpy released by the total of the acrylate double bond, in J.g⁻¹

$\Delta H_{theoretical}$ was calculated according to this relation:

$$\Delta H'_{theoretical} = \frac{f \times E \times x_M}{M} \quad (A.4)$$

with

f, the monomer functionality

E, the energy necessary to break the reactive function

x_M , the monomer fraction within the formulation

M, the monomer molecular weight

The polymerization rate is the slope of the conversion profile and can be defined as follows:

$$\frac{d\alpha}{dt} = \frac{\left[\frac{d(\Delta H_t)}{dt} \right]}{\Delta H_{theoretical}} \quad (A.5)$$

The photoDSC was used to characterize the kinetics of the photopolymerization of our systems (cf Chapter II). The experiments were performed by means of the DSC Q200 from TA instruments. The formulations were placed into uncovered aluminium hermetic

pans. The sample weight was about 2 mg. They were constantly submitted to a nitrogen purge (50mL/min) in order to remove residual air within the resin and facilitate the heat transfer phenomenon. The sample was irradiated by an Hg-Xe hamamatsu lamp (cf Annexl.1) whose light intensity was about 21mW/ cm². Universal Analysis program software from TA instruments was used to generate the results from these experiments.

Table 1 summarizes both the strengths and the limitations of the RT FTIR spectroscopy and the photoDSC.

Table 1: Advantages and drawbacks of RT FTIR spectroscopy and the photoDSC

	RT FTIR	PhotoDSC
Monitored phenomenon	Disappearance of the reactive function	Enthalpy of reaction
Slow polymerization (>10 s)	+++	+++
Fast polymerization (< 1s)	+++	-
Light intensity	+++	++
Controlled atmosphere	+	+++
Temperature of polymerization	-	+++

Annexe III: Thermoanalytical techniques

Annex III.1: Dynamic Mechanical Analysis (DMA)

Dynamic Mechanical Analysis (DMA) is used to characterize the polymer viscoelastic properties. The technique consists in applying a sinusoidal deformation at a given frequency to the sample and the resulting material response is measured as a function of time. Under these conditions, a time shift is observed between the stress and the deformation, as it is illustrated in Figure 11. This phase angle is called δ ($0 < \delta < 90^\circ$ for viscoelastic materials) ⁵. For accuracy sake, the amplitude of the material deformation must be within the linear viscoelastic region of the material. Indeed, in this region, the material response does not depend on the magnitude of deformation and the material structure is not modified.

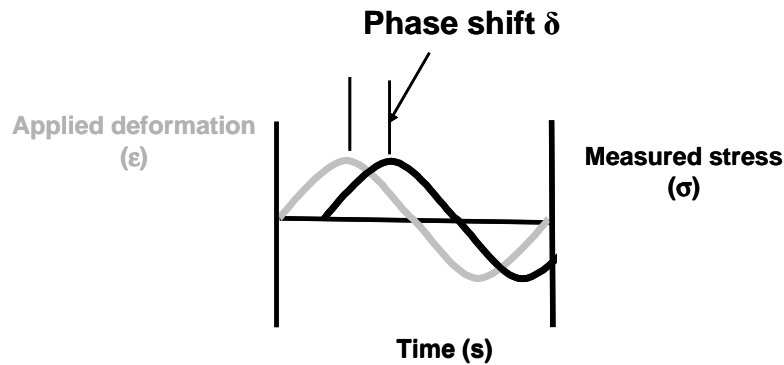


Figure 11 : Phase shift between the stress and the strain for viscoelastic materials

From the determination of δ , the storage modulus E' which refers to the sample's elastic behavior, the loss modulus E'' which measures the sample ability to dissipate the energy and the loss factor $\tan \delta = (E''/E')$ also called damping (evaluation of the capacity of damping) can be determined. Their respective signals in a DMA thermogram are represented in Figure 12.

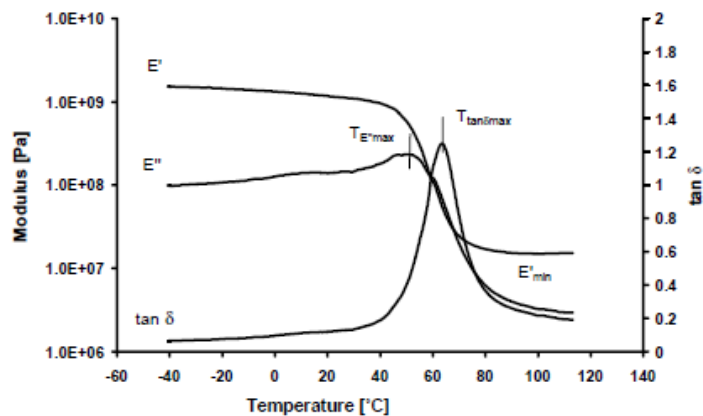


Figure 12 : Typical DMA signals ⁵

DMA can be used to determine the glass transition temperature (T_g) corresponding to the transition temperature between the glassy and the rubbery state (usually, the temperature of the maximum of the loss factor, $T_{\tan\delta\max}$).

The Young's modulus referring to the stiffness of the material can also be determined. It is the ratio of stress to strain. Experimentally, the determination of Young's modulus lies in slightly increasing the amount of stress, whilst measuring the sample elongation at each stress level. It corresponds to the initial slope of the stress-strain curve, as it is depicted in Figure 13.

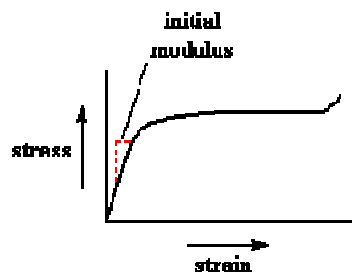


Figure 13 : Calculation of the Young's modulus

Preparation of the samples:

The formulations were applied onto glass substrate by means of an automatic wire wound applicator. They were polymerized under the UV conveyor belt according to the irradiation conditions in Annex I.2. The sample thickness varies from 65 to 90 μm depending on the viscosity of the formulation. As a consequence, the sample thickness was checked with a micrometer. A rectangular specimen was stripped from the substrate. Its dimensions were about 3 cm*0.6 cm.

DMA experimental conditions

Dynamic mechanical analyses were conducted with DMA Q800 from TA instruments, at a frequency of 1Hz in tensile mode. The $\tan\delta$ curves were obtained as a function of temperature at a constant heating rate of 3°C/min. Usually, the temperature was ramped from 0°C to 250-300°C. The interpretation of the results was achieved with Universal Analysis program from TA instruments.

Young Modulus experimental conditions

The experiments were performed at room temperature. The force ramp rate was 2 N/min. The maximum force applied was 18 N.

Annex III.2: Modulated Differential Scanning Calorimetry (MDSC)

Differential Scanning Calorimetry (DSC) is an analytical technique that gives some interesting qualitative and quantitative information about endothermic and exothermic sample transitions. The main interests of this method are the ease to prepare the sample, the possibility to analyze liquids, powders, films..., the relative rapidity of measurement and a wide temperature operational range. However, standard DSC displays some limitations for differentiating processes occurring at the same time especially for a mixture with several components ⁶.

To overcome this problem, Modulated Differential Scanning Calorimetry (MDSC) can be employed. Contrary to standard DSC where the heating rate is only changing linearly, in MDSC, a sinusoidal heating rate is superimposed to the linear heating rate (See Figure 14) ⁷.

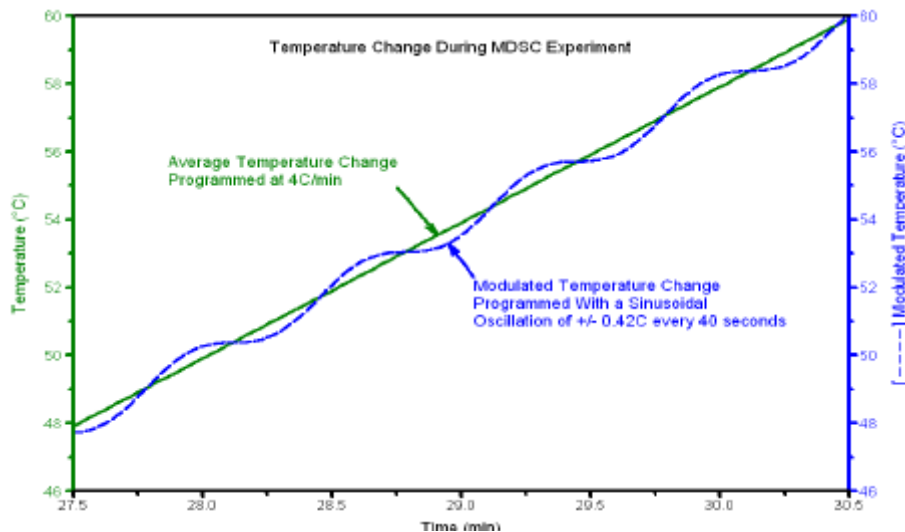


Figure 14: Temperature profile from a MDSC experiment

MDSC is a more sensitive method than traditional DSC since it permits to distinguish the thermal events occurring at a specific temperature or time during a run. Indeed, the total heat flow measured by conventional DSC comprises two components, as it can be seen from the following equation ⁸.

$$\frac{dH}{dt} = C_p \frac{dT}{dt} + f(T, t)$$

(A.6)

The first component depends on the sample's heat capacity and the heating rate. Meanwhile, the second component is a function of absolute temperature and time. It is called the kinetic component.

In MDSC, the linear heating rate is used to calculate the total heat flow, $\frac{dH}{dT}$ the same signal measures in DSC.

$C_p \frac{dT}{dt}$: This component is commonly named the Reversing heat flow or the heat capacity component of the total heat flow. It is calculated from the heat capacity. It corresponds to the fraction of the heat flow which is due to a heating rate modification. Basically, the glass transition temperature is assessed with this signal.

$f(T,t)$: This component is called Nonreversing heat flow. It corresponds to the difference between the total heat flow and the reversing signal. Evaporation, cristallisation and polymerization phenomena are commonly observed with this signal.

To sum up, the MDSC has the advantage to split the overlaid transitions (See Figure 15), to directly calculate the heat capacity, to enhance the sensitivity for determining the polymer initial crystallinity and measuring weak transitions.

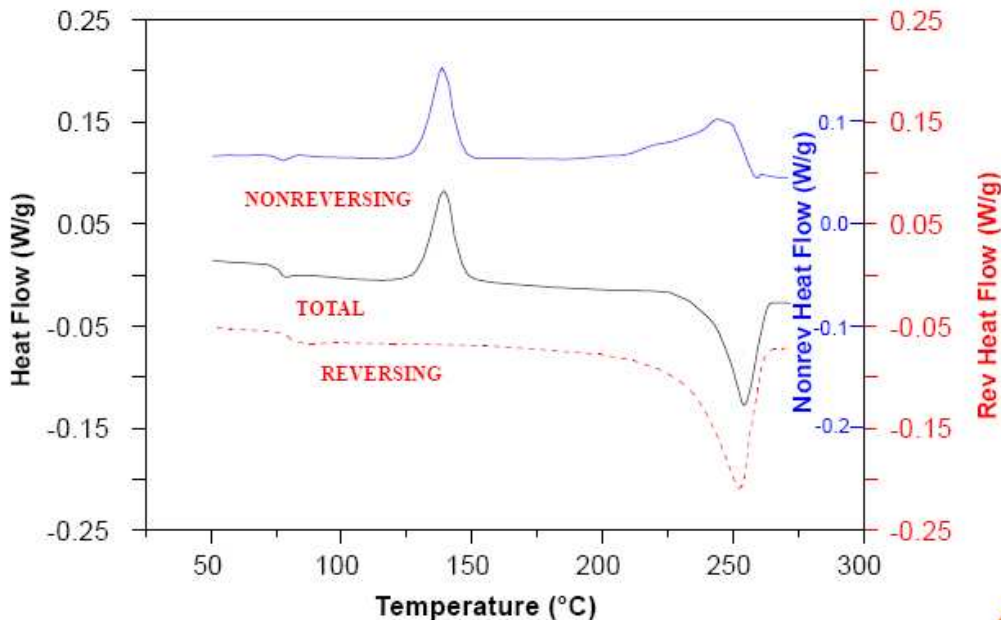


Figure 15: PET MDSC signals from MDSC training course TA instruments

The MDSC experiments were performed in order to determine the glass transition for the homopolymers and for hybrid formulations in Chapter II. The experiments require two steps:

1. The curing of the photosensitive resins

The samples were photocured with DSC Q200 equipped with a photocalorimetry accessory from TA instruments. They were placed into uncovered aluminium hermetic pans. For sensitivity sake, the sample weight was about 10 mg. A special attention was given to the sample preparation to get a flat surface to optimize the heat transfer with the pan. They were irradiated by an Hg-Xe hamamatsu lamp (cf Annex I.1) whose light intensity was about 21mW/ cm².

2. MDSC experiments

After UV curing, the pans were hermetically sealed and MDSC experiments were carried out with the same apparatus but with the MDSC option coupled with a cooling unit RCS. The temperature was ramped at 2°C/min from 0°C to 2 50°C and modulated at ± 2°C/min every 60s. The DSC traces were exploited with the Universal Analysis program from TA instruments.

Annexe IV: Electronic microscopy technique

Annex IV.1: Scanning Electronic Microscopy (SEM)

Scanning electron microscopy (SEM) is a powerful method for observing a sample surface topography. It is based on the scanning of a high energy electron beam onto the sample. The beam of electrons is generated by the heat of a metallic filament located on top of the microscope. Then, the beam is focused on the sample thanks to electromagnetic lenses. The interaction between the electrons and the sample atoms leads to the ejection of sample backscattered and secondary electrons. These latter are detected and turned into a signal producing a surface image on a screen. In SEM, samples must be conductive at their surface to avoid any accumulation of electrostatic charge at their surface. If the specimens are insulators, they must be coated with gold vapour.

This device can also be employed for examining the sample morphology in the bulk on condition that the sample is fractured. Usually, the sample is frozen by liquid nitrogen and then broken.

The experiments were performed at l'Institut de Science des Matériaux de Mulhouse (IS2M) by Dr Loic vidal.

Preparation of the samples:

The formulations were applied onto glass substrate by means of an automatic wire wound applicator. They were polymerized under the UV conveyor belt according to the irradiation conditions in Annex I.2. Transparent tacky free films of approximately 40 μm thickness were obtained. Afterwards, the samples were metallised with gold, frozen in liquid nitrogen and fractured. Electron micrographs were made at a magnification 25 000x with the Philips XL 30 LaB6 Scanning Electron Microscop (SEM).

Annexe V: Rheological technique

Annex V.1: Combination of Real time dynamic ultrasound reflectometry and time resolved near infrared spectroscopy

The Deutsches Kunststoff-Institut in Germany (DKI) has set up a new technique based on the association of Real time dynamic ultrasound reflectometry and time resolved near infrared spectroscopy to monitor simultaneously in real time the shear modulus and the conversion versus time during the photopolymerization of acrylate resins^{9,10}.

The device is a measuring cell having at the top and at the bottom fused quartz bars. The fused quartz bar at the bottom was metallised with gold for NIR reflection. At the edges of the cell, there are two piezo transducers: one transmitter and one receiver of shear waves (resonant frequency of 5 MHz). Under the effect of an electrical pulse, the excited transmitter engenders a transversal wave into the quartz bar. The shear wave is reflected on the sample substrate interface (sample thickness~200 µm) and turns towards the receiver. Due to the presence of the coating in the interface, the reflected wave is shifted in terms of amplitude and phase with regard to the value obtained only for the quartz bar. As a result, the complex reflection coefficient can be determined. Finally, from this coefficient and acoustic impedances of both the viscoelastic sample and the quartz cell substrate, the complex dynamic shear modulus can be calculated.

Through the use of optical fibers and a lens system, NIR measurements can be simultaneously carried out. For an optimum sample absorption, the NIR beam passes six times through the coating. The determination of the the reactive function conversion is achieved by following the disappearance of the typical NIR absorption band of the reactive function versus time. A simplified scheme of this method is presented in Figure 16.

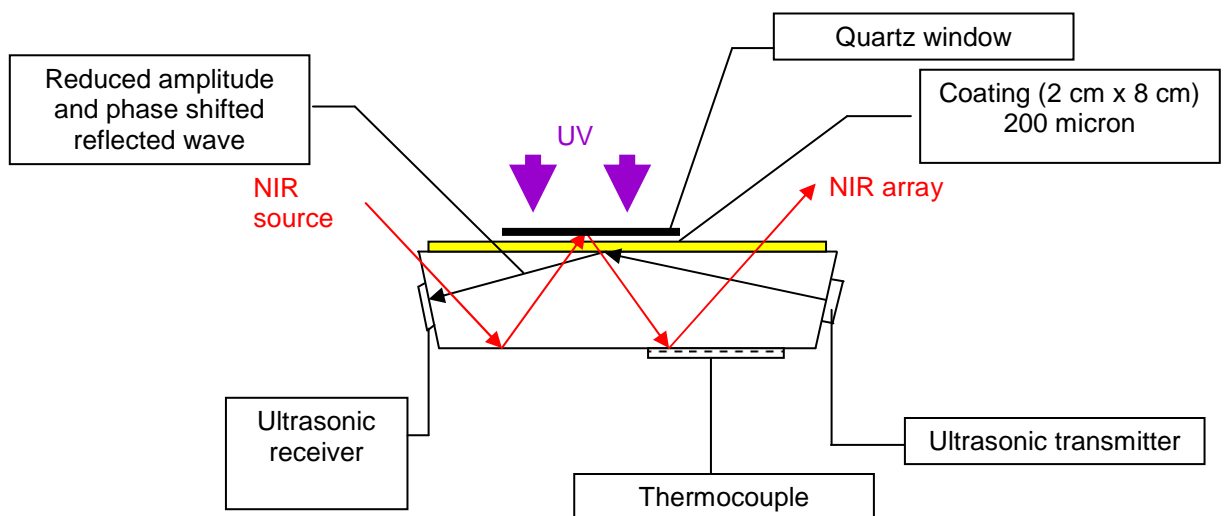


Figure 16: Hyphenated Real time dynamic ultrasound reflectometry and time resolved near infrared spectroscopy

The device is placed in aluminium housing with a fused quartz window transparent to UV illumination. Both the temperature (between 15 to 85°C) and the atmosphere (nitrogen flow) are controlled. The cure of the sample is performed by means of a microwave UV lamp (Nordson UV-Mac) (emission wavelength between 200 nm and 500 nm). The sample thickness is around 200 µm and the light intensity is roughly 35 mW/cm².

Synthesis procedures

The molecules were synthesized at both the laboratory Chimie Organique et Bioorganique and the Department of Photochemistry.

Annexe VI: Synthesis of liquid bismaleimides

Given the lack of commercial available difunctional maleimide compounds especially liquid ones, we decided to synthesize a poly(propylene glycol bismaleimide) (PPGBMI) (molecular weight~390 g.mol⁻¹)

The poly(propylene glycol bismaleimide), PPGBMI was prepared in two steps. The overall process is pictured in Figure 17 ¹¹.

The first step was the preparation of poly(propylene glycol) bis (2-propyl ether maleamic acid) intermediate. The second step was the preparation of PPGBMI from bismaleamic acid, which was cyclodehydrated in situ. A solution of poly(propylene glycol) bis (2-aminopropyl ether) (noted PPGA) of Mw of 230 g.mol⁻¹ (30 g, 0.130 mol) in THF (30 mL) was added dropwise at room temperature to a stirred solution of maleic anhydride (26.86 g, 0.274 mol) in THF (~100 mL). The reaction was carried out under argon atmosphere. During the addition process, the solution changed from colorless to light yellow. The resulting reaction mixture was then stirred for an additional hour, after which ZnBr₂ (61 g, 0.271 mol) was added in one portion. While the resulting reaction mixture was heated (40 °C), a solution of 1,1,1,3,3,3-Hexamethyldisilazane (HMDS) (66.3 g, 0.411 mol) in THF (50 mL) was slowly added over a period of 1 h 30 min, and the mixture was heated (40 °C) during 1 h 30 min with a reflux. After cooling to room temperature, the mixture was filtered and the solvent evaporated. The resulting brown viscous residue was purified using a packed silica gel column eluted with 70% cyclohexane/ 30% ethyl acetate. The eluent was reduced in volume at the rotary evaporator. The corresponding maleimide was obtained in 50 % yield. The purity is about 95%.

NMR: δ_{H} (400 MHz, CDCl₃) 1.01 (6H, m); 1.33 (6H, m); 3.45 (10H, m); 4.34 (2H, m); 6.65 (4H, s)

$\delta_{13\text{C}}$ (400 MHz, CDCl₃) 171; 134; 75-69; 46; 17; 15 ppm

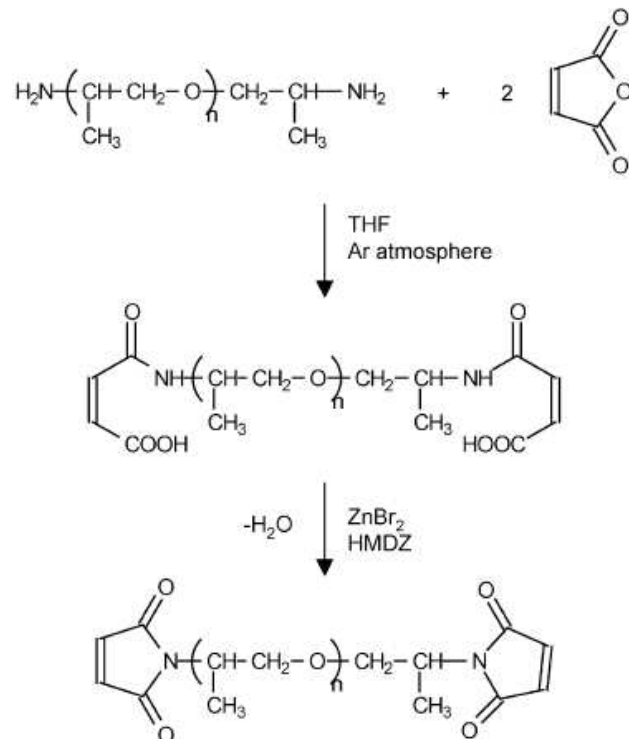
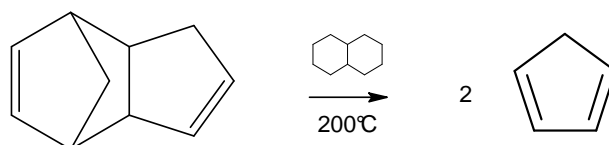


Figure 17: Synthesis of a poly(propylene glycol bismaleimide) (PPGBMI)

Annexe VII: Synthesis of norbornenes

The synthesis of the norbornenes can be divided into two steps.

The first step consists in cracking the dicyclopentadiene in order to obtain the cyclopentadiene. The cracking was accomplished by using a distillation apparatus. In a two-neck round bottom flask equipped with a dropping funnel and a condenser cooled with iced water, 10 mL of dicyclopentadiene (bp~170°C¹²) (0.08 mol) was stirred with 15 mL of decalin (0.10 mol) (bp ~189-191°C¹³) at 200°C. Decalin played the role of body heat transfer due to its high boiling point. In the dropping funnel, 15 mL of dicyclopentadiene (0.11 mol) was added dropwise to the bottom flask while the cyclopentadiene distilled progressively at a temperature around 40°C (bp ~41.5°C¹⁴). 25 mL of cyclopentadiene is finally obtained. The product is immediately stored in ice to inhibit the slow dimerization that occurs at room temperature. The distillation procedure takes 1h30 to 4 hours depending on the desired amount of cyclopentadiene.

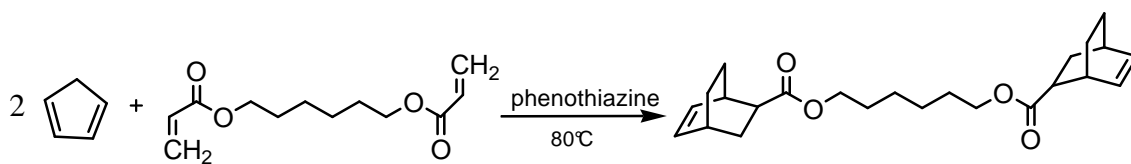


The second step corresponds to a Diels-Alder reaction between the cyclopentadiene and the acrylate. Three different acrylates were selected for the synthesis: 1,6-hexanediol diacrylate (SR 238), polyethyleneglycol (200) diacrylate (SR 259) and ethoxylated (4) bisphenol A diacrylate (SR 601E). Their structure is represented in Table 2.

Table 2: Chemical structures of the selected acrylates

Acrylate name	Chemical structure
SR 238	
SR 259	
SR 601E	

The second step will be only described for SR 238 but it is the same procedure for the two acrylates left. The scheme of the Diels-Alder reaction is given below:



In a 250 mL three neck round-bottom flask equipped with a dropping funnel, a condenser and a nitrogen inlet was charged with a dropping funnel, a condenser and an Argon inlet, 0.82 g of phenothiazine (~2000 ppm), a thermal stabilizer was mixed with 50 g of SR 238 (0.22 mol). The mixture was preheated to 80°C and 37 g of cyclopentadiene monomer (0.56 mol) was progressively added to SR 238 by means of a dropping funnel. After the complete addition of cyclopentadiene, the mixture was heated under reflux during further four hours.

At this stage, the yield of the dinorbornene named HDDNEC was 90%. Some residues of cyclopentadiene and dicyclopentadiene were still present about 5%. We faced some problems for the purification of our product. The attempt to performing a column chromatography eluted with 70% cyclohexane/30% ethyl acetate was not successful. A yield of 5 % was found.

NMR: δ_H (400 MHz, $CDCl_3$) 1.19-2.21 (17H, m); 2.78-3.20 (5H, m); 3.97-4.10 (4H, m); 5.91-6.20 (4H, m)

RT FTIR experiments were carried out with purified fraction and the non-purified one. Mixtures comprising an equimolar ratio of each norbornene fraction with N-tertbutylmaleimide in presence of 5 wt% of TPO were prepared. The experiments were carried out under air, at 366 nm and at a light intensity of 21 mW/cm². The results have shown a similar reactivity for both purified fraction and the non-purified one.

The purification of the other dinorbornenes by column chromatography was not possible because the products got stuck into the silica column owing to their acidity.

Consequently, taking into account the RT FTIR results for both purified and non purified HDDNEC fractions, RT FTIR experiments for the other dinorbornenes could be carried out on the non-purified resins.

REFERENCES

1. Dalibart, M.; Servant, L. *Techniques de l'Ingénieur, traité Analyse et Caractérisation*, **2000**, DOC P2845.
2. Decker, C.; Moussa, K. *European Polymer Journal* **1990**, *26*, 393-401.
3. Decker, C. *Polymer International* **1998**, *45*, 133-141.
4. Bayou, S.; Mouzali, M.; Abadie, M. J. M. *Comptes Rendus Chimie* **2005**, *8*, 903-910.
5. Schlesing, W.; Buhk, M.; Osterhold, M. *Progress in Organic Coatings* **2004**, *49*, 197-208.
6. Verdonck, E.; Schaap, K.; Thomas, L. C. *International Journal of Pharmaceutics* **1999**, *192*, 3-20.
7. Thomas, L. C. *TA Instruments Technical Paper TP 006*.
8. Thomas, L. C. *TA Instruments Technical Paper TP 007*.
9. Alig, I.; Steeman, P. A. M.; Lellinger, D.; Dias, A. A.; Wienke, D. *Progress in Organic Coatings* **2006**, *55*, 88-96.
10. Alig, I.; Oehler, H.; Lellinger, D.; Tadjbach, S. *Progress in Organic Coatings* **2007**, *58*, 200-208.
11. Vázquez, C. P.; Joly-Duhamel, C.; Boutevin, B. *Macromolecular Chemistry and Physics* **2009**, 9999, NA.
12. Birmingham, J. M. U.S. Patent 5877366, 1999.
13. Gu, H.; Soucek, M. D. *Chemistry of Materials* **2007**, *19*, 1103-1110.
14. Gaku, M.; Nobuyuki, I. U.S. Patent 4 469 859, 1980.